Resonant and Nonresonant Interactions in Cold Quantum Gases

by

Jochen Wachter

Vordiplom, Universität Konstanz, Germany, 1998

M. S., University of Colorado at Boulder, 2000

A thesis submitted to the

Faculty of the Graduate School of the

University of Colorado in partial fulfillment

of the requirements for the degree of

Doctor of Philosophy

Department of Physics

2007

This thesis entitled:
Resonant and Nonresonant Interactions in Cold Quantum Gases
written by Jochen Wachter
has been approved for the Department of Physics

Prof. Murray Holland

Prof. John L. Bohn

Date

The final copy of this thesis has been examined by the signatories, and we find that both the content and the form meet acceptable presentation standards of scholarly work in the above mentioned discipline.

Wachter, Jochen (Ph. D.)

Resonant and Nonresonant Interactions in Cold Quantum Gases

Thesis directed by Prof. Murray Holland

In the first part of this thesis, we present a unified kinetic theory that describes the finite-temperature, non-equilibrium dynamics of a Bose–Einstein condensed gas interacting with a thermal cloud in a trap. This theory includes binary interactions to second order in the interaction potential and reduces to a diagonal quantum Boltzmann equation for Bogoliubov quasiparticles. The Hartree–Fock–Bogoliubov interactions include the pairing field and are expressed as many-body T matrices to second order. The interactions thus include the correct renormalized scattering physics. This renormalized theory is automatically gapless. Thus, the excited Bogoliubov modes are naturally orthogonal to the condensate ground state. This kinetic theory is a complete second-order theory that reduces to the Gross–Pitaevskii equation and the quantum Boltzmann equation in the respective limits and thus is capable of describing the system over a wide temperature range.

In the second part, we consider a many-body theory of a dilute Fermi gas near a Feshbach resonance. Experiments explore the crossover physics between the Bardeen–Cooper–Schrieffer (BCS) superfluidity of a two-spin Fermi gas, and the Bose–Einstein condensation (BEC) of composite bosons. We consider correlations between a composite boson and a fermion pair and show that such correlations are the minimal ingredients needed in a many-body theory to generate the correct boson-boson scattering length in the Bose–Einstein limit of the crossover.

We also use imaginary-time propagation to find zero-temperature ground states in the BCS/BEC crossover. A cumulant expansion allows us to systematically include higher-order interactions between bosons and fermions. In particular, we calculate the Hartree term across the resonance. We further apply the cumulant-expansion method to thermal fermions and composite bosons interacting above the transition temperature in the normal phase. We numerically calculate the full time dependence in ramps across the resonance in this regime and find dif-

ferent two-body and many-body time scales in the system. We calculate molecular conversion efficiencies as a function of temperature and phase-space density, and find good agreement with results from JILA potassium experiments.

Acknowledgements

I acknowledge financial support from the National Science Foundation, the German-American Fulbright commission, the German National Merit Foundation, the W. M. Keck Foundation, the National Security Agency, and the American Physical Society. The cast of Holland-group characters that have contributed to this thesis includes: Murray Holland, Jinx Cooper, Marilu Chiofalo, Reinhold Walser, Servaas Kokkelmans, Chiara Menotti, Simon Gardiner, Satyan Bhongale, Josh Milstein, Rob Chiaramonte, Meret Krämer, Dominic Meiser, Jami Kinnunen, Rajiv Bhat, Brian Seaman, Sarah McGee, Brandon Peden, Ron Pepino, Boris Nowak, and Dave Tieri. There are yet more people to thank for maintaining my sanity.

Contents

List of Figures

Chapter 1

Introduction

In 1924, S. N. Bose and A. Einstein predicted the phenomenon of Bose–Einstein condensation (BEC) [1, 2], where a macroscopic number of noninteracting bosons (particles with integer total spin, for example ^{87}Rb atoms) collapse into a single quantum state. This behavior is a consequence of quantum statistics, which modifies the physical properties of the gas at very low temperatures.

The superfluid transition in liquid Helium was discovered in 1938 [4, 5]. Shortly thereafter in the same year, F. London suggested that the observed superfluid λ-transition (see Fig. 1.1) was due to BEC [6]. However, even at zero temperature, only 10% of the Helium atoms actually condense into a single state, because Helium is a strongly interacting liquid, whereas Bose and

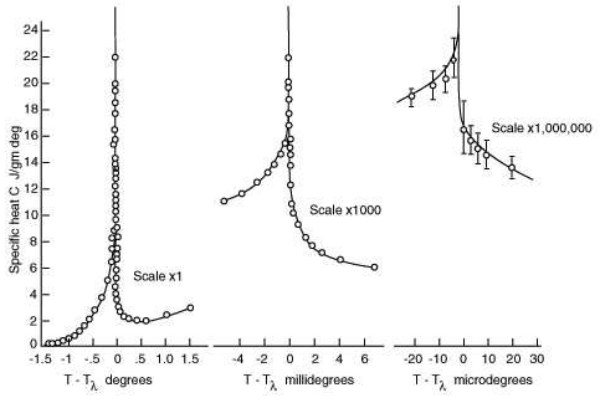

Figure 1.1: Superfluid transition in liquid ^{4}He [3]. The specific heat as a function of temperature shows the characteristic λ behavior at $T_\lambda = 2.71\,\mathrm{K}$. Note that the λ-shape is scale invariant over six orders of magnitude in temperature, indicating that the superfluid transition is a second-order phase transition.

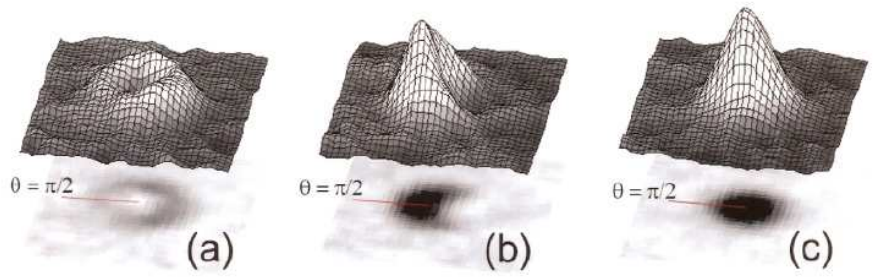

Figure 1.2: Vortex in a trapped ^{87}Rb BEC [11]. Images (a) through (c) show nondestructive absorption images (density plots) of the condensate. The images are 0.1 mm × 0.1 mm, which is macroscopic. Image (a) shows a quantized-vortex state, (c) a non-rotating state, and (b) the superposition of states (a) and (c). Due to the phase winding of the vortex in (a), the particles interfere constructively/destructively on the left/right sides of cloud (b).

Einstein predicted complete condensation for the case of a non-interacting, ideal gas.

The observation of BEC in a dilute, weakly interacting quantum gas of atomic ^{87}Rb at JILA [7] and shortly after in ^{23}Na at MIT [8] and ^{7}Li at Rice [9] thus opened a new field, in which corrections to the ideal-gas model of BEC could be calculated directly. The experimental systems are usually contained in harmonic trapping potentials, which is a complication compared to the homogeneous Helium case. Many interesting consequences of macroscopically occupied quantum states have since been observed experimentally: interference fringes between condensates [10], quantized vortices (see Fig. 1.2 (a)), superposition of condensate wave-functions or matter waves (ibid. (b)), and more. These systems exhibit quantum phenomena on macroscopic length scales; the plots in Fig. 1.2, for example, have a scale of a tenth of a millimeter.

These quantum phenomena can be understood as a consequence of $U(1)$ symmetry breaking below the transition temperature [12]. The breaking of the gauge symmetry causes the existence of a well-defined phase in the condensate. Only phase differences are physically observable; the absolute value of the phase can thus be changed without energy cost. There thus exists a low-frequency phonon mode, the zero-energy Goldstone mode [13]. This means that the collective-excitation spectrum is gapless and linear for small momenta. Another consequence of the broken gauge symmetry is the existence of long-range order [14]. This means that in a

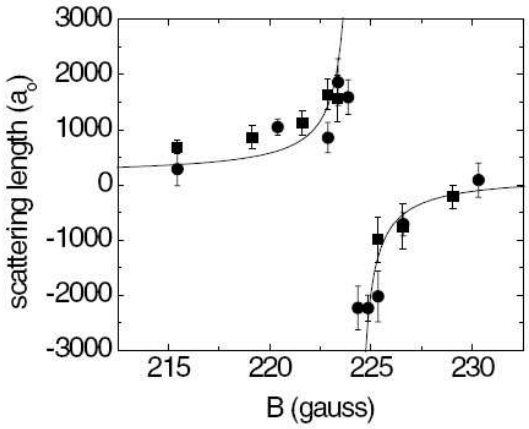

Figure 1.3: A Feshbach resonance in ^{40}K [17]. The scattering length as a function of magnetic field shows the $|9/2, -5/2\rangle$-$|9/2, -9/2\rangle$ Feshbach resonance.

condensate correlations between distant points exist. These correlations allow the low-energy collective excitations required by the Goldstone theorem.

The new cooling and trapping techniques [15] that lead to the creation of BECs were then also applied to fermions, which have half-integral total spin and at low temperatures obey quantum statistics that differ from those of bosons. In fact, Fermi-Dirac statistics predicts a maximum population of one particle per state (Pauli exclusion principle), such that at zero temperature all available quantum states up to the Fermi energy are singly occupied. This Pauli-blocking behavior was first observed in a dilute gas of ^{40}K at JILA in 1999 [16]. This experiment was performed with an equal mixture of two different magnetic sublevels ($|F = 9/2, m_F = 7/2\rangle$ and $|F = 9/2, m_F = 9/2\rangle$) of the hyperfine ground state with total atomic spin F and magnetic quantum number m_F, because s-wave scattering and thus thermalization during evaporation for one species is suppressed for due to the fermion's anti-symmetry requirement.

An intriguing possibility for fermion systems is pairing of two fermions to form a bosonic molecule. One inspiration for this idea is the Bardeen–Cooper–Schrieffer (BCS) theory of superconductivity [18]. It explains the resistance-less conduction below the transition temperature by the formation of weakly bound Cooper pairs, which are made up of two electrons interacting via

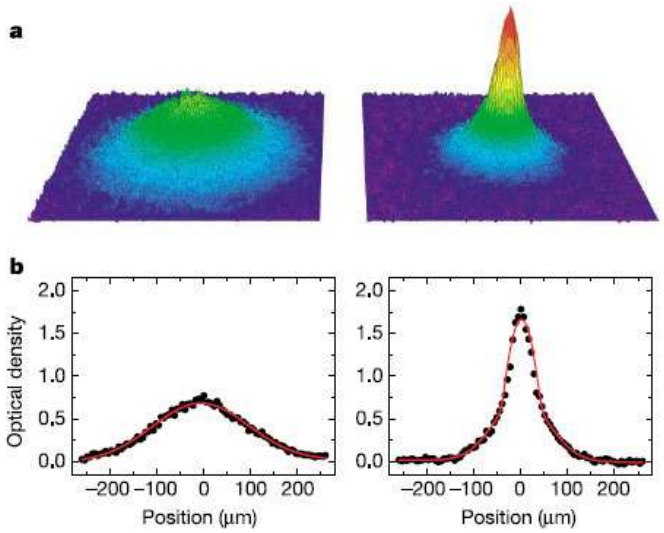

Figure 1.4: Time-of-flight images of a molecular cloud in ^{40}K [21]. Left images are above the BEC transition temperature (470, 000 molecules), right images below (200, 000 molecules). a) Surface plots of the optical density. b) Cross-sections through above images (dots) with bimodal fits (red lines).

lattice vibrations of the conductor. However, it turns out that the BCS transition temperatures for typical non-resonant s-wave scattering in a cold quantum gas are a few orders of magnitude below temperatures that can be reached in experiments.

Fortunately, the BCS transition temperature rises with increasing interaction strength, so that resonantly enhanced interactions near a Feshbach resonance opened the possibility of realizing BCS states in dilute quantum gases [19]. A Feshbach resonance is a scattering resonance with an energetically closed channel that strongly modifies the scattering in the open channel (see Chap. 5 for a more detailed introduction to Feshbach scattering). The relative position of the open and closed channels can be shifted by the Zeeman effect with an external magnetic field, which leads to the characteristic scattering behavior shown in Fig. 1.3. The Figure shows that the two-component Fermi gas is brought to the strongly interacting regime [20, 17]. Specifically, the Feshbach resonance connects loosely bound Cooper pairs on the attractive BCS limit on the right side of Fig. 1.3 to tightly bound molecules with weak repulsive interactions of the BEC (left) side of the figure.

The next series of results from groups all over the world reported the condensation of long-lived molecules on the BEC side of the resonance [22, 23, 24, 25]. These molecules are immersed in the residual Fermi sea of unbound atoms, which stabilizes the molecules due to Pauli blocking of final states for molecular decay. Figure 1.4 shows the resulting absorption images for the JILA experiment. Finally, many groups have reported observing condensation all the way through the BCS–BEC crossover [21, 26, 27, 28].

1.1 Theoretical Treatment

An exact many-body treatment of finite-temperature boson or fermion systems—even if we only considered two-body interactions—would have to involve correlations between as many particles as the system contains, because a tree of binary collisions would eventually entangle a single atom with every other atom in the system.

Fortunately, these many-body correlations are typically suppressed in the case of dilute, weakly interacting gases, because the duration of a collision τ is very small compared to the time between collisions $\Delta\tau$, so that the atoms oscillate essentially interaction-free in the external potential between isolated collision events [29]. This separation of time scales allows the high-order correlations to decay between collision events and thus justifies a coarse-grained description with a reduced set of Master variables that only contain correlation functions between two or three particles, because for times long compared to the duration of a collision τ, the higher-order correlations can be expressed as functionals of these variables [30]. We calculate the time evolution of these Master variables using the Markov approximation.

1.2 Separation of Time Scales

The diluteness of a gas is characterized by the following relation between its average number density n and its two-particle interaction strength, as given by the s-wave scattering

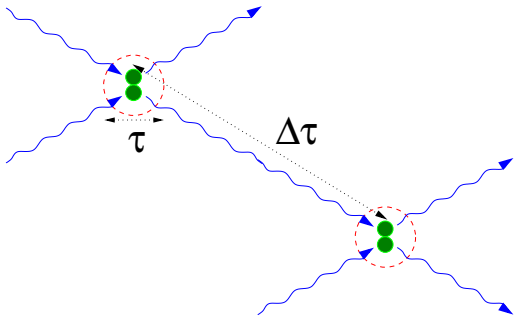

Figure 1.5: Separation of collision time scales: The duration of a collision τ is small compared to the time between subsequent collision $\Delta\tau$. The red circles illustrate the range of the binary interaction potential. Note that this range remains small even when the interactions are resonantly enhanced.

length a_s,

$$na_s^3 \ll 1. \tag{1.1}$$

This means that, on average, the volume available for each atom is large compared to its interaction volume. See Fig. 1.5 for an schematic illustration. In the case of a Feshbach resonance, where the scattering length diverges, the diluteness criterion is given by the range of the two-body potential r_0 as $nr_0^3 \ll 1$. Equation (1.1) is equivalent to the following relation between the duration of a collision τ and the time between collisions $\Delta\tau$

$$\tau = \frac{a_s}{v} \ll \frac{1}{na_s^2 v} = \Delta\tau, \tag{1.2}$$

where v is the average velocity. This quasi-classical argument shows that the diluteness of the system causes a separation of time scales. Choosing realistic experimental parameters for a cloud at 100 nK, we get, for example, $\tau \approx 5\,\mu$s and $\Delta\tau \approx 0.4$ s. Since many collision events for each particle are needed to establish local or even global equilibrium, the times associated with these states are again orders of magnitude larger than $\Delta\tau$. Some BEC experiments are performed on the time scale of $\Delta\tau$, which means that the observed system is far from equilibrium and should be described by a non-equilibrium theory.

We can distinguish between three distinct stages of evolution of a dilute quantum-gas system:

- The dynamical stage, where we follow the system on time scales shorter than the du-

ration of a collision $t \lesssim \tau$. On this time scale, the system is mostly dependent on its initial condition. In the case of an initially uncorrelated system, the time scale is too short to build up high-order correlations and a reduced description is still possible. If, however, the initial condition is highly correlated, the evolution in the dynamical stage is non-Markovian and we need the full N-particle density matrix to describe the system.

- The kinetic stage of evolution is characterized by time scales on the order of the time between collisions $t \approx \Delta\tau$. Here, we can assume that the correlations decay because of the long separation between successive collisions and the presence of large intermediate fluctuations. This allows us to make the Markov approximation and track the system with a reduced set of low-order Master variables. As pointed out above, this is the time scale on which many quantum-gas experiments are performed. Thus the kinetic description of these systems given in Chapters 2 to 4 is very useful.

- Finally, the hydrodynamic stage of evolution takes place on time scales large compared the time between collisions $t \gg \Delta\tau$, that is, when the system has come into a state of local equilibrium. Hydrodynamic equations for trapped Bose gases have been derived [31]. However, this state is more relevant in strongly interacting Bose systems, such as superfluid ^{4}He, where the kinetic stage vanishes ($\tau \approx \Delta\tau$).

1.3 Markov Approximation

The separation of time scales explained in the last Section allows us to make the far-reaching Markov approximation, which renders the problem of a kinetic theory for dilute, trapped, Bose–Einstein condensed gases feasible. It consists of the principle of rapid attenuation of quantum correlations: Individual collision events can correlate and entangle multiple particles. However, the separation of time scales leads to a decay of these correlations due to intermediate fluctuations.

Since correlations are the result of the past evolution of the system, we can interpret

the Markov approximation as saying that the future evolution is exclusively determined by the present state of the system. This is the defining property of a Markov process in the theory of stochastic differential equations, and is exactly the same property that is used for deriving the quantum-optical Master equation [32].

Another important feature of this approximation is that it implies the key observable Master variables that completely describe the system's irreversible evolution: The decay of higher-order correlation and distribution functions suggest using only few-particle quantities in a reduced but macroscopically sufficient description of the system. On the other hand, this decay means that information is lost in approximating the reversible, microscopic many-body treatment including N-particle correlations by a reduced description. This information loss is exactly the way in which irreversibility is usually introduced in statistical mechanics: The gigantic loss of information in going from a completely microscopic description in terms of atom coordinates to a macroscopic description in terms of thermodynamic quantities makes the latter appear irreversible. (Looking at decoherence in quantum systems, we see that similarly tracing over unobserved degrees of freedom, which involves loss of information, irreversibly replaces pure states by mixtures, which have to be described by density matrices.)

This principle of rapid attenuation of correlations was historically introduced by Bogoliubov [33, 29] to explain Boltzmann's assumption of molecular chaos (Stoßzahlansatz) in the derivation of his collision equation. He furthermore used it as a boundary condition in solving the Bogoliubov–Born–Green–Kirkwood–Yvon (BBGKY) hierarchy of recursively coupled equations of motion for s-particle distribution functions, where each couples to the $s+1$-particle distribution.

In the Markov approximation, the reduced set of Master variables completely describes the system, that is, its full N-particle density operator can be approximated by a density operator that is a functional of these variables only and does not contain an explicit time dependence. This is analogous to the Chapman-Enskog procedure used in classical statistical mechanics [29]. The reduced description is equivalent to coarse graining the quantum Liouville equation over

a kinetic time interval. Coarse graining is performed in the derivation of the quantum-optical Master equation to incorporate the weak-coupling approximation, which here corresponds to the rapid decay of correlations.

Within the Chapman-Enskog approach [34], expectation values are performed with the reduced density operator. Since the Markovian Master variables are our sole dynamic quantities and we can change many of the degrees of freedom of this density operator without changing these expectation values of the relevant operators, we can replace the reduced density operator by a more convenient Gaussian reference distribution, which is an exponential of quadratic combinations of the field operators. This reference distribution then enables one to expand the expectation values of operator products, which appear in the Heisenberg equations of motion for the relevant operators, using Wick's theorem [35, 36, 37, 38].

1.4 Overview

This thesis has two parts. The first begins with Chap. 2, where we derive a quantum-kinetic theory for atomic BECs using the Kadanoff–Kane Green-function formalism. In Chap. 3 we show explicitly that this theory has a gapless energy spectrum and discuss the scattering properties to second order in the binary interaction. In Chap. 4 we express the full quantum dynamics of the BEC in terms of quasiparticles interacting via a Boltzmann collision integral.

In the second part, we discuss dilute Fermi gases, in particular the crossover between BCS superfluidity and BEC of composite molecules. In Chap. 5 we discuss one- and two-channel models of Feshbach resonances. In Chap. 6 we introduce an imaginary-time method to find zero-temperature ground states for these strongly interacting fermion systems. In Chap. 7 we use a cumulant expansion to find a zero-temperature many-body theory that correctly describes the scattering physics of the BCS–BEC crossover. We also develop a cumulant expansion in the normal phase above the transition temperature in Chap. 8 and show numerical results for the full time dependence of thermal bosons and fermions across a resonance. We conclude in

Chap. 9 with the summary and outlook.

Chapter 2

The Kadanoff–Kane Formulation of Kinetic Theory [39]

2.1 Introduction

Binary collisions are the essential mechanism for the formation of a Bose–Einstein condensate in an atomic gas. Moreover, many aspects of the system's dynamics require two-particle collisions, for example, sound propagation, the damping of elementary excitations, and the very mechanism that leads to the quantum phase transition—evaporative cooling. However, the conventional Hartree–Fock–Bogoliubov approach to generalize the Gross–Pitaevskii equation for dilute, trapped gases includes binary collisional interactions only as first-order energy shifts. Second-order kinetic theories that include collisional redistributions of excited atoms offer a more complete microscopic description of the gaseous system.

Why is a simplified kinetic description possible, when the evolution of the Bose–Einstein condensate might involve correlations between as many particles as the system contains? Would not binary collisions eventually entangle the quantum state of each atom in the system with that of every other atom? Fortunately, such complexity is not necessary to describe the measurable properties of a dilute, weakly interacting gas, because the duration of a collision, τ, is very short compared to the essentially interaction-free oscillation in the external potential between isolated collision events [29].

Because of this characteristic separation of time scales, correlations that arise during an individual collision decay rapidly before the next collision takes place. This rapid decay, in turn, implies the possibility of a Markov approximation, which assumes that only the current config-

uration of the system determines its future evolution. Furthermore, this decay of correlations allows us to parameterize the system's state by a reduced set of master variables, because we are interested in the system's time evolution only on the kinetic time scale, that is, for times large compared to the duration of a collision τ. This reduced description with a set of master variables is possible, because for kinetic times the higher-order correlation functions can be expressed as functionals of these variables [30].

This set of master variables is common to both the kinetic theories that we discuss: In the Kadanoff–Baym approach, abstract real-time Green's functions parameterize the condensating gas, whereas in the Walser et al. case [40], single-time density matrices, which contain the physical density and coherences of thermal atoms, as well as the mean field, represent the system. The equivalence of these two approaches is a general principle in nonequilibrium statistical mechanics [41, 42]. However, it is not trivial to verify this fact in detail by explicitly connecting the complementary microscopic equations. Strictly speaking, we find equivalence after the Kadanoff–Baym theory has been restricted to single-time quantities using the Markov approximation.

We present the formulation of the quantum kinetic theory of dilute Bose–Einstein condensed gases in terms of nonequilibrium, real-time Green's functions and their Kadanoff–Baym equations of motion [43], which were generalized in Refs. [44, 45] to include the condensate.

By transforming these equations to the single-particle energy basis and taking the single-time limit of the two-time Green's functions by means of the Markov approximation, we reproduce the equations of motion of the Walser et al. kinetic theory as presented in Ref. [40], thus providing an independent confirmation of these equations. Following Imamović-Tomasović and Griffin [46], we use the gapless Beliaev approximation for the self-energies in the Kadanoff–Baym equations, and thus prove the Walser et al. kinetic theory to be gapless as well.

2.2 Nonequilibrium Green's Functions

We begin the introduction to the Kadanoff–Baym description of the dilute Bose gas by defining its variables. Neglecting three-body interactions, the second-quantized many-body Hamiltonian H describing the atoms is

$$H = \int d\boldsymbol{x} \int d\boldsymbol{y} \, \left[a^\dagger(\boldsymbol{x}) \, \langle \boldsymbol{x} | \, H^{(0)} \, | \boldsymbol{y} \rangle \, a(\boldsymbol{y}) + \frac{1}{2} \, a^\dagger(\boldsymbol{x}) a^\dagger(\boldsymbol{y}) \, V_{\mathrm{bin}}(\boldsymbol{x} - \boldsymbol{y}) \, a(\boldsymbol{y}) a(\boldsymbol{x}) \right], \tag{2.1}$$

where $a^\dagger(\boldsymbol{x})$ is the bosonic creation operator and $V_{\mathrm{bin}}(\boldsymbol{x} - \boldsymbol{y})$ the binary interaction potential. The single-particle Hamiltonian

$$H^{(0)} = \frac{\boldsymbol{p}^2}{2m} + V_{\mathrm{ext}}(\boldsymbol{x}) \tag{2.2}$$

contains the kinetic energy of a boson with mass m and the external potential $V_{\mathrm{ext}}(\boldsymbol{x})$.

To represent the master variables in terms of nonequilibrium Green's functions, we first write the system's degrees of freedom in terms of spinor operators [47]

$$A(1) = \begin{pmatrix} a(1) \\ a^\dagger(1) \end{pmatrix} \quad \text{and} \quad A^\dagger(1) = \begin{pmatrix} a^\dagger(1) & a(1) \end{pmatrix}, \tag{2.3}$$

where we now follow Kadanoff–Baym and abbreviate $(1) = (\boldsymbol{x}_1, t_1)$. The master variables are then contained in the following two-time propagators:

$$h(1,2) = -i\langle A(1) \rangle \langle A^\dagger(2) \rangle, \tag{2.4}$$

$$g(1,2) = -i\big\langle T\big\{ A(1) A^\dagger(2) \big\}\big\rangle, \tag{2.5}$$

where $\langle \cdot \rangle$ denotes the grand-canonical average and $T\{\cdot\}$ the time ordering operator, which sorts its arguments in order of decreasing time. These two propagators are defined for real times by analytic continuation of the finite-temperature propagators for imaginary time, following [43, Chap. 8]. We subtract the condensate propagator h from the full propagator g and thus define the Green's function for the fluctuations

$$\tilde{g}(1,2) = g(1,2) - h(1,2). \tag{2.6}$$

The two time orderings of $\tilde{g}$,

$$\tilde{g}^<(1,2) = \tilde{g}(1,2) \quad \text{for} \quad t_1 < t_2 \tag{2.7}$$

and

$$\tilde{g}^{>}(1,2) = \tilde{g}(1,2) \quad \text{for} \quad t_1 > t_2, \tag{2.8}$$

define the generalized two-time fluctuation-density matrices. This can be seen by explicitly writing these two time orderings in terms of the fluctuating part $\tilde{a}(1)$ of the field operators,

$$\tilde{a}(1) = a(1) - \langle a(1) \rangle = a(1) - \alpha(1), \tag{2.9}$$

as follows:

$$\tilde{g}^{<}(1,2) = \begin{pmatrix} \tilde{f}_{12} & \tilde{m}_{12} \\ \tilde{m}^{*}_{12} & (1+\tilde{f})^{*}_{12} \end{pmatrix}, \tag{2.10}$$

$$\tilde{g}^{>}(1,2) = \sigma_z + \tilde{g}^{<}(1,2), \tag{2.11}$$

where we defined the two-time normal ($\tilde{f}$) and anomalous ($\tilde{m}$) averages of the fluctuations in the position basis as

$$\tilde{f}_{12} = \left\langle \tilde{a}^{\dagger}(2)\tilde{a}(1) \right\rangle \quad \text{and} \quad \tilde{m}_{12} = \left\langle \tilde{a}(2)\tilde{a}(1) \right\rangle. \tag{2.12}$$

In the case $t_1 = t_2$, the propagators in Eqs. (2.10) and (2.11) correspond to the dynamical quantities in the kinetic equations for the fluctuations given in Eqs. (24) and (25) of Ref. [40]; for $t_1 = t_2$, the averages in Eq. (2.12) correspond to the density of thermal atoms around the condensate and correlations between these atoms. We have thus represented the condensate (h) and its fluctuations ($\tilde{g}^{<}$) and can now look for their corresponding evolution equations.

2.3 Kadanoff–Baym Equations

The equations of motion for the nonequilibrium Green's functions h and $\tilde{g}^{<}$ are the Kadanoff–Baym equations; these equations are equivalent to the Dyson equation. In the second part of this Section, we discuss the second-order Beliaev approximation for the self-energies that we use. For the condensed part of the atom cloud, which is parameterized by the propagator $h(1,2)$ defined in Eq. (2.4), we can write the Kadanoff–Baym equations as [44]

$$\int_{-\infty}^{\infty} d\bar{1} \left\{ g_0^{-1}(1,\bar{1}) - S_{\rm HF}(1,\bar{1}) \right\} h(\bar{1},2) = \int_{-\infty}^{t_1} d\bar{1} \ \left\{ S^{>}(1,\bar{1}) - S^{<}(1,\bar{1}) \right\} h(\bar{1},2) \tag{2.13}$$

and

$$\int_{-\infty}^{\infty} d\bar{1}\; h(1,\bar{1})\left\{g_0^{-1}(\bar{1},2) - S_{\mathrm{HF}}(\bar{1},2)\right\} = -\int_{-\infty}^{t_2} d\bar{1}\; h(1,\bar{1})\left\{S^{>}(\bar{1},2) - S^{<}(\bar{1},2)\right\}. \tag{2.14}$$

We write the corresponding equations for the fluctuations $\tilde{g}^{<}(1,2)$ and $\tilde{g}^{>}(1,2)$ [Eqs. (2.10) and (2.11)] around the condensate mean field as

$$\begin{aligned}&\int_{-\infty}^{\infty} d\bar{1}\left\{g_0^{-1}(1,\bar{1}) - \Sigma_{\mathrm{HF}}(1,\bar{1})\right\}\tilde{g}^{\gtrless}(\bar{1},2) \\ &= \int_{-\infty}^{t_1} d\bar{1}\;\left\{\Sigma^{>}(1,\bar{1}) - \Sigma^{<}(1,\bar{1})\right\}\tilde{g}^{\gtrless}(\bar{1},2) - \int_{-\infty}^{t_2} d\bar{1}\;\Sigma^{\gtrless}(1,\bar{1})\left\{\tilde{g}^{>}(\bar{1},2) - \tilde{g}^{<}(\bar{1},2)\right\}\end{aligned} \tag{2.15}$$

and

$$\begin{aligned}&\int_{-\infty}^{\infty} d\bar{1}\;\tilde{g}^{\gtrless}(1,\bar{1})\left\{g_0^{-1}(\bar{1},2) - \Sigma_{\mathrm{HF}}(\bar{1},2)\right\} \\ &= \int_{-\infty}^{t_1} d\bar{1}\;\left\{\tilde{g}^{>}(1,\bar{1}) - \tilde{g}^{<}(1,\bar{1})\right\}\Sigma^{\gtrless}(\bar{1},2) - \int_{-\infty}^{t_2} d\bar{1}\;\tilde{g}^{\gtrless}(1,\bar{1})\left\{\Sigma^{>}(\bar{1},2) - \Sigma^{<}(\bar{1},2)\right\}.\end{aligned} \tag{2.16}$$

In Eqs. (2.13) through (2.16), we use the definition of the matrix inverse of the interaction-free propagator g_0,

$$g_0^{-1}(1,2) = \left\{i\sigma^z\frac{\mathrm{d}}{\mathrm{d}t_1} + \frac{\nabla_1^2}{2m} - V_{\mathrm{ext}}(1) + \mu\right\}\delta(1,2), \tag{2.17}$$

with the third Pauli matrix $\sigma^z = \mathrm{diag}(\mathbb{1}, -\mathbb{1})$ and an energy shift μ, which removes mean-field oscillations. We define the δ function by $\delta(1,2) = \delta(\boldsymbol{x}_1 - \boldsymbol{x}_2)\delta(t_1 - t_2)$ and integration $d\bar{1}$ as integration $dt_{\bar{1}}$ over time within the given time limits and $d\boldsymbol{x}_{\bar{1}}$ over all space. The approximations we choose for the Hartree–Fock self-energies for the condensate S_{HF} and for the fluctuations Σ_{HF} as well as the second-order collisional self-energies $S^{<}$ and $\Sigma^{<}$ are discussed below.

Kadanoff and Baym derived these equations without including the condensate [43] and de Dominicis and Martin formulated a very general mathematical account [48]. The Green's function formalism traces back to Schwinger [49] and originally made use of the correspondence between the partition function and the time evolution operator in imaginary time ($e^{\beta H} = e^{iHt}$ for $t = -i\beta$). To get information about measurable quantities, the dynamic variables and equations of motion were extended to real times by analytic continuation (see [43, Chap. 8] and [50, 51, 42] for more details).

This nonequilibrium Green's function description was developed 40 years ago to eventually explain the behavior of superfluid helium [52]. Since this description involves a weak-coupling approximation but helium atoms are strongly interacting, the results at that time were disappointing and, for example, could not explain all predictions of the phenomenological Landau model. However, since the Green's function description holds for a dilute, weakly interacting gas, its application to Bose–Einstein condensation in this system is more appropriate.

To complete our exposition of the Kadanoff–Baym equations (2.13) through (2.16), we have to choose the Hartree–Fock and collisional self-energies. We draw the Hartree–Fock self-energy diagrams for both the condensate h and the thermal cloud $\tilde{g}^<$ in Fig. 2.1 and write them, respectively, as

$$S_{\rm HF}(1,2) = \frac{i}{2}\int d\bar{2}\; v(1,\bar{2}){\rm Tr}\left\{g(\bar{2},\bar{2})\right\}\delta(1,2) \;+\; iv(1,2)\tilde{g}(1,2) \tag{2.18}$$

and

$$\Sigma_{\rm HF}(1,2) = \frac{i}{2}\int d\bar{2}\; v(1,\bar{2}){\rm Tr}\left\{g(\bar{2},\bar{2})\right\}\delta(1,2) \;+\; iv(1,2)g(1,2), \tag{2.19}$$

with the local-time, binary interaction potential $v(1,2) = V_{\rm bin}(\boldsymbol{x}_1 - \boldsymbol{x}_2)\;\delta(t_1 - t_2)$ and the matrix trace Tr. When we evaluate the time-ordered propagator g at equal times, we follow the convention $T\{a(1)a^\dagger(2)\} = a^\dagger(2)a(1)$.

For the second-order collisional self-energies $\Sigma^{\gtrless}$ we choose the gapless and energy- and number-conserving Beliaev approximation [46, 53, 54]. This means that, compared to Kane and Kadanoff [44], we include the exchange terms, which they deliberately excluded to obtain the simplest conserving approximation as proven in [55], and compared to Hohenberg and Martin [45], we include the terms containing no condensate contributions, which give rise to the quantum Boltzmann terms for the fluctuations.

We depict the resulting self-energy diagrams in Fig. 2.2 and represent them mathemati-

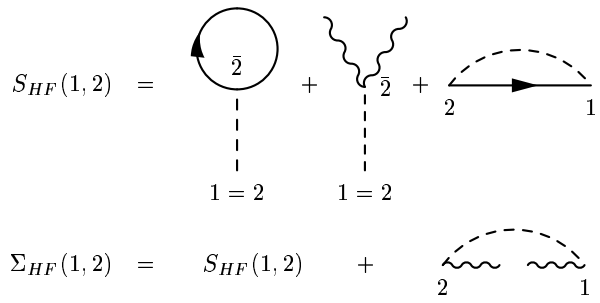

Figure 2.1: The first-order Hartree–Fock self-energy diagrams. The solid lines depict the non-condensate propagator $\tilde{g}$, the wiggly lines the condensate propagator h, and the dashed lines the interaction potential v. The first two terms give the energy shifts due to both the mean field U_{f^c} and the normal fluctuations $U_{\tilde{f}}$. The third term in $S_{\rm HF}$ gives rise to a factor of 2 for $U_{\tilde{f}}$ and to $V_{\tilde{m}}$. The fourth term which only appears in $\Sigma_{\rm HF}$ causes the difference in the mean-field shifts that are experienced by the condensate and the fluctuations, respectively.

cally as

$$S^{>}_{<}(1,2) = -\frac{1}{2}\int d\bar{2}\int d\bar{3}\; v(1,\bar{2})v(2,\bar{3}) \qquad \Big[\tilde{g}^{>}_{<}(1,2)\mathrm{Tr}\Big\{\tilde{g}^{<}_{>}(\bar{3},\bar{2})\tilde{g}^{>}_{<}(\bar{2},\bar{3})\Big\} \qquad (2.20)$$
$$+2\tilde{g}^{>}_{<}(1,\bar{3})\tilde{g}^{<}_{>}(\bar{3},\bar{2})\tilde{g}^{>}_{<}(\bar{2},2)\Big]$$

for the condensed part and

$$\begin{aligned}\Sigma^{>}_{<}(1,2) \;=\; & -\frac{1}{2}\int d\bar{2}\int d\bar{3}\; v(1,\bar{2})v(2,\bar{3}) \qquad (2.21)\\ & \times\Big[\tilde{g}^{>}_{<}(1,2)\mathrm{Tr}\Big\{g^{<}_{>}(\bar{3},\bar{2})g^{>}_{<}(\bar{2},\bar{3}) - h(\bar{3},\bar{2})h(\bar{2},\bar{3})\Big\} + h(1,2)\mathrm{Tr}\Big\{\tilde{g}^{<}_{>}(\bar{3},\bar{2})\tilde{g}^{>}_{<}(\bar{2},\bar{3})\Big\}\\ & +2\tilde{g}^{>}_{<}(1,\bar{3})\Big\{g^{<}_{>}(\bar{3},\bar{2})g^{>}_{<}(\bar{2},2) - h(\bar{3},\bar{2})h(\bar{2},2)\Big\} + 2h(1,\bar{3})\Big\{\tilde{g}^{<}_{>}(\bar{3},\bar{2})\tilde{g}^{>}_{<}(\bar{2},2)\Big\}\Big]\end{aligned}$$

for the fluctuations.

Instead of using lines for the matrix-valued propagators $\tilde{g}$ and h as in Fig. 2.2, one can also draw diagrams for the four elements of the matrix separately. The resulting diagrams for the first-order and second-order Beliaev terms can be seen in Figs. 15 and 17 of Ref. [56], where the interaction potential is replaced by a two-body T matrix.

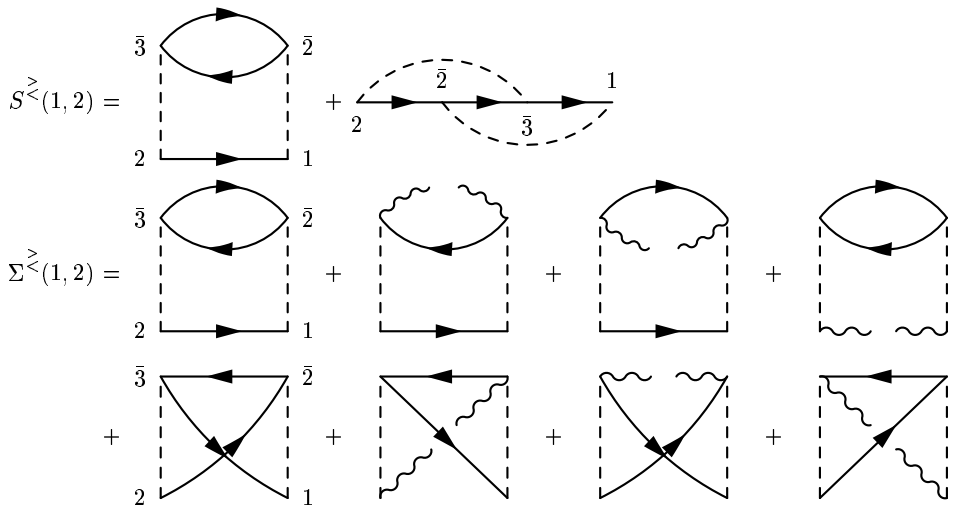

Figure 2.2: The second-order, collisional self-energies in the gapless Beliaev approximation. The solid lines depict the noncondensate propagator $\tilde{g}$, the wiggly lines the condensate propagator h, and the dashed lines the binary interaction potential v. The second diagram of S corresponds to the last four of Σ, when we replace each of the three fluctuation propagators by an open condensate one.

2.4 Transformation to the Energy Basis

We now demonstrate the key steps that connect the kinetic theory presented in the previous Section to the work of Walser et al. presented in [40]: We rewrite the Kadanoff–Baym Eqs. (2.13) through (2.16) in the single-particle energy (SPE) basis and obtain the equations of motion for the master variables—the measurable quantities in our reduced description of the system—in this basis, exactly as given in the Walser et al. paper.

First, we define our master variables in the SPE basis $\{|1'\rangle\}_{1'} = \{|\epsilon_{1'}\rangle\}_{\epsilon_{1'}}$ and determine the relation to their position basis counterparts, the Green's functions given in Eqs. (2.4), (2.10), and (2.11). The time-dependent, two-component mean-field state vector

$$\chi = \begin{pmatrix} \alpha \\ \\ \alpha^* \end{pmatrix} \tag{2.22}$$

is defined in terms of $\alpha = \alpha_{1'}\,|1'\rangle = \sum_{1'}\langle a_{1'}\rangle\,|1'\rangle$ and also contains the time-reversed mean field α^*. The time-dependent, fluctuating annihilation and creation operators $\tilde{a}$ and $\tilde{a}^\dagger$ transform

as

$$\tilde{a}(1) = \langle 1\,|\,1'\rangle \tilde{a}_{1'} \quad \text{and} \quad \tilde{a}^\dagger(1) = \langle 1'\,|\,1\rangle \tilde{a}^\dagger_{1'}, \tag{2.23}$$

where $|1\rangle = |\boldsymbol{x}_1\rangle$ are the position eigen states. The fluctuating part of the master variables is then contained in the single-time fluctuation-density matrix $\tilde{G}^<$, which we define as

$$\tilde{G}^< = \begin{pmatrix} \tilde{f} & \tilde{m} \\ \tilde{m}^* & (1+\tilde{f})^* \end{pmatrix}, \tag{2.24}$$

with the normal fluctuation density $\tilde{f} = \langle \tilde{a}^\dagger_{2'} \tilde{a}_{1'} \rangle\, |1'\rangle \otimes \langle 2'|$ and the anomalous average $\tilde{m} = \langle \tilde{a}_{2'} \tilde{a}_{1'} \rangle\, |1'\rangle \otimes |2'\rangle$ in the SPE basis.

Second, we can recognize the fluctuation-density matrix $\tilde{G}^<$ as the single-time limit of its position-basis counterpart $\tilde{g}^<(1,2)$ in Eq. (2.10). The mean-field state vector χ, on the other hand, can be combined with its Hermitian conjugate into the matrix $-i\chi\chi^\dagger$, which corresponds to $h(1,2)$ in Eq. (2.4). We thus define $\chi(1) = \langle A(1)\rangle$. This allows us to explicitly connect the condensate mean-field state vectors $\chi(1)$ expressed in the position basis and $\chi(t_1)$ in the SPE basis as follows:

$$\chi(1) = \begin{pmatrix} \langle 1\,|\,1'\rangle & 0 \\ 0 & \langle 1'\,|\,1\rangle \end{pmatrix} \begin{pmatrix} \alpha_{1'}(t_1) \\ \alpha^*_{1'}(t_1) \end{pmatrix} = T(1)\,\chi(t_1), \tag{2.25}$$

with a time-independent $2 \times 2n$ transformation matrix $T(1) = T(\boldsymbol{x}_1)$. Because of the completeness of the position basis, we can also write

$$\chi(t_1) = \int d\boldsymbol{x}_1\, T^\dagger(1)\chi(1). \tag{2.26}$$

For the fluctuation density, we obtain similarly

$$i\,\tilde{g}^<(1,2)\big|_{t_1=t_2} = T(1)\tilde{G}^<(t_1)T^\dagger(2) \tag{2.27}$$

and

$$-i\,\tilde{G}^<(t_1) = \int d\boldsymbol{x}_1 \int d\boldsymbol{x}_2\, T^\dagger(1)\tilde{g}^<(1,2)T(2)\big|_{t_1=t_2}. \tag{2.28}$$

We can now use the transformation Eq. (2.27) to write the condensate's Hartree–Fock self-energy $S_{\mathrm{HF}}(1,\bar{1})$ in Eq. (2.18) as

$$T(1)\begin{pmatrix} U_{f^c}+2U_{\tilde{f}} & V_{\tilde{m}} \\ V_{\tilde{m}}^{\dagger} & U_{f^c}^{\dagger}+2U_{\tilde{f}}^{\dagger} \end{pmatrix} T^{\dagger}(\bar{1})\delta(t_1-t_{\bar{1}}). \tag{2.29}$$

We here use the definitions of [40], where energy shifts due to both the mean field and the normal fluctuations are given by the matrices

$$U_f = 2\,\phi^{1'2'3'4'} f_{3'2'}\,|1'\rangle \otimes \langle 4'|\,, \tag{2.30}$$

whereas the first-order anomalous coupling strength is given by

$$V_{\tilde{m}} = 2\,\phi^{1'2'3'4'}\tilde{m}_{3'4'}\,|1'\rangle \otimes |2'\rangle\,. \tag{2.31}$$

The symmetrized two-body interaction matrix elements ϕ are here defined by

$$\phi^{1'2'3'4'} = \frac{1}{4}(\phi_u^{1'2'3'4'} + \phi_u^{1'2'4'3'} + \phi_u^{2'1'3'4'} + \phi_u^{2'1'4'3'}), \tag{2.32}$$

$$\phi_u^{1'2'3'4'} = \int d\boldsymbol{x}_1 \int d\boldsymbol{x}_2\ \langle 1'|1\rangle\langle 2'|2\rangle\ \frac{V_{\mathrm{bin}}(\boldsymbol{x}_1-\boldsymbol{x}_2)}{2}\ \langle 1|3'\rangle\langle 2|4'\rangle. \tag{2.33}$$

Like the first-order Hartree–Fock self-energies, we can rewrite the second-order self-energies in Eqs. (2.20) and (2.21) using the transformations in Eqs. (2.25) to (2.28) and (2.33). In particular, we now have to transform two potential factors, which makes the computation more complicated. Furthermore, the integrals over time to t_1 and t_2 in Eqs. (2.13) through (2.16) modify one of the binary potentials according to Eq. (65) of [37] to an approximately energy-conserving two-particle matrix element

$$\phi_\eta^{1'2'3'4'} = \phi^{1'2'3'4'}\left\{\pi\delta_\eta(\Delta) + i\,\mathcal{P}_\eta\frac{1}{\Delta}\right\}, \tag{2.34}$$

with an energy difference Δ between the incoming and outgoing states of the collision event. This definition of the matrix elements ϕ_η introduces the Markov approximation into the Kadanoff–Baym equations. We obtain the second-order damping rates and energy shifts $\Upsilon^{\gtrless}$ for the

condensate, corresponding to $S(1,2)$ in Eq. (2.20), and $\Gamma^{\gtrless}$ for the fluctuations, corresponding to $\Sigma(1,2)$ in Eq. (2.21); these are the collision integrals defined in [40]. These second-order terms appear in combinations $\Gamma^{<}\tilde{G}^{>} - \Gamma^{>}\tilde{G}^{<}$ that contain, for example, the Boltzmann collision terms

$$\begin{aligned} \left\{\Gamma_{\tilde{f}\tilde{f}(1+\tilde{f})}(1+\tilde{f}) \right. &- \left. \Gamma_{(1+\tilde{f})(1+\tilde{f})\tilde{f}}\tilde{f}\right\}_{1'5'} = \\ 8\phi^{1'2'3'4'}\phi_{\eta}^{1''2''3''4''} &\left\{ \tilde{f}_{3'1''}\tilde{f}_{4'2''}(1+\tilde{f})_{4''2'}(1+\tilde{f})_{3''5'} \right. \\ &- \left. (1+\tilde{f})_{3'1''}(1+\tilde{f})_{4'2''}\tilde{f}_{4''2'}\tilde{f}_{3''5'}\right\} \end{aligned} \tag{2.35}$$

and similar contributions involving the anomalous averages $\tilde{m}$ and $\tilde{m}^*$. See Appendix A for a detailed derivation of the collisional terms in the SPE basis.

We can now exactly reproduce the coupled equations for the condensed fraction as well as the normal and anomalous fluctuations stated in Eqs. (10) and (26) of Ref. [40]. Considering the first column of the matrix Eq. (2.13) for the condensate at $t_1 = t_2$, we obtain the generalized Gross–Pitaevskii equation

$$\frac{\mathrm{d}}{\mathrm{d}t}\chi = (-i\,\Pi + \Upsilon^{<} - \Upsilon^{>})\chi, \tag{2.36}$$

with the symplectic first-order propagator

$$\Pi = \begin{pmatrix} \Pi_{\mathcal{N}} & \Pi_{\mathcal{A}} \\ -\Pi_{\mathcal{A}}^{*} & -\Pi_{\mathcal{N}}^{*} \end{pmatrix}. \tag{2.37}$$

This propagator consists of the normal Hermitian Hamiltonian

$$\Pi_{\mathcal{N}} = H^{(0)} + U_{f^c} + 2U_{\tilde{f}} - \mu, \tag{2.38}$$

which contains the usual single-particle Hamiltonian $H^{(0)}$ given in Eq. (2.2) and the mean-field and fluctuation shifts U_f given in Eq. (2.30); furthermore, the symmetric anomalous coupling

$$\Pi_{\mathcal{A}} = V_{\tilde{m}} \tag{2.39}$$

is defined in Eq. (2.31). The propagator Π contains the Hartree–Fock shifts, which are given in Eq. (2.29), and originally were contained in $S_{\mathrm{HF}}(1,2)$ [see Eq. (2.18)].

To obtain the equation of motion for the fluctuations, we subtract Eq. (2.15) from (2.16) and evaluate at $t_1 = t_2$ to obtain

$$\frac{\mathrm{d}}{\mathrm{d}t}\tilde{G}^{<} = -i\,\Sigma\tilde{G}^{<} + \Gamma^{<}\tilde{G}^{>} - \Gamma^{>}\tilde{G}^{<} + \text{H.c.} \tag{2.40}$$

The reversible evolution of the fluctuations $\tilde{G}^{<}$ is governed by the Hartree–Fock–Bogoliubov self-energy operator

$$\Sigma = \begin{pmatrix} \Sigma_{\mathcal{N}} & \Sigma_{\mathcal{A}} \\ -\Sigma_{\mathcal{A}}^{*} & -\Sigma_{\mathcal{N}}^{*} \end{pmatrix}, \tag{2.41}$$

which in turn consists of the Hermitian Hamiltonian

$$\Sigma_{\mathcal{N}} = H^{(0)} + 2U_{f^c} + 2U_{\tilde{f}} - \mu \tag{2.42}$$

and the symmetric anomalous coupling

$$\Sigma_{\mathcal{A}} = V_m. \tag{2.43}$$

The propagator Σ corresponds to $\Sigma_{\mathrm{HF}}(1,2)$ in Eq. (2.19). Its mean-field shift is twice as large as that of the condensate propagator Π, which is a well known property of first-order Hartree–Fock–Bogoliubov theories. Further details of this transformation can be found in Appendix A.

2.5 Conclusion

We independently rederive the kinetic equations of Walser et al. from the Kadanoff–Baym nonequilibrium Green's function formulation of kinetic theory, and recover identical factors in all second-order damping rates and energy shifts. This shows that for dilute, weakly interacting gases the Kadanoff–Baym nonequilibrium, real-time Green's function approach is microscopically equivalent to the density-matrix approach used by Walser et al. [40]. The latter approach is more physical in two respects: First, its variables are measurable quantities: the mean field and the density and coherences of thermal atoms. Second, the variables' equations of motion reduce to the Gross–Pitaevskii equation and the quantum Boltzmann equation in the low- and high-temperature limits, respectively.

Starting from the gapless Beliaev approximation for the collisional self-energy in the Kadanoff–Baym equations, we furthermore learn that the full second-order kinetic theory of Walser et al. is gapless itself [54, 46]. This shows that the gap that appears in the first-order Hartree–Fock–Bogoliubov spectrum [57] is closed by the second-order energy shifts.

Furthermore, this work connects the kinetic theory of Walser et al. with work done by M. Imamović-Tomasović et al. [46, 53, 58], because they start from the same Kadanoff–Baym equations.

Chapter 3

Gaplessness—T Matrices [59]

3.1 Introduction

The extension of finite-temperature theories of Bose–Einstein condensation (BEC) to the real-time domain has been a very active field of study. The goal is a unified description of a dilute, atomic gas of bosons in a harmonic trap in terms of a condensate mean field interacting with a thermal cloud. The success of the zero-temperature Gross–Pitaevskii (GP) theory in describing BEC experiments spurred interest in effects not contained in this framework. Examples are damping of collective excitations and condensate growth through collisional redistributions of thermal atoms. This redistribution cannot be treated in theories that are still of first order in the binary interaction, such as, for example, Hartree–Fock–Bogoliubov (HFB) theories.

We present a kinetic theory of second order in the interaction, which is formulated in terms of Bogoliubov quasiparticles and contains collisional terms beyond the HFB approximation. The HFB interactions are expressed as many-body T matrices to second order in the binary potential and thus include the correct renormalized scattering physics. This theory thus contains no ultraviolet divergences and has a gapless energy spectrum. We extend the papers of Walser et al. [37, 40], which are the basis of the present results, by clearly demonstrating these two essential aspects of the theory.

We go beyond theoretical approaches that drop the anomalous pair matrix $\tilde{m} = \langle \tilde{a}\tilde{a} \rangle$ in the Popov approximation [31, 60, 53, 61]. Monte Carlo simulations based on the semi-classical Zaremba–Nikuni–Griffin theory [31, 62, 63, 64] show very good agreement for experimentally

observed damping rates and response frequencies [65]. However, recent experiments [66] and their theoretical explanations [67, 68] have shown that the pairing field plays an important role in Bose gases with resonance interactions.

Keeping the pair matrix $\tilde{m}$ in this theory would cause ultraviolet divergences if we replaced the non-local interaction potential with a contact-potential, whose strength is given by s-wave scattering length a_s. The vacuum part of the pairing field's self interaction, for example, diverges, because the delta-function potential contains unphysically high energy contributions. These divergences can be resolved by writing the interactions in terms of scattering T matrices, which subsume the divergent sums over intermediate scattering states and correctly reduce to the scattering length a_s in the zero-energy and -momentum limit [69, 70, 71, 72, 73, 74, 75, 76]. Using these scattering T matrices, we can consistently eliminate all divergences to second order in the interaction.

We thus obtain a renormalized HFB operator, which has a gapless spectrum. The zero-energy eigen space is spanned by the condensate, and excitations with non-vanishing energy are thus automatically orthogonal to the condensate. This is similar to the renormalized gapless HFB equations proposed in Ref. [71]. Other approaches have to explicitly project the excitations orthogonal to the condensate [77, 72, 78]. Using the condensate as the ground state of this adiabatic basis also simplifies the representation of a condensate band in the Gardiner-Zoller master equation formulation [79, 80].

The Monte Carlo simulations of Jackson and Zaremba [62, 63] show that considering dynamic population-exchange between the condensate and the thermal cloud and within the thermal cloud leads to good agreement with the observed response spectra. We include these kinetic effects, thus going beyond collisionless descriptions [81, 82].

Our presentation builds on the papers by Walser et al. [37, 40] and we begin by summarizing the kinetic equations derived in these papers in Sec. 3.2. In Sec. 3.3, we examine the first-order HFB self energy and rewrite it in terms of second-order T matrices, by including second-order energy shifts and adiabatically eliminating the pairing field $\tilde{m}$. This shows that

the theory is explicitly gapless and renormalized. We then make use of the gaplessness and write the kinetic equations in terms of Bogoliubov quasiparticles, which are orthogonal to the condensate by construction. The results in Chap. 4 show that the complicated collision terms presented in the Walser et al. papers can be simplified dramatically by a basis transformation. Practical calculations of the quantum Boltzmann equation then require only diagonal elements of the quasiparticle population matrix.

3.2 Single-Particle Kinetic Equations

We present the Walser et al. formulation of kinetic theory [40], which was originally derived using a statistical operator approach [37]. In Chap. 2, we derived the kinetic theory from the Kadanoff–Baym [43, 44] theory of non-equilibrium Green functions. We used the gapless second-order Beliaev approximation [53, 83] and showed equivalence to the work of Walser et al. under the Markov approximation. Further, another independent derivation [84, 85] connects this approach to kinetic theories by Morgan and Proukakis. Rey et al. [86, 87, 88] use an effective-action formalism for calculations in optical lattices that also includes Beliaev effects and reduces to the Kadanoff–Baym equations in the two-time limit.

Neglecting three-body and higher interactions, we can describe the weakly interacting, dilute gas by the following Hamiltonian

$$H = {H^{(0)}}^{1'2'} a^\dagger_{1'} a_{2'} + \phi^{1'2'3'4'} a^\dagger_{1'} a^\dagger_{2'} a_{3'} a_{4'}, \tag{3.1}$$

where ${H^{(0)}}^{1'2'} = \langle 1'| H^{(0)} |2'\rangle$ denotes the matrix elements of the interaction-free single-particle Hamiltonian

$$H^{(0)} = \frac{\boldsymbol{p}^2}{2m} + V_{\text{ext}}(\boldsymbol{x}) \tag{3.2}$$

with external harmonic potential V_{ext}. The bosonic creation operator $a^\dagger_{1'}$ creates a particle in the state $|1'\rangle$, where $1'$ stands for a complete set of quantum numbers, which label a constant, single-particle energy basis, such as, for example, harmonic oscillator states or eigen states of

the GP equation. We use the summation convention for these abbreviated indices and indicate the single-particle basis with primes.

The two-particle matrix elements of the binary interaction potential $V_{\mathrm{bin}}(\boldsymbol{x}_1, \boldsymbol{x}_2)$ are defined by

$$\begin{aligned}\phi^{1'2'3'4'} = \frac{1}{4} \int d\boldsymbol{x}_1 \, d\boldsymbol{x}_2 \, \langle 1' \,|\, \boldsymbol{x}_1 \rangle \langle 2' \,|\, \boldsymbol{x}_2 \rangle V_{\mathrm{bin}}\big(|\boldsymbol{x}_1 - \boldsymbol{x}_2|\big) \\ \times \Big\{ \langle \boldsymbol{x}_1 \,|\, 3' \rangle \langle \boldsymbol{x}_2 \,|\, 4' \rangle + \langle \boldsymbol{x}_1 \,|\, 4' \rangle \langle \boldsymbol{x}_2 \,|\, 3' \rangle \Big\}. \end{aligned} \tag{3.3}$$

These matrix elements are symmetric in the first and last two indices:

$$\phi^{1'2'3'4'} = \phi^{2'1'3'4'} = \phi^{1'2'4'3'}. \tag{3.4}$$

To determine the measurable quantities we want to calculate in this theory, we first define the condensate mean field α as the expectation value of the destruction operator

$$\alpha = \alpha_{1'} \, |1'\rangle = \langle a_{1'} \rangle \, |1'\rangle \, . \tag{3.5}$$

The total density matrix f is defined by

$$f = \langle a^\dagger_{2'} a_{1'} \rangle \, |1'\rangle \otimes \langle 2'| \, . \tag{3.6}$$

Subtracting the condensate density matrix

$$f^c = \alpha \otimes \alpha^* = \alpha^*_{2'} \alpha_{1'} \, |1'\rangle \otimes \langle 2'| \, , \tag{3.7}$$

we obtain the density matrix of thermal atoms $\tilde{f} = f - f^c$. The anomalous average m is split analogously

$$m = \langle a_{1'} a_{2'} \rangle \, |1'\rangle \otimes |2'\rangle = m^c + \tilde{m}, \tag{3.8}$$

in the condensate part $m^c = \alpha \otimes \alpha$ and fluctuations $\tilde{m}$.

This set of variables contains all possible combinations of up to two field operators. The reference distribution parameterized by these variables is thus Gaussian, and we can use Wick's theorem [36] to truncate the coupling to higher-order correlation functions, that is, expectation values of more than two field operators. This approximation is valid because of the diluteness

of the condensed gas. In a dilute gas the duration of a collision event is short compared to the essentially free evolution between collisions, which allows higher-order correlations to dampen. The full coarse-grained density operator includes higher-order non-Gaussian corrections, which give rise to collisional redistributions of populations.

The procedure followed by Walser et al. [37] is then to write the Heisenberg equations of motion for the variables above and expand the expectation values using Wick's theorem. Walser et al. thus obtain the equations of motion given in the following two Sections [40].

3.2.1 Mean-Field Equations

Since the anomalous fluctuations $\tilde{m}$ couple the mean field α to its conjugate $\alpha^* = \alpha^*_{1'} \langle 1'|$, it is convenient to write the generalized Gross–Pitaevskii (GP) equation in a two-by-two matrix form

$$\frac{\mathrm{d}}{\mathrm{d}t}\chi = (-i\Pi + \Upsilon^{<} - \Upsilon^{>})\chi, \tag{3.9}$$

where the two-component state vector

$$\chi = \begin{pmatrix} \alpha \\ \alpha^* \end{pmatrix} \tag{3.10}$$

is defined in terms of $\alpha = \alpha_{1'} |1'\rangle$ and also contains the conjugate mean field α^*.

The generalized GP operator representing the reversible evolution of χ is defined as

$$\Pi = \begin{pmatrix} \Pi_{\mathcal{N}} & \Pi_{\mathcal{A}} \\ -\Pi^*_{\mathcal{A}} & -\Pi^*_{\mathcal{N}} \end{pmatrix}. \tag{3.11}$$

This symplectic operator consists of the Hermitian Hamiltonian

$$\Pi_{\mathcal{N}} = H^{(0)} + U_{f^c} + 2U_{\tilde{f}} - \mu, \tag{3.12}$$

where μ removes rapid oscillations of the mean field, and the symmetric anomalous coupling

$$\Pi_{\mathcal{A}} = V_{\tilde{m}}. \tag{3.13}$$

The energy shifts due to both the mean field and the normal fluctuations are given by the matrices

$$U_f = 2\,\phi^{1'2'3'4'} f_{3'2'}\,|1'\rangle \otimes \langle 4'|\,, \tag{3.14}$$

whereas the first-order anomalous coupling-strength is given by

$$V_m = 2\,\phi^{1'2'3'4'} m_{3'4'}\,|1'\rangle \otimes |2'\rangle\,. \tag{3.15}$$

The second-order irreversible evolution, consisting of damping rates and energy shifts, is given by the collision operator

$$\Upsilon^{<} = \begin{pmatrix} \Upsilon^{<}_{\mathcal{N}} & \Upsilon^{<}_{\mathcal{A}} \\ -\Upsilon^{>*}_{\mathcal{A}} & -\Upsilon^{>*}_{\mathcal{N}} \end{pmatrix} \tag{3.16}$$

and its time-reversed counterpart $\Upsilon^{>} = -\sigma_1 \Upsilon^{<*} \sigma_1$, where σ_1 is the first Pauli matrix exchanging the positive- and negative-energy components of vectors. The matrix elements of the collision operator are given by the in-rates

$$\Upsilon^{<}_{\mathcal{N}} = \Gamma_{\tilde{f}\tilde{f}(1+\tilde{f})} + 2\Gamma_{\tilde{f}\tilde{m}\tilde{m}^*}, \tag{3.17a}$$

$$\Upsilon^{<}_{\mathcal{A}} = \Gamma_{\tilde{m}\tilde{m}\tilde{m}^*} + 2\Gamma_{\tilde{f}\tilde{m}(1+\tilde{f})}, \tag{3.17b}$$

and the out-rates

$$\Upsilon^{>}_{\mathcal{N}} = \Gamma_{(1+\tilde{f})(1+\tilde{f})\tilde{f}} + 2\Gamma_{(1+\tilde{f})\tilde{m}\tilde{m}^*}, \tag{3.17c}$$

$$\Upsilon^{>}_{\mathcal{A}} = \Gamma_{\tilde{m}\tilde{m}\tilde{m}^*} + 2\Gamma_{(1+\tilde{f})\tilde{m}\tilde{f}}, \tag{3.17d}$$

which are defined in terms of individual collisions Γ. These elementary collision processes are defined explicitly as

$$\Gamma_{fff} = 8\phi^{1'2'3'4'}\,\phi_\eta^{1''2''3''4''}\,f_{3'1''}f_{4'2''}f_{4''2'}\,|1'\rangle \otimes \langle 3''|\,, \tag{3.18a}$$

$$\Gamma_{fmf} = 8\phi^{1'2'3'4'}\,\phi_\eta^{1''2''3''4''}\,f_{3'2''}m_{4'3''}f_{4''2'}\,|1'\rangle \otimes |1''\rangle\,, \tag{3.18b}$$

$$\Gamma_{fmm^*} = 8\phi^{1'2'3'4'}\,\phi_\eta^{1''2''3''4''}\,f_{3'1''}m_{4'4''}m^*_{2''2'}\,|1'\rangle \otimes \langle 3''|\,, \tag{3.18c}$$

$$\Gamma_{mmm^*} = 8\phi^{1'2'3'4'}\,\phi_\eta^{1''2''3''4''}\,m_{3'4''}m_{4'3''}m^*_{2''2'}\,|1'\rangle \otimes |1''\rangle\,. \tag{3.18d}$$

The in-rates of the collision operator Υ are depicted in Fig. 3.1.

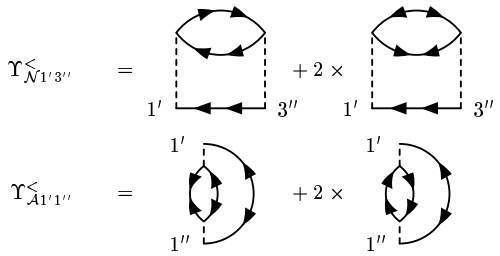

Figure 3.1: These diagrams depict the second-order terms $\Upsilon^<$ in the GP equation (3.9). The dashed potential lines correspond to the symmetrized binary potential ϕ in the single-particle energy basis. The directed propagators represent the normal density $\tilde{f}$, the remaining ones the anomalous average $\tilde{m}$ and its conjugate. Note that all diagrams are topologically equivalent, and only propagators are exchanged.

In this theory, collisional interactions are considered to second order. The effect of higher order terms, which lead to a finite duration of a collision, can be modeled by introducing a parameter η, such that every second-order collision operator contains dispersive as well as dissipative parts from the complex-valued matrix element

$$\phi_\eta^{1''2''3''4''} = \phi^{1''2''3''4''} \frac{1}{\eta - i\Delta\epsilon}, \tag{3.19}$$

where the energy difference $\Delta\epsilon$ has to be smaller than the energy uncertainty η to get a sizable contribution. The energy difference $\Delta\epsilon = -(\epsilon^0_{1''} + \epsilon^0_{2''}) + \epsilon^0_{3''} + \epsilon^0_{4''}$ is defined in terms of the single-particles eigen energies $H^{(0)} \left|\epsilon^0_{1'}\right\rangle = \epsilon^0_{1'} \left|\epsilon^0_{1'}\right\rangle$. Note that the papers [37, 40] contain a sign error in the definition of $\Delta\epsilon$. For small η we obtain

$$\frac{1}{\eta - i\Delta\epsilon} \quad \underset{\eta\to 0}{\longrightarrow} \quad \pi\delta_\eta(\Delta\epsilon) + i\mathcal{P}_\eta \frac{1}{\Delta\epsilon}, \tag{3.20}$$

where $\mathcal{P}$ indicates that the Cauchy principal value has to be taken upon integration. The parameter η thus represents off-the-energy-shell propagation after a collision. Most off-the-energy-shell coherences decay during subsequent propagation, but, due to the finite time between collisions $\Delta\tau$, energy cannot be conserved exactly, because η has to be larger than the collision rate $1/\Delta\tau$.

3.2.2 Equations for Normal Densities and Anomalous Fluctuations

The equations of motion for the fluctuation densities $\tilde{f}$ and $\tilde{m}$ are coupled and can also conveniently be written in terms of two-by-two matrices. To achieve this, we define the generalized single-time fluctuation-density matrix $\tilde{G}^<$ as

$$\tilde{G}^< = \begin{pmatrix} \tilde{f} & \tilde{m} \\ \tilde{m}^* & (1+\tilde{f})^* \end{pmatrix}, \tag{3.21}$$

where $\tilde{f} = \tilde{f}_{1'2'} \, |1'\rangle \otimes \langle 2'|$ and $\tilde{m} = \tilde{m}_{1'2'} \, |1'\rangle \otimes |2'\rangle$ are the matrix representations of the master variables. In Ref. [39], we use the property that this density matrix is the single-time limit of the corresponding time-ordered two-time Green's function. This showed that the other time ordering is given by

$$\tilde{G}^> = \begin{pmatrix} (1+\tilde{f}) & \tilde{m} \\ \tilde{m}^* & \tilde{f}^* \end{pmatrix} = \sigma_1 \tilde{G}^{<*} \sigma_1 = \sigma_3 + \tilde{G}^<. \tag{3.22}$$

Here, we use the third Pauli matrix $\sigma_3 = \mathrm{diag}(\mathbb{1}, -\mathbb{1})$. Note that our naming of the fluctuation-density matrices $\tilde{G}^<$ and $\tilde{G}^>$ is consistent with the two-time formalism in Ref. [39], but differs from Ref. [40].

The generalized Boltzmann equation of motion for this fluctuation-density matrix can be written as

$$\frac{\mathrm{d}}{\mathrm{d}t}\tilde{G}^< = -i\Sigma\tilde{G}^< + \Gamma^<\tilde{G}^> - \Gamma^>\tilde{G}^< + \mathrm{H.c.} \tag{3.23}$$

This equation has to be solved under the constraints

$$\alpha^*\tilde{f} = 0 \quad \text{and} \quad \alpha^*\tilde{m} = 0, \tag{3.24}$$

which force the fluctuations to be orthogonal to the condensate.

Again, the equation of motion (3.23) has two parts: The reversible evolution is governed by the Hartree–Fock–Bogoliubov self-energy operator

$$\Sigma = \begin{pmatrix} \Sigma_{\mathcal{N}} & \Sigma_{\mathcal{A}} \\ -\Sigma_{\mathcal{A}}^* & -\Sigma_{\mathcal{N}}^* \end{pmatrix}, \tag{3.25}$$

which in turn consists of the Hermitian Hamiltonian

$$\Sigma_{\mathcal{N}} = H^{(0)} + 2U_{f^c} + 2U_{\tilde{f}} - \mu \tag{3.26}$$

and the symmetric anomalous coupling

$$\Sigma_{\mathcal{A}} = V_{m^c} + V_{\tilde{m}}. \tag{3.27}$$

The irreversible evolution introduced by second-order collisional contributions now consists of the collisional operator

$$\Gamma^{<} = \begin{pmatrix} \Gamma^{<}_{\mathcal{N}} & \Gamma^{<}_{\mathcal{A}} \\ -\Gamma^{>*}_{\mathcal{A}} & -\Gamma^{>*}_{\mathcal{N}} \end{pmatrix}, \tag{3.28}$$

and its time-reversed counterpart $\Gamma^{>} = -\sigma_1 \Gamma^{<*} \sigma_1$. The diagonal components of the collision operator are defined as

$$\begin{aligned} \Gamma^{<}_{\mathcal{N}} &= \Gamma_{(\tilde{f}+f^c)\tilde{f}(1+\tilde{f})} + \Gamma_{\tilde{f}f^c(1+\tilde{f})} + \Gamma_{\tilde{f}\tilde{f}f^c} \\ &\quad +2\big\{\Gamma_{(\tilde{f}+f^c)\tilde{m}\tilde{m}^*} + \Gamma_{\tilde{f}m^c\tilde{m}^*} + \Gamma_{\tilde{f}\tilde{m}m^{c*}}\big\}, \end{aligned} \tag{3.29}$$

$$\begin{aligned} \Gamma^{>}_{\mathcal{N}} &= \Gamma_{(1+\tilde{f}+f^c)(1+\tilde{f})\tilde{f}} + \Gamma_{(1+\tilde{f})f^c\tilde{f}} + \Gamma_{(1+\tilde{f})(1+\tilde{f})f^c} \\ &\quad +2\big\{\Gamma_{(1+\tilde{f}+f^c)\tilde{m}\tilde{m}^*} + \Gamma_{(1+\tilde{f})m^c\tilde{m}^*} + \Gamma_{(1+\tilde{f})\tilde{m}m^{c*}}\big\}, \end{aligned} \tag{3.30}$$

and the off-diagonal, anomalous components as

$$\begin{aligned} \Gamma^{<}_{\mathcal{A}} &= \Gamma_{(\tilde{m}+m^c)\tilde{m}\tilde{m}^*} + \Gamma_{\tilde{m}m^c\tilde{m}^*} + \Gamma_{\tilde{m}\tilde{m}m^{c*}} \\ &\quad +2\big\{\Gamma_{(\tilde{f}+f^c)\tilde{m}(1+\tilde{f})} + \Gamma_{\tilde{f}m^c(1+\tilde{f})} + \Gamma_{\tilde{f}\tilde{m}f^c}\big\}, \end{aligned} \tag{3.31}$$

$$\begin{aligned} \Gamma^{>}_{\mathcal{A}} &= \Gamma_{(\tilde{m}+m^c)\tilde{m}\tilde{m}^*} + \Gamma_{\tilde{m}m^c\tilde{m}^*} + \Gamma_{\tilde{m}\tilde{m}m^{c*}} \\ &\quad +2\big\{\Gamma_{(1+\tilde{f}+f^c)\tilde{m}\tilde{f}} + \Gamma_{(1+\tilde{f})m^c\tilde{f}} + \Gamma_{(1+\tilde{f})\tilde{m}f^c}\big\}. \end{aligned} \tag{3.32}$$

Both the diagonal and off-diagonal incoming rates are depicted diagrammatically in Fig. 3.2. For every term that appears in the collisional terms of the generalized GP equation in $\Upsilon^{<}$ [Fig. (3.1)], we here [Fig. (3.2)] have three additional terms, where in each of them,

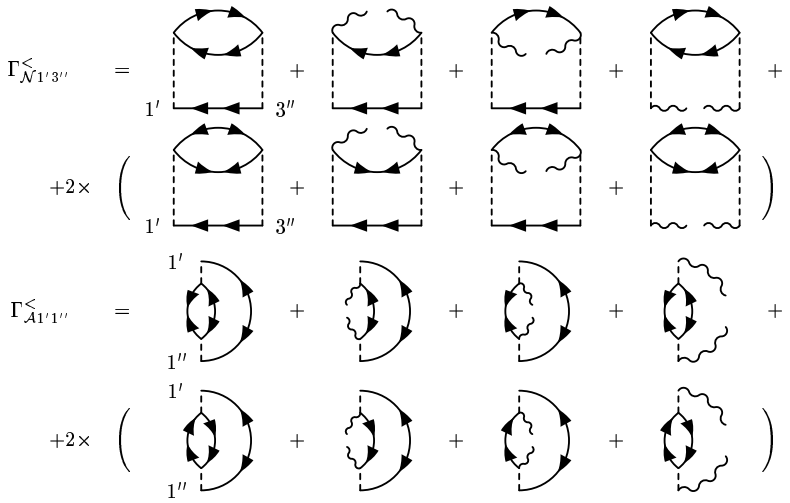

Figure 3.2: These diagrams correspond to the second-order terms $\Gamma^{<}$ in the generalized Boltzmann equation (3.23). The dashed lines depict the symmetrized binary potential ϕ in the single-particle energy basis. The directed propagators represent the normal density $\tilde{f}$, the remaining ones the anomalous average $\tilde{m}$ and its conjugate. The first column of diagrams is identical to those depicted in Fig. 3.1. The remaining diagrams each have one of the three propagators replaced with an open condensate line.

one of the three fluctuating contributions is replaced with the corresponding mean-field quantity. This replacement rule can be seen in the Beliaev collisional self energies presented in Ref. [39] and is a consequence of the fact that the Boltzmann equation (3.23) can be generated from the GP equation (3.9) by functional differentiation [45].

When the collision operator $\Gamma^{<}$ is multiplied by $\tilde{G}^{>}$ as in Eq. (3.23), we get terms like

$$\Gamma_{\tilde{f}\tilde{f}(1+\tilde{f})}(1+\tilde{f}) - \Gamma_{(1+\tilde{f})(1+\tilde{f})\tilde{f}}\tilde{f}, \tag{3.33}$$

where the second part comes from the time-reversed contribution $\Gamma^{>}\tilde{G}^{<}$. The diagonal parts are exactly the in and out terms of the quantum Boltzmann equation for the single-particle distribution function $\tilde{f}$. The remaining second-order contributions couple to the anomalous fluctuations $\tilde{m}$ and do not have an analogue in the quantum Boltzmann equation. In Chap. 4, we rewrite the kinetic equations presented here in terms of Bogoliubov quasiparticles. Then all collisional contributions take the form of Boltzmann terms.

3.3 Gaplessness—T Matrices

Our goal in this Section is to explicitly show that the kinetic equations (3.23) and (3.9) are gapless. This should on one hand be obvious, because the previous Chapter showed them to be equivalent to the Kadanoff–Baym equations [43, 44] in the gapless Beliaev approximation [53, 54]. The first-order HFB self energy Σ, which appears in the kinetic equations, is, on the other hand, known to exhibit a non-physical energy gap in the long-wavelength, homogeneous limit [57].

We resolve this discrepancy by including second-order collisional energy shifts $\mathcal{P}\{\Gamma\}$ into the HFB operator and adiabatically eliminating the anomalous average $\tilde{m}$ in the first-order anomalous potential $V_{\tilde{m}}$ (3.15). This upgrades the bare interaction potentials in the first-order operators Σ and Π to the real parts of many-body T matrices. We then have a systematic way to approximate the many-body T matrices by two-body T matrices, whose low-energy limit is the s-wave scattering length. We can thus find a contact-scattering model without incurring ultra-violet divergences.

The upgraded HFB self energy Σ, where all binary interactions are written as many-body T matrices, is explicitly gapless and thus obeys the Hugenholtz-Pines theorem [89]. The self energy thus has zero-energy modes, which are completely specified by the value of the condensate α. If we use the non-zero energy Bogoliubov modes of Σ as a basis for the thermal excitations, the excitations will automatically be orthogonal to the condensate. We follow this idea in Chap. 4.

3.4 Off-Diagonal Potentials

Here, we update the off-diagonal potentials $V_{(m^c+\tilde{m})}$ in the HFB self energy Σ by adiabatically eliminating the pairing field $\tilde{m}$. We integrate the first-order equation of motion for the anomalous average $\tilde{m}$

$$\frac{\mathrm{d}}{\mathrm{d}t}\tilde{m} = -i\Sigma_{\mathcal{N}}\tilde{m} - i\tilde{m}\Sigma_{\mathcal{N}} - i\Sigma_{\mathcal{A}}(1+\tilde{f})^* - i\tilde{f}\Sigma_{\mathcal{A}}, \tag{3.34}$$

which is obtained by taking the $\tilde{m}$ component of the generalized Boltzmann equation (3.23) and dropping the second-order terms, because we want to substitute the result for $\tilde{m}$ into the anomalous potential $V_{\tilde{m}}$ and only keep terms up to second order. In stationarity, that is, for vanishing time derivatives, we solve for $\tilde{m}$ in the dressed eigen basis of $\Sigma_{\mathcal{N}}$,

$$\Sigma_{\mathcal{N}} \left|\epsilon_{1'}\right\rangle = (\epsilon_{1'} - \mu) \left|\epsilon_{1'}\right\rangle, \tag{3.35}$$

and obtain

$$\tilde{m}_{1'2'} = \mathcal{P}\frac{\Sigma_{\mathcal{A}}^{1'2''}(1+\tilde{f})_{2'2''} + \tilde{f}_{1'2''}\Sigma_{\mathcal{A}}^{2''2'}}{2\mu - (\epsilon_{1'} + \epsilon_{2'})} \tag{3.36}$$

as an adiabatic solution. Adiabatic here means that this solution only includes time-variations with characteristic times long compared to the duration of a collision. We use the Cauchy principal value $\mathcal{P}$ to indicate omission of the divergent term in an energy integral or sum. This divergent δ-function term gives rise to the imaginary part. We insert this result into the off-diagonal potential (3.15),

$$V_{\tilde{m}}^{1'2'} = 4\mathcal{P}\frac{\phi^{1'2'3''4''}(1+2\tilde{f})_{4''2''}\phi^{3''2''3'4'}}{2\mu - (\epsilon_{3''} + \epsilon_{4''})} m^{c}_{3'4'}, \tag{3.37}$$

where we dropped the recursive $V_{\tilde{m}}$ term in the anomalous coupling $\Sigma_{\mathcal{A}}$ in order to keep Eq. (3.37) at second order. We discuss the recursive term in Sec. 3.7.

We then recognize that we can write the off-diagonal element of the HFB operator $\Sigma_{\mathcal{A}}$ as the real part of a many-body T matrix

$$\Sigma_{\mathcal{A}} \quad = \quad V_{m^c} + V_{\tilde{m}} = T_{m^c}(2\mu), \tag{3.38}$$

which is defined by

$$T^{1'2'3'4'}(\epsilon) = 2\phi^{1'2'3'4'} + 4\mathcal{P}\frac{\phi^{1'2'3''4''}(1+2\tilde{f})_{4''2''}\phi^{3''2''3'4'}}{\epsilon - (\epsilon_{3''} + \epsilon_{4''})}. \tag{3.39}$$

The energies $\epsilon_{1'}$ are dressed by the normal and mean-field shifts, but are not the full quasiparticle energies, because they do not include the effect of the pairing field, which comes in at higher order. Contractions of this T matrix with anomalous averages are defined by

$$T_m^{1'2'}(\epsilon) = T^{1'2'3'4'}(\epsilon) m_{3'4'}. \tag{3.40}$$

The T matrix defined in Eq. (3.39) is a function of energy through its last two indices in the sense that its argument $\epsilon = \epsilon_{3'} + \epsilon_{4'}$.

3.5 Diagonal Potentials

In this Section, we want to redefine the diagonal potentials U_{f^c} and $U_{\tilde{f}}$ as the real parts of T matrices by using the second-order energy shifts $\mathcal{P}\{\Gamma\}$. With $\mathcal{P}\{\Gamma\}$ we here denote the principal-value part of the collisional terms in Eqs. (3.28) and (3.16) according to Eq. (3.20). We begin by considering the condensate potential.

$$\begin{aligned} &-i\,2U_{f^c} + \mathcal{P}\big\{2\Gamma_{f^c\tilde{f}(1+\tilde{f})} + \Gamma_{\tilde{f}\tilde{f}f^c} \\ &\qquad\qquad -2\Gamma_{f^c(1+\tilde{f})\tilde{f}} - \Gamma_{(1+\tilde{f})(1+\tilde{f})f^c}\big\} \\ &= -i\,2U_{f^c} - \mathcal{P}\{\Gamma_{1(1+2\tilde{f})f^c}\} \end{aligned} \tag{3.41}$$

We here assume real eigen functions for the single-particle energy basis and do not include any Γ terms involving the anomalous average $\tilde{m}$, because they are at least of order $V_{\rm bin}^3/(\Delta\epsilon)^2$ according to Eq. (3.36). The second-order terms that contain only normal fluctuations $\tilde{f}$ are used in Eq. (3.46) to rewrite the fluctuation potential $U_{\tilde{f}}$. The term in Eq. (3.41) can again be written in terms of a many-body T matrix

$$U_{f^c} + \frac{1}{2i}\mathcal{P}\{\Gamma_{1(1+2\tilde{f})f^c}\} = T_{f^c}, \tag{3.42}$$

which is given by

$$T^{1'2'3'4'}(\epsilon) = 2\phi^{1'2'3'4'} + 4\mathcal{P}\frac{\phi^{1'2'3''4''}(1+2\tilde{f})_{4''2''}\phi^{3''2''3'4'}}{\epsilon - (\epsilon_{3''} + \epsilon_{2''})}. \tag{3.43}$$

The slight difference compared to Eq. (3.39) is resolved when we assume diagonal quasiparticle populations $P_{\bar{1}\bar{2}} = P_{\bar{1}}\delta_{\bar{1}\bar{1}}$ as will be justified in Chap. 4:

$$\tilde{f}_{1'2'} = U_{1'}^{\bar{1}} P_{\bar{1}} U_{2'}^{\bar{1}*} = \tilde{f}_{2'1'}, \tag{3.44}$$

where U is the transformation matrix to the quasiparticle basis. Alternatively, we note that the T matrix is essentially constant for energy differences up to the duration of a collision.

Contractions of the T matrix with normal averages are performed according to

$$T_f^{1'4'} = T^{1'2'3'4'}(\epsilon_{3'} + \epsilon_{4'})f_{3'2'}. \tag{3.45}$$

We now consider the fluctuation potential $U_{\tilde{f}}$, again include only the truly second-order energy shifts, and obtain

$$\begin{aligned} &-i\,2U_{\tilde{f}} + \mathcal{P}\{\Gamma_{\tilde{f}\tilde{f}(1+\tilde{f})} - \Gamma_{(1+\tilde{f})(1+\tilde{f})\tilde{f}}\} \\ &= -i\,2U_{\tilde{f}} - \mathcal{P}\{\Gamma_{1(1+\tilde{f})\tilde{f}}\} = -i\,2T'_{\tilde{f}}, \end{aligned} \tag{3.46}$$

where we get a different T matrix defined by

$$T'^{1'2'3'4'}(\epsilon) = 2\phi^{1'2'3'4'} + 4\mathcal{P}\frac{\phi^{1'2'3''4''}(1+\tilde{f})_{4''2''}\phi^{3''2''3'4'}}{\epsilon - (\epsilon_{3''} + \epsilon_{2''})}, \tag{3.47}$$

which does not have a factor of 2 in the intermediate-population term $(1 + \tilde{f})$. This difference is due to the fact that the mean field α is not bosonically enhanced. If we assume diagonal population $\tilde{f}_{1'2'} = \delta_{1'2'}\tilde{f}_{1'1'}$, which is not a good approximation in this basis, we reproduce the results of Ref. [90] for the GP equation to second order in the interaction potential. In particular, the factor of 2 in their many-body T matrix in the term corresponding to Eq. (3.46) gets canceled with a negative term from adiabatically eliminating their triple average.

3.6 Renormalized Self Energies

Using the T matrices defined in the previous Sections, we can now rewrite the generalized GP operator Π given in Eq. (3.11) and the generalized Boltzmann operator Σ given in Eq. (3.25).

The Hamiltonian of the GP equation is now

$$\Pi'_{\mathcal{N}} = H^{(0)} + T_{f^c} + 2T'_{\tilde{f}} - \mu, \tag{3.48}$$

and the anomalous coupling $\Pi'_{\mathcal{A}}$ vanishes, because of the identity

$$V_{\tilde{m}}\alpha^* = \{T_{m^c}(2\mu) - V_{m^c}\}\,\alpha^* = \{T_{f^c}(2\mu) - U_{f^c}\}\,\alpha. \tag{3.49}$$

This means that the coupling between α and α^* vanishes and they are no longer independent quantities, and that we can without loss of generality treat α as real.

When we write the Boltzmann operator in terms of T matrices, we can explicitly show that the energy spectrum is gapless; this theory thus fulfills the Hugenholtz-Pines theorem [89]. The diagonal part of the operator Σ is now

$$\Sigma'_{\mathcal{N}} = H^{(0)} + 2T_{f^c} + 2T'_{\tilde{f}} - \mu, \tag{3.50}$$

and the anomalous coupling is

$$\Sigma'_{\mathcal{A}} = T_{m^c}(2\mu). \tag{3.51}$$

We now show that this renormalized Boltzmann operator Σ' has a zero-energy eigen vector, that is, its spectrum is gapless. We begin by writing the generalized GP equation for the condensate ground state

$$\left\{H^{(0)} + T_{f^c}(2\mu) + 2T'_{\tilde{f}}(2\mu)\right\}\alpha = \mu\alpha. \tag{3.52}$$

This equation can be written in terms of the renormalized GP Hamiltonian (3.48) as $\Pi_{\mathcal{N}}\alpha = 0$, where the energies are now measured relative to the adiabatic chemical potential μ. An immediate consequence of Eq. (3.52) is that the quasiparticle ground state

$$P_\alpha = \frac{1}{\sqrt{2N_c}}\begin{pmatrix} \alpha \\ \\ -\alpha^* \end{pmatrix}, \tag{3.53}$$

is a zero-energy eigen vector of the renormalized Σ', because of the identity

$$T_{m^c}(2\mu)\alpha^* = T_{f^c}(2\mu)\alpha. \tag{3.54}$$

The ground state P_α is normalized by the number of condensate atoms

$$N_c = \alpha^\dagger\alpha, \tag{3.55}$$

as we find in Sec. 4.1.

These zero-energy eigen vectors of the HFB operator are proportional to the condensate mean field α. All non-zero-energy eigen vectors $W_{E_{\bar{1}}\neq 0}$ of Σ are thus automatically orthogonal to the condensate, and we can use the complete set $\{\alpha, W_{E_{\bar{1}}\neq 0}\}$ as a basis to describe the

condensate interacting with thermal excitations [91]. Other approaches to finite-temperature theories [72, 77] have to explicitly orthogonalize their bases using projection operators. We discuss this new basis in Chap. 4.

3.7 Ladder Approximation

We can extend the second-order T matrices introduced in the previous Sections to include ladder diagrams to all orders by using consistency arguments. We first note that by keeping the recursive $V_{\tilde{m}}$ term on the right side of Eq. (3.37), we can extend our definition of the off-diagonal T matrix to

$$T^{1'2'3'4'}(\epsilon) = 2\phi^{1'2'3'4'} + 4\mathcal{P}\frac{\phi^{1'2'3''4''}(1+2\tilde{f})_{4''2''}T^{3''2''3'4'}(\epsilon)}{\epsilon - (\epsilon_{3''}+\epsilon_{4''})}. \tag{3.56}$$

This is the real part of the many-body T matrix in the ladder approximation.

In the previous Section, we showed that the HFB operator Σ is gapless with the T matrices defined to second order. If we used the ladder T in Eq. (3.56) on the off-diagonal while keeping the second-order T in Eq. (3.43) in the diagonal, we would find an energy gap of third order, because the cancellation in Eq. (3.54) only works if the two Ts are identical. However, the Hugenholtz-Pines theorem tells us that the full theory should again be gapless. We thus conclude that we have to upgrade the T matrix on the diagonal of Σ to the ladder approximation as well.

We would like to finish our discussion of the scattering matrices in terms of the single-particle energy basis with two remarks. First, as the Liouville-space formulation [92] of density-matrix evolution shows, the scattering should really be formulated in terms of Liouville-space scattering $\mathcal{T}$ matrices [93], which can be expressed in terms of Hilbert-space T matrices as

$$\mathcal{T} = T \otimes \mathbb{1} + \mathbb{1} \otimes T^\dagger + T \otimes T^\dagger. \tag{3.57}$$

Since we only consider Hilbert-space T matrices, we thus would miss higher-order terms of the type $T \otimes T^\dagger$, even if we included the full many-body Hilbert-space scattering matrix. The imaginary part of $\mathcal{T}$ gives rise to the inelastic rates in the kinetic equations in Chap. 4.

Second, since the asymptotic states in this scattering problem are typically trapped harmonic-oscillator states for dilute, trapped atomic gases, we are strictly speaking dealing with bound-state R matrices [94] instead of T matrices.

Chapter 4

Quasiparticle Kinetic Equations [59]

4.1 Quasiparticle Basis

We now want to write the kinetic equations (3.23) in the Bogoliubov quasiparticle basis. In this basis, the complicated and non-linear evolution due to the HFB self energy Σ' is replaced with a simple commutator with the eigen energies and a slow basis rotation. As this theory is gapless, the $E \neq 0$ quasiparticle states together with the condensate α form an orthogonal basis, that is, the thermal fluctuations are by definition orthogonal to the condensate. Another motivation for transforming to a diagonal first-order Hamiltonian is that the reversible first-order evolution leaves the quasiparticle populations constant. Thus, in the quasiparticle basis, only the second-order collisional terms change the populations. A more detailed account of the transformation to the quasiparticle basis can be found in Appendix B.

Since the quasiparticles consist of the eigen vectors of the self-energy operator Σ', we consider the operator's $2n$ by $2n$ (n is the number of single-particle states considered) eigen-vector matrix W defined by

$$\Sigma' W = W E \tag{4.1}$$

at each time with the diagonal quasiparticle eigen-energy matrix E, which is labeled with the quasiparticle indices $\bar{1} = E_{\bar{1}}$. The eigen-value equations (4.1) are the Bogoliubov-de-Gennes equations. We decompose their solution W into two n by $2n$ matrices U and V^*,

$$W = \begin{pmatrix} U \\ \\ V^* \end{pmatrix} = \begin{pmatrix} u_+ & u_- \\ \\ v_+^* & v_-^* \end{pmatrix}, \tag{4.2}$$

which are in turn split into n by n matrices for positive (u_+, v_+^*) and negative quasiparticle energies (u_-, v_-^*). These quasiparticle eigen energies $\bar{1}$ are the column indices and the original single-particle energies $1'$ the row indices.

Since the operator $\sigma_3\Sigma'$ is positive semi-definite, the eigen values E in Eq. (4.1) are real and come in positive and negative pairs of equal magnitude [95]. We demonstrated in the previous Section that there exists a zero-energy eigen vector P_α defined in Eq. (3.53). This means that the operator Σ' is defective and has two zero-energy eigen values. The eigen-value equation (4.1), however, does not yield the second linearly independent zero-energy eigen vector. Instead, the associated vector Q_α is given by [95]

$$\Sigma' Q_\alpha = -i\frac{P_\alpha}{M}, \tag{4.3}$$

with a positive constant M. In our case, we find

$$Q_\alpha = -i\frac{1}{\sqrt{2N_c}}\begin{pmatrix}\alpha\\ \\ \alpha^*\end{pmatrix}. \tag{4.4}$$

In order to find a complete set of basis states, we now define the quadrature components of P_α and Q_α:

$$W^{+0} = \frac{1}{\sqrt{2}}(P_\alpha + iQ_\alpha) = \frac{1}{\sqrt{N_c}}\begin{pmatrix}\alpha\\ \\ 0\end{pmatrix}, \tag{4.5a}$$

$$W^{-0} = -\frac{1}{\sqrt{2}}(P_\alpha - iQ_\alpha) = \frac{1}{\sqrt{N_c}}\begin{pmatrix}0\\ \\ \alpha^*\end{pmatrix}. \tag{4.5b}$$

These linearly independent and normalizable vectors are not zero-energy eigen vectors, but they span the space corresponding to $E = 0$. If we now substitute these two states W^{+0} and W^{-0} into the zero-energy columns of W, we can normalize all eigen vectors using the symplectic norm

$$W^\dagger \sigma_3 W = \sigma_3. \tag{4.6}$$

The negative-energy states thus have negative norm, and the positive-energy states positive norm. In particular, the zero-energy vector W^{+0} has positive norm and thus belongs to the positive-energy part of W.

The completeness relation for the quasiparticle basis also has symplectic structure

$$W\sigma_3 W^\dagger \sigma_3 = \mathbb{1}_{2n}, \tag{4.7}$$

where $\mathbb{1}_{2n}$ indicates the $2n$-dimensional unit-matrix. The symplectic structure of the orthonormalization and completeness relations Eqs. (4.6) and (4.7), that is, the appearance of the matrix σ_3 in these expressions, guarantees that the transformation to the quasiparticle basis is canonical [95]. Canonical here means that the new quasiparticle operators obey the boson commutation relations.

To further examine the structure of the quasiparticle states W, we consider the following symmetry of the HFB operator Σ'

$$\Sigma' = -\sigma_1 \Sigma'^* \sigma_1, \tag{4.8}$$

which holds according to its definition in Eq. (3.25). This symmetry implies [40, IV.B.] the following relation for the quasiparticle states W:

$$W = \begin{pmatrix} u_+ & u_- \\ v_+^* & v_-^* \end{pmatrix} = \begin{pmatrix} u_+ & v_+ \\ v_+^* & u_+^* \end{pmatrix}. \tag{4.9}$$

This relation in Eq. (4.9) shows that the positive- and negative-energy eigen vectors of Σ' are not independent but related by

$$W^{\bar{1}} = \sigma_1 W^{-\bar{1}*}. \tag{4.10}$$

Inserting W from Eq. (4.9) into the full completeness relation Eq. (4.7), we find a completeness relation for the independent elements of W alone:

$$\frac{1}{N_c}\alpha\alpha^\dagger + \sum_{\bar{1}>0}(u_+^{\bar{1}} u_+^{\bar{1}\dagger} - v_+^{\bar{1}} v_+^{\bar{1}\dagger}) = \mathbb{1}_n. \tag{4.11}$$

This is the basis we want to use for the kinetic equations. The explicit split in a condensate mode α and the orthogonal fluctuation modes $u^{\bar{1}>0}$ and $v^{\bar{1}>0}$ is similar to the formalism of Ref. [91]. While the condensate mode α evolves according to Eq. (3.9) with the updated operator Π', we have to find an evolution equation for the quasiparticle populations.

We thus write the generalized single-time fluctuation-density matrix $\tilde{G}^<$ defined in Eq. (3.21) in terms of quasiparticles as

$$\tilde{G}^< = WPW^\dagger = \begin{pmatrix} UPU^\dagger & UPV^\top \\ V^*PU^\dagger & V^*PV^\top \end{pmatrix}, \tag{4.12}$$

where P is the not necessarily diagonal $2n$ by $2n$ quasiparticle population matrix. The time-reversed density matrix $\tilde{G}^>$ transforms according to its definition Eq. (3.22). From the same equation, we can also deduce that the quasiparticle population matrix P is Hermitian and fulfills a similar identity:

$$\sigma_3 + P = \sigma_1 P^* \sigma_1 = \sigma_1 P^\top \sigma_1. \tag{4.13}$$

This identity implies that P can be written as

$$P = \begin{pmatrix} p & q \\ q^* & (1+p)^* \end{pmatrix}, \tag{4.14}$$

in a structure similar to $\tilde{G}^<$ in Eq. (3.21). Since the classical mean field α only undergoes stimulated emission, the ground-state factors $P_{+0+0} = P_{-0-0}$ do not contain enhancement terms. Thus, the zero-energy components of σ_3 in Eq. (4.13) and similar enhancement terms associated with α actually have to be zero.

We also represent the condensate state vector (3.10) by a population matrix P^c in the quasiparticle basis

$$\chi\chi^\dagger = WP^cW^\dagger. \tag{4.15}$$

In order to maintain orthogonality between the condensate and the thermal excitations, we have to demand an analogue to the constraints $\alpha^*(t)\tilde{f} = 0$ and $\alpha^*(t)\tilde{m} = 0$ in the quasiparticle basis. We here have to distinguish two cases.

In the first case, the system evolves slowly enough that the ground-state of the adiabatic basis given in Eq. (4.11) is the true condensate state $\alpha(t) = \alpha$ (real). We can then explicitly give the condensate matrix as

$$P^c = N_c e_0 e_0^\dagger, \tag{4.16}$$

with a vector $e_0^{\bar{1}} = \delta_{\bar{1},\pm 0}$, such that all non-zero-energy components of P_c vanish. To implement the orthogonality constraint, we then explicitly set the $E = \pm 0$ elements of the quasiparticle matrix P to zero:

$$P_{0\bar{1}} = P_{\bar{1}0} = 0, \quad \text{for all } \bar{1}. \tag{4.17}$$

In the second case, the system evolves too fast for the quasiparticle basis to follow. Then, the condensate matrix contains components of non-zero energy. In this case, the more general orthogonality constraint

$$\langle \alpha(t)| \, P = \langle \alpha(t) \, |\, \bar{1}\rangle P_{\bar{1}\bar{2}} \, \langle \bar{2}| = 0 \tag{4.18}$$

has to be fulfilled. This constraint is particularly important when the condensate is coherently excited in linear response. For adiabatic evolution, Eq. (4.18) reduces to Eq. (4.17). In the next Section, we find the evolution equation for P.

4.2 Kinetic Equations

With these ingredients, we can now try to obtain an equation of motion for the occupation number matrix P from the kinetic equation (3.23). We use Eq. (4.12) to substitute the fluctuation-density matrices $\tilde{G}$ and obtain

$$\begin{aligned} \frac{\mathrm{d}}{\mathrm{d}t}P &= -i[E,P]_- + \Big\{ W^{-1}\frac{dW}{dt}P + \text{H.c.} \Big\} \\ &+ \Big\{ W^{-1}\Gamma^{<}\, W(\sigma_3 + P) - W^{-1}\Gamma^{>} W P + \text{H.c.} \Big\}. \end{aligned} \tag{4.19}$$

We are now left with the task of transforming the collisional contributions to the quasiparticle basis. To this end, we define new two-particle matrix elements in the quasiparticle energy basis by

$$\Phi^{\bar{1}\bar{2}\bar{3}\bar{4}} = \phi^{1'2'3'4'}\; V_{1'}^{\bar{1}*} V_{2'}^{\bar{2}*} U_{3'}^{\bar{3}} U_{4'}^{\bar{4}}. \tag{4.20}$$

These quasiparticle matrix elements have the same symmetries as the original ones given in Eq. (3.4). Furthermore, they fulfill

$$\Phi^{*\bar{1}\bar{2}\bar{3}\bar{4}} = \left(\Phi^{\bar{1}\bar{2}\bar{3}\bar{4}}\right)^* = \Phi^{-\bar{3}-\bar{4}-\bar{1}-\bar{2}}. \tag{4.21}$$

The careful examination of symmetries in Appendix B shows that the collision operator Eq. (3.28) reduces to terms containing the completely symmetric matrix elements

$$\psi^{\bar{1}\bar{2}\bar{3}\bar{4}} = \frac{1}{\sqrt{3}} \sum_{\pi} \Phi^{\pi(\bar{1}\bar{2}\bar{3}\bar{4})}, \tag{4.22}$$

which are defined as a sum over all index permutations π.

The resulting kinetic equations for the quasiparticle populations P are

$$\frac{\mathrm{d}}{\mathrm{d}t} P = -iEP + B_W P + C_{PP} + C_{\alpha P} + \text{H.c.}, \tag{4.23}$$

with the non-adiabatic basis-rotation term

$$B_W = W^{-1} \frac{dW}{dt} = \sigma_3 W^{\dagger} \sigma_3 \frac{dW}{dt}, \tag{4.24}$$

and the Boltzmann collision rates between fluctuations

$$\begin{aligned} C_{PP} &= C^{<}_{PP}(\sigma_3 + P) - C^{>}_{PP} P \\ &= \Gamma_{PP(\sigma_3+P)}(\sigma_3 + P) - \Gamma_{(\sigma_3+P)(\sigma_3+P)P} P \end{aligned} \tag{4.25}$$

and between fluctuations and the condensate

$$C_{\alpha P} = 3\Gamma_{P^c P(\sigma_3+P)}(\sigma_3 + P) - 3\Gamma_{P^c(\sigma_3+P)P} P. \tag{4.26}$$

These collision rates are defined in terms of the quasiparticle collision operator

$$\sigma_3 \Gamma_{PPP} = \frac{1}{2} \psi^{\bar{1}\bar{2}\bar{3}\bar{4}} \psi_{\eta}^{\bar{1}'\bar{2}'\bar{3}'\bar{4}'} P_{-\bar{1}-\bar{1}'} P_{-\bar{2}-\bar{2}'} P_{\bar{4}'\bar{4}} \left|\bar{3}\right\rangle \otimes \left\langle\bar{3}'\right|. \tag{4.27}$$

In this operator, P can stand for any one of the three possibilities P, $(\sigma_3 + P)$, or P^c, as needed in Eqs. (4.25) and (4.26). The approximately energy conserving matrix element ψ_η is explicitly given by

$$\psi_{\eta}^{\bar{1}'\bar{2}'\bar{3}'\bar{4}'} = \psi^{\bar{1}'\bar{2}'\bar{3}'\bar{4}'} \pi \delta_{\eta}(E_{\bar{1}'} + E_{\bar{2}'} + E_{\bar{3}'} + E_{\bar{4}'}), \tag{4.28}$$

where the quasiparticle energies can be positive or negative depending on their index. In an on-shell scattering event, this delta function forces two of the indices to be positive and the remaining two to be negative. This has to be considered in interpreting the collision terms C_{PP}

and $C_{\alpha P}$, because there all the sums run over positive and negative indices. The principal-value part in Eq. (3.20), which appears in the single-particle kinetic equations, is absorbed in the T matrices in Sec. 3.3 and thus does not appear anymore in the quasiparticle equations.

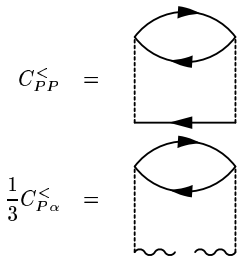

Figure 4.1: The incoming collision rates for collisions between thermal atoms $C^<_{PP}$ and between a thermal and a condensate atom $C^<_{\alpha P}$. The potential lines are now totally symmetric according to Eq. (4.22). The propagator lines represent the quasiparticle propagator P, which contains both the anomalous average $\tilde{m}$ and the normal density $\tilde{f}$. Because of the total symmetry of the interaction line, the three distinct condensate diagrams on each row of Fig. 2.2 reduce to one diagram with a weight of 3.

To complete the presentation of the quasiparticle kinetic equations, we write the generalized Gross–Pitaevskii equation (3.9) with the updated GP operator Π' and the second-order collisional contributions expressed in terms of quasiparticle populations P and obtain

$$\frac{\mathrm{d}}{\mathrm{d}t}\chi = -i\Pi'\chi + W\sigma_3\big(\Gamma_{PP(\sigma_3+P)} - \Gamma_{(\sigma_3+P)(\sigma_3+P)P}\big)W^{-1}\chi \tag{4.29}$$

In Sec. 4.6, we write this equation for $\alpha(t)$ alone. This equation together with Eq. (4.23) gives a complete description in terms of Bogoliubov quasiparticles of a condensate coupled to a thermal cloud at finite temperatures.

4.3 Orders of Magnitude

We now want to discuss the orders of magnitude of several of the quantities of this theory. This suggests some approximations to the full quasiparticle kinetic equations (4.23).

We first consider the basis transformation W. The completeness relation for the quasi-

particle basis Eq. (4.7) tells us that

$$W = \mathcal{O}(1). \tag{4.30}$$

For example, for high-energy eigen functions, the effect of the condensate becomes small, and the quasiparticle transformation reduces to

$$u \longrightarrow 1 \quad \text{and} \quad v \longrightarrow 0, \quad \text{as } E \longrightarrow \infty. \tag{4.31}$$

Now, considering the basis-rotation term defined in Eq. (4.24) we find

$$B_W = W^{-1}\frac{dW}{dt} = \frac{\mathcal{O}(1)}{dt} = \mathcal{O}(\Gamma) < \mathcal{O}\Big(\frac{1}{\Delta\tau}\Big), \tag{4.32}$$

because the time-scale for population changes, which change the quasiparticle basis W, is limited by the time between collisions $dt > \Delta\tau$. In equilibrium, the populations are constant due to detailed balance of the in and out rates. Thus, the net collision rate $\Gamma = C_{PP} + C_{\alpha P} + \text{H.c.}$ gives a better estimate for population changes $dt \approx \Gamma^{-1}$. This also confirms that $B_W = 0$ in equilibrium, since $dW/dt = 0$.

We now show that the stationary solutions P of the Boltzmann equation (4.23) are diagonal. Considering the stationary solution $\frac{\mathrm{d}}{\mathrm{d}t}P_{\bar{1}\bar{2}} = 0$ of Eq. (4.23) for an off-diagonal element with $\bar{1} \neq \bar{2}$, we obtain

$$P_{\bar{1}\neq\bar{2}} = i\frac{B_W P + C_{PP} + C_{\alpha P} + \text{H.c.}}{E_{\bar{2}} - E_{\bar{1}}} = \mathcal{O}\Big(\frac{\Gamma}{\Delta\epsilon}\Big). \tag{4.33}$$

This shows that the off-diagonal elements of the quasiparticle population are small compared to the diagonal ones, which are of the order of the number of particles N, and vanish at equilibrium.

4.4 Quasiparticle T Matrices

The T matrix in Eq. (3.39) (or the ladder extension Eq. (3.56)) has been obtained appropriately to second order. The second-order term with the factor of 1 in Eq. (3.39) is the divergent part, which is renormalized in Eq. (3.56) when replaced by the T-matrix. The term containing $2\tilde{f}$ of Eq. (3.39) is a convergent many-body second-order term. It is thus reasonable

to replace the T of Eq. (3.56) with

$$T^{1'2'3'4'}(E) = T_{2B}^{1'2'3'4'}(E+2\mu) + 8\mathcal{P}\frac{\phi^{1'2'3''4''}\tilde{f}_{4''2''}\phi^{3''2''3'4'}}{E-(E_{3''}+E_{4''})}, \tag{4.34}$$

where we replaced the single-particle energies in the denominator by quasiparticle energies, because the difference is of higher order. We here use the following two-body T matrix

$$T_{2\mathrm{B}}^{1'2'3'4'}(\epsilon) = 2\phi^{1'2'3'4'} + 4\mathcal{P}\frac{\phi^{1'2'3''4''}\phi^{3''4''3'4'}}{\epsilon-(\epsilon^0_{3''}+\epsilon^0_{4''})}, \tag{4.35}$$

which is given in terms of single-particle energies ϵ^0 defined by

$$H^{(0)}\left|\epsilon^0_{1'}\right\rangle = \left(\frac{\boldsymbol{p}^2}{2m}+V_{\mathrm{ext}}(\boldsymbol{x})\right)\left|\epsilon^0_{1'}\right\rangle = \epsilon^0_{1'}\left|\epsilon^0_{1'}\right\rangle. \tag{4.36}$$

The collisional terms of the kinetic equations (4.23) correspond to the imaginary part of a Liouville-space $\mathcal{T}$-matrix (3.57). Examining the argument of the δ_η-function in Eq. (4.28), which defines ψ_η, in comparison with the ladder T in Eq. (3.56) shows that (when the energies are correlated with the appropriate elements of W, see Appendix B) two of the energies in the denominator must be positive and two negative, which, together with the fact that P is diagonal close to equilibrium, leads to terms in the kinetic equation of the form $PP(1+P)(1+P)$, etc. The kinetic equation (4.23) then becomes the quantum Boltzmann equation for quasiparticle populations. The equilibrium solution is therefore the expected Bose–Einstein distribution for the quasiparticles, as the steady-state solution of Eqs. (4.23) and (4.29) shows [40, Sec. V]. The interaction matrix elements ϕ in Eq. (4.20) can also be upgraded to Ts. These equations in terms of T are now consistent with an impact approximation treatment (with elastic scattering not contributing when $T\otimes T^\dagger$ terms are considered, cf Eq. (3.57)).

4.5 Conservation Laws

Because of the non-vanishing pairing field, the trace of the quasiparticle density matrix P is in general not equal to the number of excited particles in the system. Hence, the number of quasi-particles is not conserved. Our single-particle kinetic equations (3.9) and (3.23) do,

however, conserve the mean total number

$$\langle N\rangle = \alpha^\dagger\alpha + \mathrm{Tr}\{\tilde{f}\} = N_c + \mathrm{Tr}\{\tilde{f}\} = \mathrm{const}; \tag{4.37}$$

this can be proven explicitly by inserting these kinetic equations into $\frac{\mathrm{d}}{\mathrm{d}t}\langle N\rangle$ and canceling terms. We thus adopt a self-consistent procedure for the quasiparticle kinetic equations Eqs. (4.23) and (4.29), by requiring

$$\langle N\rangle = N_c + \mathrm{Tr}\{UPU^\dagger\} = \mathrm{const}. \tag{4.38}$$

This equation self-consistently constrains the number of condensate atoms N_c: in equilibrium at temperature β^{-1}, the quasiparticle matrix P consists of $q = 0$ and

$$p(E) = \frac{1}{e^{\beta(E-\mu)} - 1} \tag{4.39}$$

according to Eq. (4.14) with the chemical potential μ given by the GP equation (3.52). As temperature tends to zero, we obtain the usual corrections for the anomalous average and condensate depletion [72]. Note that the number of excited atoms is not given by the trace of p, but has to include the basis transformation U as discussed above. If we drop the basis-rotation term B_W in numerical simulations, we incur number-non-conservation on the order of Γ, while away from equilibrium.

Since we use a Markovian collision integral with a damping function of finite width η in order to include off-the-energy-shell propagation, this theory is not exactly energy conserving. Markovian theories fail to track the decay of initial correlations and thus do not account for the decay of the correlation energy [96]. In our case, with a self-consistent η, energy is conserved to order η, which is consistent with the order of approximation. For a detailed discussion of these memory effects and how they affect the conservation laws see [97].

4.6 Summary

We summarize the main results of Chapters 3 and 4. We formulate a kinetic theory in terms of Bogoliubov quasiparticle modes W, which are defined by the eigen value equation for

the renormalized Hartree–Fock–Bogoliubov operator Σ'

$$\begin{pmatrix} H^{(0)} + 2T_{f^c} + 2T'_{\tilde{f}} - \mu & T_{m^c} \\ -\Sigma'^{*}_{\mathcal{A}} & -\Sigma'^{*}_{\mathcal{N}} \end{pmatrix} W = WE. \tag{4.1}$$

The T matrices are defined to second order in Eqs. (3.39) and (3.47) and Eq. (3.56) gives an extension to the ladder approximation. The Gross–Pitaevskii equation

$$\Big\{H^{(0)} + T_{f^c}(2\mu) + 2T'_{\tilde{f}}(2\mu)\Big\}\,\alpha = \mu\alpha \tag{4.52}$$

for the ground state α is contained in Eq. (4.1), because the renormalized Σ' is gapless. The GP equation defines the value of the chemical potential μ. To find a complete basis W, we have to find the second zero-energy mode and form quadrature components as discussed in Sec. 4.1.

We find the following Boltzmann equation for the thermal excitations in terms of Bogoliubov quasiparticles:

$$\begin{aligned} \frac{\mathrm{d}}{\mathrm{d}t}P &= -i[E,P] + \Big\{\sigma_3 W^\dagger \sigma_3 \frac{dW}{dt} P + \text{H.c.}\Big\} \\ &+ \Big\{\Gamma_{PP(\sigma_3+P)}(\sigma_3+P) - \Gamma_{(\sigma_3+P)(\sigma_3+P)P}P + \text{H.c.}\Big\} \\ &+ 3\Big\{\Gamma_{P^cP(\sigma_3+P)}(\sigma_3+P) - \Gamma_{P^c(\sigma_3+P)P}P + \text{H.c.}\Big\}. \end{aligned} \tag{4.23}$$

The basis-rotation term containing $\frac{\mathrm{d}}{\mathrm{d}t}W$ can be dropped for adiabatic evolution. However, this is not the case if the system is driven, as in linear response calculations. The quasiparticle density matrix P is diagonal close to equilibrium, and its elements obey an equilibrium Bose–Einstein distribution as the second and third lines show. The collision terms containing the general condensate matrix P^c defined in Eq. (4.15) represent population exchange between the thermal cloud and the condensate. They are balanced in the following equation for the condensate

$$\begin{aligned} \frac{\mathrm{d}}{\mathrm{d}t}\alpha(t) &= \big\{H^{(0)} + T_{f^c} + 2T'_{\tilde{f}} - \mu\big\}\alpha(t) \\ &+ U\sigma_3\big\{\Gamma_{PP(\sigma_3+P)} - \Gamma_{(\sigma_3+P)(\sigma_3+P)P}\big\}\sigma_3 \\ &\quad\times\big\{U^\dagger\alpha(t) - V^\top\alpha^*(t)\big\}. \end{aligned} \tag{4.29}$$

In general, $\alpha(t)$ can be different from the α used as the ground state of the adiabatic basis. A non-adiabatic change in a driving force, for example, would cause $\alpha(t)$ to change quickly.

The coupled Eqs. (4.23) and (4.29) have to be solved under the orthogonality constraints (4.18) or (4.17) depending on whether the evolution is adiabatic or not. Furthermore, the total particle number has to fulfill the self-consistent constraint Eq. (4.38).

4.7 Conclusions

We have extended the non-equilibrium kinetic theory of Walser et al. [37, 40] in two important respects. First, we write the binary interactions as many-body T matrices to second order in the interaction by subsuming ultra-violet divergent terms. This procedure removes divergences caused by the anomalous average $\tilde{m}$ and contained in the second-order terms. We can then replace the low-energy limit of the T matrix with the s-wave scattering length for numerical calculations. We present a consistent treatment of these difficulties associated with the anomalous average in a theory that includes second-order collisional terms. The updated Hartree–Fock–Bogoliubov operator Σ' is then gapless, which greatly facilitates a consistent treatment of the condensate coupled to thermal fluctuations.

The second extension of the Walser et al. theory makes use of the gapless HFB operator by using its quasiparticle eigen modes to parameterize the thermal fluctuations, which are then automatically orthogonal to the condensate mean field. We find that this basis greatly simplifies the second-order collision terms of the Walser et al. theory. Another important result reported here is that, in equilibrium, the Bogoliubov modes diagonalize the quasiparticle population matrix P. This means that, close to equilibrium, the second-order terms can be evaluated in n^4 operations, where n is the number of energy levels considered. This is a vast improvement compared to n^8 operations for a basis that does not diagonalize the population matrix, such as, for example, the single-particle basis used by Walser et al.

Chapter 5

Resonance Theory for Fermions [98]

In this Chapter, we formulate a many-body theory of a dilute gas focusing specifically on the description of a scattering resonance. This situation is relevant to current experiments on quantum gases in atomic physics involving Feshbach resonances. Utilizing a Feshbach resonance, experimentalists are able to probe the crossover physics between the Bardeen–Cooper–Schrieffer (BCS) superfluidity of a two-spin Fermi gas, and the Bose–Einstein condensation (BEC) of composite bosons. The physical situation giving rise to a Feshbach resonance, a two-channel system, is the principal focus of this Chapter. In particular, we highlight the criteria necessary for a two-channel model to be reducible to a single-channel situation. When such reduction is not possible, additional microscopic parameters which characterize the resonance itself are found to play an essential role in the many-body problem.

We begin with an overview of the main ideas of superfluid quantum gases, and examine the general problem of describing resonance interactions.

5.1 Bose–Einstein Condensation and Superfluidity

Bose–Einstein condensation, as the textbook problem was originally posed, occurs in a non-interacting gas at equilibrium as a consequence of the bosonic statistics of the particles. Perhaps the most striking aspect is the phenomenon that below a critical temperature a finite fraction of all the particles are found in a single quantum state, the ground state of the system, representing the Bose–Einstein condensate. This persists even when one considers the limit in

which the single quantum ground state is a state of zero integral measure, for example in the case of a continuous spectrum. Although Bose–Einstein condensation is remarkable in itself, there is an even more subtle and profound aspect which is the connection with superfluidity.

The phenomenon of superfluidity requires that there be interactions between the particles. Superfluidity occurs in a variety of physical systems bridging many fields of physics and a wide range of energetic and spatial scales. Superfluidity can be defined in a number of ways, but perhaps the most powerful is the connection of superfluidity with the presence of an order parameter or macroscopic wave function which describes all the superfluid particles. As in any scalar field of complex numbers, a macroscopic wave function $\psi(\boldsymbol{x})$ contains precisely two degrees of freedom at each point in space, which may be interpreted in terms of the local superfluid density $n(\boldsymbol{x})$ and the local superfluid phase $\phi(\boldsymbol{x})$, that is, $\psi(\boldsymbol{x}) = \sqrt{n(\boldsymbol{x})}\exp(i\phi(\boldsymbol{x}))$. Since the global phase of a wave function is not measurable and plays no physical role, it is only the variation in space of the superfluid phase that is of physical significance.

To make this clear, we point out that for the simple situation of a de Broglie matter wave of a free particle of mass m with wave vector $\boldsymbol{k}$, the wave function is simply a plane wave proportional to $\exp(i\boldsymbol{k}\cdot\boldsymbol{x})$. In this case it is the gradient of the quantum mechanical phase multiplied by $\hbar/m$ which leads to the particle's velocity, that is, $\hbar\boldsymbol{k}/m$. We define the superfluid velocity in analogous manner from the gradient in the phase of the macroscopic wave function

$$\boldsymbol{v} = \frac{\hbar}{m}\nabla\phi. \tag{5.1}$$

While this may appear straightforward, such a construction has truly nontrivial consequences. Any vector field formed from the gradient of a scalar field is irrotational, that is, $\nabla\times\boldsymbol{v} = 0$. This means that a superfluid in which the density is non-zero everywhere cannot contain circulation. The natural question which immediately arises therefore is how can a superfluid possibly rotate?

The dilemma is naturally resolved by accounting for the fact that it is not required that the density be non-zero everywhere, and indeed a superfluid can rotate if there are lines of zero superfluid density which penetrate the fluid. These are known as vortex lines and have

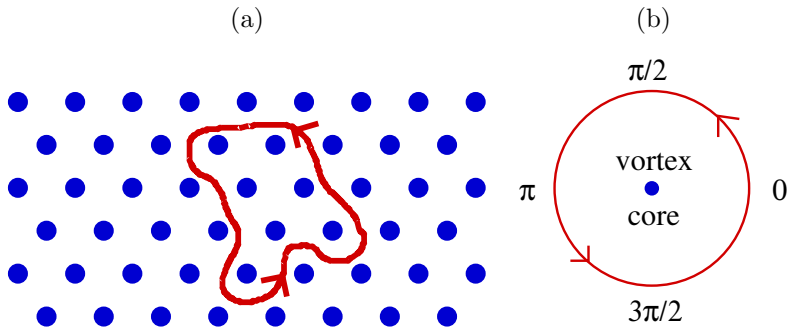

Figure 5.1: (a) The circulation integral in a superfluid depends on the number of vortex lines enclosed by the loop, in this case seven. (b) A characteristic phase pattern around a vortex core.

been imaged in a number of physical systems, including by direct methods in dilute atomic gases [11, 99]. Interestingly, when there are many vortex lines, it is generally the case that the motion of the vortex lines themselves mimics that of rigid body rotation of the system. In any case, when one performs a circulation integral inside any superfluid, as illustrated in Fig. 5.1, the circulation is quantized

$$\oint_{\text{loop}} \boldsymbol{v} \cdot \mathrm{d}\boldsymbol{l} = n\frac{h}{m} \tag{5.2}$$

where n is an integer and is equal to the number of vortex lines enclosed by the loop.

Figure 5.2 shows an example of the density and phase profile of a vortex in a dilute atomic gas trapped in a harmonic potential. For the state $\left|1\right\rangle$ the situation shown is a Bose–Einstein condensate with no vortex cores and a flat phase profile. In $\left|2\right\rangle$, a single quantized vortex is shown, and the characteristic 2π phase winding around the vortex line of zero density is evident. The density drops to zero in the center of the vortex core since the superfluid velocity diverges in the region. The characteristic size of this density dip—the vortex core—coincides with the region in which the superfluid velocity exceeds the speed of sound. Compare also to the experimental images in Fig. 1.2, where (c) corresponds to state $\left|1\right\rangle$ and (a) to state $\left|2\right\rangle$ above.

Of course, it is never guaranteed that in any given quantum system a single macroscopic wave function exists to define the superfluid. The condensate can, at least in principle, be

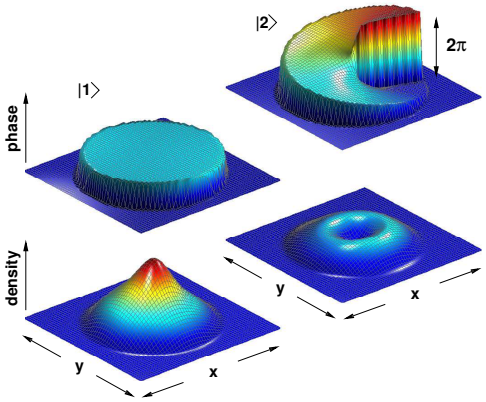

Figure 5.2: $|1\rangle$ The phase (top) and density (bottom) profile of a Bose–Einstein condensate in a harmonic trap in the ground state. $|2\rangle$ As for $|1\rangle$ but showing a condensate containing a single quantized vortex [100].

fragmented over a few quantum states. Indeed, there are many situations in which a more sophisticated description is necessary. A few examples include strongly correlated gases where the interaction effects are large or resonantly enhanced, gases where the ground state has a macroscopic degeneracy (a situation which occurs for harmonically confined gases at high rotation), and gases in the vicinity of critical points where the ground state symmetry changes.

5.2 Description of a Superfluid in a Dilute Atomic Gas

In a dilute atomic gas, typically composed of ground state alkali-metal atoms, the description of interactions in the superfluid phase is typically straightforward and depends on very few microscopic quantities. The primary physical reason for this is that the de Broglie wavelength associated with the atoms in the temperature scale at which Bose–Einstein condensation occurs is much larger than the characteristic range R of the interaction potential.

This characteristic range is determined by matching the spatial scale at which the kinetic energy coincides with the potential energy for collisions of alkali-metal atoms. If we assume the thermal collision energy to be sufficiently low, and the atoms to be in the ground internal state, then only the long-range part of the van der Waals potential plays an important role. The van der Waals potential is given in general form by C_6/R^6 where C_6 is a constant coefficient which

encapsulates the induced polarizability. In this case, the matching is given by the spatial scale R for which

$$\frac{\hbar^2}{mR^2} = \frac{C_6}{R^6}. \tag{5.3}$$

In a dilute gas, the resulting scale R for alkali-metal atoms is generally much less than the typical inter-particle spacing so that the simple picture of contact interactions is relevant. Furthermore, at low temperature, that is, when the de Broglie wavelength is much larger than R, one can expect that the low-energy scattering properties do not depend on the detailed structure of the interaction potential at small internuclear separation.

A further simplification occurs when one considers the effects of quantized angular momentum. Collisions between atoms which have a non-zero value for the orbital angular-momentum quantum number l see a centrifugal barrier proportional to $\hbar^2 l(l+1)/mr^2$, which becomes large and repulsive at short internuclear separation r. At sufficiently low temperature, the presence of a centrifugal barrier prevents the atoms reaching small enough separation for the true interatomic potential to have appreciable effect. In that case, collisions only occur in the $l = 0$ channel where the centrifugal barrier is absent. This channel is known as the s-wave channel.

Thus, in ultracold quantum gases, the interactions are generally parameterized by the s-wave scattering phase shift which may be expressed in length units as the s-wave scattering length a, which then determines the zero-energy two-body scattering T-matrix, $T = 4\pi\hbar^2 a/m$. A consequence is that the theory of superfluidity in dilute Bose–Einstein condensates, for the most part, has involved solutions of the nonlinear Schrödinger equation known as the Gross–Pitaevskii equation

$$i\hbar\frac{\mathrm{d}\psi}{\mathrm{d}t} = \left(-\frac{\hbar^2}{2m}\nabla^2 + V(\boldsymbol{x}) + T|\psi|^2\right)\psi. \tag{5.4}$$

The full condensate evolution depends here on three energy contributions in the bracketed expression on the right hand side of the equation: the kinetic energy, the potential energy $V(\boldsymbol{x})$ of an externally applied potential, and the internal mean-field energy proportional to both the two-body T-matrix and condensate density $|\psi|^2$. The fact that interactions are parameterized

by this particularly concise form of a constant T-matrix is not the only simplification. The many-body state is also taken to be completely factorisable into orbitals which depend only on a single coordinate; an approximation equivalent to completely dropping explicit two-particle and higher correlations. In the next Section, we begin to consider the effects of a failure of this approximation.

5.3 Breakdown of the Mean-Field Picture—Resonance Superfluids

There are important and relevant situations in which this approach fails. Scattering resonances can modify the qualitative character since it is possible to tune the two-body scattering length through infinity by appropriate modification of the details of the potential. When the scattering length is infinity, clearly the Gross–Pitaevskii equation cannot be applied as written. The resonance can be of many types: a direct Feshbach resonance, a shape resonance, a potential resonance, or even a Feshbach resonance induced through photo-associative laser coupling. Regardless of the detailed mechanism, the principles we now outline are almost universally applicable. The case of a Feshbach resonance is illustrated in Fig. 5.3. A closed-channel potential, typically corresponding to a distinct spin configuration, can support bound states with energies in close proximity to the scattering threshold. The difference in the magnetic moments of the open and closed channels allow the detuning $\bar{\nu}$ to be varied by application of an external magnetic field.

When the bound state crosses threshold, the scattering length passes from positive infinity to negative infinity. In the vicinity of this point, the two-body T-matrix is not constant and becomes strongly dependent on the scattering energy. The T-matrix may even acquire a substantial imaginary component as shown in Fig. 5.4. The assumption that the fields factorize into single-particle orbitals is no longer valid and quantum correlations must be included as an essential part of the description. For a single Feshbach resonance, as considered here, the

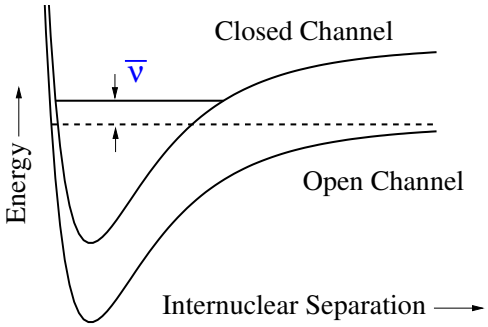

Figure 5.3: A Feshbach resonance. A bound state of a closed potential is in close proximity (with detuning $\bar{\nu}$) to the scattering threshold (dashed line)

behavior of the scattering length as a function of magnetic field is universal and is shown in the inset of Fig. 5.4. Note that the separation of scales arguments that were discussed previously apply here as well. In its minimal form only two parameters are required to characterize this resonance: the matrix element between the open and closed channels g, and the detuning from resonance $\bar{\nu}$. The behavior of the scattering length in this approximation is given by

$$T = \frac{4\pi\hbar^2 a}{m} = -\frac{g^2}{\bar{\nu}}. \tag{5.5}$$

5.4 Single-Channel versus Two-Channel Approaches

We now turn to the formulation of a many-body description of a dilute gas including scattering resonances. In accomplishing this task, it is necessary to ensure that the microscopic physics just explained is correctly incorporated. We begin by presenting two alternative starting points and then proceed to establish their connection. We focus our attention solely on a system of fermions, rather than considering directly bosons as described by the Gross–Pitaevskii theory. This is a good starting point, since a dilute gas of bosons emerges indirectly when the interaction properties are tuned, such that the fermions pair-up to form composite bosonic molecules.

Since fermions require an anti-symmetric wave function under exchange, s-wave interactions require at least two spin components, which we label as $\uparrow$ and $\downarrow$. We may then write a

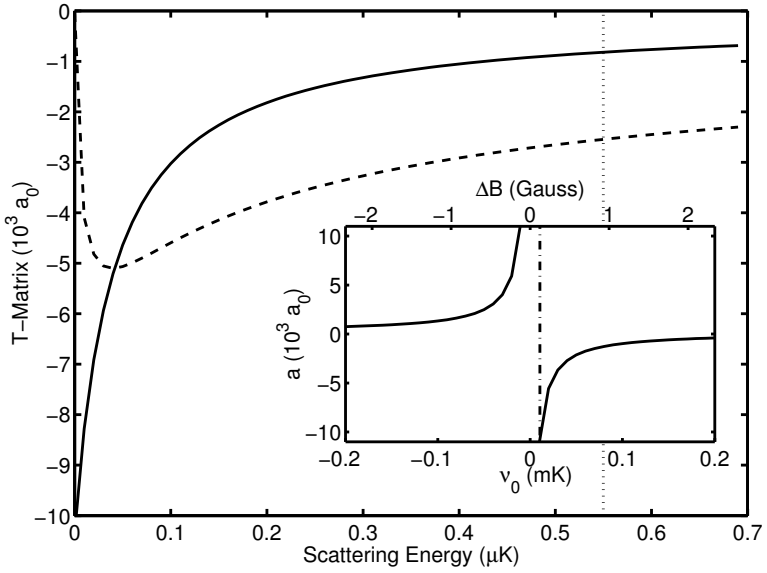

Figure 5.4: Real (solid line) and imaginary (dashed line) components of the two-body T-matrix for collisions of the lowest two spin states of ^{40}K at a detuning of $20\,\epsilon_{\rm F}$ ($\epsilon_{\rm F}$ is a typical Fermi energy for a dilute gas), shown in length dimensions, that is, $T/(4\pi\hbar^2/m)$ [101]. The scattering length is the intercept at zero scattering energy which for this case is approximately $-10000\,a_0$, where a_0 is the Bohr radius. The inset shows the scattering length as a function of detuning, with $20\,\epsilon_{\rm F}$ detuning indicated by the dashed-dot line.

Hamiltonian for the system, keeping pairwise or binary interactions of general form,

$$H_{\rm single} = \sum_{\boldsymbol{k}\sigma} \epsilon_{\boldsymbol{k}} c^\dagger_{\boldsymbol{k}\sigma} c_{\boldsymbol{k}\sigma} + \sum_{\boldsymbol{q}\boldsymbol{k}\boldsymbol{k}'} U_{\boldsymbol{k},\boldsymbol{k}'}\, c^\dagger_{\boldsymbol{q}/2+\boldsymbol{k}\uparrow} c^\dagger_{\boldsymbol{q}/2-\boldsymbol{k}\downarrow} c_{\boldsymbol{q}/2-\boldsymbol{k}'\downarrow} c_{\boldsymbol{q}/2+\boldsymbol{k}'\uparrow}, \tag{5.6}$$

where $\epsilon_{\boldsymbol{k}} = \hbar^2 k^2/2m$ is the free-fermion dispersion relation. The operators $c^{(\dagger)}_{\boldsymbol{k}\sigma}$ annihilate (create) fermions with momentum $\boldsymbol{k}$ and spin σ, and the momentum indices enforce momentum conservation. The interaction potential U need not be the physical interaction potential for the atoms being considered, because there is no unique potential that reproduces the physical two-body T-matrix for the given atoms over the relevant energy scale. In other words, one is free to choose U to be of a particularly simple and convenient form, a procedure known as renormalization. One way of doing this is to impose the constraint that the potential be independent of momentum and to cut all momentum sums in the theory off at a maximum momentum, K. This leads to the following relationship between U and T:

$$T = \frac{U}{1-\alpha U}, \tag{5.7}$$

where $\alpha = mK/(2\pi^2\hbar^2)$.

There exists an alternative approach to the many-body formulation. This is based on constructing the many-body Hamiltonian by considering the microscopic formation and dissociation of molecules in the Feshbach resonance state [19, 102]

$$H_{\rm res} = \sum_{\boldsymbol{k},\sigma=\uparrow,\downarrow} \epsilon_{\boldsymbol{k}} a^\dagger_{\boldsymbol{k}\sigma} a_{\boldsymbol{k}\sigma} + \sum_{\boldsymbol{q}} \Big(\frac{\epsilon_{\boldsymbol{q}}}{2} + \nu\Big) b^\dagger_{\boldsymbol{q}} b_{\boldsymbol{q}} + \sum_{\boldsymbol{q}\boldsymbol{k}} g_{\boldsymbol{k}} \Big(b^\dagger_{\boldsymbol{q}} a_{\boldsymbol{q}/2-\boldsymbol{k}\downarrow} a_{\boldsymbol{q}/2+\boldsymbol{k}\uparrow} + \text{H.c.}\Big), \tag{5.8}$$

where $g_{\boldsymbol{k}}$ is the matrix element relating two free fermions in the open channel to the closed-channel bound state near threshold, and ν is the bare detuning of the bound state, which we relate to the physical detuning by renormalization below. The operators $a^{(\dagger)}_{\boldsymbol{k}\sigma}$ annihilate (create) open-channel fermions with momentum $\boldsymbol{k}$ and spin σ, while $b^{(\dagger)}_{\boldsymbol{k}}$ annihilate (create) closed-channel bosons. See Appendix D for a discussion of when a pair of fermions can be treated as a boson. Said Appendix also discusses a more general Hamiltonian that includes a non-resonant background interaction for the fermions.

So we may pose the question: what is the connection between the single- and two-channel formulations? The relationship can be well understood by considering the two-fermion relative wave function. An eigen state of Eq. (5.8) can be constructed by considering the following linear combination of basis states

$$\Psi_{\boldsymbol{k}} = \chi_{\boldsymbol{k}} + C_{\boldsymbol{k}}\phi, \tag{5.9}$$

where $\chi_{\boldsymbol{k}} = \langle a_{-\boldsymbol{k}\downarrow} a_{\boldsymbol{k}\uparrow}\rangle$ and $\phi = \langle b_0\rangle$. The coefficient $C_{\boldsymbol{k}}$ will be determined later. The evolution of $\Psi_{\boldsymbol{k}}$ is given by taking vacuum expectation values of the Heisenberg equations of motion generated by the resonance Hamiltonian in Eq. (5.8):

$$i\hbar \frac{\mathrm{d}\Psi_{\boldsymbol{k}}}{\mathrm{d}t} = i\hbar \frac{\mathrm{d}}{\mathrm{d}t}\left(\chi_{\boldsymbol{k}} + C_{\boldsymbol{k}}\phi\right) = 2\epsilon_{\boldsymbol{k}}\chi_{\boldsymbol{k}} + g_{\boldsymbol{k}}\phi + C_{\boldsymbol{k}}\left(\nu\phi + \sum_{\boldsymbol{k}'} g_{\boldsymbol{k}'}\chi_{\boldsymbol{k}'}\right). \tag{5.10}$$

This can be rewritten to eliminate the explicit dependence on the open-channel fermions by substituting $\chi_{\boldsymbol{k}} = \Psi_{\boldsymbol{k}} - C_{\boldsymbol{k}}\phi$ to give

$$i\hbar \frac{\mathrm{d}\Psi_{\boldsymbol{k}}}{\mathrm{d}t} = 2\epsilon_{\boldsymbol{k}}\Psi_{\boldsymbol{k}} + C_{\boldsymbol{k}}\sum_{\boldsymbol{k}'} g_{\boldsymbol{k}'}\Psi_{\boldsymbol{k}'} + \left[g_{\boldsymbol{k}} + C_{\boldsymbol{k}}\Big(\nu - 2\epsilon_{\boldsymbol{k}} - \sum_{\boldsymbol{k}'} g_{\boldsymbol{k}'}C_{\boldsymbol{k}'}\Big)\right]\phi, \tag{5.11}$$

where the term in brackets contains the residual explicit dependence on the bosons in the Feshbach resonance state. If this term in brackets vanishes, we obtain an effective single-channel theory for the dressed eigen-state solution $\Psi_{\boldsymbol{k}}$

$$i\hbar\frac{\mathrm{d}\Psi_{\boldsymbol{k}}}{\mathrm{d}t} = 2\epsilon_{\boldsymbol{k}}\Psi_{\boldsymbol{k}} + C_{\boldsymbol{k}}\sum_{\boldsymbol{k}'} g_{\boldsymbol{k}'}\Psi_{\boldsymbol{k}'}. \tag{5.12}$$

The following choice for the coefficient $C_{\boldsymbol{k}}$ in Eq. (5.9) gives us the above single-channel solution

$$C_{\boldsymbol{k}} = \mathcal{P}\frac{g_{\boldsymbol{k}}}{2\epsilon_{\boldsymbol{k}} - E}, \tag{5.13}$$

where $\mathcal{P}$ denotes the Cauchy Principal Value and E is defined by the solution of an integral equation

$$E = \nu - \mathcal{P}\sum_{\boldsymbol{k}}\frac{g_{\boldsymbol{k}}^2}{2\epsilon_{\boldsymbol{k}} - E}\,. \tag{5.14}$$

The nature of the solution depends on the presence or absence of a bound state indicated by the sign of the renormalized detuning $\bar{\nu}$. This is defined as

$$\bar{\nu} = \nu - \sum_{\boldsymbol{k}}\frac{g_{\boldsymbol{k}}^2}{2\epsilon_{\boldsymbol{k}}}, \tag{5.15}$$

and is physically related to the magnetic field shift from the Feshbach resonance [103]. The case of $\bar{\nu} < 0$ corresponds to the side of the resonance in which the scattering length is positive. There, a bosonic dimer bound state exists and the solution of Eq. (5.14) coincides at small detuning with the bound-state energy $E = -\hbar^2/ma^2$ [104, 105, 67]. For $\bar{\nu} > 0$ there is no bound state and the solution is $E = \bar{\nu}$.

5.5 Poles of the Molecular Propagator

Finding the correct physical solutions for the energy in Eq. (5.14) requires some care. If we simply were to drop the principal value from Eq. (5.14), we would find the following equations

for a complex-frequency pole of the molecular propagator

$$\omega = \nu - \frac{g^2}{2\pi^2}\int_0^\infty \mathrm{d}k\, \frac{k^2}{\hbar^2 k^2/m - \omega + i\delta}\,, \quad \delta = 0+ \tag{5.16a}$$

$$= \bar{\nu} - \frac{g^2}{2\pi^2}\frac{m}{\hbar^2}\int_0^\infty \mathrm{d}k\, \frac{\omega}{\hbar^2 k^2/m - \omega + i\delta} \tag{5.16b}$$

$$= \bar{\nu} - \frac{g^2}{4\pi^2}\frac{m^{3/2}}{\hbar^3}\int \mathrm{d}z\, \frac{\omega}{z^2 - \omega + i\delta}. \tag{5.16c}$$

The subtle point here is that the solution one finds depends on the integration path in the complex plane. If we perform the integral, the poles arise as roots of the following quadratic equation

$$z^2 \pm i\frac{g^2}{4\pi}\frac{m^{3/2}}{\hbar^3}z - \bar{\nu}\,, \quad \sqrt{\omega} = z. \tag{5.17}$$

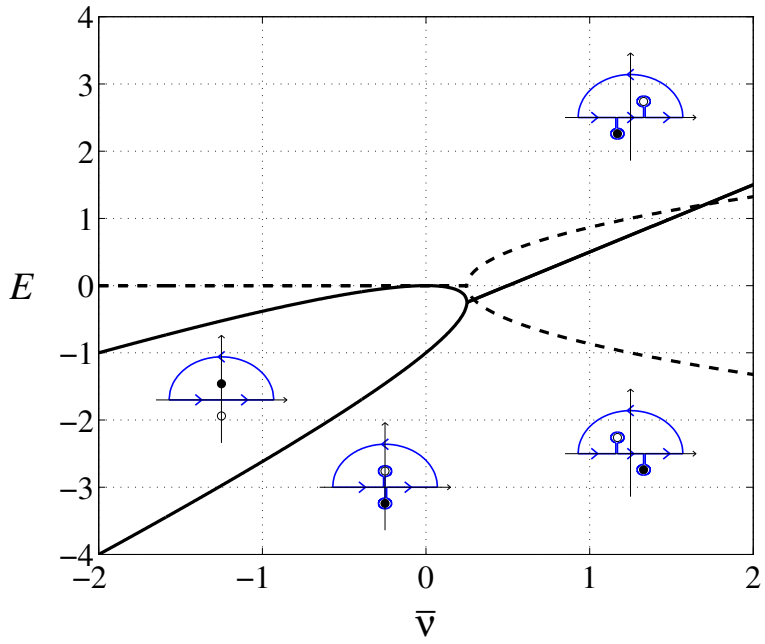

Figure 5.5: Poles of the molecular propagator as a function of detuning (solid line) real part, (dashed line) imaginary part. The insets show the various integration contours which lead to the solutions shown. The true bound state is the upper solid curve for $\bar{\nu} < 0$.

Figure 5.5 shows the various possible solutions. Note the prediction of two bound-state solutions on the positive side of the resonance ($\bar{\nu} > 0$), and the shift of the real part of the

pole to higher detunings than $\bar{\nu}$ at large detuning. With the exception of the true bound state at negative detuning ($\bar{\nu} < 0$), these curves are misleading and do not correspond to physical solutions of the two-channel scattering problem.

5.6 The Equivalent Single-Channel Theory

Using the definition for E in Eq. (5.14), we may write the prefactor bracket of ϕ in Eq. (5.11) as

$$\frac{g_{\boldsymbol{k}}}{2\epsilon_{\boldsymbol{k}} - E}\left[(2\epsilon_{\boldsymbol{k}} - E) + \nu - 2\epsilon_{\boldsymbol{k}} - \mathcal{P}\sum_{\boldsymbol{k}'}\frac{g_{\boldsymbol{k}}g_{\boldsymbol{k}'}}{2\epsilon_{\boldsymbol{k}'} - E}\right], \tag{5.18}$$

and substituting Eq. (5.14), which defines E, this is

$$\frac{g_{\boldsymbol{k}}}{2\epsilon_{\boldsymbol{k}} - E}\left[2\epsilon_{\boldsymbol{k}} - E + \nu - 2\epsilon_{\boldsymbol{k}} - \nu + E\right] = 0, \tag{5.19}$$

as required. The evolution of $\Psi_{\boldsymbol{k}}$ is then given by

$$i\hbar\frac{\mathrm{d}\Psi_{\boldsymbol{k}}}{\mathrm{d}t} = 2\epsilon_{\boldsymbol{k}}\Psi_{\boldsymbol{k}} + \mathcal{P}\sum_{\boldsymbol{k}'}\frac{g_{\boldsymbol{k}}g_{\boldsymbol{k}'}}{2\epsilon_{\boldsymbol{k}} - E}\Psi_{\boldsymbol{k}'}. \tag{5.20}$$

This is nothing more than a time-dependent Schrödinger equation for an effective single-channel problem. In other words, an effective single-channel theory has now been shown to be encapsulated by the resonance Hamiltonian theory. The interaction potential, defined in Eq. (5.6), can be directly read off from Eq. (5.20)

$$U_{\boldsymbol{k},\boldsymbol{k}'} = \mathcal{P}\frac{g_{\boldsymbol{k}}g_{\boldsymbol{k}'}}{2\epsilon_{\boldsymbol{k}} - E}. \tag{5.21}$$

What remains is to show that this potential generates the correct scattering length at all detunings $\bar{\nu}$. To this end, we must obtain the two-body T-matrix by solving the Lippmann-Schwinger equation [106]

$$T_{\boldsymbol{k},\boldsymbol{k}'} = U_{\boldsymbol{k},\boldsymbol{k}'} + \sum_{\boldsymbol{q}}\frac{U_{\boldsymbol{k},\boldsymbol{q}}T_{\boldsymbol{q},\boldsymbol{k}'}}{2\epsilon_{\boldsymbol{k}'} - 2\epsilon_{\boldsymbol{q}} + i\delta}, \quad \delta \to 0^{+}. \tag{5.22}$$

We wish to solve this in the limit of zero scattering energy $\epsilon_{\boldsymbol{k}} \to 0$ and constant $g_{\boldsymbol{k}} \to g$. Equation (5.22) can then be rewritten as a series by recursive substitutions

$$T = -\frac{g^2}{E} + \frac{g^2}{E}\mathcal{P}\sum_{\boldsymbol{k}''}\frac{g^2}{2\epsilon_{\boldsymbol{k}''}(2\epsilon_{\boldsymbol{k}''} - E)} + \dots\ . \tag{5.23}$$

Now from the definition of E in Eq. (5.14)

$$E = \nu - \mathcal{P}\sum_{\boldsymbol{k}} \frac{g^2}{2\epsilon_{\boldsymbol{k}} - E} \tag{5.24a}$$

$$= \nu - \mathcal{P}\sum_{\boldsymbol{k}} \frac{g^2(2\epsilon_{\boldsymbol{k}} - E + E)}{2\epsilon_{\boldsymbol{k}}(2\epsilon_{\boldsymbol{k}} - E)} \tag{5.24b}$$

$$= \bar{\nu} - \mathcal{P}\sum_{\boldsymbol{k}} \frac{g^2 E}{2\epsilon_{\boldsymbol{k}}(2\epsilon_{\boldsymbol{k}} - E)}, \tag{5.24c}$$

which leads to

$$\mathcal{P}\sum_{\boldsymbol{k}''} \frac{g^2}{2\epsilon_{\boldsymbol{k}}(2\epsilon_{\boldsymbol{k}} - E)} = \frac{\bar{\nu} - E}{E}. \tag{5.25}$$

Substituting this expression into Eq. (5.23) and continuing similarly for the rest of the terms, we arrive at the geometric series

$$T = -\frac{g^2}{E}\left(1 + \frac{E - \bar{\nu}}{E} + \left(\frac{E - \bar{\nu}}{E}\right)^2 + \dots\right) \tag{5.26a}$$

$$= -\frac{g^2}{E(1 - ((1 - \bar{\nu})/E))} \tag{5.26b}$$

$$= -\frac{g^2}{\bar{\nu}}. \tag{5.26c}$$

Equation (5.26) provides the correct behavior of the tuning of the scattering length around resonance, with the usual definition $T = 4\pi\hbar^2 a/m$, and confirms that the potential $U_{\boldsymbol{k},\boldsymbol{k}'}$ leads to the correct effective fermion interaction properties.

We have thus presented a detailed mathematical proof of the equivalence of the two initial Hamiltonians for the single- and two-channel models describing the scattering of two fermions in vacuum. One must extend this result to consider the equivalence in systems that contain more than two fermions. The structure of the mathematical proof can be continued along the presented lines. The result for the important case of four fermions is that the equivalence between the single and two-channel theories has been shown to hold, but requires that the width of the Feshbach resonance be sufficiently broad [107].

5.7 Connection with the Theory of Feshbach Resonances

We can equivalently express the two-channel model in terms of the original language of the open P and closed Q channels as done by Feshbach [108, 109, 110]. In terms of these separate Hilbert subspaces, the time-independent Schrödinger equation takes the following coupled form:

$$E\left|\Psi_{\mathrm{P}}\right\rangle = H_{\mathrm{PP}}\left|\Psi_{\mathrm{P}}\right\rangle + H_{\mathrm{PQ}}\left|\Phi_{\mathrm{Q}}\right\rangle, \tag{5.27a}$$

$$E\left|\Phi_{\mathrm{Q}}\right\rangle = H_{\mathrm{QQ}}\left|\Phi_{\mathrm{Q}}\right\rangle + H_{\mathrm{QP}}\left|\Psi_{\mathrm{P}}\right\rangle. \tag{5.27b}$$

We may formally solve Eq. (5.27a),

$$\left|\Psi_{\mathrm{P}}\right\rangle = \frac{1}{E - H_{\mathrm{PP}}} H_{\mathrm{PQ}}\left|\Phi_{\mathrm{Q}}\right\rangle, \tag{5.28}$$

and substitute the result into Eq. (5.27b) and obtain

$$\left(E - H_{\mathrm{QQ}} - H_{\mathrm{QP}}\frac{1}{E - H_{\mathrm{PP}}} H_{\mathrm{PQ}}\right)\left|\Phi_{\mathrm{Q}}\right\rangle = 0. \tag{5.29}$$

The effective interaction due to the coupled spaces is therefore

$$H_{\mathrm{QQ}}^{\mathrm{eff}} = H_{\mathrm{QQ}} + H_{\mathrm{QP}}\frac{1}{E - H_{\mathrm{PP}}} H_{\mathrm{PQ}}. \tag{5.30}$$

This expression is, in fact, similar to Eq. (5.14); except that in this case it is in operator form, whereas Eq. (5.14) is represented in a basis. The chosen basis involves a continuum $\left|\boldsymbol{k}\right\rangle$ for the P subspace, a single quantum resonance state $\left|\phi\right\rangle$ for the Q subspace, and an explicit form for the matrix elements of momentum dependent coupling. The mapping is thus $\left\langle\phi\right|H_{\mathrm{QQ}}\left|\phi\right\rangle = \nu$, $\left\langle\boldsymbol{k}\right|H_{\mathrm{PP}}\left|\boldsymbol{k}\right\rangle = 2\epsilon_{\boldsymbol{k}}$, and $\left\langle\phi\right|H_{\mathrm{QP}}\left|\boldsymbol{k}\right\rangle = \left\langle\boldsymbol{k}\right|H_{\mathrm{PQ}}\left|\phi\right\rangle = g_{\boldsymbol{k}}$.

5.8 The BCS–BEC Crossover

One of the first attempts to understand the crossover between the phenomena of BCS and BEC was put forth by Eagles in a 1969 paper on pairing in superconducting semiconductors [111]. He proposed moving between these two limits by doping samples, in this case by decreasing the carrier density in systems of $SrTiO_3$ doped with Zr. In a 1980 paper by Leggett [112],

motivated by the early ideas of quasi-chemical equilibrium theory, he modeled the crossover at zero temperature by way of a variational wave function:

$$\psi_{\mathrm{BCS}} = \prod_k (u_k + v_k a_k^\dagger a_{-k}^\dagger)|0\rangle. \tag{5.31}$$

This wave function is simply the BCS wave function and assumes that at $T = 0$ all the fermions form Cooper pairs. What Leggett was able to show was that he could smoothly interpolate between conventional BCS theory and the occurrence of BEC.

In 1985, Nozières and Schmitt-Rink (NSR) extended this theory to finite temperatures, in order to calculate the critical temperature T_{C} [113]. NSR derived the conventional BCS gap and number equations, but introduced into the number equation the self-energy associated with the particle-particle ladder diagram (or scattering T-matrix) to lowest order. This very influential paper was built upon by many other groups and was transformed into a functional form by Randeria et al. [114].

A compelling motivation for understanding the crossover problem comes from the fact that many high-T_{C} superconductors fall within the intermediate region between loosely bound BCS pairs and a BEC of tightly bound pairs. In the copper oxides, for instance, the coherence length of the Cooper pairs has been measured to be only a few times the lattice spacing. In contrast, in conventional superconductors, the coherence lengths are usually much greater than the lattice spacings. An understanding of the crossover may be one of the keys to understanding and manipulating high-T_{C} materials.

Dilute quantum gases have already played a very important role in experimentally probing the BCS–BEC crossover. This crossover is, in fact, a special case of a more general framework of resonance superfluids. In the broad resonance limit, which is generally the experimentally relevant one, the system maps on to the BCS–BEC crossover problem originally introduced in the context of condensed matter systems. Figure 5.6 illustrates some of the important distinctions of resonance superfluids. In particular, the pairing in a weakly coupled BCS superconductor

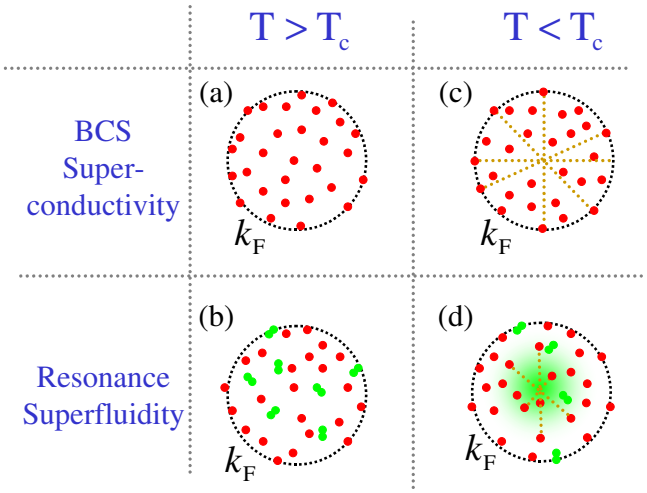

Figure 5.6: Schematic comparison of BCS theory and the BCS–BEC crossover theory of resonance superfluidity. Resonance superfluidity describes closed-channel, tightly bound pairs of fermions (green) in addition to the loosely bound BCS pairs (red/yellow). Below the transition temperature T_C, the closed-channel pairs condense and also mediate pairing of open-channel fermions away from the Fermi sphere.

occurs primarily at the Fermi surface in momentum space and the superfluid appears out of the degenerate Fermi sea at a critical temperature T_C much less than the Fermi temperature. As Fig. 5.6 illustrates, the physical situation for resonance superfluids can be quite different, with pairing throughout the Fermi surface, and molecular condensation of the composite bosons. Furthermore the critical temperature for superfluidity in this case can be comparable to the Fermi temperature. This is very important, since current experiments in dilute quantum gases can, at the lowest, reach temperatures on the order of a tenth of the Fermi temperature, which is far above the critical temperatures predicted by simple BCS theory in the region in which it can be applied.

Chapter 6

Imaginary-Time Propagation for Fermions [98]

6.1 Imaginary-Time Methods for Single- and Two-Channel BCS Models

The method of steepest descents has been widely applied for finding condensate wave functions in Boson systems. In this Section, we want to generalize this method and calculate the single- and two-channel BCS solution for interacting fermions. Our imaginary-time approach can be generalized to include beyond-BCS interactions.

The most important advantage of our imaginary-time method for fermions is that it gives direct access to zero-temperature ground states for fermion systems without diagonalizing the BCS self-energy matrix. One could, for example, study topological excitations of the BCS superfluid by imposing symmetry constraints. For example, imposing a 2π phase winding around a central core results in a vortex state as depicted in Fig. 5.2.

6.1.1 Single-Channel BCS Theory

BCS theory is a single-channel theory for fermions, whose interactions are characterized by the scattering length a as the single microscopic parameter [18]. The BCS Hamiltonian can be diagonalized analytically by solving the following number and gap equations

$$n = \int_0^\infty \mathrm{d}k \frac{k^2}{2\pi^2} \left(1 - \frac{\epsilon_k - \mu_\mathrm{F}}{\sqrt{(\epsilon_k - \mu)^2 + \Delta^2}} \right) \quad \text{and} \tag{6.1a}$$

$$\frac{m}{4\pi\hbar^2 a} = \int_0^\infty \mathrm{d}k \frac{k^2}{4\pi^2} \left(\frac{1}{\epsilon_k} - \frac{1}{\sqrt{(\epsilon_k - \mu_\mathrm{F})^2 + \Delta^2}} \right), \tag{6.1b}$$

where $\epsilon_k = \hbar^2 k^2/(2m)$ is the kinetic energy, μ_F the chemical potential, Δ the superfluid gap and $n = n_\uparrow + n_\downarrow$ the total particle density. These equations are self-consistently solved for the chemical potential and the gap, and one obtains the Bogoliubov quasi-particle modes u_k and v_k, which are given by

$$u_k^2 = 1 - v_k^2 = \frac{1}{2}\left(1 - \frac{\epsilon_k - \mu_\mathrm{F}}{\sqrt{(\epsilon_k - \mu_\mathrm{F})^2 + \Delta^2}}\right) \tag{6.2}$$

The normal and anomalous averages $f_{\boldsymbol{k}}$ and $m_{\boldsymbol{k}}$ at zero temperature are then given by

$$f_{\boldsymbol{k}\uparrow} = \langle a^\dagger_{\boldsymbol{k}\uparrow} a_{\boldsymbol{k}\uparrow}\rangle = v_k^2 \quad \text{and} \tag{6.3a}$$

$$m_{\boldsymbol{k}} = \langle a_{-\boldsymbol{k}\downarrow} a_{\boldsymbol{k}\uparrow}\rangle = u_k v_k \tag{6.3b}$$

The normal average $f_{\boldsymbol{k}\uparrow}$ is the density of spin-up atoms at momentum $\boldsymbol{k}$, and the anomalous average a pair-correlation function between atoms of opposite momentum and spin. We want to find the solutions (6.3) for the averages by using imaginary-time propagation.

6.1.2 Imaginary-Time Propagation for Bosons

How does imaginary-time propagation work for bosons? The basic idea is to replace the time variable t in the Gross–Pitaevskii (GP) equation for the condensate wave-function ψ,

$$i\hbar\frac{\mathrm{d}\psi}{\mathrm{d}t} = \left(-\frac{\hbar^2}{2m}\nabla^2 + V + T|\psi|^2\right)\psi = H_\mathrm{GP}\psi, \tag{6.4}$$

with the imaginary time variable $-it$. The time-evolution under the GP equation (6.4) can be written in terms of its eigen states ϕ_n, which are defined by $H_\mathrm{GP}\phi_n = E_n\phi_n$, with the eigen energies E_n:

$$\psi(t) = \sum_n c_n \exp\left(-\frac{iE_n t}{\hbar}\right)\phi_n, \tag{6.5}$$

where the coefficients c_n are defined by the expansion of the initial condition $\psi(t=0) = \sum_n c_n\phi_n$. Propagating the GP equation in imaginary time changes the above time evolution to

$$\psi(t) = \sum_n c_n \exp\left(-\frac{E_n t}{\hbar}\right)\phi_n. \tag{6.6}$$

The unitary time-evolution in Eq. (6.5) has turned into an exponential decay.

The algorithm for the imaginary-time method is now to use the imaginary-time evolution over a time interval and renormalizing the resulting wave function after each step using a normalization condition or number equation, in this case,

$$N = \int \mathrm{d}^3\boldsymbol{x}|\psi(\boldsymbol{x})|^2. \tag{6.7}$$

This procedure converges on the lowest-energy ground state solution ϕ_0

$$\psi(t) \quad \xrightarrow{-it} \quad \phi_0, \tag{6.8}$$

provided that the ground state is nondegenerate. Due to numerical errors, this even works if the initial wave function $\psi(t = 0)$ does not contain a contribution of the ground state, that is if $c_0 = 0$. The convergence can, however, be accelerated in practice by choosing $\psi(t = 0)$ appropriately.

Imaginary-time propagation can include symmetry, topological, or orthogonality constraints, and one can thus calculate topological condensate states or higher-excited states of the Hamiltonian. See Fig. 5.2 for an example of a vortex state calculated using imaginary-time propagation. We now generalize this powerful approach to fermions.

6.1.3 Imaginary-Time Propagation for Fermions

In the case of bosons above, we learned how to propagate a wave-function equation in imaginary time and thus find ground-state solutions. Time-dependent BCS theory, which is the simplest single-channel theory for interacting fermions, has two equations for the normal $f_{\boldsymbol{k}}$ and anomalous density $m_{\boldsymbol{k}}$,

$$i\hbar\frac{\mathrm{d}f_{\boldsymbol{k}\uparrow}}{\mathrm{d}t} = i2U\Im\left(p^* m_{\boldsymbol{k}}\right), \qquad \text{and} \tag{6.9a}$$

$$i\hbar\frac{\mathrm{d}m_{\boldsymbol{k}}}{\mathrm{d}t} = 2(\epsilon_{\boldsymbol{k}} - \mu_{\mathrm{F}})m_{\boldsymbol{k}} + Up\left(1 - f_{\boldsymbol{k}\uparrow} - f_{\boldsymbol{k}\downarrow}\right), \tag{6.9b}$$

with the pairing field $p = \sum m_{\boldsymbol{k}}$ and the renormalized potential U, which is derived from the T-matrix, and where $\Im$ indicates the imaginary part. The second equation for the pairing correlation can be evolved like the GP equation in Sec. 6.1.2. The first equation for the density,

however, is a density matrix equation, which does not evolve like a wave function. Density matrices evolve under two time-evolution operators called tetradics with positive and negative energies, such that the diagonal elements do not evolve at all. The conventional imaginary-time algorithm would thus not change the initial particle distribution function.

We here propose a new solution to finding the evolution of the density matrix equation by using the Bloch–Messiah at zero temperature.

Bloch–Messiah Theorem

In this Section, we use the Bloch–Messiah theorem [115, 116, 117] to find a relation between the density $f_{\boldsymbol{k}}$ and the pairing correlation $m_{\boldsymbol{k}}$ that we can use instead of the density-matrix equation to determine the evolution of $f_{\boldsymbol{k}}$.

We motivate the theorem by first discussing the Cauchy–Schwartz inequality. The inequality holds for any inner-product space and can be written in the usual bra-ket notation as

$$\langle\alpha|\alpha\rangle\langle\beta|\beta\rangle \geq |\langle\beta|\alpha\rangle|^2. \tag{6.10}$$

Choosing values for $|\alpha\rangle$ and $|\beta\rangle$, we can prove the following relation

$$\langle a^\dagger_{\boldsymbol{k}\uparrow} a_{\boldsymbol{k}\uparrow}\rangle\langle a_{-\boldsymbol{k}\downarrow} a^\dagger_{-\boldsymbol{k}\downarrow}\rangle \geq |\langle a_{-\boldsymbol{k}\downarrow} a_{\boldsymbol{k}\uparrow}\rangle|^2. \tag{6.11}$$

At zero temperature, this relation becomes an identity

$$f_{\boldsymbol{k}\uparrow}(1 - f_{\boldsymbol{k}\downarrow}) = |m^2_{\boldsymbol{k}}|, \tag{6.12}$$

as one can see from the quasi-particle vacuum relations Eqs. (6.3) and the properties of the Bogoliubov modes in Eq. (6.2). One can prove the identity in Eq. (6.12) at zero temperature for any set of evolution equations for which one can find a quasi-particle transformation. This is the Bloch–Messiah theorem. It can be generalized [118, 119] and extended to finite temperature [120, 121], and has also been discussed for Bosons [122, 123].

In order to be able to use Eq. (6.12) as planned, we have to assume spin symmetry

$$f_{\boldsymbol{k}\uparrow} = f_{\boldsymbol{k}\downarrow} = f_{\boldsymbol{k}}. \tag{6.13}$$

On closer examination, we note that the solution for $f_{\boldsymbol{k}}$ of Eq. (6.12) has two branches

$$f_{\boldsymbol{k}} = \frac{1}{2} + \mathrm{sgn}(\mu_{\mathrm{F}} - \epsilon_{\boldsymbol{k}})\sqrt{\frac{1}{4} - |m_{\boldsymbol{k}}|^2}. \tag{6.14}$$

The sign function here picks the positive branch for energies below the chemical potential and the negative branch for higher energies, as is the case for the BCS solutions given in Eqs. (6.3).

6.1.4 Imaginary-Time Algorithm for the Single-Channel Model

With these ingredients, we can now formulate the new algorithm for finding zero-temperature ground states in interacting fermion systems.

1. Pick an initial pairing correlation $m_{\boldsymbol{k}}$ and chemical potential μ_{F}.

2. Calculate the pairing field $p = \sum m_{\boldsymbol{k}}$ and the density $f_{\boldsymbol{k}}$ according to Eq. (6.14).

3. Evolve the anomalous density $m_{\boldsymbol{k}}$ for a time step $\mathrm{d}t$ in imaginary time using

$$\hbar\frac{\mathrm{d}m_{\boldsymbol{k}}}{\mathrm{d}t} = -2(\epsilon_{\boldsymbol{k}} - \mu_{\mathrm{F}})m_{\boldsymbol{k}} - Up\left(1 - f_{\boldsymbol{k}\uparrow} - f_{\boldsymbol{k}\downarrow}\right). \tag{6.15}$$

4. Repeat (2) and (3) until convergence.

5. Adjust chemical potential μ_{F} in (1) until total density $n = \sum_{\boldsymbol{k},\sigma} f_{\boldsymbol{k}\sigma}$ is correct.

We have verified numerically that this algorithm yields the BCS solution both for local and a Gaussian, non-local potential. One can, in fact, show analytically that the BCS equations are a solution to the imaginary-time equations. See Fig. 6.1 for the results for the local potential. Can we generalize this algorithm to the two-channel case?

6.1.5 Imaginary-Time Propagation for the Two-Channel Model

The two-channel model with contact interactions is equivalent to a single-channel model with non-local interactions. However, models with contact interactions are much easier computationally. We further show in the following Sections how we can extend the two-channel contact

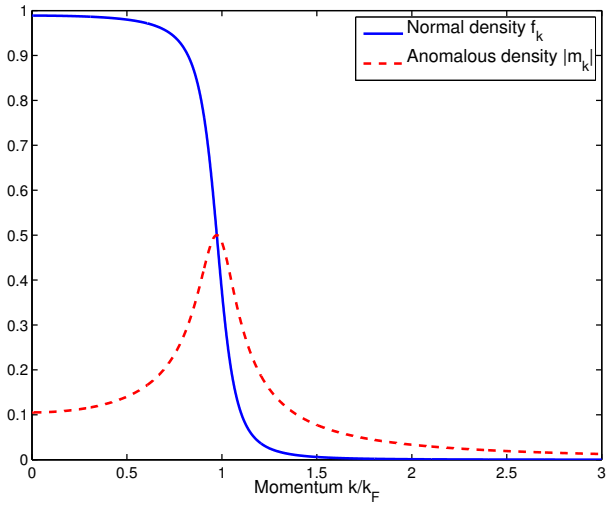

Figure 6.1: Normal (full line) and anomalous (dashed) density for a single-channel model at $k_{\mathrm{F}}a = -1$. The paired fermions predominantly occupy states near the Fermi energy.

model to sufficiently high-order correlations to properly reproduce the composite boson-boson scattering length. This extension is not feasible for the single-channel model with a contact interaction.

Two-Channel Equations of Motion

We begin by deriving the equations of motion of the relevant mean fields for the two-channel model. The crossover Hamiltonian for a homogeneous system is, again, given by

$$H = \sum_{\boldsymbol{k},\sigma=\uparrow,\downarrow} \epsilon_{\boldsymbol{k}}\, a^{\dagger}_{\boldsymbol{k}\sigma} a_{\boldsymbol{k}\sigma} + \sum_{\boldsymbol{q}} \Big(\frac{\epsilon_{\boldsymbol{q}}}{2} + \nu\Big) b^{\dagger}_{\boldsymbol{q}} b_{\boldsymbol{q}} + \sum_{\boldsymbol{q}\boldsymbol{k}} g_{\boldsymbol{k}} \Big(b^{\dagger}_{\boldsymbol{q}} a_{\boldsymbol{q}/2-\boldsymbol{k}\downarrow} a_{\boldsymbol{q}/2+\boldsymbol{k}\uparrow} + \mathrm{H.c.} \Big), \tag{6.16}$$

where we now have composite-boson fields $b_{\boldsymbol{q}}$ coupling to the fermions.

The minimal set of mean fields that we now have to derive equations of motion for is the anomalous density $m_{\boldsymbol{k}}$ and now also the condensate wave function $\phi_{\mathrm{m}} = \langle b_0 \rangle$. The normal density is again given by the Bloch–Messiah result in Eq. (6.14). We ignore the lowest-order thermal molecular mean fields $\langle\!\langle b^{\dagger}_{\boldsymbol{q}} b_{\boldsymbol{q}} \rangle\!\rangle \equiv \langle b^{\dagger}_{\boldsymbol{q}} b_{\boldsymbol{q}} \rangle - |\phi_{\mathrm{m}}|^2\, \delta_{\boldsymbol{q}0}$ and $\langle\!\langle b_{-\boldsymbol{q}} b_{\boldsymbol{q}} \rangle\!\rangle \equiv \langle b_{-\boldsymbol{q}} b_{\boldsymbol{q}} \rangle - \phi^2_{\mathrm{m}}\, \delta_{\boldsymbol{q}0}$, which neglects the quantum depletion of the molecular condensate. Note that there is no thermal depletion, since we only consider zero-temperature ground states.

To derive the equations of motion for the relevant mean fields, we first write the Heisen-

berg equations of motion for the three individual operators

$$i\hbar\frac{\mathrm{d}a_{\boldsymbol{k}\uparrow}}{\mathrm{d}t} = \epsilon_{\boldsymbol{k}} a_{\boldsymbol{k}\uparrow} + \sum_{\boldsymbol{q}} g_{-\boldsymbol{q}/2+\boldsymbol{k}} a^{\dagger}_{\boldsymbol{q}-\boldsymbol{k}\downarrow} b_{\boldsymbol{q}}, \tag{6.17a}$$

$$i\hbar\frac{\mathrm{d}a_{\boldsymbol{k}\downarrow}}{\mathrm{d}t} = \epsilon_{\boldsymbol{k}} a_{\boldsymbol{k}\downarrow} - \sum_{\boldsymbol{q}} g_{\boldsymbol{q}/2-\boldsymbol{k}} a^{\dagger}_{\boldsymbol{q}-\boldsymbol{k}\uparrow} b_{\boldsymbol{q}}, \quad \text{and} \tag{6.17b}$$

$$i\hbar\frac{\mathrm{d}b_{\boldsymbol{q}}}{\mathrm{d}t} = \Big(\frac{\epsilon_{\boldsymbol{q}}}{2} + \nu\Big) b_{\boldsymbol{q}} + \sum_{\boldsymbol{k}} g_{\boldsymbol{k}} a_{\boldsymbol{q}/2-\boldsymbol{k}\downarrow} a_{\boldsymbol{q}/2+\boldsymbol{k}\uparrow}. \tag{6.17c}$$

We then take the average of Eq. (6.17c) to obtain the equation of motion for the condensate wave function ϕ_{m}

$$i\hbar\frac{\mathrm{d}\phi_{\mathrm{m}}}{\mathrm{d}t} = \nu\phi_{\mathrm{m}} + g\sum_{\boldsymbol{k}} m_{\boldsymbol{k}} = \nu\phi_{\mathrm{m}} + gp. \tag{6.18}$$

We similarly combine Eqs. (6.17a) and (6.17b) to obtain the equation of motion for the anomalous density $m_{\boldsymbol{k}}$

$$i\hbar\frac{\mathrm{d}m_{\boldsymbol{k}}}{\mathrm{d}t} = 2\epsilon_{\boldsymbol{k}}\, m_{\boldsymbol{k}} + g\phi_{\mathrm{m}}\left(1 - f_{\boldsymbol{k}\uparrow} - f_{\boldsymbol{k}\downarrow}\right) - 2g\sum_{\boldsymbol{q}} \left\langle\!\!\left\langle b_{\boldsymbol{q}} a^{\dagger}_{\boldsymbol{q}+\boldsymbol{k}\uparrow} a_{\boldsymbol{k}\uparrow}\right\rangle\!\!\right\rangle. \tag{6.19}$$

This equation for the anomalous density $m_{\boldsymbol{k}}$ couples to the three-operator cumulant $\left\langle\!\!\left\langle ba^{\dagger}a\right\rangle\!\!\right\rangle$. The cumulant notation again indicates that the lower-order factorized averages have been subtracted out. We drop this cumulant for now, but in Sec. 6.2 we discuss its importance for reproducing the correct molecule-molecule scattering length on the BEC side of the crossover.

With these two equations of motion (6.18) and (6.19), we can now update the algorithm for the steepest-descent method.

Imaginary-Time Algorithm for the Two-Channel Model

The algorithm now has two coupled wave functions that need to be evolved.

1. Pick an initial pairing correlation $m_{\boldsymbol{k}}$, condensate wave function ϕ_{m}, and chemical potential μ_{F}.

2. Calculate the pairing field $p = \sum m_{\boldsymbol{k}}$ and the density $f_{\boldsymbol{k}}$ according to Eq. (6.14).

3. Evolve the anomalous density $m_{\boldsymbol{k}}$ and condensate wave function ϕ_{m} for a time step $\mathrm{d}t$

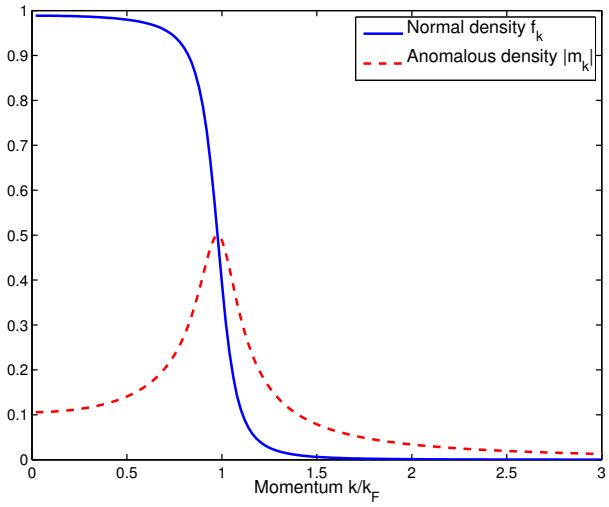

Figure 6.2: Normal (full line) and anomalous (dashed) density for a two-channel model at $k_\mathrm{F}a = -1$. This is calculated for the broad resonance in ^{6}Li at 834 G, with a bare molecular fraction of $4 \cdot 10^{-6}$ [124]. One can see the good agreement with the single-channel result in Fig. 6.1 in the broad resonance limit.

in imaginary time using

$$\hbar \frac{\mathrm{d}\phi_\mathrm{m}}{\mathrm{d}t} = -(\nu - 2\mu_\mathrm{F})\phi_\mathrm{m} - gp \quad \text{and} \tag{6.20a}$$

$$\hbar \frac{\mathrm{d}m_{\boldsymbol{k}}}{\mathrm{d}t} = -2(\epsilon_{\boldsymbol{k}} - \mu_\mathrm{F})m_{\boldsymbol{k}} - g\phi_\mathrm{m}\left(1 - f_{\boldsymbol{k}\uparrow} - f_{\boldsymbol{k}\downarrow}\right). \tag{6.20b}$$

4. Repeat (2) and (3) until convergence.

5. Adjust chemical potential μ_F in (1) until total density $n = \sum_{\boldsymbol{k},\sigma} f_{\boldsymbol{k}\sigma} + 2|\phi_\mathrm{m}|^2$ is correct.

In Fig. 6.2, we show results for this algorithm for a contact two-channel model. They look very similar to the ones we found in the single-channel case in Fig. 6.1. Is that what we would expect? The superfluid gaps of both theories turn out to be the same

$$\Delta = Up = g\phi_\mathrm{m}. \tag{6.21}$$

However, the number equations are slightly different. In the single-channel case discussed in Sec. 6.1.3, only the dressed fermions are summed over

$$n_\mathrm{1C} = \sum_{\boldsymbol{k}\sigma} f_{\boldsymbol{k}\sigma}, \tag{6.22}$$

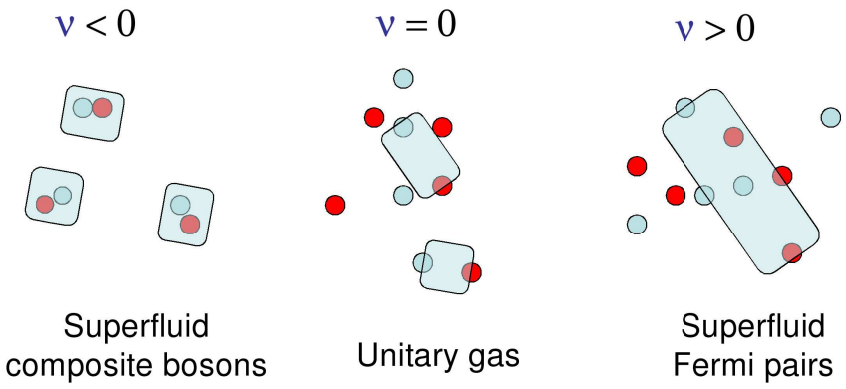

Figure 6.3: Schematic illustrating the crossover between fermions, whose interactions can be described by BCS theory with scattering length a, and composite bosonic molecules, with interactions given by $0.6a$, as a function of detuning $\bar{\nu}$, that is, magnetic field.

whereas, in the two-channel case, both the bare fermions and bare molecules contribute to the total fermion density

$$n_{2C} = \sum_{\boldsymbol{k}\sigma} f_{\boldsymbol{k}\sigma} + 2|\phi_m|^2. \tag{6.23}$$

Each molecule contributes two fermions to the total density. This difference results in a correction to the chemical potential μ_F; a small correction in the broad-resonance case.

6.2 A Mean-Field Description for the Crossover Problem

In this Section, we want to determine the minimal ingredients for a mean-field theory that wants to correctly reproduce the molecule-molecule scattering between composite bosons on the BEC side of the resonance. Consider first a schematic picture of the crossover in Fig. 6.3. The picture shows how the overlapping, loosely bound Cooper pairs on the right side of the resonance contract as the detuning is lowered and changes sign. On the BEC side, at negative detuning, the pairs turn into tightly bound molecules, which are interacting with a molecule-molecule scattering length of approximately $0.6a$ [125], where a is the atom-atom scattering length.

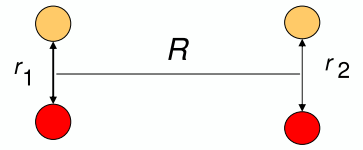

Figure 6.4: Schematic of the interaction between two dimers of paired fermions.

6.2.1 Boson Scattering Length

To find an expression for the dimer-dimer scattering length a_{dd}, which is the effective interaction of the composite bosonic molecules, Petrov et al. [125] start with a four-body Schrödinger equation in the set of coordinates defined in Fig. 6.4,

$$\begin{aligned} -\left(\nabla^2_{\boldsymbol{r}_1}+\nabla^2_{\boldsymbol{r}_2}+\frac{1}{2}\nabla^2_{\boldsymbol{R}}+\frac{mE}{\hbar^2}\right)\Psi = \\ -\frac{m}{\hbar^2}\left(U(\boldsymbol{r}_1)+U(\boldsymbol{r}_2)+\sum_{\pm}U\left(\frac{\boldsymbol{r}_1+\boldsymbol{r}_2}{2}\pm\boldsymbol{R}\right)\right)\Psi, \end{aligned} \tag{6.24}$$

where $U(\boldsymbol{r})$ is the two-body potential in real space. This equation is simplified by assuming a pseudopotential boundary condition

$$\Psi(\boldsymbol{r}_1,\boldsymbol{r}_2,\boldsymbol{R}) \overset{\boldsymbol{r}_1\to 0}{\longrightarrow} f(\boldsymbol{r}_2,\boldsymbol{R})\left(\frac{1}{r_1}-\frac{1}{a}\right), \tag{6.25}$$

which is valid, because the effective range of the interatomic potential U is small compared to the scattering length a. The factor multiplying $f(\boldsymbol{r}_2,\boldsymbol{R})$ on the right-hand side of Eq. (6.25) is an expansion of the bound-state wave function $\exp(-r_1/a)/r_1$ near threshold. This boundary condition Eq. (6.25) implies that we do not need the full four-body wave function Ψ, which is six-dimensional in a homogeneous system, to describe the dimer-dimer scattering correctly. Instead, it suffices to solve for the reduced wave function $f(\boldsymbol{r}_2,\boldsymbol{R})$, which has only three independent dimensions in a homogeneous system. This simplification allowed the authors of [125] to solve the scattering equation (6.24) and find the dimer-dimer scattering length as $a_{\mathrm{dd}}\approx 0.6a$, a result that has been supported experimentally [126, 127, 28].

What is the physical meaning of the wave function $f(\boldsymbol{r}_2,\boldsymbol{R})$? The schematic in Fig. 6.5 depicts $f(\boldsymbol{r}_2,\boldsymbol{R})$ as an atom-molecule correlation function between a tightly bound dimer and

two loosely bound fermions. As we have seen in Sec. 6.1, this correlation function is not part of BCS theory or the lowest-order mean-field picture of the crossover we discussed in Sec. 6.1.5. We did, however, see in that Section how to extend the equations of motion: Equation (6.19) couples to a three-operator correlation function that is of the same vector structure as $f(\boldsymbol{r}_2, \boldsymbol{R})$. To extend the set of equations in Sec. 6.1.5, we would have to derive an equation of motion for the new correlation function $\langle\!\langle ba^\dagger a \rangle\!\rangle$. This correlation in turn couples to other three-operator correlation functions. We assume that we can drop all couplings to still higher-order correlations and solve the coupled three-operator equations. This yields a theory that includes the Hartree self-energy shift in the crossover and yields the observed dimer-dimer scattering length within our approximations as discussed above.

We may thus anticipate that one should be able to combine the quantity $f(\boldsymbol{r}_2, \boldsymbol{R})$ with the mean-field description of the crossover that we began to present in Sec. 6.1.5 to get a more complete picture of the crossover as presented in Table 6.1.

6.2.2 Beyond Pair Correlations

In the last Section, we learned that we need to include four-particle correlation functions in order find the correct value for the molecule-molecule interactions on the BEC side. Here, we want to revisit the single- and two-channel models discussed in the context of BCS theory in Sec. 6.1 and see how they can be extended to include these beyond-pair correlations.

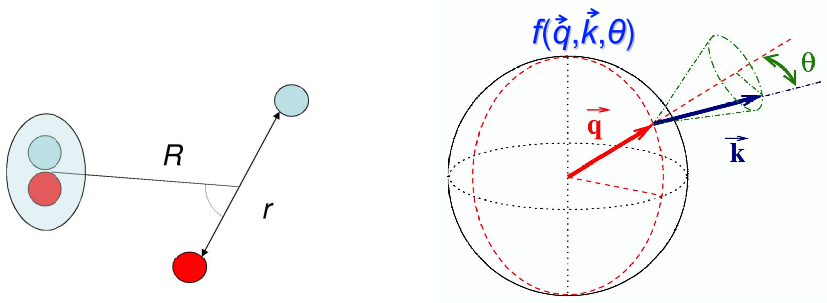

Figure 6.5: This atom-molecule correlation function is the minimum ingredient needed to recover the boson-boson scattering length for the composite molecules as $0.6a$. The schematic on the right shows the dimensionality of $f(\boldsymbol{r}_2, \boldsymbol{R})$ in momentum space.

Table 6.1: A more complete picture of the crossover

$\phi_{\rm m} = \langle b_0 \rangle$	BEC: Interactions mediated by fermions
$\Uparrow$	
$\langle\!\langle b_{-\boldsymbol{q}} a_{\boldsymbol{q}/2-\boldsymbol{k}\downarrow} a_{\boldsymbol{q}/2+\boldsymbol{k}\uparrow} \rangle\!\rangle$	Crossover
$\Downarrow$	
$m_{\boldsymbol{k}} = \langle a_{-\boldsymbol{k}\downarrow} a_{\boldsymbol{k}\uparrow} \rangle$	BCS: Interactions mediated by bosons

Four-Particle Correlations in the Single-Channel Model

The Hamiltonian of the single-channel model is

$$H = \sum_{\boldsymbol{k}\sigma} \epsilon_{\boldsymbol{k}} a^\dagger_{\boldsymbol{k}\sigma} a_{\boldsymbol{k}\sigma} + \sum_{\boldsymbol{q}\boldsymbol{k}\boldsymbol{k}'} U_{\boldsymbol{k}-\boldsymbol{k}'} a^\dagger_{\boldsymbol{q}/2+\boldsymbol{k}\uparrow} a^\dagger_{\boldsymbol{q}/2-\boldsymbol{k}\downarrow} a_{\boldsymbol{q}/2-\boldsymbol{k}'\downarrow} a_{\boldsymbol{q}/2+\boldsymbol{k}'\uparrow}. \tag{6.26}$$

The minimum necessary mean-field to include the required four-particle correlations in this model is

$$\langle\!\langle a_{-\boldsymbol{q}/2-\boldsymbol{k}\downarrow} a_{-\boldsymbol{q}/2+\boldsymbol{k}\uparrow} a_{\boldsymbol{q}/2-\boldsymbol{k}'\downarrow} a_{\boldsymbol{q}/2+\boldsymbol{k}'\uparrow} \rangle\!\rangle. \tag{6.27}$$

With this Hamiltonian, it is impossible to contract a fermion pair into a boson directly, so we have to treat all four particles explicitly. The four-particle correlation above is a function of three vectors, and thus has six degrees of freedom in a homogeneous system, which is numerically very difficult.

Four-Particle Correlations in the Two-Channel Model

Let us now see whether the two-channel model has an advantage in describing the necessary four-particle correlations. The Hamiltonian for this model is

$$H = \sum_{\boldsymbol{k},\sigma=\uparrow,\downarrow} \epsilon_{\boldsymbol{k}}\ a^\dagger_{\boldsymbol{k}\sigma} a_{\boldsymbol{k}\sigma} + \sum_{\boldsymbol{q}} \Big(\frac{\epsilon_{\boldsymbol{q}}}{2} + \nu \Big) b^\dagger_{\boldsymbol{q}} b_{\boldsymbol{q}} + g \sum_{\boldsymbol{q}\boldsymbol{k}} \Big(b^\dagger_{\boldsymbol{q}} a_{\boldsymbol{q}/2-\boldsymbol{k}\downarrow} a_{\boldsymbol{q}/2+\boldsymbol{k}\uparrow} + \text{H.c.} \Big), \tag{6.28}$$

which shows that this model contains composite molecules explicitly. The minimum correlation function to include four-particle interactions is now

$$\langle\!\langle b_{-\boldsymbol{q}} a_{\boldsymbol{q}/2-\boldsymbol{k}\downarrow} a_{\boldsymbol{q}/2+\boldsymbol{k}\uparrow} \rangle\!\rangle, \tag{6.29}$$

which is a function of only two momentum vectors. The dimensionality of this correlation function is thus only three in a homogeneous system, which is directly accessible in numerical calculations.

The two-channel model thus gives naturally a minimal description that is at this level of approximation consistent with the vacuum scattering properties of four-particle scattering discussed in Sec. 6.2.1.

6.3 Summary

Atomic physics has provided a wealth of information on a variety of aspects of superfluidity, both in bosonic and fermionic systems. We have presented the foundation concepts of superfluids, and discussed the vortices which support rotation in superfluid systems. We have shown how the separation of scales, both in energy and in physical space, lead to a simplified parametrization of the interaction effects in dilute quantum gases. Of particular interest has been Feshbach resonances, which allow the collision effects to be resonantly enhanced.

We have shown that for two fermions in vacuum, one is able to prove the equivalence between the two-channel approach which arises naturally in the description of Feshbach resonances, and the single-channel approach which is a typical starting point for condensed matter theories. We should emphasize here that in the case of a many-body system, the single-channel and two-channel theories do not generally coincide if simple contact potentials are chosen.

The description of Feshbach resonances in dilute atomic gases has required the development of a many-body theory able to describe strong correlations and specifically the point of infinite scattering length. Careful consideration must therefore be made of the breakdown of simple mean-field approaches which contain the scattering length explicitly. We have shown how one may include the two-channel Feshbach formulation in the many-body Hamiltonian. This problem is relevant to the theoretical description of many current experimental efforts, exploring the formation and dissociation of molecules around Feshbach resonances, and the crossover from

fermionic to bosonic superfluidity.

Chapter 7

Zero-Temperature Correlation Effects the BCS–BEC Crossover

In this Chapter, we formulate a many-body mean-field theory of the BCS–BEC crossover problem. In particular, we want to extend the imaginary-time method presented in Chap. 6 to go beyond pair correlations. Figure 7.1 shows the deviation between an experiment in the Jin group at JILA [129] and a theory that is calculated to include only pair correlations [128]. Including higher-order correlations, beginning with the Hartree term, might remedy this discrepancy.

We first need a suitable description of correlations and introduce the notion of a cumulant

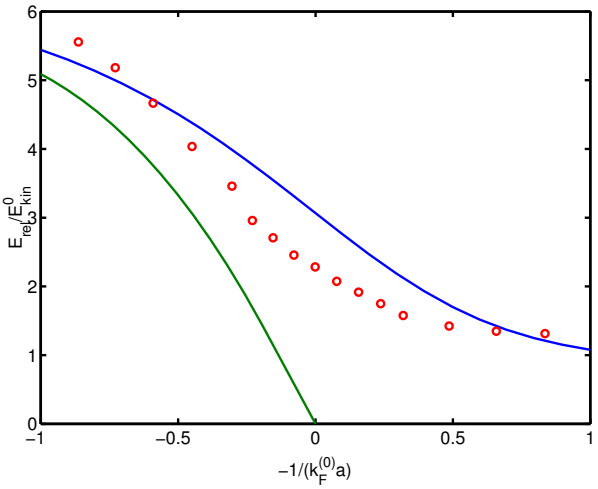

Figure 7.1: Released energy of a harmonically trapped gas as a function of the detuning $-1/(k_{\rm F}^0 a(0))$ for a ramp rate of 2μs/G (blue line) [128]. The red circles are the experimental results from Ref. [129]. The blue theory line is calculated with pair correlations only. The lower, green line is the corresponding result solving the two-body problem associated with the molecular state. The energy is normalized to the kinetic energy of the non-interacting gas $E^0_{\rm kin} = 3\epsilon^0_{\rm F}/8$.

mean field, which is a many-particle correlation function. The order of a cumulant is given by the number of particles—more precisely, the number of operators— involved. The equations of motion for cumulants form a hierarchy, because the evolution of a cumulant of order n is dependent on lower-order cumulants and only the cumulant of order $n+1$. In a dilute system, this Bogoliubov–Born–Green–Kirkwood–Yvon (BBGKY) hierarchy can be cut, because higher-order correlations rapidly dampen between subsequent two-body collisions [33, 29]. This cut of the hierarchy gives a closed set of coupled equations, which can be simplified further by adiabatically eliminating the remaining highest-order cumulants using a secular approximation. We show how this elimination renormalizes the detuning as previously discussed in Chap. 5. This renormalization removes the cutoff dependence of the bare detuning and relates it to the applied magnetic field in the experiments.

We present two examples for this method of cumulant expansion using the two-channel BCS–BEC crossover Hamiltonian Eq. (5.8):

1. Condensed bosonic molecules and fermions interacting at zero temperature. In this case, we use the imaginary-time methods discussed in the preceding Chap. 6.

2. Thermal bosons and fermions interacting in the normal phase, that is, above the critical temperature, as discussed in the following Chap. 8. We show how the cumulant expansion gives rise to rate equations similar to those found by Williams et al. [130, 131].

We begin by defining the type of correlation function we use to derive the BBGKY hierarchy.

7.1 Cumulants

A cumulant expansion is a systematic way of classifying correlation functions of different orders [132, 133, 134, 74]. The order of a cumulant is given by the number of operators involved, that is, the number of operators in the correlation function. Cumulants are essentially expectation values of operators, where the lower-order contributions, which can be obtained by

factorization, are removed. We have already encountered several of these correlation functions for composite bosons $b_{\boldsymbol{q}}$ and fermions $a_{\boldsymbol{k}\uparrow\downarrow}$ in a homogeneous system:

$$\text{Bare molecular wave function} \quad \phi_{\mathrm{m}} = \langle b_0 \rangle. \tag{7.1}$$

$$\text{Fermion density} \quad f_{\boldsymbol{k}\uparrow} = \langle a^\dagger_{\boldsymbol{k}\uparrow} a_{\boldsymbol{k}\uparrow} \rangle. \tag{7.2}$$

$$\text{Pairing correlation} \quad m_{\boldsymbol{k}} = \langle a_{-\boldsymbol{k}\downarrow} a_{\boldsymbol{k}\uparrow} \rangle. \tag{7.3}$$

These lowest-order correlation functions are just given by the thermal average, because they do not factorize. The single-operator averages for fermions vanish, since macroscopic occupation of a single state is not possible for fermions, that is, they do not Bose–Einstein condense. We here use a symmetry-breaking approach as discussed in [135, 136], where it is shown that this approach can be rigorously justified for Bose–Einstein condensed systems. Alternative number-conserving approaches [137, 138, 139, 78] yield equivalent results, but may differ in the formal details.

A simple example of an actual cumulant is the density of thermal molecules:

$$\left\langle\!\left\langle b^\dagger_{\boldsymbol{q}} b_{\boldsymbol{q}} \right\rangle\!\right\rangle = \langle b^\dagger_{\boldsymbol{q}} b_{\boldsymbol{q}} \rangle - |\phi_{\mathrm{m}}|^2 \, \delta_{\boldsymbol{q}0}, \tag{7.4}$$

where δ is the Kronecker delta function. Here, the average $\langle b^\dagger_{\boldsymbol{q}} b_{\boldsymbol{q}} \rangle$ contains the factorizable component $|\phi_{\mathrm{m}}|^2$, which gets subtracted out in the case of zero momentum to define the two-boson cumulant $\left\langle\!\left\langle b^\dagger_{\boldsymbol{q}} b_{\boldsymbol{q}} \right\rangle\!\right\rangle$. The pairing function of the molecules is analogously given by:

$$\left\langle\!\left\langle b_{-\boldsymbol{q}} b_{\boldsymbol{q}} \right\rangle\!\right\rangle = \langle b_{-\boldsymbol{q}} b_{\boldsymbol{q}} \rangle - \phi^2_{\mathrm{m}} \, \delta_{\boldsymbol{q}0}. \tag{7.5}$$

A more complicated three-operator correlation between a boson and a pair of fermions is

$$\left\langle\!\left\langle b_{\boldsymbol{q}} a^\dagger_{\boldsymbol{q}+\boldsymbol{k}\uparrow} a_{\boldsymbol{k}\uparrow} \right\rangle\!\right\rangle = \langle b_{\boldsymbol{q}} a^\dagger_{\boldsymbol{q}+\boldsymbol{k}\uparrow} a_{\boldsymbol{k}\uparrow} \rangle - \phi_{\mathrm{m}} f_{\boldsymbol{k}} \, \delta_{\boldsymbol{q}0}. \tag{7.6}$$

The following four-fermion average contains two lower-order contributions, which have to be removed to define the cumulant

$$\left\langle\!\left\langle a^\dagger_{\boldsymbol{q}/2+\boldsymbol{k}\uparrow} a^\dagger_{\boldsymbol{q}/2-\boldsymbol{k}\downarrow} a_{\boldsymbol{q}/2-\boldsymbol{k}'\downarrow} a_{\boldsymbol{q}/2+\boldsymbol{k}'\uparrow} \right\rangle\!\right\rangle = \langle a^\dagger_{\boldsymbol{q}/2+\boldsymbol{k}\uparrow} a^\dagger_{\boldsymbol{q}/2-\boldsymbol{k}\downarrow} a_{\boldsymbol{q}/2-\boldsymbol{k}'\downarrow} a_{\boldsymbol{q}/2+\boldsymbol{k}'\uparrow} \rangle \tag{7.7}$$

$$- m^*_{\boldsymbol{k}} m_{\boldsymbol{k}'} \, \delta_{\boldsymbol{q}0} - f_{\boldsymbol{k}'\uparrow} f_{-\boldsymbol{k}\downarrow} \, \delta_{\boldsymbol{q}0}. \tag{7.8}$$

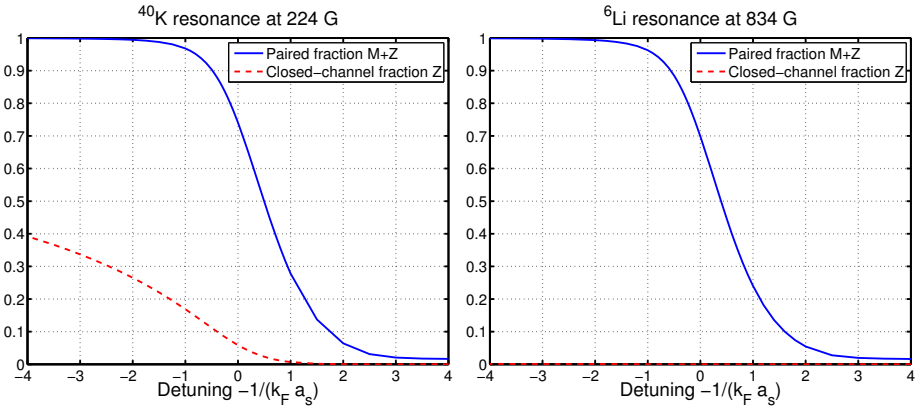

Figure 7.2: Pair fractions of the total fermion number for the resonance at 224.2 G in ^{40}K (left) and the wide resonance at 843 G in ^{6}Li (right).

To apply the cumulant method, we discuss the extension of the imaginary-time propagation method for finding zero-temperature ground states presented in Chap. 6 to include higher-order correlations. We begin by discussing some results we obtained for our two-channel model.

7.2 Pairs in the BCS–BEC Crossover

In a two-channel model, pairing takes place both in the open and closed scattering channels. However, the closed- ($Z = 2|\phi_{\mathrm{m}}|^2$) and open-channel ($M = 2\sum_{\boldsymbol{k}} |m_{\boldsymbol{k}}|^2$) contributions in Fig. 7.2 are just projections of the physical molecular bound state onto the Feshbach subspaces. In the case of ^{6}Li on the right side of the Figure, it seems that the closed-channel contribution is very small and thus insignificant. Remember, however, that with our model Hamiltonian (5.8) the fermions do not interact directly. The pairing in the open channel is thus only due to the small closed-channel contribution. Furthermore, the closed-channel part of the ^{6}Li has actually been observed, as can be seen in Fig. 7.3. The experiment measures the photoexcitation rate of the singlet closed-channel bound state to a free state [124]. The open-channel pairs are in a triplet state, and thus do not get excited. The agreement of our zero-temperature simulation with the experimental points is very good on the BEC side of the resonance (left), which indicates that neglecting thermal molecules is a good approximation. On the BCS side (right),

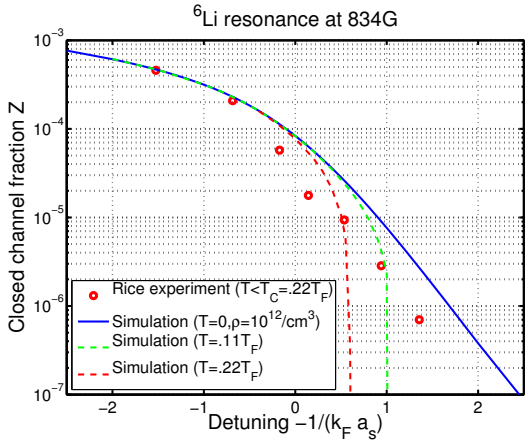

Figure 7.3: Closed-channel fraction for the wide resonance in ^{6}Li [124].

finite-temperature effects are more important for reducing the closed-channel fraction, as our finite-temperature results show. Finite temperature effects can thus account for the discrepancy between zero-temperature theory and experiment. Note in particular that the finite-temperature theory lines coincide with the zero-temperature results on the BEC side. We use a generalization of the imaginary-time procedure using an equilibrium distribution for the excited quasiparticle states. The self-energy operator defining the quasiparticle states can include the Hartree and Bose mean-field corrections discussed below, and we can derive a quantum-Boltzmann equation for the quasiparticles, along the lines of Chap. 4.

7.3 Mean Fields

The model we consider for the imaginary-time algorithm is a homogeneous system at zero temperature with symmetrically populated spins up and down. There is no pairing within each spin state, because s-wave interactions are suppressed. We thus use the following set of

elementary mean-field correlation functions:

$$\text{Bare molecular wave function} \quad \phi_{\mathrm{m}} = \langle b_0 \rangle, \tag{7.9}$$

$$\text{Fermion density} \quad f_{\boldsymbol{k}\uparrow} = \langle a^\dagger_{\boldsymbol{k}\uparrow} a_{\boldsymbol{k}\uparrow} \rangle = f_{\boldsymbol{k}\downarrow} \qquad \text{(spin symmetry)}, \tag{7.10}$$

$$\text{Pairing correlation} \quad m_{\boldsymbol{k}} = \langle a_{-\boldsymbol{k}\downarrow} a_{\boldsymbol{k}\uparrow} \rangle. \tag{7.11}$$

We also neglect the following correlation functions:

$$\text{Cross-level magnetization} \quad \langle a^\dagger_{\boldsymbol{k}\uparrow} a_{\boldsymbol{k}\downarrow} \rangle = 0, \tag{7.12}$$

$$\text{Pairing for equal spins} \quad \langle a_{-\boldsymbol{k}\sigma} a_{\boldsymbol{k}\sigma} \rangle = 0 \qquad \text{(no } s\text{-wave pairing for fermions)}, \tag{7.13}$$

$$\text{Thermal molecules} \quad \langle\!\langle b^\dagger_{\boldsymbol{q}} b_{\boldsymbol{q}} \rangle\!\rangle = \langle\!\langle b_{-\boldsymbol{q}} b_{\boldsymbol{q}} \rangle\!\rangle = 0 \qquad \text{(zero temperature)}. \tag{7.14}$$

The number of particles is fixed by the following density equation

$$n_{\mathrm{tot}} = \sum_{\boldsymbol{k}\sigma} f_{\boldsymbol{k}\sigma} + 2|\phi_{\mathrm{m}}|^2, \tag{7.15}$$

where the momentum sums are spherically symmetric and evaluated as follows

$$\sum_{\boldsymbol{k}} F(k) = \frac{1}{2\pi^2} \int k^2 F(k)\, dk. \tag{7.16}$$

The next Section shows how these sets couple to higher-order cumulants, and how we obtain closed equations for the above mean fields by adiabatic elimination.

7.4 Equations of Motion

In this Section, we show how to obtain closed equations for the mean fields listed in Sec. 7.3 by adiabatically eliminating three- and four-operator cumulants. Figure 7.4 schematically shows the BBGKY hierarchy of correlation functions, which we cut by dropping the coupling to five-operator correlation functions. This amounts to a kinetic approximation, which is valid in a dilute system, where the inter-particle distance $n^{-1/3}$ is small compared to the range of the two-body potential r_0,

$$n r_0^3 \ll 1, \tag{7.17}$$

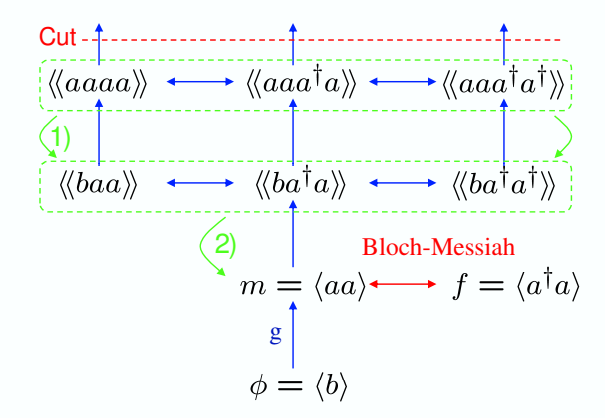

Figure 7.4: Schematic of the cumulant hierarchy. We cut the coupling to five-operator cumulants and adiabatically eliminate the steady-state solutions at levels 1) and 2) to obtain a closed equation for the pair correlation $m_{\boldsymbol{k}}$.

and many-particle correlations can thus decay between collisions. The first elimination step 1) of the four-operator cumulants introduces the renormalization of the detuning $\bar{\nu}$. The second elimination 2) of the resulting three-operator equations yields an updated equation for the pair function $m_{\boldsymbol{k}}$ including the Hartree and higher-order interaction terms.

We begin by repeating the coupled equations for the molecular wave function ϕ_{m} (6.18) and the pair function $m_{\boldsymbol{k}}$ (6.19), which we have derived from the Heisenberg equations (6.17) previously:

$$i\hbar \frac{\mathrm{d}\phi_{\mathrm{m}}}{\mathrm{d}t} = \nu\phi_{\mathrm{m}} + g\sum_{\boldsymbol{k}} m_{\boldsymbol{k}} \tag{7.18}$$

$$i\hbar \frac{\mathrm{d}m_{\boldsymbol{k}}}{\mathrm{d}t} = 2\epsilon_{\boldsymbol{k}}\, m_{\boldsymbol{k}} + g\phi_{\mathrm{m}}\left(1 - f_{\boldsymbol{k}\uparrow} - f_{\boldsymbol{k}\downarrow}\right) - 2g\sum_{\boldsymbol{q}} \left\langle\!\left\langle b_{\boldsymbol{q}} a^\dagger_{\boldsymbol{q}+\boldsymbol{k}\uparrow} a_{\boldsymbol{k}\uparrow} \right\rangle\!\right\rangle \tag{7.19}$$

The normal density is again calculated from the Bloch-Messiah theorem [140, 141]:

$$f_{\boldsymbol{k}\uparrow}(1 - f_{\boldsymbol{k}\downarrow}) = |m_{\boldsymbol{k}}|^2. \tag{7.20}$$

The pair correlation $m_{\boldsymbol{k}}$ couples to the three-operator cumulant $\left\langle\!\left\langle b_{\boldsymbol{q}} a^\dagger_{\boldsymbol{q}+\boldsymbol{k}\uparrow} a_{\boldsymbol{k}\uparrow} \right\rangle\!\right\rangle$, whose

equation of motion,

$$i\hbar\frac{\mathrm{d}\langle\!\langle b_{\boldsymbol{q}}a^{\dagger}_{\boldsymbol{q}+\boldsymbol{k}\uparrow}a_{\boldsymbol{k}\uparrow}\rangle\!\rangle}{\mathrm{d}t} = \Big(\nu - 2\epsilon_{\boldsymbol{q}/2+\boldsymbol{k}} + 2\epsilon_{\boldsymbol{k}}\Big)\langle\!\langle b_{\boldsymbol{q}}a^{\dagger}_{\boldsymbol{q}+\boldsymbol{k}\uparrow}a_{\boldsymbol{k}\uparrow}\rangle\!\rangle - g\; f_{\boldsymbol{q}+\boldsymbol{k}\uparrow}\; m_{\boldsymbol{k}} + g\sum_{\boldsymbol{k}'}\langle\!\langle a_{\boldsymbol{q}/2-\boldsymbol{k}'\downarrow}a_{\boldsymbol{q}/2+\boldsymbol{k}'\uparrow}a^{\dagger}_{\boldsymbol{q}+\boldsymbol{k}\uparrow}a_{\boldsymbol{k}\uparrow}\rangle\!\rangle - g\phi^{*}_{\mathrm{m}}\langle\!\langle b_{\boldsymbol{q}}a_{-\boldsymbol{k}-\boldsymbol{q}\downarrow}a_{\boldsymbol{k}\uparrow}\rangle\!\rangle + g\phi_{\mathrm{m}}\langle\!\langle b_{\boldsymbol{q}}a^{\dagger}_{\boldsymbol{q}+\boldsymbol{k}\uparrow}a^{\dagger}_{-\boldsymbol{k}\downarrow}\rangle\!\rangle, \tag{7.21}$$

is also derived from the Heisenberg equations (6.17). The equation of motion for the three-operator correlation again couples up to the next order. We have, however, already dropped the coupling to the four-operator correlation $\langle\!\langle bb^{\dagger}aa\rangle\!\rangle$, because this correlation function does not contribute to the four-fermion scattering problem. In writing the following equation for the other required four-operator correlation function we cut the BBGKY hierarchy and drop the coupling to five-operator correlations:

$$i\hbar\frac{\mathrm{d}}{\mathrm{d}t}\langle\!\langle a_{\boldsymbol{q}/2-\boldsymbol{k}'\downarrow}a_{\boldsymbol{q}/2+\boldsymbol{k}'\uparrow}a^{\dagger}_{\boldsymbol{q}+\boldsymbol{k}\uparrow}a_{\boldsymbol{k}\uparrow}\rangle\!\rangle \tag{7.22}$$

$$= (-2\epsilon_{\boldsymbol{q}/2+\boldsymbol{k}} + 2\epsilon_{\boldsymbol{k}} + 2\epsilon_{\boldsymbol{k}'})\langle\!\langle a_{\boldsymbol{q}/2-\boldsymbol{k}'\downarrow}a_{\boldsymbol{q}/2+\boldsymbol{k}'\uparrow}a^{\dagger}_{\boldsymbol{q}+\boldsymbol{k}\uparrow}a_{\boldsymbol{k}\uparrow}\rangle\!\rangle \tag{7.23}$$

$$+ g\langle\!\langle b_{\boldsymbol{q}}a^{\dagger}_{\boldsymbol{q}+\boldsymbol{k}\uparrow}a_{\boldsymbol{k}\uparrow}\rangle\!\rangle \tag{7.24}$$

$$= 2\mu\langle\!\langle a_{\boldsymbol{q}/2-\boldsymbol{k}'\downarrow}a_{\boldsymbol{q}/2+\boldsymbol{k}'\uparrow}a^{\dagger}_{\boldsymbol{q}+\boldsymbol{k}\uparrow}a_{\boldsymbol{k}\uparrow}\rangle\!\rangle. \tag{7.25}$$

We also neglect all many-body terms proportional to the normal density and pair function and only keep two-body terms, because the two-body terms dominate in the high-momentum limit that is important for the renormalization. We set the time-derivative on the left-hand side equal to a global phase given by the steady-state energy 2μ, which is determined by the number of creation and destruction operators. Each fermion creation operator evolves with $-\mu$ and each destruction operator with μ, which results in the 2μ given above. The boson operators each evolve with 2μ, respectively. The steady-state energy 2μ is constrained by the total number. If we included correlations to all orders and were in full thermodynamic equilibrium, μ would be the chemical potential of the fermions. Since we cut the correlation hierarchy, we need to explicitly examine the change in energy as a particle is added to find the chemical potential [142].

This steady-state approximation allows us to adiabatically eliminate the four-operator

correlation as

$$\left\langle\!\left\langle a_{\boldsymbol{q}/2-\boldsymbol{k}'\downarrow} a_{\boldsymbol{q}/2+\boldsymbol{k}'\uparrow} a^\dagger_{\boldsymbol{q}+\boldsymbol{k}\uparrow} a_{\boldsymbol{k}\uparrow} \right\rangle\!\right\rangle = -\frac{g}{\Delta E} \left\langle\!\left\langle b_{\boldsymbol{q}} a^\dagger_{\boldsymbol{q}+\boldsymbol{k}\uparrow} a_{\boldsymbol{k}\uparrow} \right\rangle\!\right\rangle, \tag{7.26}$$

where the energy denominator is given by

$$\Delta E = -2\mu - 2\epsilon_{\boldsymbol{q}/2+\boldsymbol{k}} + 2\epsilon_{\boldsymbol{k}} + 2\epsilon_{\boldsymbol{k}'}. \tag{7.27}$$

We can substitute this result (7.26) into the full equation for the three-operator correlation (7.21) and find that the new term enters the kinetic energy.

$$\begin{aligned} i\hbar \frac{\mathrm{d}\left\langle\!\left\langle b_{\boldsymbol{q}} a^\dagger_{\boldsymbol{q}+\boldsymbol{k}\uparrow} a_{\boldsymbol{k}\uparrow} \right\rangle\!\right\rangle}{\mathrm{d}t} &= \Big(\nu - \mathcal{P}\sum_{\boldsymbol{k}'} \frac{g^2}{\Delta E} - 2\epsilon_{\boldsymbol{q}/2+\boldsymbol{k}} + 2\epsilon_{\boldsymbol{k}}\Big) \left\langle\!\left\langle b_{\boldsymbol{q}} a^\dagger_{\boldsymbol{q}+\boldsymbol{k}\uparrow} a_{\boldsymbol{k}\uparrow} \right\rangle\!\right\rangle \\ &\quad - g\, f_{\boldsymbol{q}+\boldsymbol{k}\uparrow}\, m_{\boldsymbol{k}} - g\phi^*_{\mathrm{m}} \left\langle\!\left\langle b_{\boldsymbol{q}} a_{-\boldsymbol{k}-\boldsymbol{q}\downarrow} a_{\boldsymbol{k}\uparrow} \right\rangle\!\right\rangle + g\phi_{\mathrm{m}} \left\langle\!\left\langle b_{\boldsymbol{q}} a^\dagger_{\boldsymbol{q}+\boldsymbol{k}\uparrow} a^\dagger_{-\boldsymbol{k}\downarrow} \right\rangle\!\right\rangle. \end{aligned} \tag{7.28}$$

We here only keep the real principal-part contribution according to the relation

$$\frac{1}{\Delta E + i\epsilon} = \mathcal{P}\frac{1}{\Delta E} - i\pi\delta(\Delta E). \tag{7.29}$$

In Appendix E, we demonstrate in the normal phase how the imaginary delta-function terms give rise to the collisional quantum-Boltzmann rates, which determine equilibrium. This allows us to define a diagonal quasiparticle representation for fermions and composite bosons, which can be used to prove the Bloch-Messiah theorem Eq. (7.20).

The new term in Eq. (7.28) renormalizes the bare detuning ν to the physical value

$$\bar{\nu} = \nu - \mathcal{P}\sum_{\boldsymbol{k}'} \frac{g^2}{2\epsilon_{\boldsymbol{k}'}} = \nu - g^2 \frac{4\pi}{8\pi^3} \mathcal{P}\int_0^K \frac{mk'^2}{\hbar^2 k'^2} dk' = \nu - \frac{mK}{2\pi^2\hbar^2} g^2, \tag{7.30}$$

as discussed in Sec. 5.4.

Adiabatically eliminating the coupling to the four-operator cumulant thus updates the bare detuning ν to the renormalized physical detuning $\bar{\nu}$. This happens analogously in the equations for all three-operator correlation functions.

7.5 Adiabatic Elimination of Three-Operator Correlations

We now continue by further eliminating the three-operator correlations, in order to obtain closed equations for the pairing function and molecular mean field. At first, we only keep terms to

order g^2 to illustrate the lowest-order corrections. We start by finding the steady-state solution of Eq. (7.28),

$$E_1 \left\langle\!\left\langle b_{\boldsymbol{q}} a^\dagger_{\boldsymbol{q}+\boldsymbol{k}\uparrow} a_{\boldsymbol{k}\uparrow} \right\rangle\!\right\rangle = -g\, f_{\boldsymbol{q}+\boldsymbol{k}\uparrow}\, m_{\boldsymbol{k}} + \frac{g^2}{E_2}\, \phi^*_{\mathrm{m}}\, m_{\boldsymbol{q}+\boldsymbol{k}}\, m_{\boldsymbol{k}} + \frac{g^2}{E_3}\, \phi_{\mathrm{m}}\, f_{\boldsymbol{q}+\boldsymbol{k}\uparrow}\, f_{\boldsymbol{k}\downarrow}, \tag{7.31}$$

with the following energy denominators

$$E_1 = 2\mu - \bar{\nu} + 2\epsilon_{\boldsymbol{q}/2+\boldsymbol{k}} - 2\epsilon_{\boldsymbol{k}}, \tag{7.32a}$$

$$E_2 = 4\mu - \bar{\nu} - \epsilon_{\boldsymbol{q}} - 2\epsilon_{\boldsymbol{q}/2+\boldsymbol{k}}, \text{and} \tag{7.32b}$$

$$E_3 = 2\epsilon_{\boldsymbol{q}/2+\boldsymbol{k}} - \bar{\nu}. \tag{7.32c}$$

Substituting Eq. (7.31) into Eq. (7.19) for the pairing field we obtain the following set of equations

$$i\hbar \frac{\mathrm{d}\phi_{\mathrm{m}}}{\mathrm{d}t} = (\nu - 2\mu)\phi_{\mathrm{m}} + g \sum_{\boldsymbol{k}} m_{\boldsymbol{k}}, \tag{7.33}$$

$$\begin{aligned} i\hbar \frac{\mathrm{d}m_{\boldsymbol{k}}}{\mathrm{d}t} &= 2(\epsilon_{\boldsymbol{k}} + U_{\boldsymbol{k}} + V_{\boldsymbol{k}} - \mu) m_{\boldsymbol{k}} \\ &\quad + g\phi_{\mathrm{m}} \Big(1 - f_{\boldsymbol{k}\uparrow} - f_{\boldsymbol{k}\downarrow} - 2\,\mathcal{P} \sum_{\boldsymbol{q}} \frac{g^2}{E_1 E_3} f_{\boldsymbol{q}+\boldsymbol{k}\uparrow}\, f_{\boldsymbol{k}\downarrow} \Big), \end{aligned} \tag{7.34}$$

together with the Bloch-Messiah relation (7.20). The lowest-order correction terms are the Hartree term,

$$U_{\boldsymbol{k}} = g^2 \mathcal{P} \sum_{\boldsymbol{q}} \frac{f_{\boldsymbol{q}+\boldsymbol{k}}}{E_1}, \tag{7.35}$$

and a Bose term, which is the lowest contribution to the molecular self-energy on the BEC side of the resonance,

$$V_{\boldsymbol{k}} = -g^3 \mathcal{P} \sum_{\boldsymbol{q}} \frac{\phi^*_{\mathrm{m}} m_{\boldsymbol{q}+\boldsymbol{k}}}{E_1 E_2}. \tag{7.36}$$

In the following, we neglect the last term in Eq. (7.34), because it is a higher-order correction to the many-body Pauli-blocking factor $(1 - f_{\boldsymbol{k}\uparrow} - f_{\boldsymbol{k}\downarrow})$. We now consider the resulting equation of motion for the dressed paired state to find how the Bose term (7.36) enters the molecular self-energy.

7.6 Dressed Pair Correlations

We are looking for an eigenvalue solution for Eqs. (7.33) and (7.34) at energy E. This solution describes a dressed pair. We replace the steady-state energy 2μ with the eigen energy E and try the following Ansatz for a pair wave function

$$\chi_m = N\Big(\phi_\mathrm{m} + \mathcal{P}\sum_{\boldsymbol{k}} \frac{g}{E - 2\epsilon_{\boldsymbol{k}}} m_{\boldsymbol{k}}\Big), \tag{7.37}$$

with eigen energy

$$E = \nu + \mathcal{P}\sum_{\boldsymbol{k}} \frac{g^2\big(1 - f_{\boldsymbol{k}\uparrow} - f_{\boldsymbol{k}\downarrow}\big)}{E - 2\epsilon_{\boldsymbol{k}}}, \tag{7.38}$$

and a normalization constant N which is chosen so that the norm of χ_m matches the density of pairs

$$|\chi_m|^2 = n_p = \sum_{\boldsymbol{k}} |m_{\boldsymbol{k}}|^2 + |\phi_\mathrm{m}|^2. \tag{7.39}$$

The density of unpaired fermions can then be defined as $n_f = n_\mathrm{tot} - 2n_p$. The eigen energy E only coincides with the steady-state energy 2μ if all higher-order correlations are included and we are in full thermodynamic equilibrium.

In the two-body case, the Pauli-blocking factor in the expression for the energy in Eq. (7.38) vanishes and we have

$$E_\mathrm{2B} = \nu + \mathcal{P}\sum_{\boldsymbol{k}} \frac{g^2}{E - 2\epsilon_{\boldsymbol{k}}}, \tag{7.40}$$

for the two-body dressed energy. Equation (7.40) corresponds to Eqs. (7) and (8) in Ref. [143]. In that paper, Fano discusses the interaction of a discrete state with a continuum of states and finds the numerator of Eq. (7.40) to be the absolute value squared of a matrix element of the Hamiltonian. This is the case for the two-body formula above. The full many-body case in Eq. (7.38), however, has a Pauli-blocking factor in the numerator, which can become negative and can thus not be written as the square of a matrix element. This means, that the many-body dressed state above is not an eigenstate of a two-body Hamiltonian. The dressed pairs can thus not be interpreted as two-body molecules, because of their inherent many-body nature. A generalization of BCS quasiparticles along the lines of Chap. 4 for the boson case is a more

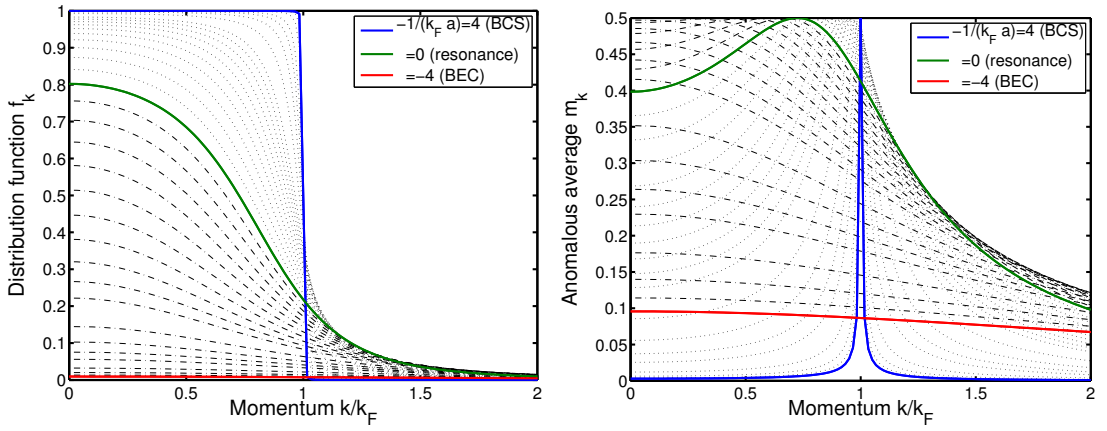

Figure 7.5: Correlation functions in the BCS/BEC crossover. We plot the normal density $f_{\boldsymbol{k}}$ (left) and pair correlation function $m_{\boldsymbol{k}}$ (right) as a function of momentum for different detunings $-1/(k_{\rm F}a)$. The blue line is in the BCS regime, the green line on resonance, and the red line in the BEC limit.

appropriate picture for the pairs. See also App. D for a discussion of a density matrix for the paired fermions.

Using Eqs. (7.33) and (7.34) for closed and open channel pairs, we obtain the following equation for the dressed pair correlation,

$$i\hbar\frac{\mathrm{d}\chi_m}{\mathrm{d}t} = E\chi_m + 2g\,\mathcal{P}\sum_{\boldsymbol{k}}\frac{U_{\boldsymbol{k}}+V_{\boldsymbol{k}}}{E-2\epsilon_{\boldsymbol{k}}}m_{\boldsymbol{k}}. \tag{7.41}$$

7.7 Numerical Results

We use the imaginary-time algorithm discussed in the previous Chapter and now use Eqs. (7.33) and (7.34), which include the Hartree and Bose correlation corrections to the self energy. We iterate the equations and calculate new self-energy corrections at each step, to obtain a self-consistent result. The final change in the distribution functions is below 10^{-4}, indicating a good level of convergence. In Fig. 7.5 we show the resulting correlation functions across the BCS/BEC crossover. In the BCS limit (blue line), the fermions obey a sharp Fermi-Dirac distribution, and pairing is limited to close to the Fermi momentum. With decreasing detuning, pairing spreads through the Fermi sphere, as can also be seen in Fig. 7.2.

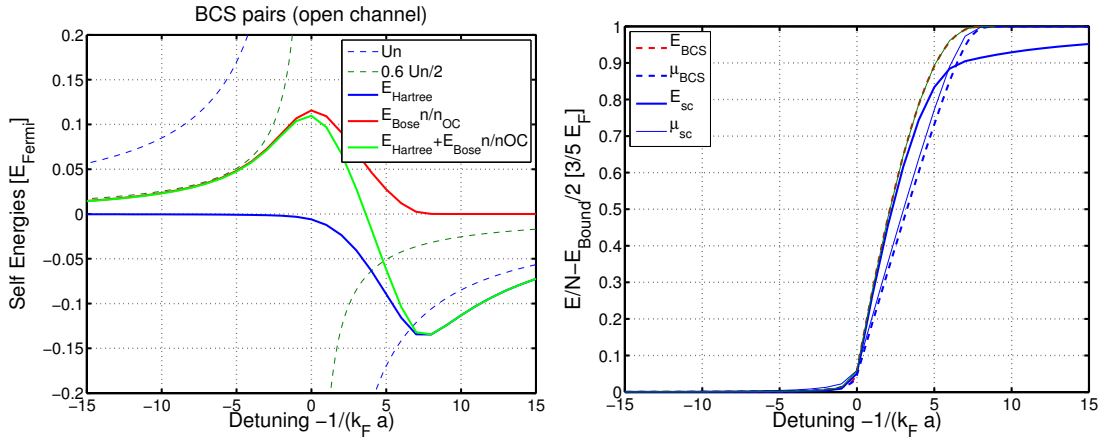

Figure 7.6: Energy plot for the narrow resonance in ^{6}Li at 543 G as a function of detuning $-1/(k_\mathrm{F}a)$. On the left we plot the Hartree and Bose contributions to the self energy, together with the dashed asymptotic values for the BCS side (positive detuning) in blue and the BEC side (negative detuning) in green. On the right we plot the steady-state energy 2μ and energy per particle, after subtracting the binding energy on the BEC side, which is the asymptotic value for these quantities. The plot on the right is in units of the ideal-gas energy per particle $3/5E_\mathrm{F}$.

In Fig. 7.6 we show energy plots for the narrow resonance at 543 G in ^{6}Li. On the left, we plot the Hartree- and Bose-contributions to the self energy as a function of detuning. The asymptotic value for the self-energy corrections on the BCS side (blue dashed) is given by

$$Un = \frac{4\pi\hbar^2 a}{m} n, \tag{7.42}$$

where n is the density of fermions, m is their mass, and a the s-wave scattering length. On the BEC side, the expected dimer-dimer scattering length is $a_\mathrm{dd} = 0.6a$ [125], which reduces the asymptotic value of the self-energy correction (green dashes). We divide the Bose term by the open-channel fraction n_OC/n to match the asymptotic behavior. The numerical results interpolate between the two limits. On the right, we plot the energy per particle minus the asymptotic value on the BEC side in units of the ideal-gas value of $3/5E_\mathrm{F}$. Including the self-energy corrections lowers the total energy.

To calculate the energy per particle, we evaluate the expectation value of the Hamiltonian (5.8). We first consider the BCS level, where we drop correlations beyond pairs:

$$E_\mathrm{BCS} = \langle H_\mathrm{res} \rangle = \sum_{\boldsymbol{k},\sigma} \epsilon_{\boldsymbol{k}} f_{\boldsymbol{k}\sigma} + \nu|\phi_\mathrm{m}|^2 + 2g \sum_{\boldsymbol{k}} \Re(\phi_\mathrm{m}^* m_{\boldsymbol{k}}). \tag{7.43}$$

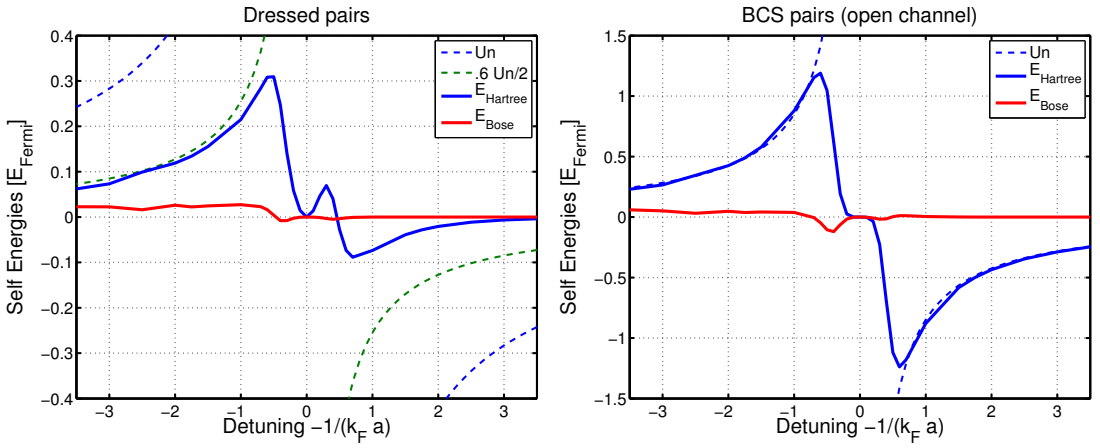

Figure 7.7: Self energy plots for ^{40}K as a function of detuning $-1/(k_{\mathrm{F}}a)$, together with the dashed asymptotic values for the BCS side (positive detuning) in blue and the BEC side (negative detuning) in green. The plot on the right shows the self energies for the open-channel BCS pairs, on the left we show dressed pairs, which are a superposition of open- and closed-channel contributions

The self-consistent energy E_{sc}, on the other hand, includes a three-operator contribution and the energy is calculated from the self-consistent averages $f_{\boldsymbol{k}}$ and $m_{\boldsymbol{k}}$.

$$E_{\mathrm{sc}} = E_{\mathrm{BCS}} + 2g\sum_{\boldsymbol{qk}} \Re\langle\!\langle b_{\boldsymbol{q}} a^{\dagger}_{\boldsymbol{q}/2-\boldsymbol{k}\downarrow} a^{\dagger}_{\boldsymbol{q}/2+\boldsymbol{k}\uparrow}\rangle\!\rangle. \tag{7.44}$$

The right-hand side is given by the following adiabatic, principal value solution for the three-operator correlation:

$$\left(2\epsilon_{\boldsymbol{q}/2+\boldsymbol{k}} - \bar{\nu}\right)\langle\!\langle b_{\boldsymbol{q}} a^{\dagger}_{\boldsymbol{q}/2+\boldsymbol{k}\uparrow} a^{\dagger}_{\boldsymbol{q}/2-\boldsymbol{k}\downarrow}\rangle\!\rangle = g\, f_{\boldsymbol{q}+\boldsymbol{k}\uparrow}\, f_{\boldsymbol{k}\downarrow} + g\phi^{*}_{\mathrm{m}}\Big(\langle\!\langle b_{\boldsymbol{q}} a^{\dagger}_{\boldsymbol{k}+\boldsymbol{q}\downarrow} a_{\boldsymbol{k}\downarrow}\rangle\!\rangle + \langle\!\langle b_{\boldsymbol{q}} a^{\dagger}_{-\boldsymbol{k}\uparrow} a_{-\boldsymbol{k}-\boldsymbol{q}\uparrow}\rangle\!\rangle\Big) \tag{7.45}$$

In Fig. 7.7 we show the self-energy corrections for the resonance at 224 G in ^{40}K. In this wider resonance, we find that the Hartree term dominates across the resonance. On the right, we plot the corrections for the open-channel BCS pairs, and find the same asymptotic behavior on both sides of the resonance. Only considering dressed pairs (left) recovers the expected dimer-dimer scattering behavior on the BEC side.

7.8 Summary

We extend the imaginary-time algorithm developed in Chap. 6 by using a cumulant expansion to include higher-order correlation effects. In particular, we include the Hartree term, and the lowest order contribution to the molecular self-energy on the BEC side and show numerically that we obtain results consistent with the observed dimer-dimer scattering for the effective bosons. This means that our many-body mean-field theory includes the four-fermion correlations necessary to properly describe the effective bosons. It is straightforward to extend the cumulant method we use to include correlations of higher order than considered here.

Chapter 8

Many-Body Dynamics of the BCS–BEC Crossover in the Normal Phase

In this Chapter, we consider fermions coupled to bosonic composite molecules above the critical temperature for the BEC or BCS transition in a homogeneous system. We use the BCS–BEC crossover Hamiltonian (5.8), which models a Feshbach resonance with a two-channel model , and use the cumulant expansion discussed in the previous Chapter to derive equations of motion for the thermal densities of composite bosons,

$$n_{\boldsymbol{q}} = \langle\!\langle b^\dagger_{\boldsymbol{q}} b_{\boldsymbol{q}} \rangle\!\rangle, \tag{8.1}$$

and fermions,

$$f_{\boldsymbol{k}} = f_{\boldsymbol{k}\uparrow} = \langle a^\dagger_{\boldsymbol{k}\uparrow} a_{\boldsymbol{k}\uparrow} \rangle = f_{\boldsymbol{k}\downarrow}, \tag{8.2}$$

in a spin-symmetric system. We assume that the temperature is high compared to the transition temperature so that we can neglect all symmetry-broken terms, such as the fermion pair correlation $m_{\boldsymbol{k}}$ and the molecular mean field ϕ_{m}. The number equation for this model is thus

$$n_{\mathrm{tot}} = \sum_{\boldsymbol{k},\sigma} f_{\boldsymbol{k}\sigma} + 2 \sum_{\boldsymbol{q}} n_{\boldsymbol{q}}. \tag{8.3}$$

Figure 8.1 shows schematically the correlation hierarchy we find for this model. We can cut the hierarchy at the following levels:

Cut A: If we cut here, we decouple the fermions and bosons and thus cut out the physics we are interested in.

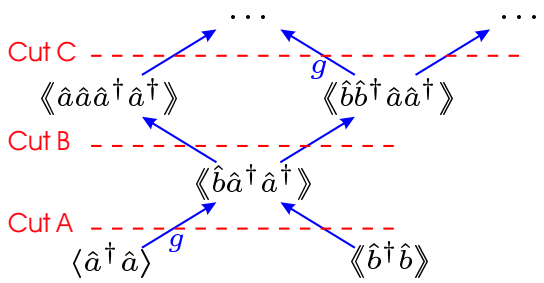

Figure 8.1: Schematic of the BBGKY cumulant hierarchy for the normal phase. The levels of this hierarchy are determined by the number of operators involved. In the dilute-gas systems we are interested in, a separation of time scales (the time between collisions is much larger than the duration of a collision) allows us to cut this hierarchy by dropping the correlation functions at a certain level.

Cut B: This yields a theory that describes the crossover problem for coupled, thermal bosons and fermions. However, we numerically find that the resulting equations are not positive definite. Furthermore, the renormalization of the detuning, Eq. (5.15), borrows terms from the next level of the hierarchy and this cut can thus not be performed cleanly.

Cut C: This is consistent with the renormalization used and yields a positive-definite theory. However, the four-operator cumulants are functions of three momenta and have too many degrees of freedom for a full numerical treatment.

In the following discussion, we derive the required equations of motion and show how adiabatic elimination of the four-operator cumulants leads to a closed set of three coupled equations, whose time dependence we numerically simulate. Simulations are performed for the narrow resonance in ^{6}Li, where the open and closed channels are coupled weakly, that is, the coupling constant g in the crossover Hamiltonian Eq. (5.8) is of order one in units of the Fermi energy and the system density. The experimentally explored wide resonances in ^{6}Li and ^{40}K have coupling constants that are two orders of magnitude larger, which makes the full time dependence very unstable. The zero-temperature method discussed in the last Chapter does not have this limitation.

Numerical results show that, above the Feshbach resonance, fermion and boson distributions stay in thermal equilibrium, even as the detuning is changed as a function of time. In Appendix E we derive effective coupled Boltzmann-type rate equations for the fermions and

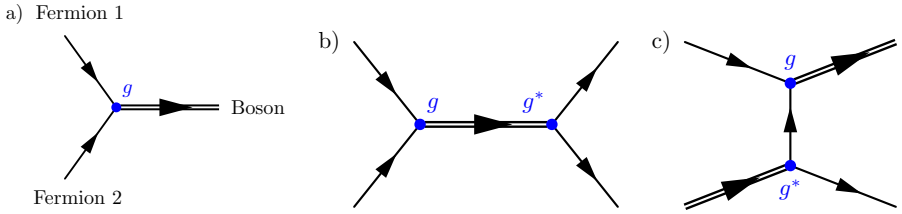

Figure 8.2: Scattering rates for the crossover Hamiltonian Eq. (5.8). a) Interaction node for the crossover Hamiltonian. This is the diagram for the first-order conversion of fermions to bosons, which is energetically suppressed on the BEC side of the resonance. b) Effective fermion-fermion interaction through intermediate boson state. c) Second-order fermion-boson interaction through particle exchange.

bosons similar to those found by Williams et al. [130, 144, 131], which explicitly show the collisional contributions depicted in Fig. 8.2. Each of these contributions contains energy-conserving delta functions between the incoming and outgoing lines. Rate b) thus allows off-shell intermediate boson states, which can not be represented by combining two collisions of type a), because they each conserve energy.

8.1 Equations of Motion

We list below the full set of normal-phase equations up to cut C illustrated in Fig. 8.1. First, we have the normal densities of fermions and composite bosons,

$$i\hbar\frac{\mathrm{d}f_{\boldsymbol{k}\uparrow}}{\mathrm{d}t} = 2ig\,\Im\Big\{\sum_{\boldsymbol{q}}\big\langle\!\big\langle b_{\boldsymbol{q}}a^\dagger_{\boldsymbol{k}\uparrow}a^\dagger_{\boldsymbol{q}-\boldsymbol{k}\downarrow}\big\rangle\!\big\rangle\Big\}, \tag{8.4a}$$

$$i\hbar\frac{\mathrm{d}n_{\boldsymbol{q}}}{\mathrm{d}t} = -2ig\,\Im\Big\{\sum_{\boldsymbol{k}}\big\langle\!\big\langle b_{\boldsymbol{q}}a^\dagger_{\boldsymbol{q}/2+\boldsymbol{k}\uparrow}a^\dagger_{\boldsymbol{q}/2-\boldsymbol{k}\downarrow}\big\rangle\!\big\rangle\Big\}, \tag{8.4b}$$

where $\Im$ indicates the imaginary part. These couple to the three-operator correlation function,

$$\begin{aligned} i\hbar\frac{\mathrm{d}\langle\!\langle b_{\boldsymbol{q}}a^\dagger_{\boldsymbol{q}/2+\boldsymbol{k}\uparrow}a^\dagger_{\boldsymbol{q}/2-\boldsymbol{k}\downarrow}\rangle\!\rangle}{\mathrm{d}t} &= (\nu-2\epsilon_{\boldsymbol{k}})\langle\!\langle b_{\boldsymbol{q}}a^\dagger_{\boldsymbol{q}/2+\boldsymbol{k}\uparrow}a^\dagger_{\boldsymbol{q}/2-\boldsymbol{k}\downarrow}\rangle\!\rangle \\ &+ g\sum_{\boldsymbol{k}'}\langle\!\langle a_{\boldsymbol{q}/2-\boldsymbol{k}'\downarrow}a_{\boldsymbol{q}/2+\boldsymbol{k}'\uparrow}a^\dagger_{\boldsymbol{q}/2+\boldsymbol{k}\uparrow}a^\dagger_{\boldsymbol{q}/2-\boldsymbol{k}\downarrow}\rangle\!\rangle \\ &- g\sum_{\boldsymbol{q}'}\Big(\langle\!\langle b_{\boldsymbol{q}}b^\dagger_{\boldsymbol{q}'}a_{\boldsymbol{q}'-\boldsymbol{q}/2+\boldsymbol{k}\uparrow}a^\dagger_{\boldsymbol{q}/2+\boldsymbol{k}\uparrow}\rangle\!\rangle + \langle\!\langle b_{\boldsymbol{q}}b^\dagger_{\boldsymbol{q}'}a_{\boldsymbol{q}'-\boldsymbol{q}/2-\boldsymbol{k}\downarrow}a^\dagger_{\boldsymbol{q}/2-\boldsymbol{k}\downarrow}\rangle\!\rangle\Big) \\ &+ g\,f_{\boldsymbol{q}/2+\boldsymbol{k}\uparrow}f_{\boldsymbol{q}/2-\boldsymbol{k}\downarrow}(1+n_{\boldsymbol{q}}) - g\,n_{\boldsymbol{q}}(1-f_{\boldsymbol{q}/2+\boldsymbol{k}\uparrow})(1-f_{\boldsymbol{q}/2-\boldsymbol{k}\downarrow}), \end{aligned} \tag{8.4c}$$

which in turn depends on the following two four-operator correlation functions,

$$\begin{aligned} i\hbar\frac{\mathrm{d}\langle\!\langle b_{\boldsymbol{q}}b^\dagger_{\boldsymbol{q}'}a_{\boldsymbol{q}'-\boldsymbol{q}/2+\boldsymbol{k},\sigma}a^\dagger_{\boldsymbol{q}/2+\boldsymbol{k},\sigma}\rangle\!\rangle}{\mathrm{d}t} &= 2\left(\epsilon_{(\boldsymbol{q}'-\boldsymbol{q})/2+\boldsymbol{k}}-\epsilon_{\boldsymbol{k}}\right)\langle\!\langle b_{\boldsymbol{q}}b^\dagger_{\boldsymbol{q}'}a_{\boldsymbol{q}'-\boldsymbol{q}/2+\boldsymbol{k},\sigma}a^\dagger_{\boldsymbol{q}/2+\boldsymbol{k},\sigma}\rangle\!\rangle \\ &\pm g\left(f_{\boldsymbol{q}/2+\boldsymbol{k},\sigma}+n_{\boldsymbol{q}}\right)\langle\!\langle b^\dagger_{\boldsymbol{q}'}a_{\boldsymbol{q}/2-\boldsymbol{k},-\sigma}a_{\boldsymbol{q}'-\boldsymbol{q}/2+\boldsymbol{k},\sigma}\rangle\!\rangle \\ &\mp g\left(f_{\boldsymbol{q}'-\boldsymbol{q}/2+\boldsymbol{k},\sigma}+n_{\boldsymbol{q}'}\right)\langle\!\langle b_{\boldsymbol{q}}a^\dagger_{\boldsymbol{q}/2+\boldsymbol{k},\sigma}a^\dagger_{\boldsymbol{q}/2-\boldsymbol{k},-\sigma}\rangle\!\rangle, \end{aligned} \tag{8.4d}$$

where the signs on the right-hand side correspond to the two possible spin directions, and,

$$\begin{aligned} i\hbar\frac{\mathrm{d}\langle\!\langle a_{\boldsymbol{q}/2-\boldsymbol{k}'\downarrow}a_{\boldsymbol{q}/2+\boldsymbol{k}'\uparrow}a^\dagger_{\boldsymbol{q}/2+\boldsymbol{k}\uparrow}a^\dagger_{\boldsymbol{q}/2-\boldsymbol{k}\downarrow}\rangle\!\rangle}{\mathrm{d}t} &= 2\left(\epsilon_{\boldsymbol{k}'}-\epsilon_{\boldsymbol{k}}\right)\langle\!\langle a_{\boldsymbol{q}/2-\boldsymbol{k}'\downarrow}a_{\boldsymbol{q}/2+\boldsymbol{k}'\uparrow}a^\dagger_{\boldsymbol{q}/2+\boldsymbol{k}\uparrow}a^\dagger_{\boldsymbol{q}/2-\boldsymbol{k}\downarrow}\rangle\!\rangle \\ &+ g\left(1-f_{\boldsymbol{q}/2+\boldsymbol{k}'\uparrow}-f_{\boldsymbol{q}/2-\boldsymbol{k}'\downarrow}\right)\langle\!\langle b_{\boldsymbol{q}}a^\dagger_{\boldsymbol{q}/2+\boldsymbol{k}\uparrow}a^\dagger_{\boldsymbol{q}/2-\boldsymbol{k}\downarrow}\rangle\!\rangle \\ &- g\left(1-f_{\boldsymbol{q}/2+\boldsymbol{k}\uparrow}-f_{\boldsymbol{q}/2-\boldsymbol{k}\downarrow}\right)\langle\!\langle b^\dagger_{\boldsymbol{q}}a_{\boldsymbol{q}/2-\boldsymbol{k}'\downarrow}a_{\boldsymbol{q}/2+\boldsymbol{k}'\uparrow}\rangle\!\rangle. \end{aligned} \tag{8.4e}$$

These equations of motion are derived from the Heisenberg equations (6.17). Equations (8.4) are exact in the normal phase, apart from the highest-order ones, Eqs. (8.4d) and (8.4e), where we dropped the couplings to five-operator cumulants to cut the BBGKY hierarchy of correlation functions.

The three-operator correlation (8.4c) is a three-dimensional quantity in a homogeneous system. This is the maximum number of degrees of freedom that can be treated numerically. We thus eliminate the four-operator cumulants Eqs. (8.4d) and (8.4e) by adiabatically solving for the four-operator cumulants and substituting into the equation for the time-dependent three-operator correlation $\langle\!\langle b_{\boldsymbol{q}}a^\dagger_{\boldsymbol{q}/2+\boldsymbol{k}\uparrow}a^\dagger_{\boldsymbol{q}/2-\boldsymbol{k}\downarrow}\rangle\!\rangle$. This yields the equations we simulate numerically.

In adiabatically solving the four-operator equations, we pick the imaginary delta-function contribution according to the following relation for energy denominators

$$\frac{1}{\Delta E - i\epsilon} = \mathcal{P}\frac{1}{\Delta E} + i\pi\delta(\Delta E), \tag{8.5}$$

for small $\epsilon > 0$. This choice gives us the collisional rates we are interested in, as can be seen in App. E. The resulting quantum-Boltzmann rates are depicted in Fig. 8.2: the couplings a) and c) are between fermions and bosons, b) is an effective fermion-fermion interaction. Only rate a) allows for particle exchange between bosons and fermions. The off-shell, principal value contributions renormalize the energy-denominators, but we neglect this correction of the intermediate-state energies. We find for the mixed four-operator cumulant:

$$\begin{aligned}\langle\!\langle b_{\boldsymbol{q}} b^\dagger_{\boldsymbol{q}'} a_{\boldsymbol{q}'-\boldsymbol{q}/2+\boldsymbol{k},\sigma} a^\dagger_{\boldsymbol{q}/2+\boldsymbol{k},\sigma}\rangle\!\rangle = -i\pi\ \delta\big(2\epsilon_{(\boldsymbol{q}'-\boldsymbol{q})/2+\boldsymbol{k}} - 2\epsilon_{\boldsymbol{k}}\big)\, g \\ \times\Big[\pm\big(f_{\boldsymbol{q}/2+\boldsymbol{k},\sigma} + n_{\boldsymbol{q}}\big)\langle\!\langle b^\dagger_{\boldsymbol{q}'} a_{\boldsymbol{q}/2-\boldsymbol{k},-\sigma} a_{\boldsymbol{q}'-\boldsymbol{q}/2+\boldsymbol{k},\sigma}\rangle\!\rangle \\ \mp\big(f_{\boldsymbol{q}'-\boldsymbol{q}/2+\boldsymbol{k},\sigma} + n_{\boldsymbol{q}'}\big)\langle\!\langle b_{\boldsymbol{q}} a^\dagger_{\boldsymbol{q}/2+\boldsymbol{k},\sigma} a^\dagger_{\boldsymbol{q}/2-\boldsymbol{k},-\sigma}\rangle\!\rangle\Big].\end{aligned} \tag{8.6}$$

We analogously consider Eq. (8.4e) and find the following adiabatic expression:

$$\begin{aligned}\langle\!\langle a_{\boldsymbol{q}/2-\boldsymbol{k}'\downarrow} a_{\boldsymbol{q}/2+\boldsymbol{k}'\uparrow} a^\dagger_{\boldsymbol{q}/2+\boldsymbol{k}\uparrow} a^\dagger_{\boldsymbol{q}/2-\boldsymbol{k}\downarrow}\rangle\!\rangle = -i\pi\ \delta(2\epsilon_{\boldsymbol{k}'} - 2\epsilon_{\boldsymbol{k}})\, g \\ \times\Big[\big(1 - f_{\boldsymbol{q}/2+\boldsymbol{k}'\uparrow} - f_{\boldsymbol{q}/2-\boldsymbol{k}'\downarrow}\big)\langle\!\langle b_{\boldsymbol{q}} a^\dagger_{\boldsymbol{q}/2+\boldsymbol{k}\uparrow} a^\dagger_{\boldsymbol{q}/2-\boldsymbol{k}\downarrow}\rangle\!\rangle \\ - \big(1 - f_{\boldsymbol{q}/2+\boldsymbol{k}\uparrow} - f_{\boldsymbol{q}/2-\boldsymbol{k}\downarrow}\big)\langle\!\langle b^\dagger_{\boldsymbol{q}} a_{\boldsymbol{q}/2-\boldsymbol{k}'\downarrow} a_{\boldsymbol{q}/2+\boldsymbol{k}'\uparrow}\rangle\!\rangle\Big].\end{aligned} \tag{8.7}$$

Substituting these expressions (8.6) and (8.7) on the right-hand side of the three-operator Eq. (8.4c) gives a closed set of cumulant equations. We are thus including four-operator correlations without explicitly keeping the four-operator functions as dynamical quantities. This procedure is necessary, because we do not assume a Gaussian reference distribution, which would lead to a straight-forward way of cutting the BBGKY hierarchy depicted in Fig. 8.1, because correlation functions beyond pairs would factorize with a Gaussian reference distribution.

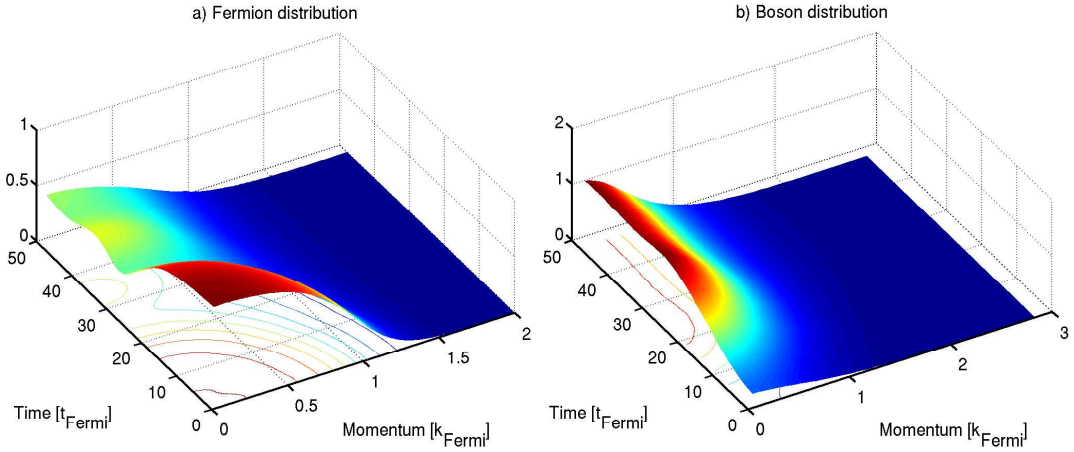

Figure 8.3: Normal-phase distribution function for a) fermions and b) bosons during a ramp from detuning $\bar{\nu} = 2E_{\mathrm{Fermi}}$ close to resonance at $T_{\mathrm{initial}} = 0.33T_{\mathrm{Fermi}}$ as a function of time and momentum. The time grid has 2000 points and is measured in units of $t_{\mathrm{Fermi}} \approx 10\,\mu$s. The momentum grids have a) 200 and b) 60 points.

8.2 Numerical Results

We here show results for the narrow resonance in ^{6}Li at 543 G [145, 146] for various detuning ramps. The initial distributions are equilibrium Bose–Einstein and Fermi–Dirac distributions at a given temperature T_{initial}, where the fermion chemical potential μ_{F} is found by root finding using a number constraint Eq. (8.3) and the chemical potential for the bosons is given by $\mu_{\mathrm{B}} = 2\mu_{\mathrm{F}}$. The time evolution is then calculated using a Runge-Kutta algorithm [147].

Figure 8.3 shows the fermion and boson distribution functions as a function of momentum and time during a ramp from an initial detuning of $\bar{\nu} = 2E_{\mathrm{Fermi}}$ to $0.2E_{\mathrm{Fermi}}$ just above the resonance. The ramp takes place in the first half of the time axis and is followed by equilibration at constant detuning. Some of the fermions get converted to composite bosons during the ramp: Fig. 8.4 shows on the left how the fermion fraction drops from an initial value of 85% to a final value of just below 30%. The plot on the right shows the resulting initial and final distributions of bosons and fermions. We can fit these distributions with equilibrium Bose–Einstein and Fermi–Dirac distributions.

From fits to the distributions in Fig. 8.3 we can extract the detuning $\bar{\nu}$, the temperatures

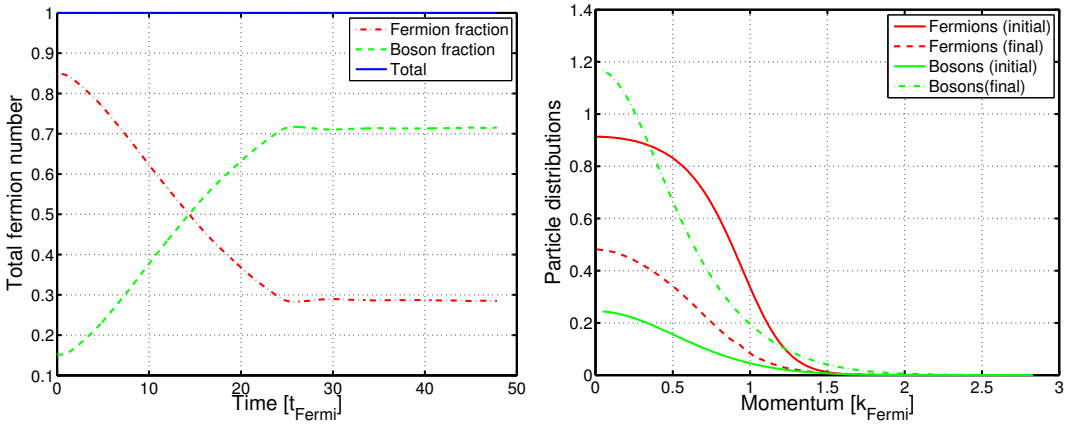

Figure 8.4: Time evolution of the population fractions during the ramp (left plot). Most of the unpaired fermions are converted to tightly bound molecules (this is for the narrow-resonance limit). The plots on the right show the initial and final distributions of the particles. These are cuts through the plots in Fig. 8.3.

of the fermion and boson distributions, and the chemical potential μ_{F} of the fermions. Figure 8.5 shows on the left the detuning as a function of time. The blue, solid line is the applied magnetic field ramp, and the dashed, green line is the detuning obtained from fitting the distributions. The fitted detuning quickly follows the ramp and briefly oscillates to the applied value after the ramp. On the right side of Fig. 8.5 we plot the temperatures of the two distributions as a function of time; the bosons and fermions are driven out of thermal equilibrium during the ramp, and reequilibrate at constant detuning after the ramp. The system also heats during the ramp and ends up at a final temperature of $T_{\mathrm{final}} = 0.47 T_{\mathrm{Fermi}}$.

Figure 8.6 shows the energy and entropy as a function of time during the ramp. The energy is given by the expectation value of the crossover Hamiltonian Eq. (5.8)

$$E_{\mathrm{tot}} = \langle H_{\mathrm{res}} \rangle = \sum_{\boldsymbol{k},\sigma} \epsilon_{\boldsymbol{k}} f_{\boldsymbol{k}\sigma} + \sum_{\boldsymbol{q}} \left(\frac{\epsilon_{\boldsymbol{q}}}{2} + \nu \right) n_{\boldsymbol{q}} + 2g \sum_{\boldsymbol{q}\boldsymbol{k}} \Re \langle\!\langle b_{\boldsymbol{q}} a^{\dagger}_{\boldsymbol{q}/2-\boldsymbol{k}\downarrow} a^{\dagger}_{\boldsymbol{q}/2+\boldsymbol{k}\uparrow} \rangle\!\rangle. \tag{8.8}$$

To calculate the entropy, we use the following formula [29, Chap. 2.2.3] for the combinatorial entropy of the two distributions and neglect the correlation contribution in this case

$$S_{\mathrm{tot}} = -\sum_{\boldsymbol{k},\sigma} \Big[f_{\boldsymbol{k}\sigma} \ln(f_{\boldsymbol{k}\sigma}) + (1 - f_{\boldsymbol{k}\sigma}) \ln(1 - f_{\boldsymbol{k}\sigma}) \Big] - \sum_{\boldsymbol{q}} \Big[n_{\boldsymbol{q}} \ln(n_{\boldsymbol{q}}) + (1 + n_{\boldsymbol{q}}) \ln(1 + n_{\boldsymbol{q}}) \Big]. \tag{8.9}$$

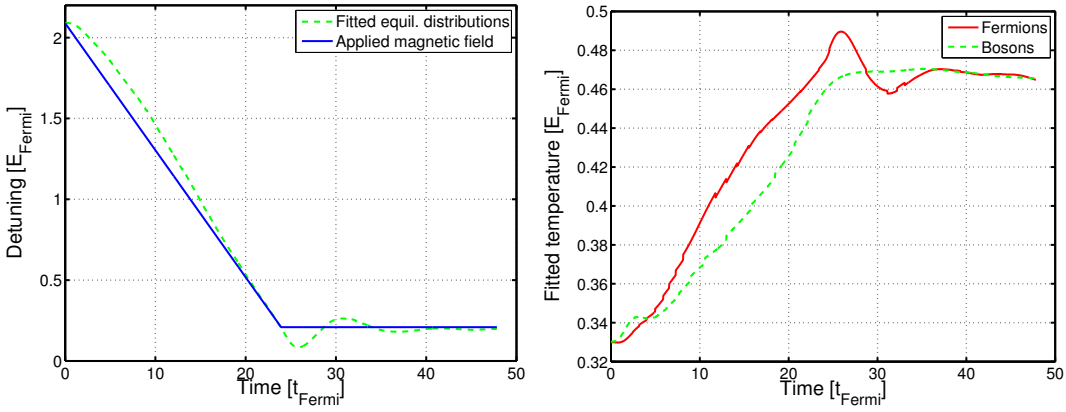

Figure 8.5: We fit the distributions shown in Fig. 8.3 to equilibrium Bose and Fermi distributions with the fermion chemical potential, the boson detuning $\bar{\nu}$ and the two temperatures as parameters. The plot on the left shows the fitted detuning and the applied detuning, that is, magnetic field as a function of time. The plot on the right shows the temperatures of the distributions.

Neglecting the correlation contribution to the entropy is not a good approximation close to the resonance, where the ramp in the previous plot ends. We will now consider a case, where we stay a Fermi energy away from the resonance.

Figure 8.7 shows ramps from a detuning of $2E_{\mathrm{Fermi}}$ to $1E_{\mathrm{Fermi}}$ and back up for three different, constant ramp speeds, now at a higher initial temperature of $T_{\mathrm{initial}} = 0.8\, T_{\mathrm{Fermi}}$. On the left, we plot the applied and fitted detunings as a function of time on a logarithmic scale. By the middle ramp, the fitted detuning already tracks the applied magnetic field very well. The plot on the right of Fig. 8.7 shows on the other hand that only the very slowest ramp brings the temperatures back to the initial value at the end of the ramp. This illustrates that the reversibility of the ramp is determined by a much longer many-body adiabaticity time scale than the transfer of populations, which is determined by a two-body adiabaticity time scale. The same difference in time scales appears in Fig. 8.8. The transfer of fermions during the ramp saturates quickly, whereas it takes longer for the entropy to return to its initial value.

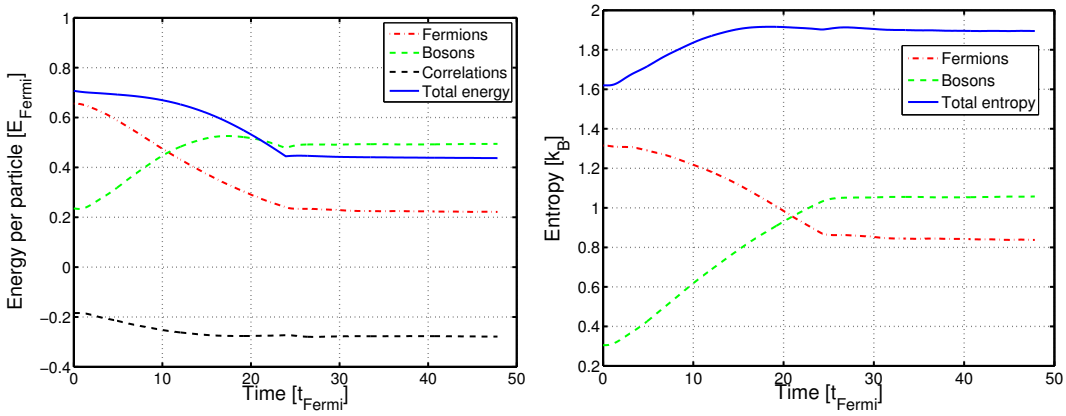

Figure 8.6: We plot the energy (left) and entropy (right) of the system as a function of time. The green, dashed line is the boson part, the red, dash-dotted line the fermion part, and the blue, full line the total number. In the energy plot, the black dotted line is the correlation energy due to the three-operator cumulant $\langle\!\langle ba^\dagger a^\dagger \rangle\!\rangle$, which is included in the total energy.

The discussion of rate equations in App. E finds that the collision processes depicted in Fig. 8.2 are the ones contained in this theory. The second-order processes b) and c) in Fig. 8.2, which maintain local equilibrium in each of the Fermi and Bose distributions, are of second order in the interaction g and are thus much slower than the first-order interaction a), which directly couples a pair of fermions to a composite boson and thus leads to global thermal equilibrium. The first-order rate, however, is energetically suppressed for negative detuning, because the bound state of the composite boson lies below the open-channel threshold of the free fermions. Figure 8.9 for a ramp across the resonance illustrates this point: The fitted

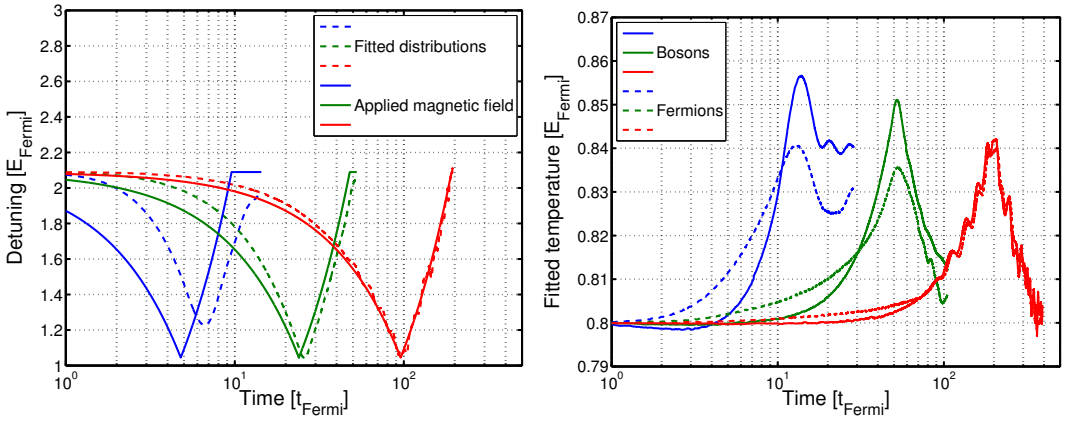

Figure 8.7: Fitted detuning and temperatures for return ramps. Shown are results for three different ramp speeds as a function of time.

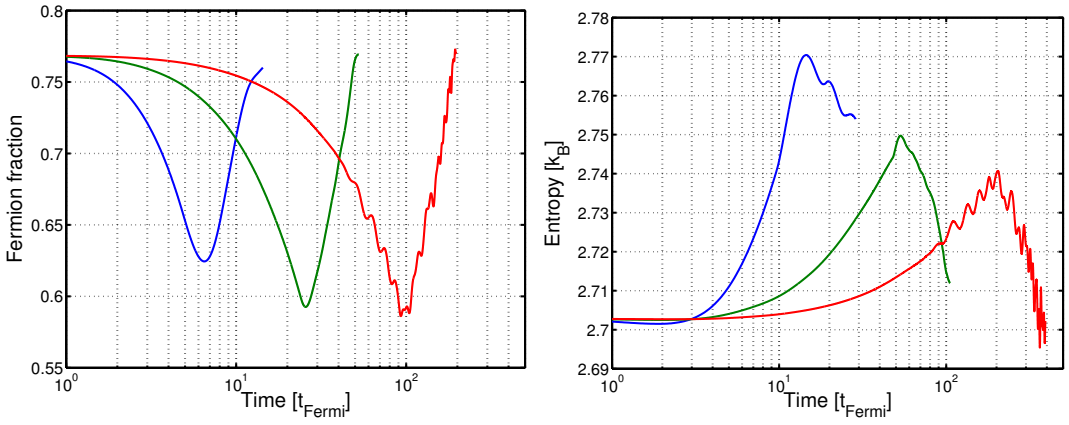

Figure 8.8: Fermion fraction (left) and entropy (right) as a function of time for return ramps at different speeds.

detuning follows the applied magnetic field until just below the resonance. At this point the first-order coupling between the fermions and bosons becomes energetically suppressed, and global equilibrium is not maintained any more as the ramp continues into the BEC regime. The plot on the right shows the much slower relaxation under the second-order rates that does not bring the temperatures of the two distributions into equilibrium any more after the ramp has finished. Three-body collisions, which we have neglected in this approach, become important in this regime and ultimately lead to thermalization.

We next consider the temperature dependence of the same ramp across the resonance from detuning $\bar{\nu} = 2E_{\mathrm{Fermi}}$ to $-2E_{\mathrm{Fermi}}$. Figure 8.10 shows on the left the initial and final boson fraction as a function of temperature. The lowest temperature points are outside the range of validity of this normal-phase theory, because they are below the Bose-Einstein transition temperature $T_{\mathrm{BEC}} = 0.35T_{\mathrm{Fermi}}$ for the experimental density and the mass of ^{6}Li. Accordingly, the initial boson population goes to zero and the final fraction does not head for the analytical zero-temperature result of full conversion given by Landau-Zener theory [149]. We have also plotted an experimental result for the narrow Lithium resonance [22], which deviates significantly from our results. Our simulation is, however, in much better quantitative agreement with results in ^{40}K experiments at JILA [148]. This is demonstrated in the graph on the right of Fig. 8.10,

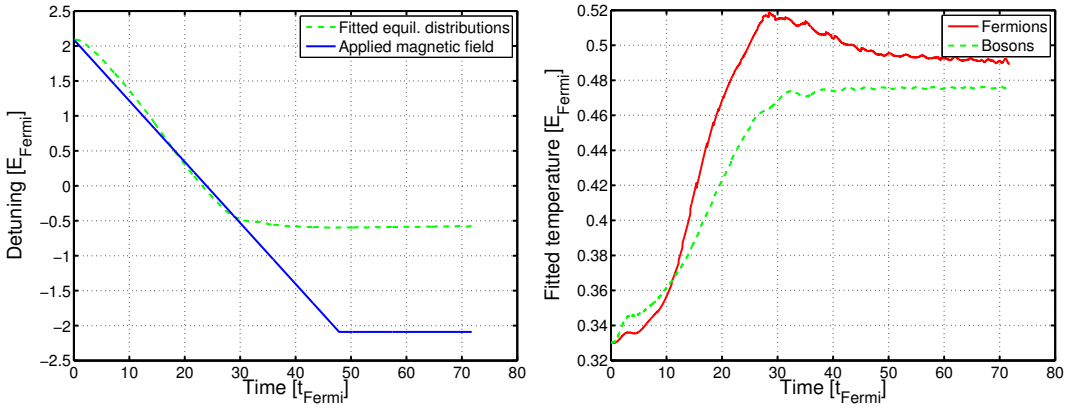

Figure 8.9: Fitted detuning (left) and temperatures (right) for a ramp across the resonance from detuning $\bar{\nu} = 2E_{\mathrm{Fermi}}$ to $-2E_{\mathrm{Fermi}}$.

where we plot the same data as a function of peak phase-space density ρ, which is given by the thermal de-Broglie wave length λ_{th} and the peak density n_{peak} at the center of the trap as

$$\rho = \lambda_{\mathrm{th}}^3 n_{\mathrm{peak}}. \tag{8.10}$$

The plot on the right of Fig. 8.10 shows that the Rice result still deviates, but the measurements at JILA [25, 148] agree very well with our quantum simulation. We also plot two theory lines due to Williams et al. [131]. The authors of the latter paper find the following transcendental equation for the molecular production efficiency χ as a function of phase-space density ρ for a two-component Fermi gas

$$2\chi + \ln\chi - \ln(1-\chi) = \ln\rho \tag{8.11}$$

They derive this relation using a classical-gas approximation and entropy conservation to relate the initial and final values of the phase-space density. We plot the numerical solution of this relation Eq. (8.11) as the green dashed line on the right side of Fig. 8.10. Williams et al. [131] also find an analytical prediction including quantum-statistical corrections, which we plot as the green full line and agrees with the 2005 JILA data better than the classical prediction, but not quite as well as our fully time-dependent quantum simulation.

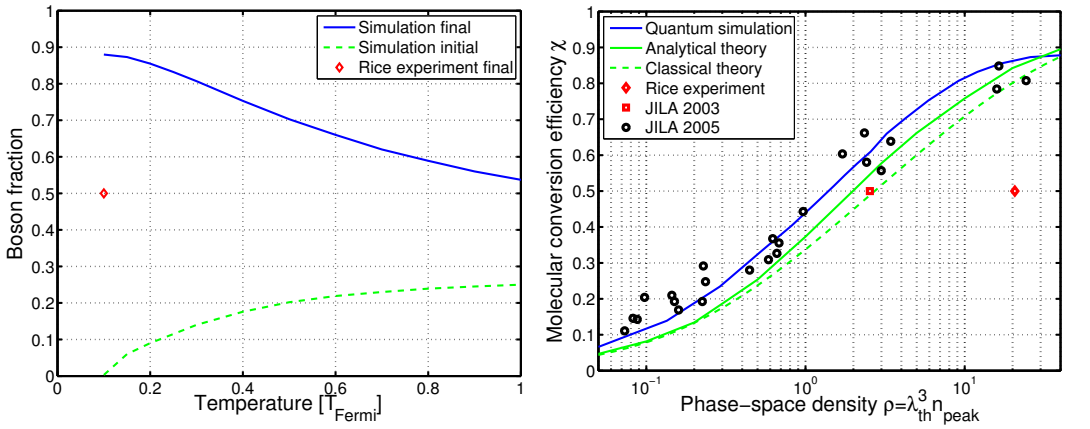

Figure 8.10: Molecular conversion efficiency as a function of temperature (left) and peak phase-space density (right) for a ramp across the resonance from detuning $\bar{\nu} = 2E_{\mathrm{Fermi}}$ to $-2E_{\mathrm{Fermi}}$. We also include experimental data from Rice [22] and JILA [25, 148] and theory results due to Williams et al. [131].

8.3 Summary

We discuss how thermal fermions and bosons in the normal phase couple in a mean-field theory of the BCS/BEC crossover near a Feshbach resonance. The cumulant method is a powerful tool for deriving a hierarchy of coupled equations of motion for distribution functions and higher-order correlations. We show how to consistently truncate this hierarchy and obtain a set of equations that we simulate numerically. The full time dependence of the crossover problem in the case of the narrow resonance at 543 G in ^{6}Li shows rapid local and global thermal equilibration of the distribution functions. The first-order rates that lead to global equilibrium are energetically suppressed below the resonance. We also find two adiabaticity time scales as the ramp speed is varied. We further examine the temperature dependence of the molecular conversion efficiency and find good agreement with experiments in ^{40}K.

Chapter 9

Summary and Outlook

In the first part of this thesis, we discussed a kinetic theory for a dilute quantum gas of bosons. In dilute gases, particles propagate freely for a long time between successive collision events, which leads to an attenuation of high-order correlations. Because of this attenuation, tracking a few, low-order correlation functions or Master variables is sufficient to describe the behavior of the system. This simplification allows us to develop microscopic theories, unlike the strongly interacting case of liquid Helium.

We used the Kadanoff–Baym nonequilibrium Green's function formalism [43, 44] to derive a kinetic theory for Bose–Einstein condensed bosons. The resulting equations reproduced the quantum-Boltzmann limit at high temperature and the Gross–Pitaevskii equation at low temperature. We also recovered the results of Walser et al. [37], who used a statistical-operator approach to derive the same kinetic equations. Next we examined the interaction diagrams present in this theory and identified many-body scattering T matrices to the level of approximation used. This allowed us to explicitly demonstrate that the excitation spectrum is gapless, as required for condensed bosons. We also diagonalized the renormalized self energies and used the resulting quasiparticle basis to write a diagonal Boltzmann equation for the dressed states.

This first part of the thesis is all theoretical, and calculating finite-temperature excitations and damping of a BEC would make comparison to experiments such as [65] and other theories possible. The work of Morgan et al. [75, 76] seems particularly interesting , since they use a number-conserving approach, which is different from the symmetry-breaking language we use.

In the second part of this thesis, we considered the BCS–BEC crossover near a Feshbach

resonance. Resonantly enhanced interactions between a pair of free fermions cause the fermions to cross over into a tightly bound, composite molecule. These effectively bosonic molecules can then condense. The bosons do not behave quite as expected. For example, the effective boson-boson scattering length is just 60% of the initial fermion-fermion interaction strength.

We first discussed one- and two-channel models of the BCS–BEC crossover and the Feshbach scattering theory that gives rise to the crossover. We then introduced an imaginary-time technique for fermions that finds zero-temperature ground states across the resonance. We used the Bloch-Messiah theorem, which relates the density and the pair function of fermions, to find a steepest-descent algorithm that works even for density-matrix evolution. We use this algorithm to find generalized BCS states.

We also examined the minimum ingredients for a mean-field theory that reproduces the observed boson-boson scattering length on the BEC side of the crossover and found that a three-point correlation function between a pair of free fermions and a composite boson needs to be treated. We introduced the concept of a cumulant, in order to include this required three-point correlation function. We then applied the imaginary-time method to the resulting equations of motion and numerically showed the observed dimer-dimer scattering behavior on the BEC side.

Next we used the cumulant expansion in a different regime and considered the coupling between thermal molecules and fermions in the normal phase above the transition temperature by numerically solving the time-dependent equations of motion including the three-point correlation function. We showed that the equations in the normal phase contain the Boltzmann rates for fermions and bosons and that the interconversion rate becomes energetically suppressed on the BEC side of the crossover. We showed numerical results in the normal phase for the narrow resonance at 543 G in ^{6}Li and discuss different time scales for many-body and two-body relaxation. We also compare molecular conversion efficiencies from our simulations to results in JILA potassium experiments and find good agreement.

To extend the work in the last two Chapters, one could imagine using the zero-temperature results of the imaginary-time method as an initial condition for a more general time-dependent

code that includes symmetry-broken mean fields. We have in fact worked with a program like that, but before we developed the imaginary-time method, and finding stable solutions proved difficult without good initial conditions. Another possible direction would be to calculate more measurable quantities, such as the superfluid gap and the universal β parameter, which describes the self-energy shift on resonance.

Appendix A

Collisional Self Energies in the Single-Particle Energy Basis

In this Appendix we give details omitted in Chap. 2, where the Kadanoff–Kane kinetic equations are written in the single-particle energy basis. The basis transformation is discussed in Section 2.4 and the steps for the collisional self energy are exactly the same as that of the first-order Hartree–Fock self energies discussed in Chap. 2. However, since the collisional self energies are quadratic in the interaction potential, this Section is more involved [150].

A.1 Mean-Field Equations

We start by writing down the analytical form of the collisional self energy given in Eq. (2.20) as

$$S^{<}(1,2) = -\frac{1}{2}\int d\bar{2}\int d\bar{3}\; v(1,\bar{2})v(2,\bar{3})\;\Big[\tilde{g}^{<}(1,2)\mathrm{Tr}\Big\{\tilde{g}^{>}(\bar{3},\bar{2})\tilde{g}^{<}(\bar{2},\bar{3})\Big\} + 2\tilde{g}^{<}(1,\bar{3})\tilde{g}^{>}(\bar{3},\bar{2})\tilde{g}^{<}(\bar{2},2)\Big]. \tag{A.1}$$

This is the gapless Beliaev approximation for the second-order contributions as pointed out in Chap. 2. Using the transformation Eq. (2.27) for the first propagator $\tilde{g}^{<}$ and their definitions Eqs. (2.7) and (2.8) for the remaining ones, we obtain for the self energy

$$S^{<}(1,2) = -\frac{1}{2}\int d\bar{2}\int d\bar{3}\; v(1,\bar{2})v(2,\bar{3})\; T_{13'}\Bigg[\tilde{G}^{<}_{3'1''}T_{1''2}\; 2i\Big\{(1+\tilde{f})_{\bar{3}\bar{2}}\tilde{f}_{\bar{2}\bar{3}} + \tilde{m}_{\bar{3}\bar{2}}\tilde{m}^{*}_{\bar{2}\bar{3}}\Big\} + \tilde{G}^{<}_{3'2'}T_{2'\bar{3}}\; 2i\begin{pmatrix} (1+\tilde{f})_{\bar{3}\bar{2}}\tilde{f}_{\bar{2}2} + \tilde{m}_{\bar{3}\bar{2}}\tilde{m}^{*}_{\bar{2}2} & (1+\tilde{f})_{\bar{3}\bar{2}}\tilde{m}_{\bar{2}2} + \tilde{m}_{\bar{3}\bar{2}}(1+\tilde{f})_{2\bar{2}} \\ \tilde{m}^{*}_{\bar{3}\bar{2}}\tilde{f}_{\bar{2}2} + \tilde{f}_{\bar{2}\bar{3}}\tilde{m}^{*}_{\bar{2}2} & \tilde{m}^{*}_{\bar{3}\bar{2}}\tilde{m}_{\bar{2}2} + \tilde{f}_{\bar{2}\bar{3}}(1+\tilde{f})_{2\bar{2}} \end{pmatrix}\Bigg]. \tag{A.2}$$

We now write all normal and anomalous fluctuation densities in the energy basis by using their respective transformation laws:

$$
\begin{aligned}
S^{<}(1,2) = -i \int d\bar{2} \int d\bar{3}\, \langle 2' \,|\, \bar{2}\rangle v(1,\bar{2}) \langle \bar{2} \,|\, 4'\rangle \, \langle 2'' \,|\, \bar{3}\rangle v(2,\bar{3}) \langle \bar{3} \,|\, 4''\rangle T_{13'} \tilde{G}^{<}_{3'1''} \\
\times \Big\{ (1+\tilde{f})_{4''2'} \tilde{f}_{4'2''} + \tilde{m}_{4''4'} \tilde{m}^{*}_{2'2''} \Big\} T_{1''2} \\
-i \int d\bar{2} \int d\bar{3}\, \langle 2' \,|\, \bar{2}\rangle v(1,\bar{2}) \langle \bar{2} \,|\, 4'\rangle \, v(2,\bar{3}) T_{13'} \tilde{G}^{<}_{3'2''} T_{2''\bar{3}} T_{\bar{3}4'} \\
\times \begin{pmatrix} (1+\tilde{f})_{4''2'} \tilde{f}_{4'1''} + \tilde{m}_{4''4'} \tilde{m}^{*}_{2'1''} & (1+\tilde{f})_{4''2'} \tilde{m}_{4'1''} + \tilde{m}_{4''4'} (1+\tilde{f})_{1''2'} \\ \tilde{m}^{*}_{4''2'} \tilde{f}_{4'1''} + \tilde{f}_{4'4''} \tilde{m}^{*}_{2'1''} & \tilde{m}^{*}_{4''2'} \tilde{m}_{4'1''} + \tilde{f}_{4'4''} (1+\tilde{f})_{1''2'} \end{pmatrix} T_{1''2}. \quad \text{(A.3)}
\end{aligned}
$$

Finally, using Eq. (2.33) to write the interaction potential in terms of its symmetrized energy matrix-elements, we obtain the condensate self energy in the energy basis projected back onto the position basis as

$$
\begin{aligned}
S^{<}(1,2) = -4i\, \phi^{1'2'3'4'}_{t_1} \phi^{1''2''3''4''}_{t_2} \begin{pmatrix} \langle 1 \,|\, 1'\rangle & 0 \\ 0 & \langle 3' \,|\, 1\rangle \end{pmatrix} \\
\times \Bigg[\begin{pmatrix} \tilde{f}_{3'1''} & \tilde{m}_{3'3''} \\ \tilde{m}^{*}_{1'1''} & (1+\tilde{f})_{3''1'} \end{pmatrix} \Big\{ (1+\tilde{f})_{4''2'} \tilde{f}_{4'2''} + \tilde{m}_{4''4'} \tilde{m}^{*}_{2'2''} \Big\} \\
+ \begin{pmatrix} \tilde{f}_{3'2''} & \tilde{m}_{3'4''} \\ \tilde{m}^{*}_{1'2''} & (1+\tilde{f})_{4''1'} \end{pmatrix} \begin{pmatrix} (1+\tilde{f})_{4''2'} \tilde{f}_{4'1''} + \tilde{m}_{4''4'} \tilde{m}^{*}_{2'1''} & 2(1+\tilde{f})_{4''2'} \tilde{m}_{4'3''} \\ 2\tilde{m}^{*}_{2''2'} \tilde{f}_{4'1''} & \tilde{m}^{*}_{2''2'} \tilde{m}_{4'3''} + \tilde{f}_{4'2''} (1+\tilde{f})_{3''2'} \end{pmatrix} \Bigg] \\
\times \begin{pmatrix} \langle 3'' \,|\, 2\rangle & 0 \\ 0 & \langle 2 \,|\, 1''\rangle \end{pmatrix}, \quad \text{(A.4)}
\end{aligned}
$$

where the time subscript of the two-particle matrix elements $\phi^{1'2'3'4'}_{t_1}$ means that the field operators that are contracted with that matrix element have to be evaluated at t_1. We can collect some terms using the symmetries of the two-particle matrix element ϕ given in Eq. (3.4) to

obtain

$$S^{<}(1,2) = -8i\,\phi_{t_1}^{1'2'3'4'}\phi_{t_2}^{1''2''3''4''}\begin{pmatrix} \langle 1\,|\,1'\rangle & 0 \\ 0 & \langle 3'\,|\,1\rangle \end{pmatrix}$$
$$\times\Bigg[\begin{pmatrix} \tilde{f}_{3'1''} & \tilde{m}_{3'3''} \\ \tilde{m}^{*}_{1'1''} & (1+\tilde{f})_{3''1'} \end{pmatrix}\Big\{(1+\tilde{f})_{4''2'}\tilde{f}_{4'2''} + \tilde{m}_{4''4'}\tilde{m}^{*}_{2'2''}\Big\}$$
$$+\begin{pmatrix} \tilde{f}_{3'2''} & \tilde{m}_{3'4''} \\ \tilde{m}^{*}_{1'2''} & (1+\tilde{f})_{4''1'} \end{pmatrix}\begin{pmatrix} 0 & (1+\tilde{f})_{4''2'}\tilde{m}_{4'3''} \\ \tilde{m}^{*}_{2''2'}\tilde{f}_{4'1''} & 0 \end{pmatrix}\Bigg]\begin{pmatrix} \langle 3''\,|\,2\rangle & 0 \\ 0 & \langle 2\,|\,1''\rangle \end{pmatrix}. \quad \text{(A.5)}$$

Now using the definition of the non-conserving collision operators

$$\Gamma^{0}_{fff} = 8\phi_{t_1}^{1'2'3'4'}\phi_{t_2}^{1''2''3''4''} f_{3'1''}f_{4'2''}f_{4''2'}\,|1'\rangle\,\langle 3''|\,, \quad \text{(A.6a)}$$

$$\Gamma^{0}_{fmf} = 8\phi_{t_1}^{1'2'3'4'}\phi_{t_2}^{1''2''3''4''} f_{3'1''}m_{4'3''}f_{4''2'}\,|1'\rangle\,|2''\rangle\,, \quad \text{(A.6b)}$$

$$\Gamma^{0}_{fmm^{*}} = 8\phi_{t_1}^{1'2'3'4'}\phi_{t_2}^{1''2''3''4''} f_{3'1''}m_{4'3''}m^{*}_{2''2'}\,|1'\rangle\,\langle 4''|\,, \text{ and} \quad \text{(A.6c)}$$

$$\Gamma^{0}_{mmm^{*}} = 8\phi_{t_1}^{1'2'3'4'}\phi_{t_2}^{1''2''3''4''} m_{3'4''}m_{4'3''}m^{*}_{2''2'}\,|1'\rangle\,|1''\rangle\,, \quad \text{(A.6d)}$$

we get the collisional self energy for the condensate in the position basis expressed in terms of the energy-basis collision operators

$$S(1,2)^{<} = -i\begin{pmatrix} \langle 1|\left(\Gamma^{0}_{\tilde{f}\tilde{f}(1+\tilde{f})} + 2\Gamma^{0}_{\tilde{f}\tilde{m}\tilde{m}^{*}}\right)|2\rangle & \langle 12|\left(\Gamma^{0}_{\tilde{m}\tilde{m}\tilde{m}^{*}} + 2\Gamma^{0}_{\tilde{f}\tilde{m}(1+\tilde{f})}\right) \\ \left(\Gamma^{0*}_{\tilde{m}\tilde{m}\tilde{m}^{*}} + 2\Gamma^{0*}_{(1+\tilde{f})\tilde{m}\tilde{f}}\right)|12\rangle & \langle 2|\left(\Gamma^{0\dagger}_{(1+\tilde{f})(1+\tilde{f})\tilde{f}} + 2\Gamma^{0\dagger}_{(1+\tilde{f})\tilde{m}\tilde{m}^{*}}\right)|1\rangle \end{pmatrix}. \quad \text{(A.7)}$$

The other time ordering $S^{>}(1,2)$ can be obtained by exchanging $\tilde{f}$ for $(1+\tilde{f})$ and vice versa.

A.2 Normal and Anomalous Fluctuations

Similar to the condensate case, the collisional self energy for the fluctuations given in Eq. (2.21) is transformed:

$$\Sigma^{<}(1,2) = -\frac{1}{2}\int d\bar{2}\int d\bar{3}\; v(1,\bar{2})v(2,\bar{3})$$
$$\times\Big[\tilde{g}^{<}(1,2)\mathrm{Tr}\Big\{g^{>}(\bar{3},\bar{2})g^{<}(\bar{2},\bar{3}) - h(\bar{3},\bar{2})h(\bar{2},\bar{3})\Big\} + h(1,2)\mathrm{Tr}\Big\{\tilde{g}^{>}(\bar{3},\bar{2})\tilde{g}^{<}(\bar{2},\bar{3})\Big\}$$
$$+2\tilde{g}^{<}(1,\bar{3})\Big\{g^{>}(\bar{3},\bar{2})g^{<}(\bar{2},2) - h(\bar{3},\bar{2})h(\bar{2},2)\Big\} + 2h(1,\bar{3})\tilde{g}^{>}(\bar{3},\bar{2})\tilde{g}^{<}(\bar{2},2)\Big]. \quad \text{(A.8)}$$

We now substitute the first propagator in each term by using Eq. (2.27) and the analogous expression for $h(1,2)$. For the remaining propagators we substitute the definitions Eqs. (2.7) and (2.8) and obtain

$$
\begin{aligned}
\Sigma^{<}(1,2) = &-\frac{1}{2}\int d\bar{2}\int d\bar{3}\; v(1,\bar{2})v(2,\bar{3})\; T_{13'} \\
&\times\Bigg[\tilde{G}^{<}_{3'1''}T_{1''2}\; 2i\Big\{(1+f)_{\bar{3}\bar{2}}f_{\bar{2}\bar{3}} + m_{\bar{3}\bar{2}}m^{*}_{\bar{2}\bar{3}} - f^{c}_{\bar{3}\bar{2}}f^{c}_{\bar{2}\bar{3}} - m^{c}_{\bar{3}\bar{2}}m^{c*}_{\bar{2}\bar{3}}\Big\} \\
&\quad + H_{3'1''}T_{1''2}\; 2i\Big\{(1+\tilde{f})_{\bar{3}\bar{2}}\tilde{f}_{\bar{2}\bar{3}} + \tilde{m}_{\bar{3}\bar{2}}\tilde{m}^{*}_{\bar{2}\bar{3}}\Big\} \\
&\quad + \tilde{G}^{<}_{3'2'}T_{2'\bar{3}}\; 2i\begin{pmatrix} (1+f)_{\bar{3}\bar{2}}f_{\bar{2}2} + m_{\bar{3}\bar{2}}m^{*}_{\bar{2}2} & (1+f)_{\bar{3}\bar{2}}m_{\bar{2}2} + m_{\bar{3}\bar{2}}(1+f)_{2\bar{2}} \\ m^{*}_{\bar{3}\bar{2}}f_{\bar{2}2} + f_{\bar{2}\bar{3}}m^{*}_{\bar{2}2} & m^{*}_{\bar{3}\bar{2}}m_{\bar{2}2} + f_{\bar{2}\bar{3}}(1+f)_{2\bar{2}} \end{pmatrix} \\
&\quad - \tilde{G}^{<}_{3'2'}T_{2'\bar{3}}\; 2i\begin{pmatrix} f^{c}_{\bar{3}\bar{2}}f^{c}_{\bar{2}2} + m^{c}_{\bar{3}\bar{2}}m^{c*}_{\bar{2}2} & f^{c}_{\bar{3}\bar{2}}m^{c}_{\bar{2}2} + m^{c}_{\bar{3}\bar{2}}f^{c}_{\bar{2}\bar{2}} \\ m^{c*}_{\bar{3}\bar{2}}f^{c}_{\bar{2}2} + f^{c}_{\bar{2}\bar{3}}m^{c*}_{\bar{2}2} & m^{c*}_{\bar{3}\bar{2}}m^{c}_{\bar{2}2} + f^{c}_{\bar{2}\bar{3}}f^{c}_{\bar{2}\bar{2}} \end{pmatrix} \\
&\quad + H_{3'2'}T_{2'\bar{3}}\; 2i\begin{pmatrix} (1+\tilde{f})_{\bar{3}\bar{2}}\tilde{f}_{\bar{2}2} + \tilde{m}_{\bar{3}\bar{2}}\tilde{m}^{*}_{\bar{2}2} & (1+\tilde{f})_{\bar{3}\bar{2}}\tilde{m}_{\bar{2}2} + \tilde{m}_{\bar{3}\bar{2}}(1+\tilde{f})_{2\bar{2}} \\ \tilde{m}^{*}_{\bar{3}\bar{2}}\tilde{f}_{\bar{2}2} + \tilde{f}_{\bar{2}\bar{3}}\tilde{m}^{*}_{\bar{2}2} & \tilde{m}^{*}_{\bar{3}\bar{2}}\tilde{m}_{\bar{2}2} + \tilde{f}_{\bar{2}\bar{3}}(1+\tilde{f})_{2\bar{2}} \end{pmatrix}\Bigg]. \qquad \text{(A.9)}
\end{aligned}
$$

Now writing all normal and anomalous fluctuation densities in the energy basis, we obtain

$$
\begin{aligned}
\Sigma^{<}(1,2) = &-i\int d\bar{2}\int d\bar{3}\; \langle 2'\,|\,\bar{2}\rangle v(1,\bar{2})\langle\bar{2}\,|\,4'\rangle\; \langle 2''\,|\,\bar{3}\rangle v(2,\bar{3})\langle\bar{3}\,|\,4''\rangle\; T_{13'} \\
&\times\Bigg[\tilde{G}^{<}_{3'1''}\Big\{(1+f)_{4''2'}f_{4'2''} + m_{4''4'}m^{*}_{2'2''} - f^{c}_{4''2'}f^{c}_{4'2''} - m^{c}_{4''4'}m^{c*}_{2'2''}\Big\} \\
&\quad + H_{3'1''}\Big\{(1+\tilde{f})_{4''2'}\tilde{f}_{4'2''} + \tilde{m}_{4''4'}\tilde{m}^{*}_{2'2''}\Big\}\Bigg]T_{1''2} \\
&-i\int d\bar{2}\int d\bar{3}\; \langle 2'\,|\,\bar{2}\rangle v(1,\bar{2})\langle\bar{2}\,|\,4'\rangle\; v(2,\bar{3})\; T_{13'} \\
&\times\Bigg[\tilde{G}^{<}_{3'2''}T_{2''\bar{3}}T_{\bar{3}4''}\begin{pmatrix} (1+f)_{4''2'}f_{4'1''} + m_{4''4'}m^{*}_{2'1''} & (1+f)_{4''2'}m_{4'1''} + m_{4''4'}(1+f)_{1''2'} \\ m^{*}_{4''2'}f_{4'1''} + f_{4'4''}m^{*}_{2'1''} & m^{*}_{4''2'}m_{4'1''} + f_{4'4''}(1+f)_{1''2'} \end{pmatrix} \\
&\quad - \tilde{G}^{<}_{3'2''}T_{2''\bar{3}}T_{\bar{3}4''}\begin{pmatrix} f^{c}_{4''2'}f^{c}_{4'1''} + m^{c}_{4''4'}m^{c*}_{2'1''} & f^{c}_{4''2'}m^{c}_{4'1''} + m^{c}_{4''4'}f^{c}_{1''2'} \\ m^{c*}_{4''2'}f^{c}_{4'1''} + f^{c}_{4'4''}m^{c*}_{2'1''} & m^{c*}_{4''2'}m^{c}_{4'1''} + f^{c}_{4'4''}f^{c}_{1''2'} \end{pmatrix} \\
&\quad + H_{3'2''}T_{2''\bar{3}}T_{\bar{3}4''}\begin{pmatrix} (1+\tilde{f})_{4''2'}\tilde{f}_{4'1''} + \tilde{m}_{4''4'}\tilde{m}^{*}_{2'1''} & (1+\tilde{f})_{4''2'}\tilde{m}_{4'1''} + \tilde{m}_{4''4'}(1+\tilde{f})_{1''2'} \\ \tilde{m}^{*}_{4''2'}\tilde{f}_{4'1''} + \tilde{f}_{4'4''}\tilde{m}^{*}_{2'1''} & \tilde{m}^{*}_{4''2'}\tilde{m}_{4'1''} + \tilde{f}_{4'4''}(1+\tilde{f})_{1''2'} \end{pmatrix}\Bigg] \\
&\times T_{1''2}. \qquad \text{(A.10)}
\end{aligned}
$$

In the next step, we use Eq. (2.33) to express the interaction potential in terms of its symmetrized matrix elements in the energy basis and obtain

$$
\begin{aligned}
\Sigma(1,2)^{<} = -4i\, \phi_{t_1}^{1'2'3'4'} \phi_{t_2}^{1''2''3''4''} & \begin{pmatrix} \langle 1\,|\,1'\rangle & 0 \\ 0 & \langle 3'\,|\,1\rangle \end{pmatrix} \\
\times \Bigg[& \begin{pmatrix} \tilde{f}_{3'1''} & \tilde{m}_{3'3''} \\ \tilde{m}^{*}_{1'1''} & (1+\tilde{f})_{3''1'} \end{pmatrix} \Big\{ (1+f)_{4''2'} f_{4'2''} + m_{4''4'} m^{*}_{2'2''} - f^{c}_{4''2'} f^{c}_{4'2''} - m^{c}_{4''4'} m^{c*}_{2'2''} \Big\} \\
& + \begin{pmatrix} f^{c}_{3'1''} & m^{c}_{3'3''} \\ m^{c*}_{1'1''} & f^{c}_{3''1'} \end{pmatrix} \Big\{ (1+\tilde{f})_{4''2'} \tilde{f}_{4'2''} + \tilde{m}_{4''4'} \tilde{m}^{*}_{2'2''} \Big\} \\
& + \begin{pmatrix} \tilde{f}_{3'2''} & \tilde{m}_{3'4''} \\ \tilde{m}^{*}_{1'2''} & (1+\tilde{f})_{4''1'} \end{pmatrix} \begin{pmatrix} (1+f)_{4''2'} f_{4'1''} + m_{4''4'} m^{*}_{2'1''} & 2(1+f)_{4''2'} m_{4'3''} \\ 2m^{*}_{2'2''} f_{4'1''} & m^{*}_{2'2''} m_{4'3''} + f_{4'2''}(1+f)_{3''2'} \end{pmatrix} \\
& - \begin{pmatrix} \tilde{f}_{3'2''} & \tilde{m}_{3'4''} \\ \tilde{m}^{*}_{1'2''} & (1+\tilde{f})_{4''1'} \end{pmatrix} \begin{pmatrix} f^{c}_{4''2'} f^{c}_{4'1''} + m^{c}_{4''4'} m^{c*}_{2'1''} & 2f^{c}_{4''2'} m^{c}_{4'3''} \\ 2m^{c*}_{2''2'} f^{c}_{4'1''} & m^{c*}_{2''2'} m^{c}_{4'3''} + f^{c}_{4'2''} f^{c}_{3''2'} \end{pmatrix} \\
& + \begin{pmatrix} f^{c}_{3'2''} & m^{c}_{3'4''} \\ m^{c*}_{1'2''} & f^{c}_{4''1'} \end{pmatrix} \begin{pmatrix} (1+\tilde{f})_{4''2'} \tilde{f}_{4'1''} + \tilde{m}_{4''4'} \tilde{m}^{*}_{2'1''} & 2(1+\tilde{f})_{4''2'} \tilde{m}_{4'3''} \\ 2\tilde{m}^{*}_{2''2'} \tilde{f}_{4'1''} & \tilde{m}^{*}_{2''2'} \tilde{m}_{4'3''} + \tilde{f}_{4'2''}(1+\tilde{f})_{3''2'} \end{pmatrix} \Bigg] \\
& \times \begin{pmatrix} \langle 3''\,|\,2\rangle & 0 \\ 0 & \langle 2\,|\,1''\rangle \end{pmatrix}. \qquad \text{(A.11)}
\end{aligned}
$$

We collect some terms making use of the symmetries of the two-particle matrix element ϕ as given in Eq. (3.4)

$$
\begin{aligned}
\Sigma(1,2)^{<} = -8i\, \phi_{t_1}^{1'2'3'4'} \phi_{t_2}^{1''2''3''4''} & \begin{pmatrix} \langle 1\,|\,1'\rangle & 0 \\ 0 & \langle 3'\,|\,1\rangle \end{pmatrix} \\
\times \Bigg[& \begin{pmatrix} \tilde{f}_{3'1''} & \tilde{m}_{3'3''} \\ \tilde{m}^{*}_{1'1''} & (1+\tilde{f})_{3''1'} \end{pmatrix} \Big\{ (1+f)_{4''2'} f_{4'2''} + m_{4''4'} m^{*}_{2'2''} - f^{c}_{4''2'} f^{c}_{4'2''} - m^{c}_{4''4'} m^{c*}_{2'2''} \Big\} \\
& + \begin{pmatrix} f^{c}_{3'1''} & m^{c}_{3'3''} \\ m^{c*}_{1'1''} & f^{c}_{3''1'} \end{pmatrix} \Big\{ (1+\tilde{f})_{4''2'} \tilde{f}_{4'2''} + \tilde{m}_{4''4'} \tilde{m}^{*}_{2'2''} \Big\} \\
& + \begin{pmatrix} \tilde{f}_{3'2''} & \tilde{m}_{3'4''} \\ \tilde{m}^{*}_{1'2''} & (1+\tilde{f})_{4''1'} \end{pmatrix} \begin{pmatrix} 0 & (1+f)_{4''2'} m_{4'3''} - f^{c}_{4''2'} m^{c}_{4'3''} \\ m^{*}_{2'2''} f_{4'1''} - m^{c*}_{2''2'} f^{c}_{4'1''} & 0 \end{pmatrix} \\
& + \begin{pmatrix} f^{c}_{3'2''} & m^{c}_{3'4''} \\ m^{c*}_{1'2''} & f^{c}_{4''1'} \end{pmatrix} \begin{pmatrix} 0 & (1+\tilde{f})_{4''2'} \tilde{m}_{4'3''} \\ \tilde{m}^{*}_{2''2'} \tilde{f}_{4'1''} & 0 \end{pmatrix} \Bigg] \begin{pmatrix} \langle 3''\,|\,2\rangle & 0 \\ 0 & \langle 2\,|\,1''\rangle \end{pmatrix}, \qquad \text{(A.12)}
\end{aligned}
$$

and express the collisional self energy in terms of the collision operators Γ^{0}:

$$
\begin{aligned}
\Sigma(1,2)^{<} = & -i \begin{pmatrix} \langle 1| \left(\Gamma^{0}_{\tilde{f}f(1+f)} + \Gamma^{0}_{\tilde{f}mm^{*}}\right)|2\rangle & \langle 12| \left(\Gamma^{0}_{f\tilde{m}(1+f)} + \Gamma^{0}_{\tilde{m}mm^{*}}\right) \\ \left(\Gamma^{0*}_{(1+f)\tilde{m}f} + \Gamma^{0*}_{\tilde{m}mm^{*}}\right)|12\rangle & \langle 2| \left(\Gamma^{0\dagger}_{(1+\tilde{f})(1+f)f} + \Gamma^{0\dagger}_{(1+\tilde{f})mm^{*}}\right)|1\rangle \end{pmatrix} \\
& + i \begin{pmatrix} \langle 1| \left(\Gamma^{0}_{\tilde{f}f^{c}f^{c}} + \Gamma^{0}_{\tilde{f}m^{c}m^{c*}}\right)|2\rangle & \langle 12| \left(\Gamma^{0}_{f^{c}\tilde{m}f^{c}} + \Gamma^{0}_{\tilde{m}m^{c}m^{c*}}\right) \\ \left(\Gamma^{0*}_{f^{c}\tilde{m}f^{c}} + \Gamma^{0*}_{\tilde{m}m^{c}m^{c*}}\right)|12\rangle & \langle 2| \left(\Gamma^{0\dagger}_{(1+\tilde{f})f^{c}f^{c}} + \Gamma^{0\dagger}_{(1+\tilde{f})m^{c}m^{c*}}\right)|1\rangle \end{pmatrix} \\
& - i \begin{pmatrix} \langle 1| \left(\Gamma^{0}_{f^{c}\tilde{f}(1+\tilde{f})} + \Gamma^{0}_{f^{c}\tilde{m}\tilde{m}^{*}}\right)|2\rangle & \langle 12| \left(\Gamma^{0}_{\tilde{f}m^{c}(1+\tilde{f})} + \Gamma^{0}_{m^{c}\tilde{m}\tilde{m}^{*}}\right) \\ \left(\Gamma^{0*}_{(1+\tilde{f})m^{c}\tilde{f}} + \Gamma^{0*}_{m^{c}\tilde{m}\tilde{m}^{*}}\right)|12\rangle & \langle 2| \left(\Gamma^{0\dagger}_{f^{c}(1+\tilde{f})\tilde{f}} + \Gamma^{0\dagger}_{f^{c}\tilde{m}\tilde{m}^{*}}\right)|1\rangle \end{pmatrix} \qquad \text{(A.13)} \\
& - i \begin{pmatrix} \langle 1|\big(\Gamma^{0}_{f\tilde{m}m^{*}} - \Gamma^{0}_{f^{c}\tilde{m}m^{c*}} + \Gamma^{0}_{\tilde{f}m^{c}\tilde{m}^{*}}\big)|2\rangle & \langle 12|\big(\Gamma^{0}_{\tilde{f}m(1+f)} - \Gamma^{0}_{\tilde{f}m^{c}f^{c}} + \Gamma^{0}_{f^{c}\tilde{m}(1+\tilde{f})}\big) \\ \big(\Gamma^{0*}_{(1+\tilde{f})mf} - \Gamma^{0*}_{(1+\tilde{f})m^{c}f^{c}} + \Gamma^{0*}_{f^{c}\tilde{m}\tilde{f}}\big)|12\rangle & \langle 2|\big(\Gamma^{0\dagger}_{(1+f)\tilde{m}m^{*}} - \Gamma^{0\dagger}_{f^{c}\tilde{m}m^{c*}} + \Gamma^{0\dagger}_{(1+\tilde{f})m^{c}\tilde{m}^{*}}\big)|1\rangle \end{pmatrix}.
\end{aligned}
$$

Using $f = f^c + \tilde{f}$ and $m = m^c + \tilde{m}$, we can rewrite this equation to obtain the final result for the collisional self energy

$$
\begin{aligned}
& i\,\Sigma(1,2)^{<} = \qquad\qquad\qquad\qquad\qquad\qquad\qquad\qquad\qquad\qquad\qquad\qquad\qquad\qquad (A.14)\\
& \begin{pmatrix} \langle 1|\big(\Gamma^{0}_{f\tilde{f}(1+\tilde{f})}+\Gamma^{0}_{\tilde{f}f^c(1+\tilde{f})}+\Gamma^{0}_{\tilde{f}\tilde{f}f^c}\big)|2\rangle & \langle 12|\big(\Gamma^{0}_{m\tilde{m}\tilde{m}^*}+\Gamma^{0}_{\tilde{m}m^c\tilde{m}^*}+\Gamma^{0}_{\tilde{m}\tilde{m}m^{c*}}\big) \\ \big(\Gamma^{0*}_{m\tilde{m}\tilde{m}^*}+\Gamma^{0*}_{\tilde{m}m^c\tilde{m}^*}+\Gamma^{0*}_{\tilde{m}\tilde{m}m^{c*}}\big)|12\rangle & \langle 2|\big(\Gamma^{0\dagger}_{(1+f)(1+\tilde{f})\tilde{f}}+\Gamma^{0\dagger}_{(1+\tilde{f})f^c\tilde{f}}+\Gamma^{0\dagger}_{(1+\tilde{f})(1+\tilde{f})f^c}\big)|1\rangle \end{pmatrix}\\
& +2\begin{pmatrix} \langle 1|\big(\Gamma^{0}_{f\tilde{m}\tilde{m}^*}+\Gamma^{0}_{\tilde{f}m^c\tilde{m}^*}+\Gamma^{0}_{\tilde{f}\tilde{m}m^{c*}}\big)|2\rangle & \langle 12|\big(\Gamma^{0}_{f\tilde{m}(1+\tilde{f})}+\Gamma^{0}_{\tilde{f}m^c(1+\tilde{f})}+\Gamma^{0}_{\tilde{f}\tilde{m}f^c}\big) \\ \big(\Gamma^{0*}_{(1+f)\tilde{m}\tilde{f}}+\Gamma^{0*}_{(1+\tilde{f})m^c\tilde{f}}+\Gamma^{0*}_{(1+\tilde{f})\tilde{m}f^c}\big)|12\rangle & \langle 2|\big(\Gamma^{0\dagger}_{(1+f)\tilde{m}\tilde{m}^*}+\Gamma^{0\dagger}_{(1+\tilde{f})m^c\tilde{m}^*}+\Gamma^{0\dagger}_{(1+\tilde{f})\tilde{m}m^{c*}}\big)|1\rangle \end{pmatrix}.
\end{aligned}
$$

As in the condensate case, the self energy $\Sigma^{>}(1,2)$ can be obtained by exchanging $\tilde{f}$ and $(1+\tilde{f})$ and vice versa.

Appendix B

Collisional Terms in the Quasiparticle Basis

This Appendix shows in detail how the symmetries of the quasiparticle basis allow us to rewrite the second-order collisional terms as shown in Sec. 4.2 [150].

We first transform only the thermal terms of the collision operator, which do not contain condensate contributions and are denoted by $\tilde{\Gamma}^{<}$. We begin by writing down their definition in terms of individual collision processes

$$\sigma^z\tilde{\Gamma}^{<} = \begin{pmatrix} \Gamma_{\tilde{f}\tilde{f}(1+\tilde{f})} + 2\Gamma_{\tilde{f}\tilde{m}\tilde{m}^*} & \Gamma_{\tilde{m}\tilde{m}\tilde{m}^*} + 2\Gamma_{\tilde{f}\tilde{m}(1+\tilde{f})} \\ \Gamma^*_{\tilde{m}\tilde{m}\tilde{m}^*} + 2\Gamma^*_{(1+\tilde{f})\tilde{m}\tilde{f}} & \Gamma^{\dagger}_{(1+\tilde{f})(1+\tilde{f})\tilde{f}} + 2\Gamma^{\dagger}_{(1+\tilde{f})\tilde{m}\tilde{m}^*} \end{pmatrix} \tag{B.1}$$

$$\equiv \tilde{\Gamma}^{<}_1 + \begin{pmatrix} \Gamma_{\tilde{f}\tilde{m}\tilde{m}^*} & \Gamma_{\tilde{f}\tilde{m}(1+\tilde{f})} \\ \Gamma^*_{(1+\tilde{f})\tilde{m}\tilde{f}} & \Gamma^{\dagger}_{(1+\tilde{f})\tilde{m}\tilde{m}^*} \end{pmatrix}. \tag{B.2}$$

For the moment, we drop the factors of two and substitute the definitions of the individual collisional operators Γ

$$\tilde{\Gamma}^{<}_1 = 8\,\phi^{1'2'3'4'}\phi^{1''2''3''4''}_{\eta} \begin{pmatrix} \tilde{f}_{3'1''}\ |1'\rangle\otimes\langle 3''| & \tilde{m}_{3'3''}\ |1'\rangle\otimes|1''\rangle \\ \tilde{m}^*_{1'1''}\ \langle 3'|\otimes\langle 3''| & (1+\tilde{f})_{3''1'}\ \langle 3'|\otimes|1''\rangle \end{pmatrix}$$
$$\times\Big\{(1+\tilde{f})_{4''2'}\tilde{f}_{4'2''} + \tilde{m}_{4'4''}\tilde{m}^*_{2'2''}\Big\}. \tag{B.3}$$

Then we replace the expectation values of the normal and anomalous densities by writing Eq. (4.12) in 2 by 2 components,

$$\tilde{G}^{<}_{1'2'} = \begin{pmatrix} \tilde{f}_{1'2'} & \tilde{m}_{1'2'} \\ \tilde{m}^*_{1'2'} & (1+\tilde{f})_{2'1'} \end{pmatrix} = \begin{pmatrix} u^{\bar{1}}_{1'}P_{\bar{1}\bar{2}}u^{\bar{2}*}_{2'} & u^{\bar{1}}_{1'}P_{\bar{1}\bar{2}}v^{\bar{2}}_{2'} \\ v^{\bar{1}*}_{1'}P_{\bar{1}\bar{2}}u^{\bar{2}*}_{2'} & v^{\bar{1}*}_{1'}P_{\bar{1}\bar{2}}v^{\bar{2}}_{2'} \end{pmatrix}. \tag{B.4}$$

and substituting in Eq. (B.3):

$$\tilde{\Gamma}_1^< = 8\,\phi^{1'2'3'4'}\phi_\eta^{1''2''3''4''}\begin{pmatrix} u_{3'}^{\bar{3}}P_{\bar{3}\bar{1}'}u_{1''}^{\bar{1}'*}\ |1'\rangle\otimes\langle 3''| & u_{3'}^{\bar{3}}P_{\bar{3}\bar{3}'}v_{3''}^{\bar{3}'}\ |1'\rangle\otimes|1''\rangle \\ v_{1'}^{\bar{1}*}P_{\bar{1}\bar{1}'}u_{1''}^{\bar{1}'*}\ \langle 3'|\otimes\langle 3''| & v_{1'}^{\bar{1}*}P_{\bar{1}\bar{3}'}v_{3''}^{\bar{3}'}\ \langle 3'|\otimes|1''\rangle \end{pmatrix} \times\Big\{v_{2'}^{\bar{2}*}P_{\bar{2}\bar{4}'}v_{4''}^{\bar{4}'}u_{4'}^{\bar{4}}P_{\bar{4}\bar{2}'}u_{2''}^{\bar{2}'*}+u_{4'}^{\bar{4}}P_{\bar{4}\bar{4}'}v_{4''}^{\bar{4}'}v_{2'}^{\bar{2}*}P_{\bar{2}\bar{2}'}u_{2''}^{\bar{2}'*}\Big\}. \tag{B.5}$$

Finally, we use Eq. (4.9) to substitute $v_{1'}^{\bar{1}}$ and $u_{1'}^{\bar{1}*}$ according to $v_{1'}^{\bar{1}}=u_{1'}^{-\bar{1}}$ and $u_{1'}^{\bar{1}*}=v_{1'}^{-\bar{1}*}$, reverse the corresponding summations, and reintroduce the weighting factors to obtain for the full collision operator

$$\sigma^z\tilde{\Gamma}^< = 8\,\phi^{1'2'3'4'}\phi_\eta^{1''2''3''4''}v_{2''}^{\bar{2}'*}u_{4''}^{\bar{4}'}P_{\bar{3}-\bar{1}'}P_{\bar{2}-\bar{4}'}P_{\bar{4}-\bar{2}'} \times\begin{pmatrix} u_{3'}^{\bar{3}}v_{1''}^{\bar{1}'*}\big\{v_{2'}^{\bar{2}*}u_{4'}^{\bar{4}}+2v_{2'}^{\bar{4}*}u_{4'}^{\bar{2}}\big\}\,|1'\rangle\otimes\langle 3''| & u_{3'}^{\bar{3}}u_{3''}^{\bar{1}'}\big\{2v_{2'}^{\bar{2}*}u_{4'}^{\bar{4}}+v_{2'}^{\bar{4}*}u_{4'}^{\bar{2}}\big\}\,|1'\rangle\otimes|1''\rangle \\ v_{1'}^{\bar{3}*}v_{1''}^{\bar{1}'*}\big\{2v_{2'}^{\bar{2}*}u_{4'}^{\bar{4}}+v_{2'}^{\bar{4}*}u_{4'}^{\bar{2}}\big\}\,\langle 3'|\otimes\langle 3''| & v_{1'}^{\bar{3}*}u_{3''}^{\bar{1}'}\big\{v_{2'}^{\bar{2}*}u_{4'}^{\bar{4}}+2v_{2'}^{\bar{4}*}u_{4'}^{\bar{2}}\big\}\,\langle 3'|\otimes|1''\rangle \end{pmatrix}. \tag{B.6}$$

To transform the collision operator $\tilde{\Gamma}^<$ to the quasiparticle basis $\{\bar{1}\}$, we multiply it from the left by $W^\dagger$ and from the right by W to obtain

$$W^\dagger\sigma^z\tilde{\Gamma}^<W = |\bar{5}\rangle\otimes\langle\bar{5}'|\begin{pmatrix} u_{5'}^{\bar{5}*}\big(\langle 5'|\otimes\mathbb{1}\big) & v_{5'}^{\bar{5}}\big(|5'\rangle\otimes\mathbb{1}\big)\end{pmatrix}\sigma^z\Gamma^<\begin{pmatrix} u_{5''}^{\bar{5}'}\ \mathbb{1}\otimes|5''\rangle \\ v_{5''}^{\bar{5}'*}\ \mathbb{1}\otimes\langle 5''|\end{pmatrix} \tag{B.7}$$

$$= 8\,\phi^{1'2'3'4'}\phi_\eta^{1''2''3''4''}v_{2''}^{\bar{2}'*}u_{4''}^{\bar{4}'}P_{\bar{3}-\bar{1}'}P_{\bar{2}-\bar{4}'}P_{\bar{4}-\bar{2}'}\ |-\bar{1}\rangle\otimes\langle\bar{3}'| \times\Big[u_{3'}^{\bar{3}}v_{1''}^{\bar{1}'*}\big\{v_{2'}^{\bar{2}*}u_{4'}^{\bar{4}}+2v_{2'}^{\bar{4}*}u_{4'}^{\bar{2}}\big\}v_{1'}^{\bar{1}*}u_{3''}^{\bar{3}'}+u_{3'}^{\bar{3}}u_{3''}^{\bar{1}'}\big\{2v_{2'}^{\bar{2}*}u_{4'}^{\bar{4}}+v_{2'}^{\bar{4}*}u_{4'}^{\bar{2}}\big\}v_{1'}^{\bar{1}*}v_{1''}^{\bar{3}'*} +v_{1'}^{\bar{3}*}v_{1''}^{\bar{1}'*}\big\{2v_{2'}^{\bar{2}*}u_{4'}^{\bar{4}}+v_{2'}^{\bar{4}*}u_{4'}^{\bar{2}}\big\}u_{3'}^{\bar{1}}u_{3''}^{\bar{3}'}+v_{1'}^{\bar{3}*}u_{3''}^{\bar{1}'}\big\{v_{2'}^{\bar{2}*}u_{4'}^{\bar{4}}+2v_{2'}^{\bar{4}*}u_{4'}^{\bar{2}}\big\}u_{3'}^{\bar{1}}v_{1''}^{\bar{3}'*}\Big]. \tag{B.8}$$

We now define new two-particle matrix elements in the quasiparticle energy basis by

$$\Phi_{(\eta)}^{\bar{1}\bar{2}\bar{3}\bar{4}} \equiv \phi_{(\eta)}^{1'2'3'4'}\ v_{1'}^{\bar{1}*}v_{2'}^{\bar{2}*}u_{3'}^{\bar{3}}u_{4'}^{\bar{4}}, \tag{B.9}$$

which have the same symmetries as the original matrix elements ϕ^{1234} [cf. Eq. (3.4)]:

$$\Phi_{(\eta)}^{\bar{1}\bar{2}\bar{3}\bar{4}} = \Phi_{(\eta)}^{\bar{2}\bar{1}\bar{3}\bar{4}} = \Phi_{(\eta)}^{\bar{1}\bar{2}\bar{4}\bar{3}}. \tag{B.10}$$

We now substitute these new matrix elements, defined in Eq. (B.9), into the collision operator

Eq. (B.8) and obtain

$$W^\dagger \sigma^z \tilde{\Gamma}^< W = 8\, P_{\bar{3}-\bar{1}'} P_{\bar{4}-\bar{2}'} P_{\bar{2}-\bar{4}'}\, |-\bar{1}\rangle \otimes \langle \bar{3}'| \times \Big[\Phi^{\bar{1}\bar{2}\bar{3}\bar{4}} \Phi_\eta^{\bar{1}'\bar{2}'\bar{3}'\bar{4}'} + 2\Phi^{\bar{1}\bar{4}\bar{3}\bar{2}} \Phi_\eta^{\bar{1}'\bar{2}'\bar{3}'\bar{4}'} + 2\Phi^{\bar{1}\bar{2}\bar{3}\bar{4}} \Phi_\eta^{\bar{3}'\bar{2}'\bar{1}'\bar{4}'} + \Phi^{\bar{1}\bar{4}\bar{3}\bar{2}} \Phi_\eta^{\bar{3}'\bar{2}'\bar{1}'\bar{4}'} + 2\Phi^{\bar{3}\bar{2}\bar{1}\bar{4}} \Phi_\eta^{\bar{1}'\bar{2}'\bar{3}'\bar{4}'} + \Phi^{\bar{3}\bar{4}\bar{1}\bar{2}} \Phi_\eta^{\bar{1}'\bar{2}'\bar{3}'\bar{4}'} + \Phi^{\bar{3}\bar{2}\bar{1}\bar{4}} \Phi_\eta^{\bar{3}'\bar{2}'\bar{1}'\bar{4}'} + 2\Phi^{\bar{3}\bar{4}\bar{1}\bar{2}} \Phi_\eta^{\bar{3}'\bar{2}'\bar{1}'\bar{4}'} \Big]. \quad \text{(B.11)}$$

The definition of the two-particle matrix elements Φ in Eq. (B.9) implies the following identity

$$\Phi^{*\bar{1}\bar{2}\bar{3}\bar{4}} \equiv \left(\Phi^{\bar{1}\bar{2}\bar{3}\bar{4}}\right)^* = \phi^{3'4'1'2'}\; v_{1'}^{\bar{1}} v_{2'}^{\bar{2}} u_{3'}^{\bar{3}*} u_{4'}^{\bar{4}*} = \phi^{3'4'1'2'}\; u_{1'}^{-\bar{1}} u_{2'}^{-\bar{2}} v_{3'}^{-\bar{3}*} v_{4'}^{-\bar{4}*} = \Phi^{-\bar{3}-\bar{4}-\bar{1}-\bar{2}}, \quad \text{(B.12)}$$

which we use to substitute the $\bar{1}$, $\bar{2}$, $\bar{3}$, and $\bar{4}$ indices and obtain, after reordering some terms,

$$W^\dagger \sigma^z \tilde{\Gamma}^< W = 8\, P_{-\bar{1}-\bar{1}'} P_{-\bar{2}-\bar{2}'} P_{-\bar{4}-\bar{4}'}\, |\bar{3}\rangle \otimes \langle \bar{3}'| \times \Big[\Big\{ \Phi^{*\bar{1}\bar{2}\bar{3}\bar{4}} + 2\Phi^{*\bar{1}\bar{4}\bar{3}\bar{2}} + 2\Phi^{*\bar{3}\bar{2}\bar{1}\bar{4}} + \Phi^{*\bar{3}\bar{4}\bar{1}\bar{2}} \Big\} \Phi_\eta^{\bar{1}'\bar{2}'\bar{3}'\bar{4}'} + \Big\{ 2\Phi^{*\bar{1}\bar{2}\bar{3}\bar{4}} + \Phi^{*\bar{1}\bar{4}\bar{3}\bar{2}} + \Phi^{*\bar{3}\bar{2}\bar{1}\bar{4}} + 2\Phi^{*\bar{3}\bar{4}\bar{1}\bar{2}} \Big\} \Phi_\eta^{\bar{3}'\bar{2}'\bar{1}'\bar{4}'} \Big] \quad \text{(B.13)}$$

$$\equiv \frac{1}{2}\, \Psi^{\bar{1}\,\bar{2}\,\bar{3}\,\bar{4}}_{\bar{1}'\bar{2}'\bar{3}'\bar{4}'}\; P_{-\bar{1}-\bar{1}'} P_{-\bar{2}-\bar{2}'} P_{-\bar{4}-\bar{4}'}\, |\bar{3}\rangle \otimes \langle \bar{3}'|\,, \quad \text{(B.14)}$$

where we have defined the combined matrix element Ψ, which is symmetrized under pairwise exchange of 1, 2, and 4 in Eq. (B.13). We use this symmetry in the second line to obtain

$$\frac{1}{16} \Psi^{\bar{1}\,\bar{2}\,\bar{3}\,\bar{4}}_{\bar{1}'\bar{2}'\bar{3}'\bar{4}'} = \Big\{ \Phi^{*\bar{1}\bar{2}\bar{3}\bar{4}} + 2\Phi^{*\bar{1}\bar{4}\bar{3}\bar{2}} + 2\Phi^{*\bar{3}\bar{2}\bar{1}\bar{4}} + \Phi^{*\bar{3}\bar{4}\bar{1}\bar{2}} \Big\} \Phi_\eta^{\bar{1}'\bar{2}'\bar{3}'\bar{4}'} + \Big\{ 2\Phi^{*\bar{1}\bar{4}\bar{3}\bar{2}} + \Phi^{*\bar{1}\bar{2}\bar{3}\bar{4}} + \Phi^{*\bar{3}\bar{4}\bar{1}\bar{2}} + 2\Phi^{*\bar{3}\bar{2}\bar{1}\bar{4}} \Big\} \Phi_\eta^{\bar{3}'\bar{4}'\bar{1}'\bar{2}'} \quad \text{(B.15)}$$

$$= \Big\{ \Phi^{*\bar{1}\bar{2}\bar{3}\bar{4}} + 2\Phi^{*\bar{1}\bar{4}\bar{3}\bar{2}} + 2\Phi^{*\bar{3}\bar{2}\bar{1}\bar{4}} + \Phi^{*\bar{3}\bar{4}\bar{1}\bar{2}} \Big\} \Big\{ \Phi_\eta^{\bar{1}'\bar{2}'\bar{3}'\bar{4}'} + \Phi_\eta^{\bar{3}'\bar{4}'\bar{1}'\bar{2}'} \Big\}. \quad \text{(B.16)}$$

We now exchange $\bar{1}^{(\prime)}$ and $\bar{2}^{(\prime)}$ in one half of the terms with a factor of two and make use of the symmetries of $\Phi_{(\eta)}^{\bar{1}\bar{2}\bar{3}\bar{4}}$ given in Eq. (B.10) to rewrite Ψ as

$$\frac{1}{16} \Psi^{\bar{1}\,\bar{2}\,\bar{3}\,\bar{4}}_{\bar{1}'\bar{2}'\bar{3}'\bar{4}'} = \Big\{ \Phi^{*\bar{1}\bar{2}\bar{3}\bar{4}} + \Phi^{*\bar{1}\bar{4}\bar{3}\bar{2}} + \Phi^{*\bar{2}\bar{4}\bar{3}\bar{1}} + \Phi^{*\bar{3}\bar{2}\bar{1}\bar{4}} + \Phi^{*\bar{3}\bar{1}\bar{2}\bar{4}} + \Phi^{*\bar{3}\bar{4}\bar{1}\bar{2}} \Big\} \Big\{ \Phi_\eta^{\bar{1}'\bar{2}'\bar{3}'\bar{4}'} + \Phi_\eta^{\bar{3}'\bar{4}'\bar{1}'\bar{2}'} \Big\} \quad \text{(B.17)}$$

$$= \Big\{ \Phi^{*\bar{1}\bar{2}\bar{3}\bar{4}} + \Phi^{*\bar{1}\bar{3}\bar{2}\bar{4}} + \Phi^{*\bar{1}\bar{4}\bar{2}\bar{3}} + \Phi^{*\bar{2}\bar{3}\bar{1}\bar{4}} + \Phi^{*\bar{2}\bar{4}\bar{1}\bar{3}} + \Phi^{*\bar{3}\bar{4}\bar{1}\bar{2}} \Big\} \Big\{ \Phi_\eta^{\bar{1}'\bar{2}'\bar{3}'\bar{4}'} + \Phi_\eta^{\bar{3}'\bar{4}'\bar{1}'\bar{2}'} \Big\}. \quad \text{(B.18)}$$

The first factor can be written in terms of a sum over all permutations Π of the indices $\bar{1}$, $\bar{2}$, $\bar{3}$, and $\bar{4}$. Again exchanging $\bar{1}^{(\prime)}$ with $\bar{4}^{(\prime)}$ and $\bar{2}^{(\prime)}$ with $\bar{4}^{(\prime)}$, each in one third of the second factor, the latter factor can also be written as a sum over index permutations

$$\begin{aligned}\Psi^{\bar{1}\,\bar{2}\,\bar{3}\,\bar{4}}_{\bar{1}'\bar{2}'\bar{3}'\bar{4}'} &= \Big\{\frac{1}{4}\sum_{\Pi}\,\Phi^{*\Pi(\bar{1}\bar{2}\bar{3}\bar{4})}\Big\}\frac{16}{3} \\ &\qquad \Big\{\Phi^{\bar{1}'\bar{2}'\bar{3}'\bar{4}'}_{\eta} + \Phi^{\bar{4}'\bar{2}'\bar{3}'\bar{1}'}_{\eta} + \Phi^{\bar{1}'\bar{4}'\bar{3}'\bar{2}'}_{\eta} + \Phi^{\bar{3}'\bar{4}'\bar{1}'\bar{2}'}_{\eta} + \Phi^{\bar{3}'\bar{1}'\bar{4}'\bar{2}'}_{\eta} + \Phi^{\bar{3}'\bar{2}'\bar{1}'\bar{4}'}_{\eta}\Big\} \quad \text{(B.19)} \\ &= \frac{1}{3}\Big\{\sum_{\Pi}\,\Phi^{*\Pi(\bar{1}\bar{2}\bar{3}\bar{4})}\Big\}\Big\{\sum_{\Pi}\,\Phi^{\Pi(\bar{1}'\bar{2}'\bar{3}'\bar{4}')}_{\eta}\Big\}. \quad \text{(B.20)}\end{aligned}$$

Using the definition of the energy-conserving two-particle matrix element Φ_η in Eq. (B.9) and Eq. (65) in [37] for the corresponding element in the single-particle energy basis, we can write Φ_η as

$$\Phi^{\bar{1}'\bar{2}'\bar{3}'\bar{4}'}_{\eta} = \phi^{1'2'3'4'}_{\eta}\; v^{\bar{1}'*}_{1'} v^{\bar{2}'*}_{2'} u^{\bar{3}'}_{3'} u^{\bar{4}}_{4'} = \int_{-\infty}^{t} dt'\; e^{\eta\tau}\phi^{1234} K_1^{1'\dagger}(\tau) K_2^{2'\dagger}(\tau) K_3^{3'}(\tau) K_4^{4'}(\tau) v^{\bar{1}'*}_{1'} v^{\bar{2}'*}_{2'} u^{\bar{3}'}_{3'} u^{\bar{4}}_{4'}, \quad \text{(B.21)}$$

where $\tau = t' - t$. The time-evolution operator K is given by the time-ordered exponential

$$K(\tau) = \mathrm{T}\; e^{i\int_{\tau}^{0} ds\; H^{(0)}(s)}. \quad \text{(B.22)}$$

For Eq. (B.21), we can approximate $K(\tau)$ by replacing $H^{(0)}(s)$ by its value $H^{(0)}(0) = H^{(0)}$ at $\tau = 0$ because the energy uncertainty η exponentially dampens earlier contributions to obtain

$$K(\tau) \approx e^{-i\tau H^{(0)}}. \quad \text{(B.23)}$$

Substituting this result back into the definition of the energy-conserving two-particle matrix element in Eq. (B.21), we obtain

$$\begin{aligned}\Phi^{\bar{1}'\bar{2}'\bar{3}'\bar{4}'}_{\eta} &\approx \int_{-\infty}^{t} dt'\; e^{\eta\tau}\phi^{1234}\; (e^{i\tau H^{(0)}})^{1'}_{1}\, v^{\bar{1}'*}_{1'}\; (e^{i\tau H^{(0)}})^{2'}_{2}\, v^{\bar{2}'*}_{2'}\; (e^{-i\tau H^{(0)}})^{3'}_{3}\, u^{\bar{3}'}_{3'}\; (e^{-i\tau H^{(0)}})^{4'}_{4}\, u^{\bar{4}'}_{4'} \\ &= \phi^{1234}\; v^{\bar{1}'*}_{1} v^{\bar{2}'*}_{2} u^{\bar{3}'}_{3} u^{\bar{4}}_{4} \int_{-\infty}^{t} dt'\; e^{\eta\tau} e^{-i\tau(\epsilon_{\bar{1}'}+\epsilon_{\bar{2}'}+\epsilon_{\bar{3}'}+\epsilon_{\bar{4}'})} \quad \text{(B.24)} \\ &= \Phi^{\bar{1}'\bar{2}'\bar{3}'\bar{4}'}\frac{1}{\eta - i\Delta} \quad \underset{\eta\to 0}{\longrightarrow} \quad \Phi^{\bar{1}'\bar{2}'\bar{3}'\bar{4}'}\Big(\pi\delta_\eta(\Delta) + i\mathcal{P}_\eta\frac{1}{\Delta}\Big), \quad \text{(B.25)}\end{aligned}$$

with the energy difference $\Delta \equiv \epsilon_{\bar{1}'} + \epsilon_{\bar{2}'} + \epsilon_{\bar{3}'} + \epsilon_{\bar{4}'}$. We can now rewrite the combined matrix element Ψ from Eq. (B.20) as

$$\Psi^{\bar{1}\,\bar{2}\,\bar{3}\,\bar{4}}_{\bar{1}'\bar{2}'\bar{3}'\bar{4}'} = \psi^{*\bar{1}\bar{2}\bar{3}\bar{4}}\psi^{\bar{1}'\bar{2}'\bar{3}'\bar{4}'}\Big(\pi\delta_\eta(\Delta) + i\mathcal{P}_\eta\frac{1}{\Delta}\Big), \quad \text{(B.26)}$$

where we again defined a new, totally symmetric, matrix element

$$\psi^{\bar{1}\bar{2}\bar{3}\bar{4}} \equiv \frac{1}{\sqrt{3}} \sum_{\Pi} \Phi^{\Pi(\bar{1}\bar{2}\bar{3}\bar{4})} = \frac{4}{\sqrt{3}} \Big\{ \Phi^{\bar{1}\bar{2}\bar{3}\bar{4}} + \Phi^{\bar{1}\bar{3}\bar{2}\bar{4}} + \Phi^{\bar{1}\bar{4}\bar{2}\bar{3}} + \Phi^{\bar{2}\bar{3}\bar{1}\bar{4}} + \Phi^{\bar{2}\bar{4}\bar{1}\bar{3}} + \Phi^{\bar{3}\bar{4}\bar{1}\bar{2}} \Big\}. \tag{B.27}$$

To obtain the collision operator $\Gamma^{<}$, which includes processes involving the condensate, from $\tilde{\Gamma}^{<}$, we define extended two-particle matrix elements, modifying Eq. (B.9)

$$\Phi^{\alpha^* \bar{2}\bar{3}\bar{4}} \equiv \phi^{1'2'3'4'}\ \alpha^*_{1'} v^{\bar{2}*}_{2'} u^{\bar{3}}_{3'} u^{\bar{4}}_{4'} \tag{B.28}$$

$$\Phi^{\bar{1}\bar{2}\alpha\bar{4}} \equiv \phi^{1'2'3'4'}\ v^{\bar{1}*}_{1'} v^{\bar{2}*}_{2'} \alpha_{3'} u^{\bar{4}}_{4'}, \tag{B.29}$$

and generalized matrix elements, modifying Eq. (B.27)

$$\psi^{\chi\bar{2}\bar{3}\bar{4}} = \frac{4}{\sqrt{3}} \Big\{ \Phi^{\alpha^*\bar{2}\bar{3}\bar{4}} + \Phi^{\alpha^*\bar{3}\bar{2}\bar{4}} + \Phi^{\alpha^*\bar{4}\bar{2}\bar{3}} + \Phi^{\bar{2}\bar{3}\alpha\bar{4}} + \Phi^{\bar{2}\bar{4}\alpha\bar{3}} + \Phi^{\bar{3}\bar{4}\alpha\bar{2}} \Big\}. \tag{B.30}$$

This new generalized matrix element is also totally symmetric, in particular

$$\psi^{\chi\bar{2}\bar{3}\bar{4}} = \psi^{\bar{2}\chi\bar{3}\bar{4}} = \psi^{\bar{4}\bar{2}\bar{3}\chi}. \tag{B.31}$$

As a consequence,

$$\Psi^{\chi\bar{2}\ \bar{3}\ \bar{4}}_{\chi\bar{2}'\bar{3}'\bar{4}'} \equiv \psi^{*\chi\bar{2}\bar{3}\bar{4}} \psi^{\chi\bar{2}'\bar{3}'\bar{4}'} \Big(\pi\delta_\eta(\Delta_1) + i\mathcal{P}_\eta \frac{1}{\Delta_1} \Big) = \Psi^{\bar{2}\ \chi\bar{3}\ \bar{4}}_{\bar{2}'\chi\bar{3}'\bar{4}'} = \Psi^{\bar{4}\ \bar{2}\ \bar{3}\ \chi}_{\bar{4}'\bar{2}'\bar{3}'\chi}. \tag{B.32}$$

The energy-conserving matrix elements that contain condensate contributions can be written analogous to Eq. (B.25) as

$$\Phi^{1''\bar{2}'\bar{3}'\bar{4}'}_{\eta} \alpha^*_{1''} = \Phi^{1'\bar{2}'\bar{3}'\bar{4}'} \alpha^*_{1'} \Big(\pi\delta_\eta(\Delta_1) + i\mathcal{P}_\eta \frac{1}{\Delta_1} \Big) \quad \text{with } \Delta_1 \equiv \mu + \epsilon_{\bar{2}'} + \epsilon_{\bar{3}'} + \epsilon_{\bar{4}'} \text{ and} \tag{B.33}$$

$$\Phi^{\bar{1}'\bar{2}'\bar{3}'4''}_{\eta} \alpha_{4''} = \Phi^{\bar{1}'\bar{2}'\bar{3}'4'} \alpha_{4'} \Big(\pi\delta_\eta(\Delta_2) + i\mathcal{P}_\eta \frac{1}{\Delta_2} \Big) \quad \text{with } \Delta_2 \equiv \mu + \epsilon_{\bar{1}'} + \epsilon_{\bar{2}'} + \epsilon_{\bar{3}'}. \tag{B.34}$$

We can now write the full collision operator $\Gamma^{<}$ as

$$\begin{aligned} W^\dagger \sigma^z \Gamma^< W = \frac{1}{2} |\bar{3}\rangle \otimes \langle \bar{3}'| \Big\{ & \Psi^{\bar{1}\ \bar{2}\ \bar{3}\ \bar{4}}_{\bar{1}'\bar{2}'\bar{3}'\bar{4}'}\ P_{-\bar{1}-\bar{1}'} P_{-\bar{2}-\bar{2}'} P_{-\bar{4}-\bar{4}'} \\ & + \Big(\Psi^{\chi\bar{2}\ \bar{3}\ \bar{4}}_{\chi\bar{2}'\bar{3}'\bar{4}'}\ P_{-\bar{2}-\bar{2}'} P_{-\bar{4}-\bar{4}'} + \Psi^{\bar{1}\ \chi\bar{3}\ \bar{4}}_{\bar{1}'\chi\bar{3}'\bar{4}'}\ P_{-\bar{1}-\bar{1}'} P_{-\bar{4}-\bar{4}'} + \Psi^{\bar{1}\ \bar{2}\ \bar{3}\ \chi}_{\bar{1}'\bar{2}'\bar{3}'\chi}\ P_{-\bar{1}-\bar{1}'} P_{-\bar{2}-\bar{2}'} \Big) \Big\}. \end{aligned} \tag{B.35}$$

Relabeling some indices, we obtain

$$\begin{aligned} W^\dagger \sigma^z \Gamma^< W = \frac{1}{2} |\bar{3}\rangle \otimes \langle \bar{3}'| \Big\{ & \Psi^{\bar{1}\ \bar{2}\ \bar{3}\ \bar{4}}_{\bar{1}'\bar{2}'\bar{3}'\bar{4}'}\ P_{-\bar{1}-\bar{1}'} P_{-\bar{2}-\bar{2}'} P_{-\bar{4}-\bar{4}'} \\ & + \Big(\Psi^{\chi\bar{2}\ \bar{3}\ \bar{4}}_{\chi\bar{2}'\bar{3}'\bar{4}'} + \Psi^{\bar{2}\ \chi\bar{3}\ \bar{4}}_{\bar{2}'\chi\bar{3}'\bar{4}'} + \Psi^{\bar{4}\ \bar{2}\ \bar{3}\ \chi}_{\bar{4}'\bar{2}'\bar{3}'\chi} \Big) P_{-\bar{2}-\bar{2}'} P_{-\bar{4}-\bar{4}'} \Big\}. \end{aligned} \tag{B.36}$$

We can now use the symmetry of the generalized matrix elements, as given in Eq. (B.32) to obtain

$$W^{\dagger}\sigma^{z}\Gamma^{<}W=\frac{1}{2}\Big\{\Psi^{\bar{1}\,\bar{2}\,\bar{3}\,\bar{4}}_{\bar{1}'\bar{2}'\bar{3}'\bar{4}'}\,P_{-\bar{1}-\bar{1}'}P_{-\bar{2}-\bar{2}'}P_{-\bar{4}-\bar{4}'}+3\,\Psi^{\chi\bar{2}\,\bar{3}\,\bar{4}}_{\chi\bar{2}'\bar{3}'\bar{4}'}\,P_{-\bar{2}-\bar{2}'}P_{-\bar{4}-\bar{4}'}\Big\}\,|\bar{3}\rangle\otimes\langle\bar{3}'|\,. \quad \text{(B.37)}$$

This is the final result for the in-rate of the second-order collisional contributions, which is much simpler than the single-particle representation of these contributions given in Eq. (3.28).

The time-reversed collision operator for the fluctuations $\tilde{\Gamma}^{>}$ describes the collisions out of the distribution $\tilde{G}^{<}$ and is given by

$$\sigma^{z}\tilde{\Gamma}^{>}=\begin{pmatrix}\Gamma_{(1+\tilde{f})(1+\tilde{f})\tilde{f}}+2\Gamma_{(1+\tilde{f})\tilde{m}\tilde{m}^{*}} & \Gamma_{\tilde{m}\tilde{m}\tilde{m}^{*}}+2\Gamma_{(1+\tilde{f})\tilde{m}\tilde{f}}\\ \Gamma^{*}_{\tilde{m}\tilde{m}\tilde{m}^{*}}+2\Gamma^{*}_{\tilde{f}\tilde{m}(1+\tilde{f})} & \Gamma^{\dagger}_{\tilde{f}\tilde{f}(1+\tilde{f})}+2\Gamma^{\dagger}_{\tilde{f}\tilde{m}\tilde{m}^{*}}\end{pmatrix}. \quad \text{(B.38)}$$

It can be transformed in the same way as shown above for the in-rates to obtain

$$\begin{aligned}
&W^{\dagger}\sigma^{z}\tilde{\Gamma}^{>}W=8\,P_{\bar{2}'-\bar{4}}P_{\bar{4}'-\bar{2}}P_{\bar{1}'-\bar{3}}\,|-\bar{1}\rangle\otimes\langle\bar{3}'|\\
&\times\Big[\Phi^{\bar{1}\bar{2}\bar{3}\bar{4}}\Phi^{\bar{1}'\bar{2}'\bar{3}'\bar{4}'}_{\eta}+2\Phi^{\bar{1}\bar{2}\bar{3}\bar{4}}\Phi^{\bar{3}'\bar{2}'\bar{1}'\bar{4}'}_{\eta}+2\Phi^{\bar{3}\bar{2}\bar{1}\bar{4}}\Phi^{\bar{1}'\bar{2}'\bar{3}'\bar{4}'}_{\eta}+\Phi^{\bar{3}\bar{2}\bar{1}\bar{4}}\Phi^{\bar{3}'\bar{2}'\bar{1}'\bar{4}'}_{\eta}\\
&\quad+2\Phi^{\bar{1}\bar{4}\bar{3}\bar{2}}\Phi^{\bar{1}'\bar{2}'\bar{3}'\bar{4}'}_{\eta}+\Phi^{\bar{1}\bar{4}\bar{3}\bar{2}}\Phi^{\bar{3}'\bar{2}'\bar{1}'\bar{4}'}_{\eta}+\Phi^{\bar{3}\bar{4}\bar{1}\bar{2}}\Phi^{\bar{1}'\bar{2}'\bar{3}'\bar{4}'}_{\eta}+2\Phi^{\bar{3}\bar{4}\bar{1}\bar{2}}\Phi^{\bar{3}'\bar{2}'\bar{1}'\bar{4}'}_{\eta}\Big] \quad \text{(B.39)}\\
&=8\,P_{\bar{2}'\bar{2}}P_{\bar{4}'\bar{4}}P_{\bar{1}'\bar{1}}\,|\bar{3}\rangle\otimes\langle\bar{3}'|\\
&\times\Big[\Phi^{*\bar{1}\bar{2}\bar{3}\bar{4}}\Phi^{\bar{1}'\bar{2}'\bar{3}'\bar{4}'}_{\eta}+2\Phi^{*\bar{1}\bar{2}\bar{3}\bar{4}}\Phi^{\bar{3}'\bar{2}'\bar{1}'\bar{4}'}_{\eta}+2\Phi^{*\bar{3}\bar{2}\bar{1}\bar{4}}\Phi^{\bar{1}'\bar{2}'\bar{3}'\bar{4}'}_{\eta}+\Phi^{*\bar{3}\bar{2}\bar{1}\bar{4}}\Phi^{\bar{3}'\bar{2}'\bar{1}'\bar{4}'}_{\eta}\\
&\quad+2\Phi^{*\bar{1}\bar{4}\bar{3}\bar{2}}\Phi^{\bar{1}'\bar{2}'\bar{3}'\bar{4}'}_{\eta}+\Phi^{*\bar{1}\bar{4}\bar{3}\bar{2}}\Phi^{\bar{3}'\bar{2}'\bar{1}'\bar{4}'}_{\eta}+\Phi^{*\bar{3}\bar{4}\bar{1}\bar{2}}\Phi^{\bar{1}'\bar{2}'\bar{3}'\bar{4}'}_{\eta}+2\Phi^{*\bar{3}\bar{4}\bar{1}\bar{2}}\Phi^{\bar{3}'\bar{2}'\bar{1}'\bar{4}'}_{\eta}\Big] \quad \text{(B.40)}\\
&=\frac{1}{2}\,P_{\bar{1}'\bar{1}}P_{\bar{2}'\bar{2}}P_{\bar{4}'\bar{4}}\,|\bar{3}\rangle\otimes\langle\bar{3}'|\,\Psi^{\bar{1}\,\bar{2}\,\bar{3}\,\bar{4}}_{\bar{1}'\bar{2}'\bar{3}'\bar{4}'}, \quad \text{(B.41)}
\end{aligned}$$

which is similar in form to Eq. (B.14).

Appendix C

Kinetic Equations for Fermions

In this Appendix, we use the formalism of the Boson kinetic equations presented in Chapters 2 through 4 to derive equations for fermions in a homogeneous system, similar to those used in the later Chapters 5 through 8. This illustrates how the two main parts of this thesis are connected. The main steps are writing the kinetic equations in the position basis, writing them in center-of-mass coordinates, and then Fourier-transforming the relative coordinate to a Wigner representation, which reduces to the usual distribution function in a homogeneous system. We only demonstrate these transformations for the first-order terms; however, it is straightforward to use the same steps for the higher-order collision terms and reproduce parts of the rate equations we derived using the cumulant formalism in Chap. 7. We begin by considering the kinetic equations for fermions in the single-particle energy basis as introduced in Chap. 2.

C.1 Kinetic Equations

We consider the following Hamiltonian

$$H = {H^{(0)}}^{1'2'} a^\dagger_{1'} a_{2'} + \phi^{1'2'3'4'} a^\dagger_{1'} a^\dagger_{2'} a_{3'} a_{4'}, \tag{C.1}$$

where ${H^{(0)}}^{1'2'} = \langle 1'| H^{(0)} |2'\rangle$ denotes the matrix elements of the interaction-free single-particle Hamiltonian

$$H^{(0)} = \frac{\boldsymbol{p}^2}{2m} + V_{\text{ext}}(\boldsymbol{x}), \tag{C.2}$$

with external harmonic potential V_{ext}. The fermionic creation operator $a^\dagger_{1'}$ creates a particle in the state $|1'\rangle$, where $1'$ stands for a complete set of quantum numbers, which label a con-

stant, single-particle energy basis $\{\varphi_{1'}\}_{1'}$, such as, for example, harmonic oscillator states. The fermionic field operator in the position basis $\psi(\boldsymbol{x})$ can be written in terms of the single-particle energy basis

$$\psi(\boldsymbol{x}) = \sum_{1'} \varphi_{1'}(\boldsymbol{x}) a_{1'} = \langle \boldsymbol{x} \,|\, 1' \rangle a_{1'}. \tag{C.3}$$

We use the summation convention for these abbreviated indices and indicate the single-particle basis with primes.

We now define the distribution functions and potentials in the single-particle energy basis. The Hermitian normal density matrix f is defined by

$$f = \langle a^\dagger_{2'} a_{1'} \rangle \, |1'\rangle \otimes \langle 2'| \tag{C.4}$$

as in the boson case. The anomalous average m is defined as

$$m = \langle a_{2'} a_{1'} \rangle \, |1'\rangle \otimes |2'\rangle \,. \tag{C.5}$$

It is anti-symmetric for fermions: $m = -m^\top$. The anti-symmetrized two-particle matrix elements of the binary, spin-dependent interaction potential $V_{\mathrm{bin}}(\boldsymbol{x}_1, \boldsymbol{x}_2)$ are defined by

$$\phi^{1'2'3'4'} = (\mathcal{A}) \frac{1}{2} \int d\boldsymbol{x}_1 \, d\boldsymbol{x}_2 \, \langle 1' \,|\, \boldsymbol{x}_1 \rangle \langle 2' \,|\, \boldsymbol{x}_2 \rangle V_{\mathrm{bin}}(\boldsymbol{x}_1 - \boldsymbol{x}_2) \langle \boldsymbol{x}_1 \,|\, 3' \rangle \langle \boldsymbol{x}_2 \,|\, 4' \rangle. \tag{C.6}$$

These matrix elements are explicitly anti-symmetrized ($\mathcal{A}$) such that:

$$\phi^{1'2'3'4'} = -\phi^{2'1'3'4'} = -\phi^{1'2'4'3'}. \tag{C.7}$$

We anti-symmetrize these matrix elements, because the symmetric parts do not contribute to the Hamiltonian in Eq. (C.1) due to the Fermi anti-commutation of the operators. The energy shift due to the normal fluctuations is given by the Hermitian matrix

$$U_f = 2 \, \phi^{1'2'3'4'} f_{3'2'} \, |1'\rangle \otimes \langle 4'| \,, \tag{C.8}$$

whereas the first-order anomalous coupling-strength is given by the anti-symmetric matrix

$$V_m = 2 \, \phi^{1'2'3'4'} m_{3'4'} \, |1'\rangle \otimes |2'\rangle \,. \tag{C.9}$$

To define the generalized density matrices, we start with the spinor

$$A = \begin{pmatrix} a \\ a^\dagger \end{pmatrix}, \tag{C.10}$$

where $a = a_{1'} |1'\rangle$ and $a^\dagger = a^\dagger_{1'} \langle 1'|$ are vectors of operators. Then, the single-time limit of one time-ordering [43, 39] can be written as

$$G^> = \langle A A^\dagger \rangle = \begin{pmatrix} (1-f) & -m \\ m^* & f^* \end{pmatrix}. \tag{C.11}$$

The other time ordering gives the usual many-body density matrix

$$G^< = -\langle \sigma_1 A A^\dagger \sigma_1 \rangle^\top = - \begin{pmatrix} f & m \\ -m^* & (1-f)^* \end{pmatrix}. \tag{C.12}$$

The generalized Boltzmann equation of motion for this fluctuation-density matrix can be written as

$$\frac{\mathrm{d}}{\mathrm{d}t} G^< = -i\Sigma G^< + \Gamma^< G^> - \Gamma^> G^< + \text{H.c.} \tag{C.13}$$

The reversible evolution above is governed by the Hartree–Fock–Bogoliubov self-energy operator

$$\Sigma = \begin{pmatrix} \Sigma_{\mathcal{N}} & \Sigma_{\mathcal{A}} \\ -\Sigma^*_{\mathcal{A}} & -\Sigma^*_{\mathcal{N}} \end{pmatrix}, \tag{C.14}$$

which in turn consists of the Hermitian Hamiltonian

$$\Sigma_{\mathcal{N}} = H^{(0)} + 2U_f - \mu \tag{C.15}$$

and the anti-symmetric anomalous coupling

$$\Sigma_{\mathcal{A}} = V_{\tilde{m}}. \tag{C.16}$$

In the following, we neglect the irreversible second-order evolution given by the collision operators Γ.

Considering the components of Eq. (C.13), we obtain the following first-order equations

for f and m alone:

$$i\frac{\mathrm{d}}{\mathrm{d}t}f = \Sigma_{\mathcal{N}}f - f\Sigma_{\mathcal{N}} - \Sigma_{\mathcal{A}}m^* + m\Sigma_{\mathcal{A}}^* \tag{C.17}$$

$$i\frac{\mathrm{d}}{\mathrm{d}t}m = \Sigma_{\mathcal{N}}m + m\Sigma_{\mathcal{N}}^\top + \Sigma_{\mathcal{A}}(1-f)^* - f\Sigma_{\mathcal{A}} \tag{C.18}$$

C.2 Transformation to the Position Basis

We explicitly identify the energy and spin parts of the single-particle energy basis by writing $|1'\rangle = |\epsilon_{1'}, s_{1'}\rangle$. We can then write the transformation to the position basis as

$$\langle 1\,|\,1'\rangle = \psi_{\epsilon_{1'}}(\boldsymbol{x}_1). \tag{C.19}$$

This wave function is used to transform the energy part of the matrices defined above to the position basis. The spin labels remain after this transformation. The completeness relations for the transformation are

$$\langle 1\,|\,1'\rangle\langle 1'\,|\,2\rangle = \delta(\boldsymbol{x}_1 - \boldsymbol{x}_2), \quad \text{and} \tag{C.20}$$

$$\int d\boldsymbol{x}_1 \langle 1'\,|\,1\rangle\langle 1\,|\,2'\rangle = \delta_{\epsilon_{1'},\epsilon_{2'}}\chi^*(s_{1'})\chi(s_{2'}), \tag{C.21}$$

where χ is a spin function and we use the summation convention for the energy basis.

We now write the distribution functions and energy shifts in the position basis. The normal average f transforms as a matrix

$$f_{s_1s_2}(\boldsymbol{x}_1, \boldsymbol{x}_2) = \langle 1\,|\,1'\rangle f_{1'2'}\langle 2'\,|\,2\rangle, \quad \text{and} \tag{C.22}$$

$$f_{1'2'} = \int d\boldsymbol{x}_1 d\boldsymbol{x}_2\ \langle 1'\,|\,1\rangle f_{s_1s_2}(\boldsymbol{x}_1, \boldsymbol{x}_2)\langle 2\,|\,2'\rangle, \tag{C.23}$$

whereas the anomalous average m transforms as a tensor according to

$$m_{s_1s_2}(\boldsymbol{x}_1, \boldsymbol{x}_2) = \langle 1\,|\,1'\rangle\langle 2\,|\,2'\rangle m_{1'2'}, \quad \text{and} \tag{C.24}$$

$$m_{1'2'} = \int d\boldsymbol{x}_1 d\boldsymbol{x}_2\ \langle 1'\,|\,1\rangle\langle 2'\,|\,2\rangle m_{s_1s_2}(\boldsymbol{x}_1, \boldsymbol{x}_2). \tag{C.25}$$

The matrix elements of the potential with explicit spin indices are

$$\phi^{1'2'3'4'} = \frac{1}{4}\int d\boldsymbol{x}_1\, d\boldsymbol{x}_2\ \langle 1'\,|\,1\rangle\langle 2'\,|\,2\rangle V_{s_1s_2s_3s_4}(\boldsymbol{x}_1 - \boldsymbol{x}_2)\Big\{\langle 1\,|\,3'\rangle\langle 2\,|\,4'\rangle + \langle 1\,|\,4'\rangle\langle 2\,|\,3'\rangle\Big\}, \tag{C.26}$$

where the energy labels under the integral are symmetric and the spin part of the binary potential is anti-symmetric

$$V_{s_1 s_2 s_3 s_4}(\boldsymbol{r}) = -V_{s_2 s_1 s_3 s_4}(\boldsymbol{r}) = -V_{s_1 s_2 s_4 s_3}(\boldsymbol{r}), \tag{C.27}$$

in order to fulfill Eq. (C.7). The energy shifts in the position basis are

$$W_{s_1 s_4}(\boldsymbol{x}_1, \boldsymbol{x}_2) = \langle 1\,|\,1'\rangle U_f^{1'4'} \langle 4'\,|\,2\rangle = V_{s_1 s_2 s_3 s_4}(\boldsymbol{x}_1 - \boldsymbol{x}_2) f_{s_3 s_2}(\boldsymbol{x}_1, \boldsymbol{x}_2), \quad \text{and} \tag{C.28}$$

$$\Delta_{s_1 s_2}(\boldsymbol{x}_1, \boldsymbol{x}_2) = \langle 1\,|\,1'\rangle\langle 2\,|\,2'\rangle V_m^{1'2'} = V_{s_1 s_2 s_3 s_4}(\boldsymbol{x}_1 - \boldsymbol{x}_2) m_{s_3 s_4}(\boldsymbol{x}_1, \boldsymbol{x}_2). \tag{C.29}$$

We now have all the elements of Eqs. (C.17) and (C.18) for the normal and anomalous average and can write these equations of motion in the position basis:

$$\begin{aligned} i\frac{\mathrm{d}}{\mathrm{d}t} f_{s_1 s_2}(\boldsymbol{x}_1, \boldsymbol{x}_2) = {} & [H^{(0)}(\boldsymbol{x}_1) - H^{(0)}(\boldsymbol{x}_2)] f_{s_1 s_2}(\boldsymbol{x}_1, \boldsymbol{x}_2) \\ & + \int d\boldsymbol{y}\, [W_{s_1 s_3}(\boldsymbol{x}_1, \boldsymbol{y}) f_{s_3 s_2}(\boldsymbol{y}, \boldsymbol{x}_2) - f_{s_1 s_3}(\boldsymbol{x}_1, \boldsymbol{y}) W_{s_3 s_2}(\boldsymbol{y}, \boldsymbol{x}_2)] \\ & - \int d\boldsymbol{y}\, [\Delta_{s_1 s_3}(\boldsymbol{x}_1, \boldsymbol{y}) m^*_{s_3 s_2}(\boldsymbol{y}, \boldsymbol{x}_2) - m_{s_1 s_3}(\boldsymbol{x}_1, \boldsymbol{y}) \Delta^*_{s_3 s_2}(\boldsymbol{y}, \boldsymbol{x}_2)], \end{aligned} \tag{C.30}$$

$$\begin{aligned} i\frac{\mathrm{d}}{\mathrm{d}t} m_{s_1 s_2}(\boldsymbol{x}_1, \boldsymbol{x}_2) = {} & [H^{(0)}(\boldsymbol{x}_1) + H^{(0)}(\boldsymbol{x}_2)] m_{s_1 s_2}(\boldsymbol{x}_1, \boldsymbol{x}_2) \\ & + \int d\boldsymbol{y}\, [W_{s_1 s_3}(\boldsymbol{x}_1, \boldsymbol{y}) m_{s_3 s_2}(\boldsymbol{y}, \boldsymbol{x}_2) + m_{s_1 s_3}(\boldsymbol{x}_1, \boldsymbol{y}) W_{s_3 s_2}(\boldsymbol{y}, \boldsymbol{x}_2)] \\ & + \int d\boldsymbol{y}\, [\Delta_{s_1 s_3}(\boldsymbol{x}_1, \boldsymbol{y})(1 - f)^*_{s_3 s_2}(\boldsymbol{y}, \boldsymbol{x}_2) - f_{s_1 s_3}(\boldsymbol{x}_1, \boldsymbol{y}) \Delta_{s_3 s_2}(\boldsymbol{y}, \boldsymbol{x}_2)], \end{aligned} \tag{C.31}$$

with the position-basis single-particle Hamiltonian

$$H^{(0)}(\boldsymbol{x}) = \frac{\nabla^2_{\boldsymbol{x}}}{2m} + V_{\mathrm{ext}}(\boldsymbol{x}). \tag{C.32}$$

C.3 Center-of-Mass Coordinates

We now transform to center-of-mass position coordinates. These coordinates are given by $\boldsymbol{R} = \frac{\boldsymbol{x}_1 + \boldsymbol{x}_2}{2}$ and $\boldsymbol{r} = \boldsymbol{x}_1 - \boldsymbol{x}_2$. We find for the distribution functions:

$$f_{s_1 s_2}(\boldsymbol{R}, \boldsymbol{r}) = f_{s_1 s_2}\Big(\boldsymbol{R} + \frac{\boldsymbol{r}}{2}, \boldsymbol{R} - \frac{\boldsymbol{r}}{2}\Big), \tag{C.33}$$

$$m_{s_1 s_2}(\boldsymbol{R}, \boldsymbol{r}) = m_{s_1 s_2}\Big(\boldsymbol{R} + \frac{\boldsymbol{r}}{2}, \boldsymbol{R} - \frac{\boldsymbol{r}}{2}\Big). \tag{C.34}$$

The energy shifts are now

$$W_{s_1 s_2}(\boldsymbol{R}, \boldsymbol{r}) = V_{s_1 s_3 s_4 s_2}(\boldsymbol{r}) f_{s_4 s_3}(\boldsymbol{R}, \boldsymbol{r}) \tag{C.35}$$

$$\Delta_{s_1 s_2}(\boldsymbol{R}, \boldsymbol{r}) = V_{s_1 s_2 s_3 s_4}(\boldsymbol{r}) m_{s_3 s_4}(\boldsymbol{R}, \boldsymbol{r}), \tag{C.36}$$

and the single-particle Hamiltonian can be written as a center-of-mass and relative contribution, because we assume a harmonic trapping potential

$$H^{(0)}(\boldsymbol{x}_1) + H^{(0)}(\boldsymbol{x}_2) = H^{(0)}(\boldsymbol{r}) + H^{(0)}(\boldsymbol{R}), \tag{C.37}$$

where the mass m in $H^{(0)}(\boldsymbol{x})$ is the appropriate reduced mass for the center of mass ($2m$) and relative ($m/2$) Hamiltonian.

Since the range of the two-body potential r_0 is small compared to the size of the system, the distribution functions are weakly dependent on the center-of-mass coordinate, and we can make the following approximations

$$f_{s_1 s_2}(\boldsymbol{R} + \boldsymbol{r}', \boldsymbol{r}) \approx f_{s_1 s_2}(\boldsymbol{R}, \boldsymbol{r}) \quad \text{for any } |\boldsymbol{r}'| \leq r_0, \tag{C.38}$$

$$m_{s_1 s_2}(\boldsymbol{R} + \boldsymbol{r}', \boldsymbol{r}) \approx m_{s_1 s_2}(\boldsymbol{R}, \boldsymbol{r}) \quad \text{for any } |\boldsymbol{r}'| \leq r_0. \tag{C.39}$$

The equations of motion (C.30) and (C.31) can now be written in terms of center-of-mass and relative coordinates:

$$\begin{aligned} i\frac{\mathrm{d}}{\mathrm{d}t} f_{s_1 s_2}(\boldsymbol{R}, \boldsymbol{r}) = {} & [H^{(0)}(\boldsymbol{R} + \frac{\boldsymbol{r}}{2}) - H^{(0)}(\boldsymbol{R} - \frac{\boldsymbol{r}}{2})] f_{s_1 s_2}(\boldsymbol{R}, \boldsymbol{r}) \\ & + \int d\boldsymbol{x}\, [W_{s_1 s_3}\big(\boldsymbol{R} + \frac{\boldsymbol{r}}{2}, \boldsymbol{x}\big) f_{s_3 s_2}(\boldsymbol{R}, \boldsymbol{r} - \boldsymbol{x}) - f_{s_1 s_3}(\boldsymbol{R}, \boldsymbol{r} - \boldsymbol{x}) W_{s_3 s_2}\big(\boldsymbol{R} - \frac{\boldsymbol{r}}{2}, \boldsymbol{x}\big)] \\ & - \int d\boldsymbol{y}\, [\Delta_{s_1 s_3}\big(\boldsymbol{R} + \frac{\boldsymbol{r}}{2}, \boldsymbol{x}\big) m^*_{s_3 s_2}(\boldsymbol{R}, \boldsymbol{r} - \boldsymbol{x}) - m_{s_1 s_3}(\boldsymbol{R}, \boldsymbol{r} - \boldsymbol{x}) \Delta^*_{s_3 s_2}\big(\boldsymbol{R} - \frac{\boldsymbol{r}}{2}, \boldsymbol{x}\big)], \end{aligned} \tag{C.40}$$

$$\begin{aligned} i\frac{\mathrm{d}}{\mathrm{d}t} m_{s_1 s_2}(\boldsymbol{R}, \boldsymbol{r}) = {} & [H^{(0)}(\boldsymbol{R}) + H^{(0)}(\boldsymbol{r})] m_{s_1 s_2}(\boldsymbol{R}, \boldsymbol{r}) + V_{s_1 s_2 s_3 s_4}(\boldsymbol{r}) m_{s_3 s_4}(\boldsymbol{R}, \boldsymbol{r}) \\ & + \int d\boldsymbol{x}\, [W_{s_1 s_3}\big(\boldsymbol{R} + \frac{\boldsymbol{r}}{2}, \boldsymbol{x}\big) m_{s_3 s_2}(\boldsymbol{R}, \boldsymbol{r} - \boldsymbol{x}) + m_{s_1 s_3}(\boldsymbol{R}, \boldsymbol{r} - \boldsymbol{x}) W_{s_3 s_2}\big(\boldsymbol{R} - \frac{\boldsymbol{r}}{2}, \boldsymbol{x}\big)] \\ & - \int d\boldsymbol{x}\, [\Delta_{s_1 s_3}\big(\boldsymbol{R} + \frac{\boldsymbol{r}}{2}, \boldsymbol{x}\big) f^*_{s_3 s_2}(\boldsymbol{R}, \boldsymbol{r} - \boldsymbol{x}) + f_{s_1 s_3}(\boldsymbol{R}, \boldsymbol{r} - \boldsymbol{x}) \Delta_{s_3 s_2}\big(\boldsymbol{R} - \frac{\boldsymbol{r}}{2}, \boldsymbol{x}\big)]. \end{aligned} \tag{C.41}$$

C.4 Wigner Representation

In this Section we perform a Fourier transform of the relative coordinate in the distribution function and obtain a Wigner representation with a spatial center-of-mass and momentum relative coordinate. We start by writing the normal and anomalous averages in the Wigner representation by Fourier transforming Eqs. (C.33) and (C.34)

$$f_{s_1 s_2}(\boldsymbol{R},\boldsymbol{k}) = \frac{1}{(2\pi)^3}\int d\boldsymbol{r}\; e^{-i\boldsymbol{k}\boldsymbol{r}} f_{s_1 s_2}(\boldsymbol{R},\boldsymbol{r}), \tag{C.42}$$

$$m_{s_1 s_2}(\boldsymbol{R},\boldsymbol{k}) = \frac{1}{(2\pi)^3}\int d\boldsymbol{r}\; e^{-i\boldsymbol{k}\boldsymbol{r}} m_{s_1 s_2}(\boldsymbol{R},\boldsymbol{r}). \tag{C.43}$$

These distribution functions are independent of the center-of-mass coordinate in a homogeneous system, and correspond to the $f_{\boldsymbol{k}}$ and $m_{\boldsymbol{k}}$ used in Chap. 6. The potential transforms to

$$V_{s_1 s_2 s_3 s_4}(\boldsymbol{k}) = \frac{1}{(2\pi)^3}\int d\boldsymbol{r}\; e^{-i\boldsymbol{k}\boldsymbol{r}} V_{s_1 s_2 s_3 s_4}(\boldsymbol{r}), \tag{C.44}$$

and the relative part of the single-particle Hamiltonian is

$$H^{(0)}(\boldsymbol{k}) = \frac{\boldsymbol{k}^2}{2m} + \frac{1}{(2\pi)^3}\int d\boldsymbol{r}\; e^{-i\boldsymbol{k}\boldsymbol{r}} V_{\rm ext}(\boldsymbol{r}). \tag{C.45}$$

The energy shifts are now

$$W_{s_1 s_2}(\boldsymbol{R},\boldsymbol{k}) = \int d\boldsymbol{k}' V_{s_1 s_3 s_4 s_2}(\boldsymbol{k}-\boldsymbol{k}') f_{s_4 s_3}(\boldsymbol{R},\boldsymbol{k}'), \tag{C.46}$$

$$\Delta_{s_1 s_2}(\boldsymbol{R},\boldsymbol{k}) = \int d\boldsymbol{k}' V_{s_1 s_2 s_3 s_4}(\boldsymbol{k}-\boldsymbol{k}') m_{s_3 s_4}(\boldsymbol{R},\boldsymbol{k}'). \tag{C.47}$$

We now obtain the equations of motion in the Wigner representation by Fourier transforming Eqs. (C.40) and (C.41):

$$\begin{aligned} i\frac{\mathrm{d}}{\mathrm{d}t} f_{s_1 s_2}(\boldsymbol{R},\boldsymbol{k}) = &-\Big\{\big(H^{(0)}(\boldsymbol{R}) + H^{(0)}(\boldsymbol{k})\big), f_{s_1 s_2}(\boldsymbol{R},\boldsymbol{k})\Big\}_{\rm PB} + \int d\boldsymbol{r}\, d\boldsymbol{k}'\; e^{-i(\boldsymbol{k}-\boldsymbol{k}')\boldsymbol{r}} \\ &\times \Big[W_{s_1 s_3}\big(\boldsymbol{R}+\frac{\boldsymbol{r}}{2},\boldsymbol{k}'\big) f_{s_3 s_2}(\boldsymbol{R},\boldsymbol{k}') - f_{s_1 s_3}(\boldsymbol{R},\boldsymbol{k}') W_{s_3 s_2}\big(\boldsymbol{R}-\frac{\boldsymbol{r}}{2},\boldsymbol{k}'\big) \\ &- \Delta_{s_1 s_3}\big(\boldsymbol{R}+\frac{\boldsymbol{r}}{2},\boldsymbol{k}'\big) m^*_{s_3 s_2}(\boldsymbol{R},\boldsymbol{k}') + m_{s_1 s_3}(\boldsymbol{R},\boldsymbol{k}') \Delta^*_{s_3 s_2}\big(\boldsymbol{R}-\frac{\boldsymbol{r}}{2},\boldsymbol{k}'\big)\Big], \end{aligned} \tag{C.48}$$

where the Poisson-bracket term $\{,\}_{\rm PB}$ is an approximation to the full single-particle term given

in [151, App. D].

$$
\begin{aligned}
i\frac{\mathrm{d}}{\mathrm{d}t}m_{s_1s_2}(\boldsymbol{R},\boldsymbol{k}) = [H^{(0)}(\boldsymbol{R})+H^{(0)}(\boldsymbol{k})]m_{s_1s_2}(\boldsymbol{R},\boldsymbol{k}) + \Delta_{s_1s_2}(\boldsymbol{R},\boldsymbol{k}) + \int d\boldsymbol{r}\, d\boldsymbol{k}'\; e^{-i(\boldsymbol{k}-\boldsymbol{k}')\boldsymbol{r}} \\
\times \Big[W_{s_1s_3}\big(\boldsymbol{R}+\frac{\boldsymbol{r}}{2},\boldsymbol{k}'\big)m_{s_3s_2}(\boldsymbol{R},\boldsymbol{k}') + m_{s_1s_3}(\boldsymbol{R},\boldsymbol{k}')W_{s_3s_2}\big(\boldsymbol{R}-\frac{\boldsymbol{r}}{2},\boldsymbol{k}'\big) \\
- \Delta_{s_1s_3}\big(\boldsymbol{R}+\frac{\boldsymbol{r}}{2},\boldsymbol{k}'\big)f^*_{s_3s_2}(\boldsymbol{R},\boldsymbol{k}') - f_{s_1s_3}(\boldsymbol{R},\boldsymbol{k}')\Delta_{s_3s_2}\big(\boldsymbol{R}-\frac{\boldsymbol{r}}{2},\boldsymbol{k}'\big)\Big].
\end{aligned}
\tag{C.49}
$$

Dropping the $\boldsymbol{r}$-dependence of the center-of-mass coordinates, these equations simplify to:

$$
\begin{aligned}
i\frac{\mathrm{d}}{\mathrm{d}t}f_{s_1s_2}(\boldsymbol{R},\boldsymbol{k}) = -\Big\{\big(H^{(0)}(\boldsymbol{R})+H^{(0)}(\boldsymbol{k})\big), f_{s_1s_2}(\boldsymbol{R},\boldsymbol{k})\Big\}_{\mathrm{PB}} \\
+ (2\pi)^3\big[W_{s_1s_3}(\boldsymbol{R},\boldsymbol{k})f_{s_3s_2}(\boldsymbol{R},\boldsymbol{k}) - f_{s_1s_3}(\boldsymbol{R},\boldsymbol{k})W_{s_3s_2}(\boldsymbol{R},\boldsymbol{k}) \\
- \Delta_{s_1s_3}(\boldsymbol{R},\boldsymbol{k})m^*_{s_3s_2}(\boldsymbol{R},\boldsymbol{k}) + m_{s_1s_3}(\boldsymbol{R},\boldsymbol{k})\Delta^*_{s_3s_2}(\boldsymbol{R},\boldsymbol{k})\big],
\end{aligned}
\tag{C.50}
$$

$$
\begin{aligned}
i\frac{\mathrm{d}}{\mathrm{d}t}m_{s_1s_2}(\boldsymbol{R},\boldsymbol{k}) = [H^{(0)}(\boldsymbol{R})+H^{(0)}(\boldsymbol{k})]m_{s_1s_2}(\boldsymbol{R},\boldsymbol{k}) + \Delta_{s_1s_2}(\boldsymbol{R},\boldsymbol{k}) \\
+ (2\pi)^3\big[W_{s_1s_3}(\boldsymbol{R},\boldsymbol{k})m_{s_3s_2}(\boldsymbol{R},\boldsymbol{k}) + m_{s_1s_3}(\boldsymbol{R},\boldsymbol{k})W_{s_3s_2}(\boldsymbol{R},\boldsymbol{k}) \\
- \Delta_{s_1s_3}(\boldsymbol{R},\boldsymbol{k})f^*_{s_3s_2}(\boldsymbol{R},\boldsymbol{k}) - f_{s_1s_3}(\boldsymbol{R},\boldsymbol{k})\Delta_{s_3s_2}(\boldsymbol{R},\boldsymbol{k})\big].
\end{aligned}
\tag{C.51}
$$

These are the first-order equations of motion in the Wigner representation. In a homogeneous system, one can specify spin states as in the following Section to compare these equations to Eqs. (72) to (75) in Ref. [103] and to the equations in [152].

C.5 Scattering Equations for the Crossover Problem

We now specify a set of spin states to model the two-channel crossover Hamiltonian Eq. (5.8) discussed in Chap. 5 and show the resulting two-body scattering equations. We use the following spin states: $1, 2$ are hyperfine ground state (open channel), $3, 4$ are hyperfine excited (closed channel), electron up and down in each case. We assume spin symmetry in the open channel, vanishing magnetizations and no populations in the closed channel,

$$
f = f_{11} = f_{22}, \tag{C.52}
$$

$$
f_{12} = f_{34} = f_{33} = f_{44} = 0. \tag{C.53}
$$

No s-wave pairing for fermions in the same state means that the pair correlations vanish in the same state,

$$m_{11} = m_{22} = m_{33} = m_{44} = 0. \tag{C.54}$$

Open channel pairs are given by the pair correlation function between spin up and down:

$$m = m_{12} = -m_{21}. \tag{C.55}$$

In the closed channel, we only consider bound pairs (see App. D for a discussion of when these pairs can be treated as bosons):

$$\phi_0 = m_{34}. \tag{C.56}$$

We define the following potential including some symmetries:

$$U_F(\boldsymbol{r}) = V_{1221}(\boldsymbol{r}) = V_{2112}(\boldsymbol{r}) = -V_{1212}(\boldsymbol{r}), \tag{C.57}$$

$$U_B(\boldsymbol{r}) = V_{3443}(\boldsymbol{r}) = V_{4334}(\boldsymbol{r}) = -V_{3434}(\boldsymbol{r}), \tag{C.58}$$

$$g(\boldsymbol{r}) = V_{1234}(\boldsymbol{r}) = V_{3412}. \tag{C.59}$$

The combinations that can not be deduced from this list vanish, for example, $V_{1111} = 0$, because there is no s-wave scattering of identical fermions.

To find the two-body scattering equations, we consider the center-of-mass equation of motion (C.41) for the pair matrix m in the absence of normal fermions ($f = 0$):

$$i\frac{\mathrm{d}}{\mathrm{d}t} m_{s_1 s_2}(\boldsymbol{R}, \boldsymbol{r}) = [H^{(0)}(\boldsymbol{R}) + H^{(0)}(\boldsymbol{r})] m_{s_1 s_2}(\boldsymbol{R}, \boldsymbol{r}) + V_{s_1 s_2 s_3 s_4}(\boldsymbol{r}) m_{s_3 s_4}(\boldsymbol{R}, \boldsymbol{r}). \tag{C.60}$$

We want to solve the eigen-value problem for the Hamiltonian on the right-hand side of the above equation. As an Ansatz, we split off the spin-independent center-of-mass component $\Psi_{\mathrm{CM}}(\boldsymbol{R})$,

$$m_{s_1 s_2}(\boldsymbol{R}, \boldsymbol{r}) = \Psi_{\mathrm{CM}}(\boldsymbol{R}) \psi_{s_1 s_2}(\boldsymbol{r}), \tag{C.61}$$

and obtain the following two eigen-value equations:

$$H^{(0)}(\boldsymbol{R}) \Psi_{\mathrm{CM}}(\boldsymbol{R}) = E \Psi_{\mathrm{CM}}(\boldsymbol{R}) \quad \text{and} \tag{C.62}$$

$$H^{(0)}(\boldsymbol{r}) \psi_{s_1 s_2}(\boldsymbol{r}) + V_{s_1 s_2 s_3 s_4}(\boldsymbol{r}) \psi_{s_3 s_4}(\boldsymbol{r}) = \epsilon \psi_{s_1 s_2}(\boldsymbol{r}). \tag{C.63}$$

The second one can be split up into spin states using the definitions in Eqs. (C.55), (C.56), (C.57), and (C.59):

$$[H^{(0)}(\boldsymbol{r}) + 2U_F(\boldsymbol{r})]m(\boldsymbol{r}) + 2g(\boldsymbol{r})\phi_0(\boldsymbol{r}) = \epsilon m(\boldsymbol{r}) \tag{C.64}$$

$$\nu\phi_0(\boldsymbol{r}) + 2g(\boldsymbol{r})m(\boldsymbol{r}) = \epsilon\phi_0(\boldsymbol{r}), \tag{C.65}$$

where ν is the eigen value to the bare closed-channel bound state ϕ_0 given by

$$[H^{(0)}(\boldsymbol{r}) + 2U_B(\boldsymbol{r})]\phi_0(\boldsymbol{r}) = \nu\phi_0(\boldsymbol{r}). \tag{C.66}$$

Equations (C.64) and (C.65) are the two-body scattering equations for the open and closed channels.

Appendix D

Fermionic Pairing

In this Appendix, we consider how a pair of fermions can be treated as an effective, composite boson. We also examine the density-matrix evolution equations for pairs that are superpositions of bosons and fermions, and show their excitation spectrum to be gapless. We here use a Hamiltonian that includes a non-resonant fermion interaction.

D.1 Pairs of Fermions as Bosons

First, we examine the commutation relation for a pair of fermions to find out when it can be treated as a boson. The two-channel Hamiltonian (5.8) makes this approximation. The fermionic field operator $a_\sigma(\boldsymbol{x})$ obeys the commutation relation

$$\Big[a_\sigma(\boldsymbol{x}), a^\dagger_{\sigma'}(\boldsymbol{x}')\Big]_+ = \delta(\boldsymbol{x}-\boldsymbol{x}')\delta_{\sigma\sigma'} \tag{D.1}$$

We define the field operator $b(\boldsymbol{R})$ of a pair of these fermions by

$$b(\boldsymbol{R}) = \int d\boldsymbol{r}\ \phi(\boldsymbol{r}) a_\downarrow(\boldsymbol{R}+\frac{\boldsymbol{r}}{2}) a_\uparrow(\boldsymbol{R}-\frac{\boldsymbol{r}}{2}), \tag{D.2}$$

where $\phi(\boldsymbol{r})$ is the normalized pair wave function as a function of the relative coordinate $\boldsymbol{r}$.

Examining the commutation relation for the pairs, we find

$$\begin{aligned}\big[b(\boldsymbol{R}), b^\dagger(\boldsymbol{R}')\big]_- &= \delta(\boldsymbol{R}-\boldsymbol{R}') \\ &- \sum_{\sigma=\downarrow,\uparrow}\int d\boldsymbol{r}\ \phi(\boldsymbol{r})\phi^*\Big(\boldsymbol{r}+2(\boldsymbol{R}'-\boldsymbol{R})\Big) a^\dagger_\sigma\Big(2\boldsymbol{R}'-\boldsymbol{R}+\frac{\boldsymbol{r}}{2}\Big) a_\sigma\Big(\boldsymbol{R}+\frac{\boldsymbol{r}}{2}\Big),\end{aligned} \tag{D.3}$$

and

$$\begin{aligned}\big[b(\boldsymbol{R}),b^\dagger(\boldsymbol{R}')\big]_- &= \delta(\boldsymbol{R}-\boldsymbol{R}') \\ &- \sum_{\sigma=\downarrow,\uparrow}\int d\boldsymbol{r}\ \phi(\boldsymbol{r}-2\boldsymbol{R}')\phi^*\Big(\boldsymbol{r}+2\boldsymbol{R}\Big)a_\sigma^\dagger\Big(\frac{\boldsymbol{r}}{2}+\boldsymbol{R}'-\boldsymbol{R}\Big)a_\sigma\Big(\frac{\boldsymbol{r}}{2}-(\boldsymbol{R}'-\boldsymbol{R})\Big),\end{aligned} \tag{D.4}$$

where we used that the pair wave function ϕ is symmetric. If the second term on the right-hand side of this equation can be neglected, we obtain a bosonic commutation relation for the pairs, that is, the pairs can be described as effective bosons. In what regime is this a good approximation?

If we assume that the integral in Eq. (D.4) is maximal for $\boldsymbol{R}=\boldsymbol{R}'$, we can write

$$\big[b(\boldsymbol{R}),b^\dagger(\boldsymbol{R}')\big]_- = \delta(\boldsymbol{R}-\boldsymbol{R}')\Big(1-\sum_{\sigma=\downarrow,\uparrow}\int d\boldsymbol{r}\ |\phi(\boldsymbol{r})|^2\, n_\sigma\Big(\boldsymbol{R}+\frac{\boldsymbol{r}}{2}\Big)\Big), \tag{D.5}$$

where n_σ is the number operator for spin σ. The pair wave function ϕ vanishes outside a relative distance of $\boldsymbol{r}\approx l_{\rm pair}$, which is determined by the size of the pair. The condition for treating pairs as bosons can then be written in terms of the number density of fermions n_σ

$$\big[b(\boldsymbol{R}),b^\dagger(\boldsymbol{R}')\big]_- = \delta(\boldsymbol{R}-\boldsymbol{R}') \qquad \text{if} \qquad n_\sigma l_{\rm pair}^3 \ll 1. \tag{D.6}$$

D.2 Pairs in a Homogeneous System

We now consider pairs of fermions and composite bosons in a homogeneous system for the following Hamiltonian

$$H = \sum_{\boldsymbol{k},\sigma=\uparrow,\downarrow}\epsilon_{\boldsymbol{k}}a_{\boldsymbol{k}\sigma}^\dagger a_{\boldsymbol{k}\sigma} + \sum_{\boldsymbol{q}}\Big(\frac{\epsilon_{\boldsymbol{q}}}{2}+\nu\Big)b_{\boldsymbol{q}}^\dagger b_{\boldsymbol{q}} + \sum_{\boldsymbol{qk}} g_{\boldsymbol{k}}\Big(b_{\boldsymbol{q}}^\dagger a_{\boldsymbol{q}/2-\boldsymbol{k}\downarrow}a_{\boldsymbol{q}/2+\boldsymbol{k}\uparrow}+\text{H.c.}\Big) \tag{D.7}$$

$$+\sum_{\boldsymbol{qkk'}}U_{\boldsymbol{k}-\boldsymbol{k}'}a_{\boldsymbol{q}+\boldsymbol{k}}^\dagger a_{\boldsymbol{q}-\boldsymbol{k}}^\dagger a_{\boldsymbol{q}-\boldsymbol{k}'}a_{\boldsymbol{q}+\boldsymbol{k}'} \tag{D.8}$$

which is similar to the Bose-Fermi Hamiltonian discussed in Eq. (5.8), but now includes a non-resonant fermion background interaction $U_{\boldsymbol{k}}$. The composite bosons and fermions obey the usual commutation relations

$$[b_{\boldsymbol{q}},b_{\boldsymbol{q}'}^\dagger]_- = \delta_{\boldsymbol{qq}'} \quad \text{and} \quad [a_{\boldsymbol{k}\uparrow},a_{\boldsymbol{k}'\uparrow}^\dagger]_+ = \delta_{\boldsymbol{kk}'}. \tag{D.9}$$

The bosons and fermions commute, that is, the bound state does not contain continuum components.

$$[a_{\boldsymbol{k}\uparrow}, b_{\boldsymbol{q}}]_- = 0 \tag{D.10}$$

The long-range fermion pairs in the open channel are defined by

$$p_{\boldsymbol{qk}} = a_{\frac{\boldsymbol{q}}{2}-\boldsymbol{k}\downarrow} a_{\frac{\boldsymbol{q}}{2}+\boldsymbol{k}\uparrow}. \tag{D.11}$$

These pairs almost obey a bosonic commutation relation

$$\langle [p_{\boldsymbol{qk}}, p^\dagger_{\boldsymbol{q'k'}}]_- \rangle = \delta_{\boldsymbol{qq'}} \delta_{\boldsymbol{kk'}} N_F(\boldsymbol{q}, \boldsymbol{k}), \tag{D.12}$$

with the Pauli-blocking factor

$$N_F(\boldsymbol{q}, \boldsymbol{k}) = 1 - G_N\left(\frac{\boldsymbol{q}}{2} - \boldsymbol{k}\right) - G_N\left(\frac{\boldsymbol{q}}{2} + \boldsymbol{k}\right), \tag{D.13}$$

which represents Pauli blocking, and fermion populations

$$G_N(\boldsymbol{k}) = \langle a^\dagger_{\boldsymbol{k}\uparrow} a_{\boldsymbol{k}\uparrow} \rangle = \langle a^\dagger_{\boldsymbol{k}\downarrow} a_{\boldsymbol{k}\downarrow} \rangle. \tag{D.14}$$

We now define a density matrix for the fluctuations around the mean fields $\langle b \rangle$ and $\langle p \rangle$. We use the pair spinor

$$A(\boldsymbol{q}, \boldsymbol{k}) = \begin{pmatrix} b_{\boldsymbol{q}} & b^\dagger_{\boldsymbol{q}} & p_{\boldsymbol{qk}} & p^\dagger_{\boldsymbol{qk}} \end{pmatrix}^\top \tag{D.15}$$

to define the density matrix

$$G_{ab}(\boldsymbol{q}, \boldsymbol{k}, \boldsymbol{q'}, \boldsymbol{k'}) = \langle A^\dagger_b(\boldsymbol{q'}, \boldsymbol{k'}) A_a(\boldsymbol{q}, \boldsymbol{k}) \rangle. \tag{D.16}$$

This density matrix contains the following correlation functions

$$G_M(\boldsymbol{q}) = \langle b^\dagger_{\boldsymbol{q}} b_{\boldsymbol{q}} \rangle, \tag{D.17}$$

$$G_C(\boldsymbol{q}, \boldsymbol{k}) = \langle b^\dagger_{\boldsymbol{q}} p_{\boldsymbol{q}(\boldsymbol{k}-\frac{\boldsymbol{q}}{2})} \rangle = \langle b^\dagger_{\boldsymbol{q}} a_{\boldsymbol{q}-\boldsymbol{k}\downarrow} a_{\boldsymbol{k}\uparrow} \rangle, \text{ and} \tag{D.18}$$

$$G_P(\boldsymbol{q}, \boldsymbol{k}, \boldsymbol{k'}) = \langle p^\dagger_{\boldsymbol{qk}} p_{\boldsymbol{qk'}} \rangle = \langle a^\dagger_{\frac{\boldsymbol{q}}{2}+\boldsymbol{k}\uparrow} a^\dagger_{\frac{\boldsymbol{q}}{2}-\boldsymbol{k}\downarrow} a_{\frac{\boldsymbol{q}}{2}-\boldsymbol{k'}\downarrow} a_{\frac{\boldsymbol{q}}{2}+\boldsymbol{k'}\uparrow} \rangle. \tag{D.19}$$

The functions G_M and G_P are the densities of closed- and open-channel molecules, respectively, and G_C describes a correlation function between the two kinds of pairs. Writing this density

matrix G in Eq. D.16 explicitly in terms of its components we obtain

$$G(\boldsymbol{q},\boldsymbol{k},\boldsymbol{k}') = \begin{pmatrix} G_M(\boldsymbol{q}) & 0 & G_C^*(\boldsymbol{q},\frac{\boldsymbol{q}}{2}+\boldsymbol{k}') & 0 \\ 0 & 1+G_M(\boldsymbol{q}) & 0 & G_C(\boldsymbol{q},\frac{\boldsymbol{q}}{2}+\boldsymbol{k}') \\ G_C(\boldsymbol{q},\frac{\boldsymbol{q}}{2}+\boldsymbol{k}) & 0 & G_P(\boldsymbol{q},\boldsymbol{k}',\boldsymbol{k}) & 0 \\ 0 & G_C^*(\boldsymbol{q},\frac{\boldsymbol{q}}{2}+\boldsymbol{k}) & 0 & \delta_{\boldsymbol{k}\boldsymbol{k}'}N_F(\boldsymbol{q},\boldsymbol{k})+G_P(\boldsymbol{q},\boldsymbol{k},\boldsymbol{k}') \end{pmatrix}. \tag{D.20}$$

We here assume that b and p are quasiparticle operators in the boson (top right) and fermion-pair (bottom right) parts of the density matrix respectively, that is, the pair (or four-point) correlation function $\langle bb\rangle$ and $\langle pp\rangle$ vanish. The equation of motion for G for evolution under the Hamiltonian (D.8) can now be written as (assuming $G_N = \text{const.}$):

$$i\hbar\frac{dG(\boldsymbol{q},\boldsymbol{k},\boldsymbol{k}')}{dt} = \sum_{\boldsymbol{k}''}\Big(\Sigma(\boldsymbol{q},\boldsymbol{k},\boldsymbol{k}'')G(\boldsymbol{q},\boldsymbol{k}'',\boldsymbol{k}') - G(\boldsymbol{q},\boldsymbol{k},\boldsymbol{k}'')\Sigma^\dagger(\boldsymbol{q},\boldsymbol{k}'',\boldsymbol{k}')\Big), \tag{D.21}$$

with the self energy

$$\Sigma(\boldsymbol{q},\boldsymbol{k},\boldsymbol{k}') = \begin{pmatrix} \delta_{\boldsymbol{k}\boldsymbol{k}'}(\epsilon_{\boldsymbol{q}}+\nu) & 0 & g_{\boldsymbol{k}'} & 0 \\ 0 & -\delta_{\boldsymbol{k}\boldsymbol{k}'}(\epsilon_{\boldsymbol{q}}+\nu) & 0 & -g_{\boldsymbol{k}'} \\ N_F(\boldsymbol{q},\boldsymbol{k})g_{\boldsymbol{k}} & 0 & U(\boldsymbol{q},\boldsymbol{k},\boldsymbol{k}') & 0 \\ 0 & -N_F(\boldsymbol{q},\boldsymbol{k})g_{\boldsymbol{k}} & 0 & -U(\boldsymbol{q},\boldsymbol{k},\boldsymbol{k}') \end{pmatrix} \tag{D.22}$$

an effective interaction

$$\begin{aligned} U(\boldsymbol{q},\boldsymbol{k},\boldsymbol{k}') &= U_{\boldsymbol{k}-\boldsymbol{k}'}N_F(\boldsymbol{q},\boldsymbol{k}) \\ &+ \delta_{\boldsymbol{k}\boldsymbol{k}'}\left(\epsilon_{\frac{\boldsymbol{q}}{2}+\boldsymbol{k}}+\epsilon_{\frac{\boldsymbol{q}}{2}-\boldsymbol{k}}+U_0\sum_{\boldsymbol{q}'}\left[G_N\left(\boldsymbol{q}'-\frac{\boldsymbol{q}}{2}+\boldsymbol{k}\right)+G_N\left(\boldsymbol{q}'-\frac{\boldsymbol{q}}{2}-\boldsymbol{k}\right)\right]\right) \end{aligned} \tag{D.23}$$

and the free-particle dispersion relation

$$\epsilon_{\boldsymbol{q}} = \frac{\hbar^2 q^2}{2m}. \tag{D.24}$$

The self energy matrix Σ is gapless, because we have zero-energy eigen state P

$$P(\boldsymbol{k}) = \begin{pmatrix} \langle b_0\rangle \\ \langle b_0^\dagger\rangle \\ -\langle p_{0\boldsymbol{k}}\rangle \\ -\langle p_{0\boldsymbol{k}}^\dagger\rangle \end{pmatrix} = \begin{pmatrix} \phi_m \\ \phi_m^* \\ -G_A(\boldsymbol{k}) \\ -G_A^*(\boldsymbol{k}) \end{pmatrix}, \tag{D.25}$$

which consists of the pair mean fields. It is a non-trivial zero-energy eigen state,

$$\sum_{\boldsymbol{k}''} \Sigma(0, \boldsymbol{k}, \boldsymbol{k}'') P(\boldsymbol{k}'') = 0, \tag{D.26}$$

in equilibrium, that is, when

$$\frac{d\phi_m}{dt} = \frac{dG_A(\boldsymbol{k})}{dt} = 0, \tag{D.27}$$

where the equations of motion of the mean fields are given by

$$i\hbar \frac{d\phi_m}{dt} = \nu \phi_m + \sum_{\boldsymbol{k}} g_{\boldsymbol{k}} G_A(\boldsymbol{k}), \text{and} \tag{D.28}$$

$$i\hbar \frac{dG_A(\boldsymbol{k})}{dt} = N_F(0, \boldsymbol{k}) g_{\boldsymbol{k}} \phi_m + \sum_{\boldsymbol{k}'} U(0, \boldsymbol{k}, \boldsymbol{k}') G_A(\boldsymbol{k}'). \tag{D.29}$$

Appendix E

Rate Equations in the Normal Phase

In this Appendix, we show how to derive effective kinetic rate equations from the cumulant expansion method discussed in Chap. 8. Step (2) discussed below is essentially the same adiabatic elimination we used in Chap. 8 to close the three-operator equations we simulate numerically.

E.1 Equations of Motion

We list below the full set of normal-phase equations up to cut C illustrated in Fig. 8.1. First, we have the normal densities of fermions and composite bosons,

$$i\hbar\frac{\mathrm{d}f_{\boldsymbol{k}\uparrow}}{\mathrm{d}t} = 2ig\,\Im\Big\{\sum_{\boldsymbol{q}}\big\langle\!\big\langle b_{\boldsymbol{q}}a^\dagger_{\boldsymbol{k}\uparrow}a^\dagger_{\boldsymbol{q}-\boldsymbol{k}\downarrow}\big\rangle\!\big\rangle\Big\}, \tag{E.1a}$$

$$i\hbar\frac{\mathrm{d}n_{\boldsymbol{q}}}{\mathrm{d}t} = -2ig\,\Im\Big\{\sum_{\boldsymbol{k}}\big\langle\!\big\langle b_{\boldsymbol{q}}a^\dagger_{\boldsymbol{q}/2+\boldsymbol{k}\uparrow}a^\dagger_{\boldsymbol{q}/2-\boldsymbol{k}\downarrow}\big\rangle\!\big\rangle\Big\}, \tag{E.1b}$$

where $\Im$ indicates the imaginary part. These couple to the three-operator correlation function,

$$\begin{aligned}
i\hbar\frac{\mathrm{d}\big\langle\!\big\langle b_{\boldsymbol{q}}a^\dagger_{\boldsymbol{q}/2+\boldsymbol{k}\uparrow}a^\dagger_{\boldsymbol{q}/2-\boldsymbol{k}\downarrow}\big\rangle\!\big\rangle}{\mathrm{d}t} &= (\nu-2\epsilon_{\boldsymbol{k}})\big\langle\!\big\langle b_{\boldsymbol{q}}a^\dagger_{\boldsymbol{q}/2+\boldsymbol{k}\uparrow}a^\dagger_{\boldsymbol{q}/2-\boldsymbol{k}\downarrow}\big\rangle\!\big\rangle \\
&\quad + g\sum_{\boldsymbol{k}'}\big\langle\!\big\langle a_{\boldsymbol{q}/2-\boldsymbol{k}'\downarrow}a_{\boldsymbol{q}/2+\boldsymbol{k}'\uparrow}a^\dagger_{\boldsymbol{q}/2+\boldsymbol{k}\uparrow}a^\dagger_{\boldsymbol{q}/2-\boldsymbol{k}\downarrow}\big\rangle\!\big\rangle \\
&\quad - g\sum_{\boldsymbol{q}'}\Big(\big\langle\!\big\langle b_{\boldsymbol{q}}b^\dagger_{\boldsymbol{q}'}a_{\boldsymbol{q}'-\boldsymbol{q}/2+\boldsymbol{k}\uparrow}a^\dagger_{\boldsymbol{q}/2+\boldsymbol{k}\uparrow}\big\rangle\!\big\rangle + \big\langle\!\big\langle b_{\boldsymbol{q}}b^\dagger_{\boldsymbol{q}'}a_{\boldsymbol{q}'-\boldsymbol{q}/2-\boldsymbol{k}\downarrow}a^\dagger_{\boldsymbol{q}/2-\boldsymbol{k}\downarrow}\big\rangle\!\big\rangle\Big) \\
&\quad + g\,f_{\boldsymbol{q}/2+\boldsymbol{k}\uparrow}f_{\boldsymbol{q}/2-\boldsymbol{k}\downarrow}(1+n_{\boldsymbol{q}}) - g\,n_{\boldsymbol{q}}(1-f_{\boldsymbol{q}/2+\boldsymbol{k}\uparrow})(1-f_{\boldsymbol{q}/2-\boldsymbol{k}\downarrow}),
\end{aligned} \tag{E.1c}$$

which in turn depends on the following two four-operator correlation functions,

$$\begin{aligned} i\hbar\frac{\mathrm{d}\langle\!\langle b_{\boldsymbol{q}}b^\dagger_{\boldsymbol{q}'}a_{\boldsymbol{q}'-\boldsymbol{q}/2+\boldsymbol{k},\sigma}a^\dagger_{\boldsymbol{q}/2+\boldsymbol{k},\sigma}\rangle\!\rangle}{\mathrm{d}t} &= 2\left(\epsilon_{(\boldsymbol{q}'-\boldsymbol{q})/2+\boldsymbol{k}}-\epsilon_{\boldsymbol{k}}\right)\langle\!\langle b_{\boldsymbol{q}}b^\dagger_{\boldsymbol{q}'}a_{\boldsymbol{q}'-\boldsymbol{q}/2+\boldsymbol{k},\sigma}a^\dagger_{\boldsymbol{q}/2+\boldsymbol{k},\sigma}\rangle\!\rangle \\ &\pm g\left(f_{\boldsymbol{q}/2+\boldsymbol{k},\sigma}+n_{\boldsymbol{q}}\right)\langle\!\langle b^\dagger_{\boldsymbol{q}'}a_{\boldsymbol{q}/2-\boldsymbol{k},-\sigma}a_{\boldsymbol{q}'-\boldsymbol{q}/2+\boldsymbol{k},\sigma}\rangle\!\rangle \\ &\mp g\left(f_{\boldsymbol{q}'-\boldsymbol{q}/2+\boldsymbol{k},\sigma}+n_{\boldsymbol{q}'}\right)\langle\!\langle b_{\boldsymbol{q}}a^\dagger_{\boldsymbol{q}/2+\boldsymbol{k},\sigma}a^\dagger_{\boldsymbol{q}/2-\boldsymbol{k},-\sigma}\rangle\!\rangle, \end{aligned} \tag{E.1d}$$

where the signs on the right-hand side correspond to the two possible spin directions, and,

$$\begin{aligned} i\hbar\frac{\mathrm{d}\langle\!\langle a_{\boldsymbol{q}/2-\boldsymbol{k}'\downarrow}a_{\boldsymbol{q}/2+\boldsymbol{k}'\uparrow}a^\dagger_{\boldsymbol{q}/2+\boldsymbol{k}\uparrow}a^\dagger_{\boldsymbol{q}/2-\boldsymbol{k}\downarrow}\rangle\!\rangle}{\mathrm{d}t} &= 2\left(\epsilon_{\boldsymbol{k}'}-\epsilon_{\boldsymbol{k}}\right)\langle\!\langle a_{\boldsymbol{q}/2-\boldsymbol{k}'\downarrow}a_{\boldsymbol{q}/2+\boldsymbol{k}'\uparrow}a^\dagger_{\boldsymbol{q}/2+\boldsymbol{k}\uparrow}a^\dagger_{\boldsymbol{q}/2-\boldsymbol{k}\downarrow}\rangle\!\rangle \\ &+ g\left(1-f_{\boldsymbol{q}/2+\boldsymbol{k}'\uparrow}-f_{\boldsymbol{q}/2-\boldsymbol{k}'\downarrow}\right)\langle\!\langle b_{\boldsymbol{q}}a^\dagger_{\boldsymbol{q}/2+\boldsymbol{k}\uparrow}a^\dagger_{\boldsymbol{q}/2-\boldsymbol{k}\downarrow}\rangle\!\rangle \\ &- g\left(1-f_{\boldsymbol{q}/2+\boldsymbol{k}\uparrow}-f_{\boldsymbol{q}/2-\boldsymbol{k}\downarrow}\right)\langle\!\langle b^\dagger_{\boldsymbol{q}}a_{\boldsymbol{q}/2-\boldsymbol{k}'\downarrow}a_{\boldsymbol{q}/2+\boldsymbol{k}'\uparrow}\rangle\!\rangle. \end{aligned} \tag{E.1e}$$

These equations are the same as listed in Chap. 8. In order to obtain rate equations for the bosons and fermions we now use the following three steps:

1. Substitute the appropriate lowest-order adiabatic solution $\langle\!\langle b_{\boldsymbol{q}}a^\dagger_{\boldsymbol{q}/2+\boldsymbol{k}\uparrow}a^\dagger_{\boldsymbol{q}/2-\boldsymbol{k}\downarrow}\rangle\!\rangle_{\mathrm{A}}$ of Eq. (E.1c) into the equations for the four-operator cumulants Eqs. (E.1d) and (E.1e). This cuts the recursive coupling of the three- and four-operator cumulants.

2. Adiabatically solve for the four-operator cumulants and substitute into the equation for the time-dependent three-operator correlation $\langle\!\langle b_{\boldsymbol{q}}a^\dagger_{\boldsymbol{q}/2+\boldsymbol{k}\uparrow}a^\dagger_{\boldsymbol{q}/2-\boldsymbol{k}\downarrow}\rangle\!\rangle$. This yields the equations we simulate numerically.

3. To make sure that we choose the right expressions for the adiabatic eliminations in the two steps above, we further eliminate the three-operator cumulant altogether and are left with coupled rate equations for the fermions and bosons. The Boltzmann collision terms can be interpreted by inspection, which validates the previous two steps.

E.2 Step (1): Cut Recursion

We first cut the recursion between the three- and four-operator equations by adiabatically solving Eq. (E.1c) without any four-operator correlations and using this solution on the right-

hand sides of Eqs. (E.1d) and (E.1e). We here pick the real principal value according to the following relation for energy denominators

$$\frac{1}{\Delta E - i\epsilon} = \mathcal{P}\frac{1}{\Delta E} + i\pi\delta(\Delta E), \tag{E.2}$$

for small $\epsilon > 0$. This choice gives us the collisional rates we are interested in in step (3). The imaginary delta-function contribution renormalizes the energy-denominators, but we here neglect this correction of the intermediate-state energies, since we expect it to be small.

The adiabatic principal-value solution of Eq. (E.1c) is

$$\left\langle\!\left\langle b_{\boldsymbol{q}} a^\dagger_{\boldsymbol{q}/2+\boldsymbol{k}\uparrow} a^\dagger_{\boldsymbol{q}/2-\boldsymbol{k}\downarrow} \right\rangle\!\right\rangle_{\mathrm{A}} = \mathcal{P}\frac{-g}{\nu - 2\epsilon_{\boldsymbol{k}}} \left[f_{\boldsymbol{q}/2+\boldsymbol{k}\uparrow} f_{\boldsymbol{q}/2-\boldsymbol{k}\downarrow} - n_{\boldsymbol{q}}\big(1 - f_{\boldsymbol{q}/2+\boldsymbol{k}\uparrow} - f_{\boldsymbol{q}/2-\boldsymbol{k}\downarrow}\big)\right], \tag{E.3}$$

which has the population factors of the collisional rate illustrated in Fig. 8.2 a):

$$\left\langle\!\left\langle b_{\boldsymbol{q}} a^\dagger_{\boldsymbol{q}/2+\boldsymbol{k}\uparrow} a^\dagger_{\boldsymbol{q}/2-\boldsymbol{k}\downarrow} \right\rangle\!\right\rangle_{\mathrm{A}} = \mathcal{P}\frac{-g}{\nu - 2\epsilon_{\boldsymbol{k}}} \left[f_{\boldsymbol{q}/2+\boldsymbol{k}\uparrow} f_{\boldsymbol{q}/2-\boldsymbol{k}\downarrow}\big(1 + n_{\boldsymbol{q}}\big) - n_{\boldsymbol{q}}\big(1 - f_{\boldsymbol{q}/2+\boldsymbol{k}\uparrow}\big)\big(1 - f_{\boldsymbol{q}/2-\boldsymbol{k}\downarrow}\big)\right], \tag{E.4}$$

This is the direct interconversion of a pair of fermions to a bare composite boson.

E.3 Step (2): Eliminate Four-Operator Cumulants

In this step, we adiabatically solve the four-operator equations (E.1d) and (E.1e) and obtain the second-order collisional interactions depicted in Fig. 8.2 b) and c), an effective fermion-fermion interaction through a virtual composite boson, and an interaction between a fermion and a composite boson by exchanging a fermion. We use the adiabatic solution from step (1) on the right-hand side, and keep only the energy-conserving delta-function contributions of the energy denominator, because the off-shell parts are energetically suppressed.

$$\begin{aligned}\left\langle\!\left\langle b_{\boldsymbol{q}} b^\dagger_{\boldsymbol{q}'} a_{\boldsymbol{q}'-\boldsymbol{q}/2+\boldsymbol{k},\sigma} a^\dagger_{\boldsymbol{q}/2+\boldsymbol{k},\sigma} \right\rangle\!\right\rangle_{\mathrm{A}} &= -i\pi\ \delta\big(2\epsilon_{(\boldsymbol{q}'-\boldsymbol{q})/2+\boldsymbol{k}} - 2\epsilon_{\boldsymbol{k}}\big)\, g \\ &\quad \times \Big[\pm \big(f_{\boldsymbol{q}/2+\boldsymbol{k},\sigma} + n_{\boldsymbol{q}}\big) \left\langle\!\left\langle b^\dagger_{\boldsymbol{q}'} a_{\boldsymbol{q}/2-\boldsymbol{k},-\sigma} a_{\boldsymbol{q}'-\boldsymbol{q}/2+\boldsymbol{k},\sigma} \right\rangle\!\right\rangle_{\mathrm{A}} \\ &\quad \mp \big(f_{\boldsymbol{q}'-\boldsymbol{q}/2+\boldsymbol{k},\sigma} + n_{\boldsymbol{q}'}\big) \left\langle\!\left\langle b_{\boldsymbol{q}} a^\dagger_{\boldsymbol{q}/2+\boldsymbol{k},\sigma} a^\dagger_{\boldsymbol{q}/2-\boldsymbol{k},-\sigma} \right\rangle\!\right\rangle_{\mathrm{A}} \Big].\end{aligned} \tag{E.5}$$

Substituting the adiabatic three-operator solution (E.4) gives the fermion-boson rate in Fig. 8.2 c):

$$\begin{aligned}\left\langle\!\left\langle b_{\boldsymbol{q}} b^\dagger_{\boldsymbol{q}'} a_{\boldsymbol{q}'-\boldsymbol{q}/2+\boldsymbol{k},\sigma} a^\dagger_{\boldsymbol{q}/2+\boldsymbol{k},\sigma}\right\rangle\!\right\rangle_{\mathrm{A}} &= -i\pi\delta\big(2\epsilon_{(\boldsymbol{q}'-\boldsymbol{q})/2+\boldsymbol{k}} - 2\epsilon_{\boldsymbol{k}}\big)\,\mathcal{P}\frac{g^2}{\nu-2\epsilon_{\boldsymbol{k}}} \\ &\quad\times\Big[-f_{\boldsymbol{q}'-\boldsymbol{q}/2+\boldsymbol{k},\sigma} n_{\boldsymbol{q}}(1-f_{\boldsymbol{q}/2+\boldsymbol{k},\sigma})(1+n_{\boldsymbol{q}'}) \\ &\quad + f_{\boldsymbol{q}/2+\boldsymbol{k},\sigma} n_{\boldsymbol{q}'}(1-f_{\boldsymbol{q}'-\boldsymbol{q}/2+\boldsymbol{k},\sigma})(1+n_{\boldsymbol{q}})\Big]\end{aligned} \tag{E.6}$$

These on-shell fermion-boson collisional rates redistribute particles, but obey number conservation, that is, they obey the following detailed-balance condition:

$$\sum_q \sum_{q'} \left\langle\!\left\langle b_{\boldsymbol{q}} b^\dagger_{\boldsymbol{q}'} a_{\boldsymbol{q}'-\boldsymbol{k},\sigma} a^\dagger_{\boldsymbol{q}-\boldsymbol{k},\sigma}\right\rangle\!\right\rangle_{\mathrm{A}} = 0. \tag{E.7}$$

We analogously consider Eq. (E.1e) and find the rates depicted in Fig. 8.2 b):

$$\begin{aligned}\left\langle\!\left\langle a_{\boldsymbol{q}/2-\boldsymbol{k}'\downarrow} a_{\boldsymbol{q}/2+\boldsymbol{k}'\uparrow} a^\dagger_{\boldsymbol{q}/2+\boldsymbol{k}\uparrow} a^\dagger_{\boldsymbol{q}/2-\boldsymbol{k}\downarrow}\right\rangle\!\right\rangle_{\mathrm{A}} &= -i\pi\ \delta(2\epsilon_{\boldsymbol{k}'} - 2\epsilon_{\boldsymbol{k}})\,\mathcal{P}\frac{g^2}{\nu-2\epsilon_{\boldsymbol{k}}} \\ &\quad\times\Big[f_{\boldsymbol{q}/2+\boldsymbol{k}'\uparrow} f_{\boldsymbol{q}/2-\boldsymbol{k}'\downarrow}(1-f_{\boldsymbol{q}/2+\boldsymbol{k}\uparrow})(1-f_{\boldsymbol{q}/2-\boldsymbol{k}\downarrow}) \\ &\quad - f_{\boldsymbol{q}/2+\boldsymbol{k}\uparrow} f_{\boldsymbol{q}/2-\boldsymbol{k}\downarrow}(1-f_{\boldsymbol{q}/2+\boldsymbol{k}'\uparrow})(1-f_{\boldsymbol{q}/2-\boldsymbol{k}'\downarrow})\Big],\end{aligned} \tag{E.8}$$

with the detailed-balance relation

$$\sum_{\boldsymbol{k}} \sum_{\boldsymbol{k}'} \left\langle\!\left\langle a_{\boldsymbol{q}/2-\boldsymbol{k}'\downarrow} a_{\boldsymbol{q}/2+\boldsymbol{k}'\uparrow} a^\dagger_{\boldsymbol{q}/2+\boldsymbol{k}\uparrow} a^\dagger_{\boldsymbol{q}/2-\boldsymbol{k}\downarrow}\right\rangle\!\right\rangle_{\mathrm{A}} = 0. \tag{E.9}$$

These collisional processes enter into the rate equations for the fermion and boson populations.

E.4 Step (3): Rate Equations

Substituting the results of steps (1) and (2) back into the equations for the fermion and boson densities (E.1a) and (E.1b), we obtain the following coupled rate equations:

$$\begin{aligned}i\hbar\frac{\mathrm{d}f_{\boldsymbol{k}\uparrow}}{\mathrm{d}t} &= -2\sum_{\boldsymbol{q}}\mathcal{P}\frac{g^2}{\nu-2\epsilon_{\boldsymbol{k}-\boldsymbol{q}/2}}\Big[\sum_{\boldsymbol{k}'}\left\langle\!\left\langle a_{\boldsymbol{q}/2-\boldsymbol{k}'\downarrow} a_{\boldsymbol{q}/2+\boldsymbol{k}'\uparrow} a^\dagger_{\boldsymbol{k}\uparrow} a^\dagger_{\boldsymbol{q}-\boldsymbol{k}\downarrow}\right\rangle\!\right\rangle_{\mathrm{A}} - \sum_{\boldsymbol{q}'}\left\langle\!\left\langle b_{\boldsymbol{q}} b^\dagger_{\boldsymbol{q}'} a_{\boldsymbol{q}'-\boldsymbol{q}+\boldsymbol{k}\uparrow} a^\dagger_{\boldsymbol{k}\uparrow}\right\rangle\!\right\rangle_{\mathrm{A}}\Big] \\ &\quad - 2\pi g^2\sum_{\boldsymbol{q}}\delta\big(\nu-2\epsilon_{\boldsymbol{k}-\boldsymbol{q}/2}\big)\ \Big[f_{\boldsymbol{k}\uparrow} f_{\boldsymbol{q}-\boldsymbol{k}\downarrow}(1+n_{\boldsymbol{q}}) - n_{\boldsymbol{q}}(1-f_{\boldsymbol{k}\uparrow})(1-f_{\boldsymbol{q}-\boldsymbol{k}\downarrow})\Big]\end{aligned} \tag{E.10a}$$

$$i\hbar\frac{\mathrm{d}f_{\boldsymbol{k}\downarrow}}{\mathrm{d}t} = -2\sum_{\boldsymbol{q}}\mathcal{P}\frac{g^2}{\nu-2\epsilon_{\boldsymbol{k}-\boldsymbol{q}/2}}\Big[\sum_{\boldsymbol{k}'}\big\langle\!\big\langle a_{\boldsymbol{q}/2-\boldsymbol{k}'\downarrow}a_{\boldsymbol{q}/2+\boldsymbol{k}'\uparrow}a^\dagger_{\boldsymbol{q}-\boldsymbol{k}\uparrow}a^\dagger_{\boldsymbol{k}\downarrow}\big\rangle\!\big\rangle_{\mathrm{A}} - \sum_{\boldsymbol{q}'}\big\langle\!\big\langle b_{\boldsymbol{q}}b^\dagger_{\boldsymbol{q}'}a_{\boldsymbol{q}'-\boldsymbol{q}+\boldsymbol{k}\downarrow}a^\dagger_{\boldsymbol{k}\downarrow}\big\rangle\!\big\rangle_{\mathrm{A}}\Big]$$
$$- 2\pi g^2\sum_{\boldsymbol{q}}\delta\Big(\nu-2\epsilon_{\boldsymbol{k}-\boldsymbol{q}/2}\Big)\Big[f_{\boldsymbol{q}-\boldsymbol{k}\uparrow}f_{\boldsymbol{k}\downarrow}(1+n_{\boldsymbol{q}}) - n_{\boldsymbol{q}}(1-f_{\boldsymbol{q}-\boldsymbol{k}\uparrow})(1-f_{\boldsymbol{k}\downarrow})\Big] \tag{E.10b}$$

$$i\hbar\frac{\mathrm{d}n_{\boldsymbol{q}}}{\mathrm{d}t} = -2\sum_{\boldsymbol{k}}\mathcal{P}\frac{g^2}{\nu-2\epsilon_{\boldsymbol{k}}}\sum_{\boldsymbol{q}'}\Big[\big\langle\!\big\langle b_{\boldsymbol{q}}b^\dagger_{\boldsymbol{q}'}a_{\boldsymbol{q}'-\boldsymbol{q}/2+\boldsymbol{k}\uparrow}a^\dagger_{\boldsymbol{q}/2+\boldsymbol{k}\uparrow}\big\rangle\!\big\rangle_{\mathrm{A}} + \big\langle\!\big\langle b_{\boldsymbol{q}}b^\dagger_{\boldsymbol{q}'}a_{\boldsymbol{q}'-\boldsymbol{q}/2-\boldsymbol{k}\downarrow}a^\dagger_{\boldsymbol{q}/2-\boldsymbol{k}\downarrow}\big\rangle\!\big\rangle_{\mathrm{A}}\Big]$$
$$+ 2\pi g^2\sum_{\boldsymbol{k}}\delta(\nu-2\epsilon_{\boldsymbol{k}})\Big[f_{\boldsymbol{q}/2+\boldsymbol{k}\uparrow}f_{\boldsymbol{q}/2-\boldsymbol{k}\downarrow}(1+n_{\boldsymbol{q}}) - n_{\boldsymbol{q}}(1-f_{\boldsymbol{q}/2+\boldsymbol{k}\uparrow})(1-f_{\boldsymbol{q}/2-\boldsymbol{k}\downarrow})\Big] \tag{E.10c}$$

These rate equations contain the scattering processes depicted in Fig. 8.2. In particular, the second line in each equation contains the quantum-Boltzmann rates for the direct interconversion of a pair of fermions and a composite boson as depicted in Fig. 8.2 a). The energy-conserving delta function in these fermion-boson rates causes them to vanish for negative detuning, because the closed-channel bound state lies below the continuum of the free fermions.

E.5 Equations of Motion to Order g^2

In this Section, we further simplify the equations of motion in Sec. E.1 by only keeping the vacuum contributions from the four-operator level and introducing damping rates Γ_1 and Γ_2 that model the neglected many-body and higher-order terms.

$$\begin{aligned}i\hbar\frac{\mathrm{d}\big\langle\!\big\langle b_{\boldsymbol{q}}a^\dagger_{\boldsymbol{q}/2+\boldsymbol{k}\uparrow}a^\dagger_{\boldsymbol{q}/2-\boldsymbol{k}\downarrow}\big\rangle\!\big\rangle}{\mathrm{d}t} &= (\nu-2\epsilon_{\boldsymbol{k}}-i\Gamma_1)\big\langle\!\big\langle b_{\boldsymbol{q}}a^\dagger_{\boldsymbol{q}/2+\boldsymbol{k}\uparrow}a^\dagger_{\boldsymbol{q}/2-\boldsymbol{k}\downarrow}\big\rangle\!\big\rangle\\ &\quad + g\sum_{\boldsymbol{k}'}\big\langle\!\big\langle a_{\boldsymbol{q}/2-\boldsymbol{k}'\downarrow}a_{\boldsymbol{q}/2+\boldsymbol{k}'\uparrow}a^\dagger_{\boldsymbol{q}/2+\boldsymbol{k}\uparrow}a^\dagger_{\boldsymbol{q}/2-\boldsymbol{k}\downarrow}\big\rangle\!\big\rangle\\ &\quad + g\,f_{\boldsymbol{q}/2+\boldsymbol{k}\uparrow}f_{\boldsymbol{q}/2-\boldsymbol{k}\downarrow}(1+n_{\boldsymbol{q}}) - g\,n_{\boldsymbol{q}}(1-f_{\boldsymbol{q}/2+\boldsymbol{k}\uparrow})(1-f_{\boldsymbol{q}/2-\boldsymbol{k}\downarrow}),\end{aligned} \tag{E.11}$$

$$i\hbar\frac{\mathrm{d}\langle\!\langle a_{\boldsymbol{q}/2-\boldsymbol{k}'\downarrow}a_{\boldsymbol{q}/2+\boldsymbol{k}'\uparrow}a^\dagger_{\boldsymbol{q}/2+\boldsymbol{k}\uparrow}a^\dagger_{\boldsymbol{q}/2-\boldsymbol{k}\downarrow}\rangle\!\rangle}{\mathrm{d}t} = (2\epsilon_{\boldsymbol{k}'}-2\epsilon_{\boldsymbol{k}}-i\Gamma_2)\langle\!\langle a_{\boldsymbol{q}/2-\boldsymbol{k}'\downarrow}a_{\boldsymbol{q}/2+\boldsymbol{k}'\uparrow}a^\dagger_{\boldsymbol{q}/2+\boldsymbol{k}\uparrow}a^\dagger_{\boldsymbol{q}/2-\boldsymbol{k}\downarrow}\rangle\!\rangle$$
$$+ gN_F(\boldsymbol{q},\boldsymbol{k}')\langle\!\langle b_{\boldsymbol{q}}a^\dagger_{\boldsymbol{q}/2+\boldsymbol{k}\uparrow}a^\dagger_{\boldsymbol{q}/2-\boldsymbol{k}\downarrow}\rangle\!\rangle - gN_F(\boldsymbol{q},\boldsymbol{k})\langle\!\langle b^\dagger_{\boldsymbol{q}}a_{\boldsymbol{q}/2-\boldsymbol{k}'\downarrow}a_{\boldsymbol{q}/2+\boldsymbol{k}'\uparrow}\rangle\!\rangle \tag{E.12}$$

with the fermion population factor

$$N_F(\boldsymbol{q},\boldsymbol{k}) = 1 - f_{\boldsymbol{q}/2+\boldsymbol{k}\uparrow} - f_{\boldsymbol{q}/2-\boldsymbol{k}\downarrow}. \tag{E.13}$$

The damping rates Γ_1 and Γ_2 also model part of the effect of the couplings to five-operator averages of the type $\langle\!\langle b^\dagger a^\dagger aaa\rangle\!\rangle$. We have neglected these couplings to close our equations and cut the BBGKY hierarchy.

We now eliminate the four-operator average $\langle\!\langle aaa^\dagger a^\dagger\rangle\!\rangle$ using an initial condition of $\langle\!\langle aaa^\dagger a^\dagger\rangle\!\rangle(t=0)=0$

$$\langle\!\langle a_{\boldsymbol{q}/2-\boldsymbol{k}'\downarrow}a_{\boldsymbol{q}/2+\boldsymbol{k}'\uparrow}a^\dagger_{\boldsymbol{q}/2+\boldsymbol{k}\uparrow}a^\dagger_{\boldsymbol{q}/2-\boldsymbol{k}\downarrow}\rangle\!\rangle =$$
$$\frac{-g}{2\epsilon_{\boldsymbol{k}'}-2\epsilon_{\boldsymbol{k}}-i\Gamma_2}\Big(N_F(\boldsymbol{q},\boldsymbol{k}')\langle\!\langle b_{\boldsymbol{q}}a^\dagger_{\boldsymbol{q}/2+\boldsymbol{k}\uparrow}a^\dagger_{\boldsymbol{q}/2-\boldsymbol{k}\downarrow}\rangle\!\rangle - N_F(\boldsymbol{q},\boldsymbol{k})\langle\!\langle b^\dagger_{\boldsymbol{q}}a_{\boldsymbol{q}/2-\boldsymbol{k}'\downarrow}a_{\boldsymbol{q}/2+\boldsymbol{k}'\uparrow}\rangle\!\rangle\Big). \tag{E.14}$$

In the limit $\epsilon_{\boldsymbol{k}'} \gg \epsilon_{\boldsymbol{k}}$ we only keep the first vacuum term

$$\begin{aligned}\langle\!\langle a_{\boldsymbol{q}/2-\boldsymbol{k}'\downarrow}a_{\boldsymbol{q}/2+\boldsymbol{k}'\uparrow}a^\dagger_{\boldsymbol{q}/2+\boldsymbol{k}\uparrow}a^\dagger_{\boldsymbol{q}/2-\boldsymbol{k}\downarrow}\rangle\!\rangle &= \frac{-g}{2\epsilon_{\boldsymbol{k}'}-i\Gamma_2}\langle\!\langle b_{\boldsymbol{q}}a^\dagger_{\boldsymbol{q}/2+\boldsymbol{k}\uparrow}a^\dagger_{\boldsymbol{q}/2-\boldsymbol{k}\downarrow}\rangle\!\rangle \\ &= \Big(-\frac{g}{2\epsilon_{\boldsymbol{k}'}} - \frac{ig\Gamma_2}{4\epsilon^2_{\boldsymbol{k}'}+\Gamma_2^2}\Big)\langle\!\langle b_{\boldsymbol{q}}a^\dagger_{\boldsymbol{q}/2+\boldsymbol{k}\uparrow}a^\dagger_{\boldsymbol{q}/2-\boldsymbol{k}\downarrow}\rangle\!\rangle,\end{aligned} \tag{E.15}$$

since all the correlation functions go to zero for large momentum arguments.

Substituting the expression for the four-fermion cumulant Eq. (E.15) into the equation of motion for the fermion-boson correlation function Eq. (E.1c), we obtain the following reduced set of equations of motion

$$\frac{\mathrm{d}f_{\boldsymbol{k}\uparrow}}{\mathrm{d}t} = 2g\,\Im\Big\{\sum_{\boldsymbol{q}'}\langle\!\langle b_{-\boldsymbol{q}'}a^\dagger_{\boldsymbol{k}\uparrow}a^\dagger_{-\boldsymbol{q}'-\boldsymbol{k}\downarrow}\rangle\!\rangle\Big\} \tag{E.16a}$$

$$\frac{\mathrm{d}n_{\boldsymbol{q}}}{\mathrm{d}t} = -2g\,\Im\Big\{\sum_{\boldsymbol{k}'}\langle\!\langle b_{\boldsymbol{q}}a^\dagger_{\boldsymbol{q}/2+\boldsymbol{k}'\uparrow}a^\dagger_{\boldsymbol{q}/2-\boldsymbol{k}'\downarrow}\rangle\!\rangle\Big\} \tag{E.16b}$$

$$i\hbar\frac{\mathrm{d}\langle\!\langle b_{\boldsymbol{q}}a^\dagger_{\boldsymbol{q}/2+\boldsymbol{k}\uparrow}a^\dagger_{\boldsymbol{q}/2-\boldsymbol{k}\downarrow}\rangle\!\rangle}{\mathrm{d}t} = (\bar\nu-2\epsilon_{\boldsymbol{k}}-i\Gamma_{\mathrm{eff}})\langle\!\langle b_{\boldsymbol{q}}a^\dagger_{\boldsymbol{q}/2+\boldsymbol{k}\uparrow}a^\dagger_{\boldsymbol{q}/2-\boldsymbol{k}\downarrow}\rangle\!\rangle$$
$$+ gf_{\boldsymbol{q}/2+\boldsymbol{k}\uparrow}f_{\boldsymbol{q}/2-\boldsymbol{k}\downarrow}(1+n_{\boldsymbol{q}}) - gn_{\boldsymbol{q}}\left(1-f_{\boldsymbol{q}/2+\boldsymbol{k}\uparrow}\right)\left(1-f_{\boldsymbol{q}/2-\boldsymbol{k}\downarrow}\right) \tag{E.16c}$$

with the renormalized detuning

$$\bar{\nu} = \nu - \sum_{\boldsymbol{k}'}^{k'=K} \frac{g^2}{2\epsilon_{\boldsymbol{k}'}} = \nu - \frac{K}{2\pi^2} g^2 = \nu - \alpha g^2 \tag{E.17}$$

and an effective damping rate

$$\Gamma_{\text{eff}} = \Gamma_1 + g^2 \sum_{\boldsymbol{k}'} \frac{\Gamma_2}{4\epsilon_{\boldsymbol{k}'}^2 + \Gamma_2^2}. \tag{E.18}$$

In the next Section, we try to find an estimate for the damping rate Γ_{eff} by looking at the rate equations for fermion and boson populations.

E.6 Rate Equations to Order g^2 and Effective Damping Rates

In this Section, we eliminate the Bose–Fermi correlation function $\langle\!\langle ba^\dagger a^\dagger \rangle\!\rangle$ to obtain a coupled set of rate equations for the populations of fermions and molecules. Adiabatically solving for the imaginary part of Eq. (E.16c), we obtain:

$$\Im\Big\{ \langle\!\langle b_{\boldsymbol{q}} a^\dagger_{\boldsymbol{q}/2+\boldsymbol{k}\uparrow} a^\dagger_{\boldsymbol{q}/2-\boldsymbol{k}\downarrow} \rangle\!\rangle \Big\} = \frac{1}{2g} \Big(\Gamma_{ba}(\boldsymbol{q},\boldsymbol{k}) - \Gamma_{ab}(\boldsymbol{q},\boldsymbol{k}) \Big), \tag{E.19}$$

with fermion $\rightarrow$ boson and boson $\rightarrow$ fermion collision rates

$$\Gamma_{ab}(\boldsymbol{q},\boldsymbol{k}) = 2g^2 \frac{\Gamma_{\text{eff}}}{(\bar{\nu} - k^2)^2 + \Gamma_{\text{eff}}^2} \, f_{\boldsymbol{q}/2+\boldsymbol{k}\uparrow} f_{\boldsymbol{q}/2-\boldsymbol{k}\downarrow} \left(1 + n_{\boldsymbol{q}}\right), \tag{E.20a}$$

$$\Gamma_{ba}(\boldsymbol{q},\boldsymbol{k}) = 2g^2 \frac{\Gamma_{\text{eff}}}{(\bar{\nu} - k^2)^2 + \Gamma_{\text{eff}}^2} \, n_{\boldsymbol{q}} \left(1 - f_{\boldsymbol{q}/2+\boldsymbol{k}\uparrow}\right) \left(1 - f_{\boldsymbol{q}/2-\boldsymbol{k}\downarrow}\right). \tag{E.20b}$$

Substituting the resulting Eq. (E.19) into the population equations (E.16a) and (E.16b), we obtain the rate equations

$$\frac{\mathrm{d}f_{\boldsymbol{k}\uparrow}}{\mathrm{d}t} = \sum_{\boldsymbol{q}'} \Big(\Gamma_{ba}(\boldsymbol{q}', \boldsymbol{k} - \frac{\boldsymbol{q}'}{2}) - \Gamma_{ab}(\boldsymbol{q}', \boldsymbol{k} - \frac{\boldsymbol{q}'}{2}) \Big), \tag{E.21a}$$

$$\frac{\mathrm{d}n_{\boldsymbol{q}}}{\mathrm{d}t} = \sum_{\boldsymbol{k}'} \Big(\Gamma_{ab}(\boldsymbol{q}, \boldsymbol{k}') - \Gamma_{ba}(\boldsymbol{q}, \boldsymbol{k}') \Big). \tag{E.21b}$$

One easily sees that these equations obey conservation of the total number

$$N = \sum_{\boldsymbol{k},\sigma} f_{\boldsymbol{k},\sigma} + 2 \sum_{\boldsymbol{q}} n_{\boldsymbol{q}} \tag{E.22}$$

We now consider the limit $\Gamma_{\text{eff}} \to 0$, where the Lorentzian in the rates in Eqs. (E.20) reduces to a Dirac delta function $\pi\delta(\bar{\nu} - 2\epsilon_{\boldsymbol{k}})$

$$\frac{\mathrm{d}f_{\boldsymbol{k}\uparrow}}{\mathrm{d}t} = 2\pi g^2 \sum_{\boldsymbol{q}'} \delta\Big(\bar{\nu} - 2\epsilon_{\boldsymbol{k}-\boldsymbol{q}'/2}\Big)\Big[n_{\boldsymbol{q}'}\left(1 - f_{\boldsymbol{k}\uparrow}\right)\left(1 - f_{\boldsymbol{q}'-\boldsymbol{k}\downarrow}\right) - f_{\boldsymbol{k}\uparrow} f_{\boldsymbol{q}'-\boldsymbol{k}\downarrow}\left(1 + n_{\boldsymbol{q}'}\right)\Big], \quad \text{(E.23a)}$$

$$\frac{\mathrm{d}n_{\boldsymbol{q}}}{\mathrm{d}t} = 2\pi g^2 \sum_{\boldsymbol{k}'} \delta(\bar{\nu} - 2\epsilon_{\boldsymbol{k}'})\Big[f_{\boldsymbol{q}/2+\boldsymbol{k}'\uparrow} f_{\boldsymbol{q}/2-\boldsymbol{k}'\downarrow}\left(1 + n_{\boldsymbol{q}}\right) - n_{\boldsymbol{q}}\left(1 - f_{\boldsymbol{q}/2+\boldsymbol{k}'\uparrow}\right)\left(1 - f_{\boldsymbol{q}/2-\boldsymbol{k}'\downarrow}\right)\Big]. \quad \text{(E.23b)}$$

We can next evaluate the remaining momentum integrals in the rate equations above using the continuum limit of the momentum sums

$$\sum_{\boldsymbol{k}'} X = \frac{2\pi}{8\pi^3} \int_{-1}^{1} \int_{0}^{K} k'^2 X \, dk' \, dx' \quad \text{(E.24)}$$

For the molecule equation, we can solve the dk'-integral and obtain

$$\frac{\mathrm{d}n_{\boldsymbol{q}}}{\mathrm{d}t} = \frac{g^2\sqrt{\bar{\nu}}}{2\pi} \int_{-1}^{1} \Big[f_{\boldsymbol{q}/2+\boldsymbol{k}'\uparrow} f_{\boldsymbol{q}/2-\boldsymbol{k}'\downarrow}\left(1 + n_{\boldsymbol{q}}\right) - n_{\boldsymbol{q}}\left(1 - f_{\boldsymbol{q}/2+\boldsymbol{k}'\uparrow}\right)\left(1 - f_{\boldsymbol{q}/2-\boldsymbol{k}'\downarrow}\right)\Big]_{k'=\sqrt{\bar{\nu}}} \frac{\mathrm{d}x'}{2} \quad \text{(E.25)}$$

In the fermion equation, it is easier to solve the dx' integral first, and we obtain

$$\frac{\mathrm{d}f_{\boldsymbol{k}\uparrow}}{\mathrm{d}t} = \frac{\pi g^2}{k} \int_{0}^{K} q' \Big[n_{\boldsymbol{q}'}\left(1 - f_{\boldsymbol{k}\uparrow}\right)\left(1 - f_{\boldsymbol{k}'\downarrow}\right) - f_{\boldsymbol{k}\uparrow} f_{\boldsymbol{k}'\downarrow}\left(1 + n_{\boldsymbol{q}'}\right)\Big]_{k'=\sqrt{q'^2/2-k^2+2\bar{\nu}}} \frac{\mathrm{d}q'}{2\pi^2} \quad \text{(E.26)}$$

We can now estimate the effective decay rate Γ_{eff} for the Bose–Fermi correlation in Eq. (E.16c) as

$$\Gamma_{\text{eff}} = \frac{1}{2}\big(\Gamma_{\text{b}} + 2\Gamma_{\text{f}}\big) \quad \text{(E.27)}$$

where the boson and fermion decay rates are taken from the rate equations above:

$$\Gamma_{\text{b}} = \frac{g^2\sqrt{\bar{\nu}}}{2\pi} \int_{-1}^{1} \Big(1 - f_{\boldsymbol{q}/2+\sqrt{\bar{\nu}}\uparrow}\Big)\Big(1 - f_{\boldsymbol{q}/2-\sqrt{\bar{\nu}}\uparrow}\Big) \frac{\mathrm{d}x'}{2} \quad \text{(E.28)}$$

$$\Gamma_{\text{f}} = \frac{\pi g^2}{k} \int_{0}^{K} q' \Big[f_{\boldsymbol{k}'\uparrow}\left(1 + n_{\boldsymbol{q}'}\right)\Big]_{k'=\sqrt{q'^2/2-k^2+2\bar{\nu}}} \frac{\mathrm{d}q'}{2\pi^2} \quad \text{(E.29)}$$

Bibliography

[1] S. N. Bose. Plancks Gesetz und Lichtquantenhypothese. *Z. Phys.*, **26**:178, 1924. 1

[2] A. Einstein. Quantentheorie des einatomigen idealen Gases. *Sitzungsber. Kgl. Preuss. Akad. Wiss.*, Page 261, 1924. Zweite Abhandlung. *ibid.*, Page 3, 1925. 1

[3] M. J. Buckingham and W. M. Fairbank. The nature of the Lambda transition. In C. J. Gorter, editor, *Progress in Low Temperature Physics*, Volume III, Page 138, Amsterdam, 1961. North-Holland Pub. Co. 1

[4] P. Kapitza. Viscosity of liquid Helium below the λ-point. *Nature*, **141**:74, January 8, 1938. 1

[5] J. F. Allen and A. D. Misner. Flow of liquid Helium II. *Nature*, **141**:75, January 8, 1938. 1

[6] F. London. The λ-phenomenon of liquid helium and the Bose–Einstein degeneracy. *Nature*, **141**:643, April 16, 1938. 1

[7] M. H. Anderson, J. R. Ensher, M. R. Matthews, C. E. Wieman, and E. A. Cornell. Observation of Bose–Einstein condensation in a dilute atomic vapor. *Science*, **269**:198, July 1995. 2

[8] K. B. Davis, M. O. Mewes, M. R. Andrews, N. J. van Druten, D. S. Durfee, D. M. Kurn, and W. Ketterle. Bose–Einstein condensation in a gas of sodium atoms. *Phys. Rev. Lett.*, **75**(22):3969, Nov 1995. 2

[9] C. C. Bradley, C. A. Sackett, J. J. Tollett, and R. G. Hulet. Evidence of Bose–Einstein condensation in an atomic gas with attractive interactions. *Phys. Rev. Lett.*, **75**(9):1687, Aug 1995. 2

[10] M. R. Andrews, C. G. Townsend, H.-J. Miesner, D. S. Durfee, D. M. Kurn, and W. Ketterle. Observation of interference between two Bose–Einstein condensates. *Science*, **275**:637, January 1997. 2

[11] M. R. Matthews, B. P. Anderson, P. C. Haljan, D. S. Hall, C. E. Wieman, and E. A. Cornell. Vortices in a Bose–Einstein condensate. *Phys. Rev. Lett.*, **83**(13):2498, September 1999. 2, 55

[12] J. O. Andersen. Theory of the weakly interacting bose gas. *Rev. Mod. Phys.*, **76**(2):599, 2004. 2

[13] J. Goldstone. Field theories with "superconductor" solutions. *Nuovo Cimento*, **19**(1):154, 1961. 2

[14] S. Ritter, A. Öttl, T. Donner, T. Bourdel, M. Köhl, and T. Esslinger. Observing the formation of long-range order during Bose–Einstein condensation. *Phys. Rev. Lett.*, **98**(9):090402, 2007. 2

[15] H. J. Metcalf and P. van der Straten. *Laser Cooling and Trapping*. Springer, Berlin, 1999. 3

[16] B. DeMarco and D. S. Jin. Onset of Fermi degeneracy in a trapped atomic gas. *Science*, **285**(5434):1703, September 1999. 3

[17] C. A. Regal and D. S. Jin. Measurement of positive and negative scattering lengths in a Fermi gas of atoms. *Phys. Rev. Lett.*, **90**(23):230404, June 2003. 3, 4

[18] J. Bardeen, L. N. Cooper, and J. R. Schrieffer. Theory of superconductivity. *Phys. Rev.*, **108**(5):1175, 1957. 3, 69

[19] M. Holland, S. J. J. M. F. Kokkelmans, M. L. Chiofalo, and R. Walser. Resonance superfluidity in a quantum degenerate Fermi gas. *Phys. Rev. Lett.*, **87**:120406, September 2001. 4, 61

[20] K. M. O'Hara, S. L. Hemmer, M. E. Gehm, S. R. Granade, and J. E. Thomas. Observation of a strongly interacting degenerate Fermi gas of atoms. *Science*, **298**:2179, December 2002. 4

[21] M. Greiner, C. A. Regal, and D. S. Jin. Emergence of a molecular Bose–Einstein condensate from a Fermi gas. *Nature*, **426**(6966):537, Dec 2003. 4, 5

[22] K. E. Strecker, G. B. Partridge, and R. G. Hulet. Conversion of an atomic Fermi gas to a long-lived molecular Bose gas. *Phys. Rev. Lett.*, **91**:080406, 2003. 5, 107, 109

[23] J. Cubizolles, T. Bourdel, S. J. J. M. F. Kokkelmans, G. V. Shlyapnikov, and C. Salomon. Production of long-lived ultracold Li_2 molecules from a Fermi gas. *Phys. Rev. Lett.*, **91**(24):240401, Dec 2003. 5

[24] S. Jochim, M. Bartenstein, A. Altmeyer, G. Hendl, C. Chin, J. H. Denschlag, and R. Grimm. Pure gas of optically trapped molecules created from fermionic atoms. *Phys. Rev. Lett.*, **91**(24):240402, Dec 2003. 5

[25] C. A. Regal, C. Ticknor, J. L. Bohn, and D. S. Jin. Creation of ultracold molecules from a Fermi gas of atoms. *Nature*, **424**:47, July 2003. 5, 108, 109

[26] S. Jochim, M. Bartenstein, A. Altmeyer, G. Hendl, S. Riedl, C. Chin, J. Hecker Denschlag, and R. Grimm. Bose–Einstein Condensation of Molecules. *Science*, **302**(5653):2101, December 2003. 5

[27] M. W. Zwierlein, C. A. Stan, C. H. Schunck, S. M. F. Raupach, S. Gupta, Z. Hadzibabic, and W. Ketterle. Observation of Bose–Einstein condensation of molecules. *Phys. Rev. Lett.*, **91**(25):250401, Dec 2003. 5

[28] T. Bourdel, L. Khaykovich, J. Cubizolles, J. Zhang, F. Chevy, M. Teichmann, L. Tarruell, S. J. J. M. F. Kokkelmans, and C. Salomon. Experimental study of the BEC–BCS crossover region in Lithium 6. *Phys. Rev. Lett.*, **93**:050401, 2004. 5, 78

[29] D. Zubarev, V. Morozov, and G. Röpke. *Statistical Mechanics of Nonequilibrium Processes*, Volume 1. Akademie Verlag GmbH, Berlin, 1997. 5, 8, 11, 84, 104

[30] A. I. Akhiezer and S. V. Peletminskii. *Methods of Statistical Physics*. Pergamon Press, Oxford, 1981. 5, 12

[31] E. Zaremba, T. Nikuni, and A. Griffin. Dynamics of trapped Bose gases at finite temperatures. *J. Low Temp. Phys.*, **116**:277, August 1999. 7, 24

[32] P. Meystre and M. Sargent III. *Elements of Quantum Optics*. Springer, third edition, 1999. 8

[33] N. N. Bogoliubov. Problems of Dynamic Theory in Statistical Physics. In J. de Boer and G. E. Uhlenbeck, editors, *Studies in Statistical Mechanics*, Volume 1. North-Holland, Amsterdam, 1962. originally published in Russian in 1946. 8, 84

[34] S. Chapman and T. G. Cowling. *The Mathematical Theory of Nonuniform Gases*. Cambridge University Press, London, 1960. 9

[35] G. C. Wick. The evaluation of the collision matrix. *Phys. Rev.*, **80**(2):268, October 1950. 9

[36] W. H. Louisell. *Quantum Statistical Properties of Radiation*, chapter 3.7/3.8, Pages 182–190. Jon Wiley & Sons, unknown. 9, 27

[37] R. Walser, J. Williams, J. Cooper, and M. Holland. Quantum kinetic theory for a condensed bosonic gas. *Phys. Rev. A*, **59**(5):3878, May 1999. 9, 20, 24, 25, 26, 28, 30, 52, 110, 123

[38] J. E. Williams. *The Preparation of Topological Modes in a Strongly-Coupled Two-Component Bose–Einstein Condensate*. PhD thesis, University of Colorado at Boulder, 1999. 9

[39] J. Wachter, R. Walser, J. Cooper, and M. Holland. Equivalence of kinetic theories of Bose–Einstein condensation. *Phys. Rev. A*, **64**:053612, November 2001. 11, 31, 33, 128

[40] R. Walser, J. Cooper, and M. Holland. Reversible and irreversible evolution of a condensed bosonic gas. *Phys. Rev. A*, **63**:013607, 2001. 12, 14, 18, 20, 21, 22, 24, 25, 26, 28, 30, 31, 43, 49, 52

[41] V. G. Morozov and G. Röpke. The "mixed" Green's function approach to quantum kinetics with initial correlations. *Ann. Phys. (N.Y.)*, **278**:127, 1999. 12

[42] D. Zubarev, V. Morozov, and G. Röpke. *Statistical Mechanics of Nonequilibrium Processes*, Volume 2. Akademie Verlag GmbH, Berlin, 1997. 12, 15

[43] L. P. Kandanoff and G. Baym. *Quantum Statistical Mechanics*. W. A. Benjamin, Inc., New York, 1962. 12, 13, 15, 26, 34, 110, 128

[44] J. W. Kane and L. P. Kadanoff. Green's functions and superfluid hydrodynamics. *J. Math. Phys.*, **6**(12):1902, December 1965. 12, 14, 16, 26, 34, 110

[45] P. C. Hohenberg and P. C. Martin. Microscopic theory of superfluid Helium. *Ann. Phys. (N.Y.)*, **34**:291, 1965. reprinted *Ann. Phys. (N.Y.)*, **281**:636, 2000. 12, 16, 33

[46] M. Imamović-Tomasović and A. Griffin. Generalized Boltzmann equation for a trapped Bose-condensed gas using the Kadanoff–Baym formalism. In M. Bonitz, editor, *Progress in Nonequilibrium Green's Functions*, Page 404, Singapore, 2000. World Scientific. arXiv:cond-mat/9911402. 12, 16, 23

[47] Y. Nambu. Quasi-particles and gauge invariance in the theory of superconductivity. *Phys. Rev.*, **117**(3):648, February 1960. 13

[48] C. de Dominicis and P. C. Martin. Stationary entropy principle and renormalization in normal and superfluid systems. I. Algebraic formulation. *J. Math. Phys.*, **5**(1):14, January 1964. II. Diagrammatic formulation. *ibid.*:31. 15

[49] J. Schwinger. On the Green's functions of quantized fields. I and II. *Proc. Natl. Acad. Sci. U.S.A.*, **37**:452, 1951. 15

[50] G. Baym and N. D. Mermin. Determination of thermodynamic Green's functions. *J. Math. Phys.*, **2**(2):232, March 1961. 15

[51] R. A. Craig. Perturbation expansion for real-time Green's functions. *J. Math. Phys.*, **9**(4):605, April 1968. 15

[52] P. C. Martin. A microscopic approach to superfluidity and superconductivity. *J. Math. Phys.*, **4**(2):208, February 1961. 16

[53] M. Imamović-Tomasović and A. Griffin. Quasiparticle kinetic equation in a trapped Bose gas at low temperatures. *J. Low Temp. Phys.*, **122**(5/6):617, March 2001. 16, 23, 24, 26, 34

[54] S. T. Beliaev. Application of the methods of quantum field theory to a system of bosons. *Sov. Phys. JETP*, **34**(2):289, August 1958. Energy-spectrum of a non-ideal Bose gas. *ibid.*:299. 16, 23, 34

[55] G. Baym and L. P. Kadanoff. Conservation laws and correlation functions. *Phys. Rev.*, **124**(2):287, October 1961. 16

[56] H. Shi and A. Griffin. Finite-temperature excitations in a dilute Bose-condensed gas. *Phys. Rep.*, **304**(1-2):1, October 1998. 17

[57] A. Griffin. Conserving and gapless approximations for an inhomogeneous Bose gas at finite temperatures. *Phys. Rev. B*, **53**(14):9341, April 1996. 23, 34

[58] M. Imamović-Tomasović and A. Griffin. Coupled Hartree–Fock–Bogoliubov kinetic equations for a trapped Bose gas. *Phys. Rev. A*, **60**(1):494, July 1999. 23

[59] J. Wachter, R. Walser, J. Cooper, and M. Holland. Gapless kinetic theory beyond the Popov approximation. arXiv:cond-mat/0212432, 2002. 24, 41

[60] U. A. Khawaja and H. T. C. Stoof. Kinetic theory of collective excitations and damping in Bose–Einstein condensed gases. *Phys. Rev. A*, **62**:053602, October 2000. 24

[61] R. Graham. Langevin equation of collective modes of Bose–Einstein condensates in traps. *J. Stat. Phys.*, **101**(1):243, October 2000. 24

[62] B. Jackson and E. Zaremba. Finite-temperature simulations of the scissors mode in Bose–Einstein condensed gases. *Phys. Rev. Lett.*, **87**:100404, September 2001. 24, 25

[63] B. Jackson and E. Zaremba. Accidental suppression of Landau damping of the transverse breathing mode in elongated Bose–Einstein condensates. *Phys. Rev. Lett.*, **89**:150402, 2002. 24, 25

[64] B. Jackson and E. Zaremba. Quadrupole collective modes in trapped finite-temperature Bose–Einstein condensates. *Phys. Rev. Lett.*, **88**:180402, 2002. 24

[65] D. Jin, M. Matthews, J. Ensher, C. Wieman, and E. Cornell. Temperature-dependent damping and frequency shifts in collective excitations of a dilute Bose–Einstein condensate. *Phys. Rev. Lett.*, **78**(5):764, February 1997. 25, 110

[66] E. A. Donley, N. R. Claussen, S. T. Thompson, and C. E. Wieman. Atom-molecule coherence in a Bose–Einstein condensate. *Nature*, **417**:529, May 30, 2002. 25

[67] S. J. J. M. F. Kokkelmans and M. J. Holland. Ramsey fringes in a Bose–Einstein condensate between atoms and molecules. *Phys. Rev. Lett.*, **89**:180401, October 2002. 25, 62

[68] T. Köhler, T. Gasenzer, and K. Burnett. Microscopic theory of atom-molecule oscillations in a Bose–Einstein condensate. *Phys. Rev. A*, **67**:013601, January 2003. 25

[69] N. P. Proukakis, S. A. Morgan, S. Choi, and K. Burnett. Comparison of gapless mean-field theories for trapped Bose–Einstein condensates. *Phys. Rev. A*, **58**(3):2435, 1998. 25

[70] H. T. C. Stoof. Coherent versus incoherent dynamics during Bose–Einstein condensation in atomic gases. *J. Low Temp. Phys.*, **144**:11, 1999. 25

[71] D. A. W. Hutchinson, K. Burnett, R. J. Dodd, S. A. Morgan, M. Rusch, E. Zaremba, N. P. Proukakis, M. Edwards, and C. W. Clark. Gapless mean-field theory of Bose–Einstein condensates. *J. Phys. B: At. Mol. Opt. Phys.*, **33**(19):3825, October 2000. 25

[72] S. A. Morgan. A Gapless Theory of Bose–Einstein Condensation in Dilute Gases at Finite Temperature. *J. Phys. B: At. Mol. Opt. Phys.*, **33**(19):3847, October 2000. 25, 39, 50

[73] M. Olshanii and L. Pricoupenko. Rigorous approach to the problem of ultraviolet divergencies in dilute Bose gases. *Phys. Rev. Lett.*, **88**:010402, January 2002. 25

[74] T. Köhler and K. Burnett. Microscopic quantum dynamics approach to the dilute condensed Bose gas. *Phys. Rev. A*, **65**:033601, February 2002. 25, 84

[75] S. A. Morgan. Response of Bose–Einstein condensates to external perturbations at finite temperature. *Phys. Rev. A*, **69**:023609, 2004. 25, 110

[76] S. A. Morgan. Quantitative test of thermal field theory for Bose–Einstein condensates. ii. *Phys. Rev. A*, **72**(4):043609, 2005. 25, 110

[77] Y. Castin and R. Dum. Instability and depletion of an excited Bose–Einstein condensate in a trap. *Phys. Rev. Lett.*, **79**(19):3553, November 1997. 25, 39

[78] S. A. Gardiner and S. A. Morgan. Number-conserving approach to a minimal self-consistent treatment of condensate and noncondensate dynamics in a degenerate Bose gas. *Phys. Rev. A*, **75**(4):043621, 2007. 25, 85

[79] M. J. Davis, C. W. Gardiner, and R. J. Ballagh. Quantum kinetic theory. VII. The influence of vapor dynamics on condensate growth. *Phys. Rev. A*, **62**:063608, November 2000. and references therein to QKI to QKVI. 25

[80] M. J. Davis, R. J. Ballagh, and K. Burnett. Dynamics of thermal Bose fields in the classical limit. *J. Phys. B: At. Mol. Opt. Phys.*, **34**:4487, 2001. 25

[81] S. Giorgini. Collisionless dynamics of dilute Bose gases: Role of quantum and thermal fluctuations. *Phys. Rev. A*, **61**:063615, 2000. 25

[82] P. O. Fedichev and G. V. Shlyapnikov. Finite-temperature perturbation theory for a spatially inhomogeneous Bose-condensed gas. *Phys. Rev. A*, **58**(4):3146, October 1998. 25

[83] S. T. Beliaev. Energy-spectrum of a non-ideal Bose gas. *Sov. Phys. JETP*, **34**(2):299, August 1958. 26

[84] N. P. Proukakis. Self-consistent quantum kinetics of condensate and non-condensate via a coupled equations of motion formalism. *J. Phys. B: At. Mol. Opt. Phys.*, **34**(23):4737, 2001. 26

[85] N. P. Proukakis and P. Lambropoulos. Basis-dependent dynamics of trapped Bose–Einstein condensates and analogies with semi-classical laser theory. *Eur. Phys. J. D*, **19**(3):335, June 2002. 26

[86] A. M. Rey, B. L. Hu, E. Calzetta, A. Roura, and C. W. Clark. Nonequilibrium dynamics of optical-lattice-loaded bose-einstein-condensate atoms: Beyond the hartree-fock-bogoliubov approximation. *Phys. Rev. A*, **69**(3):033610, 2004. 26

[87] A. M. Rey, B. L. Hu, E. Calzetta, A. Roura, and C. Clark. BEC dynamics with fluctuations: Beyond HFB approximation. *Laser Physics*, **14**(2):318, February 2004. 26

[88] A. M. Rey, B. L. Hu, E. Calzetta, and C. W. Clark. Quantum kinetic theory of a bose-einstein gas confined in a lattice. *Phys. Rev. A*, **72**(2):023604, 2005. 26

[89] N. M. Hugenholtz and D. Pines. Ground-state energy and excitation spectrum of a system of interacting bosons. *Phys. Rev.*, **116**(3):489, November 1959. 34, 38

[90] N. P. Proukakis, K. Burnett, and H. T. C. Stoof. Microscopic treatment of binary interactions in the nonequilibrium dynamics of partially Bose-condensed trapped gases. *Phys. Rev. A*, **57**(2):1230, February 1998. 37

[91] A. L. Fetter. Nonuniform states of an imperfect Bose gas. *Ann. Phys. (N.Y.)*, **70**:67, 1972. 39, 43

[92] S. Mukamel. *Principles of Nonlinear Optical Spectroscopy.* Oxford University Press, New York, Oxford, 1995. 39

[93] U. Fano. Pressure broadening as a prototype of relaxation. *Phys. Rev.*, **131**(1):259, July 1963. 39

[94] A. M. Lane and R. G. Thomas. R-matrix theory of nuclear reactions. *Rev. Mod. Phys.*, **30**(2):257, April 1958. 40

[95] J.-P. Blaizot and G. Ripka. *Quantum Theory of Finite Systems.* MIT Press, Cambridge, MA, 1986. 42, 43

[96] M. Bonitz. *Quantum Kinetic Theory.* B. G. Teubner, Stuttgart, Leipzig, 1998. 50

[97] S. G. Bhongale, R. Walser, and M. J. Holland. Memory effects and conservation laws in the quantum kinetic evolution of a dilute bose gas. *Phys. Rev. A*, **66**:043618, September 2002. 50

[98] M. Holland and J. Wachter. Two-channel models of the BCS/BEC crossover. Proceedings of the International School of Physics "Enrico Fermi", 2006. 53, 69

[99] B. P. Anderson, P. C. Haljan, C. E. Wieman, and E. A. Cornell. Vortex precession in Bose–Einstein condensates: Observations with filled and empty cores. *Phys. Rev. Lett.*, **85**(14):2857, October 2000. 55

[100] J. W. Williams and M. J. Holland. Preparing topological states of a Bose–Einstein condensate. *Nature*, **401**(6753):568, October 7, 1999. arXiv:cond-mat/9909163. 56

[101] J. L. Bohn. Cooper pairing in ultracold ^{40}K using Feshbach resonances. *Phys. Rev. A*, **61**(5):053409, 2000. 60

[102] E. Timmermans, K. Furuya, P. W. Milonni, and A. K. Kerman. Prospect of creating a composite Fermi-Bose superfluid. *Phys. Lett. A*, **285**(3):228, 2001. 61

[103] S. J. J. M. F. Kokkelmans, J. N. Milstein, M. L. Chiofalo, R. Walser, and M. J. Holland. Resonance superfluidity: Renormalization of resonance scattering theory. *Phys. Rev. A*, **65**(5):053617, 2002. 62, 133

[104] R. A. Duine and H. T. C. Stoof. Microscopic many-body theory of atomic Bose gases near a Feshbach resonance. *J. Opt. B: Quantum Semiclass. Opt.*, **5**(2):S212, 2003. 62

[105] G. M. Bruun and C. J. Pethick. Effective theory of Feshbach resonances and many-body properties of Fermi gases. *Phys. Rev. Lett.*, **92**:140404, 2004. 62

[106] C. J. Pethick and H. Smith. *Bose–Einstein Condensation in Dilute Gases*. Cambridge Univ. Press, Cambridge, 2002. 64

[107] M. Holland, C. Menotti, and L. Viverit. The role of boson-fermion correlations in the resonance theory of superfluids. arXiv:cond-mat/0404234, April 2004. 65

[108] H. Feshbach. Unified theory of nuclear reactions. *Ann. Phys. (N.Y.)*, **5**(4):357, December 1958. 66

[109] H. Feshbach. A unified theory of nuclear reactions. II. *Ann. Phys. (N.Y.)*, **19**(2):287, August 1962. 66

[110] H. Feshbach. *Theoretical Nuclear Physics*. Wiley, New York, 1992. 66

[111] D. M. Eagles. Possible pairing without superconductivity at low carrier concentrations in bulk and thin-film superconducting semiconductors. *Phys. Rev.*, **186**(2):456–463, 1969. 66

[112] A. J. Leggett. Diatomic molecules and Cooper pairs. In A. Pekalski and R. Przystawa, editors, *Modern Trends in the Theory of Condensed Matter*, Volume 115 of *Lecture Notes in Physics*, Page 13, Berlin, 1980. Springer-Verlag. 66

[113] P. Nozières and S. Schmitt-Rink. Bose condensation in an attractive fermion gas: From weak to strong coupling superconductivity. *J. Low Temp. Phys.*, **59**(3/4):195, 1985. 67

[114] M. Randeria. Crossover from BCS theory to Bose–Einstein condensation. In A. Griffin, D. Snoke, and S. Stringari, editors, *Bose–Einstein Condensation*, Page 355. Cambridge Univ. Press, Cambridge, 1995. 67

[115] C. Bloch and A. Messiah. The canonical form of an antisymmetric tensor and its application to the theory of superconductivity. *Nuclear Physics*, **39**:95, 1962. 72

[116] B. Zumino. Normal forms of complex matrices. *J. Math. Phys.*, **3**(5):1055, 1962. 72

[117] P. Ring and P. Schuck. *The Nuclear Many-Body Problem*. Springer, New York, 1980. 72

[118] K. Burzyński and J. Dobaczewski. Quadrupole-collective states in a large single-j shell. *Phys. Rev. C*, **51**(4):1825, Apr 1995. 72

[119] J. Dobaczewski. Generalization of the Bloch–Messiah–Zumino theorem. *Phys. Rev. C*, **62**(1):017301, May 2000. 72

[120] K. Tanabe and K. Sugawara-Tanabe. Bloch–Messiah theorem at finite temperature. *Z. Phys. A – Hadrons and Nuclei*, **339**:91, 1991. 72

[121] H. Umezawa, H. Matsumoto, and M. Tachiki. *Thermo Field Dynamics and Condensed States*. North-Holland, Amsterdam, 1982. 72

[122] V. Chernyak, S. Choi, and S. Mukamel. Generalized coherent state representation of Bose–Einstein condensates. *Phys. Rev. A*, **67**:053604, 2003. 72

[123] R. Walser. Ground state correlations in a trapped quasi one-dimensional Bose gas. *Opt. Comm.*, **243**:107, 2004. 72

[124] G. B. Partridge, K. E. Strecker, R. I. Kamar, M. W. Jack, and R. G. Hulet. Molecular probe of pairing in the BEC–BCS crossover. *Phys. Rev. Lett.*, **95**:020404, 2005. 76, 86, 87

[125] D. S. Petrov, C. Salomon, and G. V. Shlyapnikov. Weakly bound dimers of fermionic atoms. *Phys. Rev. Lett.*, **93**:090404, 2004. 77, 78, 95

[126] M. Bartenstein, A. Altmeyer, S. Riedl, S. Jochim, C. Chin, J. H. Denschlag, and R. Grimm. Crossover from a molecular Bose–Einstein condensate to a degenerate Fermi gas. *Phys. Rev. Lett.*, **92**:120401, 2004. 78

[127] M. W. Zwierlein, C. A. Stan, C. H. Schunck, S. M. F. Raupach, A. J. Kerman, and W. Ketterle. Condensation of pairs of fermionic atoms near a Feshbach resonance. *Phys. Rev. Lett.*, **92**:120403, 2004. 78

[128] M. L. Chiofalo, S. Giorgini, and M. Holland. Released momentum distribution of a Fermi gas in the BCS–BEC crossover. *Phys. Rev. Lett.*, **97**:070404, 2006. 83

[129] C. A. Regal, M. Greiner, S. Giorgini, M. Holland, and D. S. Jin. Momentum distribution of a Fermi gas of atoms in the BCS–BEC crossover. *Phys. Rev. Lett.*, **95**:250404, 2005. 83

[130] J. E. Williams, T. Nikuni, N. Nygaard, and C. W. Clark. Atom-molecule equilibration in a degenerate Fermi gas with resonant interactions. *J. Phys. B: At. Mol. Opt. Phys.*, **37**(21):L351, Nov 2004. 84, 100

[131] J. E. Williams, N. Nygaard, and C. W. Clark. Theory of Feshbach molecule formation in a dilute gas during a magnetic field ramp. *New J. Phys.*, **8**:150, Aug 2006. 84, 100, 108, 109

[132] R. Kubo. Generalized cumulant expansion method. *J. Phys. Soc. Jpn.*, **17**(7):1100, July 1962. 84

[133] J. Fricke. Transport equations including many-particle correlations for an arbitrary quantum system: A general formalism. *Ann. Phys. (N.Y.)*, **252**:479, 1996. 84

[134] W. Kutzelnigg and D. Mukherjee. Cumulant expansion of the reduced density matrices. *J. Chem. Phys.*, **110**(6):2800–2809, 1999. 84

[135] E. H. Lieb, R. Seiringer, J. P. Solovej, and J. Yngvason. *The Mathematics of the Bose Gas and its Condensation*, Volume 34 of *Oberwolfach Seminars*. Birkhäuser, Basel, 2005. 85

[136] E. H. Lieb, R. Seiringer, and J. Yngvason. Justification of c-number substitutions in bosonic hamiltonians. *Phys. Rev. Lett.*, **94**:080401, 2005. 85

[137] Y. Castin and R. Dum. Low-temperature Bose–Einstein condensates in time-dependent traps: Beyond the $U(1)$ symmetry-breaking approach. *Phys. Rev. A*, **57**(4):3008, April 1998. 85

[138] C. W. Gardiner. Particle-number-conserving Bogoliubov method which demonstrates the validity of the time-dependent Gross–Pitaevskii equation for a highly condensed Bose gas. *Phys. Rev. A*, **56**(2):1414, August 1997. 85

[139] S. A. Morgan. *A Gapless Theory of Bose–Einstein Condensation in Dilute Gases at Finite Temperature*. PhD thesis, Univ. Oxford, 1999. 85

[140] L. P. Gorkov and T. K. Melik-Barkhudarov. Contribution to the theory of superfluidity in an imperfect Fermi gas. *Sov. Phys. JETP*, **13**(5):1018, 1961. 89

[141] A. A. Abrikosov, L. P. Gorkov, and I. E. Dzyaloshinski. *Methods of Quantum Field Theory in Statistical Physics*. Dover, 1975. 89

[142] G. H. Wannier. *Statistical Physics*. John Wiley & Sons, Inc., 1966. 90

[143] U. Fano. Effects of configuration interaction on intensities and phase shifts. *Phys. Rev.*, **124**(6):1866, 1961. 93

[144] J. E. Williams, N. Nygaard, and C. W. Clark. Phase diagrams for an ideal gas mixture of fermionic atoms and bosonic molecules. *New J. Phys.*, **6**:123, 2004. 100

[145] K. M. O'Hara, S. L. Hemmer, S. R. Granade, M. E. Gehm, J. E. Thomas, V. Venturi, E. Tiesinga, and C. J. Williams. Measurement of the zero crossing in a Feshbach resonance of fermionic ^{6}Li. *Phys. Rev. A*, **66**(4):041401, Oct 2002. 103

[146] K. Dieckmann, C. A. Stan, S. Gupta, Z. Hadzibabic, C. H. Schunck, and W. Ketterle. Decay of an ultracold fermionic Lithium gas near a Feshbach resonance. *Phys. Rev. Lett.*, **89**(20):203201, Oct 2002. 103

[147] W. H. Press, B. P. Flannery, S. A. Teukolsky, and W. T. Vetterling. *Numerical Recipes in C: The Art of Scientific Computing*. Cambridge University Press, 1992. 103

[148] E. Hodby, S. T. Thompson, C. A. Regal, M. Greiner, A. C. Wilson, D. S. Jin, E. A. Cornell, and C. E. Wieman. Production efficiency of ultracold Feshbach molecules in bosonic and fermionic systems. *Phys. Rev. Lett.*, **94**(12):120402, 2005. 107, 108, 109

[149] T. Köhler, K. Góral, and P. S. Julienne. Production of cold molecules via magnetically tunable Feshbach resonances. *Rev. Mod. Phys.*, **78**(4):1311, 2006. 107

[150] J. Wachter. A quasiparticle Boltzmann equation—Advances in the quantum kinetic theory of condensed bosonic gases. Master's thesis, University of Colorado at Boulder, 2000. http://bdagger.colorado.edu/˜wachter/thesis.pdf. 113, 120

[151] S. A. Gardiner. *Quantum Measurement, Quantum Chaos, and Bose–Einstein Condensates*. PhD thesis, Universität Innsbruck, Jan 2000. 133

[152] G. Bruun, Y. Castin, R. Dum, and K. Burnett. BCS theory for trapped ultracold fermions. *Euro. Phys. J. D*, **7**:433, 1999. 133